GEOLOGY AND MINERALISATION OF THE SOUTHERN PRINCE LYELL DEEPS, QUEENSTOWN, TASMANIA

by

Oliver L. Raymond
BSc (Hons)

Submitted in fulfilment of the requirements
for the degree of Master of Science

Centre for Ore Deposit and Exploration Studies,
University of Tasmania,
Hobart.

November, 1992

All arguments and analytical data presented in this thesis are my own unless otherwise referenced.

Oliver L. Raymond

ABSTRACT

The Prince Lyell copper - gold - silver deposit occurs in the late Cambrian Central Volcanic Complex of the Mt Read Volcanics at Queenstown, Tasmania. The southern portion of the deposit comprises several steeply plunging, broadly conformable lenses truncated at depth by the Owen Conglomerate along the Great Lyell fault. The disseminated and stringer pyrite - chalcopyrite orebody was overturned and deformed during the mid Devonian Tabberabberan orogeny, substantially modifying primary sulphide textures.

The orebody host and structural footwall rocks are highly siliceous quartz - sericite ± chlorite rocks derived from alteration of rhyolitic to dacitic lavas and coarse grained volcaniclastic rocks. The structural hangingwall to the mineralisation is formed by chlorite - sericite - quartz altered fine grained intermediate - mafic volcaniclastic rocks. The intense alteration was texturally destructive and imparted a false fragmental appearance on the altered felsic volcanics. Alteration resulted in significant mobilisation of major and trace elements (including so - called "immobile elements") except Ti and, to a lesser extent, Zr. The Ti/Zr ratio appears to be a largely reliable discriminant between altered felsic and intermediate - mafic rocks, but not between intensely altered rhyolitic and dacitic volcanics.

Minor magnetite - apatite mineralisation occurs as largely conformable, but locally transgressive zones of stockwork vein and disseminated mineralisation. Trace elements (Ti, V, REE) and magnetite $\delta^{18}O$ ratios (~ 4‰) suggest the mineralisation was derived from a magmatic fluid. This hot, low ΣS, oxidised fluid locally remobilised copper and gold out of magnetite alteration zones. Later hematite ± siderite alteration, precipitated from oxidised fluids probably derived from the hematitic Owen Conglomerate, occurs in the structural footwall volcanics adjacent to the Great Lyell fault.

Apart from metal depleted zones attributable to magnetite alteration, significant remobilisation of copper, gold or the Cu/Au ratio in the orebody has not occurred. The geochemistry of the Great Lyell fault zone and shallowly dipping "flat faults" suggests that while Devonian metamorphic fluids may have been focussed along them, dissolution of adjacent copper mineralisation was of a local scale only.

Although extensively fractured, pyrite mineralisation has retained much of its pre-deformation internal structure, revealed by etching and *in situ* microprobe analysis. Early Co - rich pyrite (Pyrite I), coeval with chalcopyrite

mineralisation, was dissolved by later unmineralised fluids and reprecipitated as trace element - poor Pyrite II. Minor amounts of a second Co - rich pyrite (Pyrite III) was precipitated concurrently with Pyrite II.

Pyrite sulphur isotope ratios ranged from + 3 to 11‰. Isotopic variation is limited to a poorly defined zoning from higher to lower $\delta^{34}S$ values towards the centre of the ore zone. *In situ* analyses did not show any consistent $\delta^{34}S$ variation between the various stages in pyrite paragenesis, suggesting recycling of sulphur from a single Cambrian volcanogenic source and deposition of all pyrite generations from reduced volcanogenic fluids.

Hematite inclusions in Pyrite II and III indicate that this pyrite mineralisation occurred after deposition of the adjacent Owen Conglomerate, from which the hematite alteration was derived. Pyrite II and III were probably deposited during the last stages of volcanic activity, contemporaneous with initial Owen Conglomerate sedimentation in the early Ordovician.

Whole rock oxygen isotope ratios ranged from + 6.6 to 10.6‰ for the altered host rocks. Isotopic equilibrium was approached across the altered sequence. The $\delta^{18}O$ values suggest that significant isotopic exchange did not occur with a Devonian low grade metamorphic fluid. The calculated initial fluid $\delta^{18}O$ ratio (+ 4.5 - 6.0‰) suggests the fluid may have been derived from Cambrian seawater, but modified by interaction with the volcanic pile prior to mineralisation or by mixing with a relatively isotopically heavy magmatic fluid.

ACKNOWLEDGEMENTS

The author acknowledges the support and guidance of many geologists, technical staff and organisations whose assistance contributed greatly to the compilation of this thesis.

The author thanks Dr R. Large, for his supervision of the project and for providing the resources of the Key Centre for Ore Deposit and Exploration Studies at the University of Tasmania; and Prof D. Green and Dr R. Varne for making available the facilities of the Department of Geology.

The Mount Lyell Mining and Railway Company provided generous logistical support, through access to underground workings and drill core, and the provision of trace element analyses and statistical data. The working knowledge of the orebody and practical assistance of senior geologist M. Flitcroft and geologists N. Foster, M. Franks and A. Wiggins were particularly valued by the author.

Technical assistance and chemical analyses were provided by Messrs S. Stephens (thin sections), P. Robinson (XRF, AAS), W. Jablonski (electron microprobe), M. Power (snr) ($\delta^{34}S$) and M. Power (jnr) ($\delta^{18}O$) from the Geology and Chemistry Departments of the University of Tasmania; I. Barrow (XRF, AAS) from Renison Goldfields; and Dr S. Eldridge (SHRIMP $\delta^{34}S$) from the Research School of Earth Sciences at the Australian National University.

The author benefitted greatly from discussions with and thesis reviews by Drs R. Berry, A. Crawford, G. Davidson, J.B. Gemmell, G. Green, V. Guthrie, D. Huston, R. Large, J. MacPhie, M. Rattenbury, A.J. Stolz, Shen-Su Sun and Khin Zaw; and fellow postgraduate students A. Hill, P. Kitto and M. Roach.

Lastly, but by no means least, the author is forever indebted to his wife, Robyn, for maintaining both his and her own state of mind for the duration of this thesis.

The author was supported by an Australian Postgraduate Award and a Tasmanian Mining Industry Scholarship during this study.

TABLE OF CONTENTS

LIST OF TABLES *(Page number in italics indicates table appears after that page)*

LIST OF FIGURES *(Page number in italics indicates figure appears after that page)*

LIST OF MAPS *(located in pocket at back of volume)*

CHAPTER ONE

INTRODUCTION AND REGIONAL GEOLOGY

1.1 INTRODUCTION TO THE MOUNT LYELL MINING FIELD

The Mount Lyell mining field, at Queenstown on the west coast of Tasmania (Fig. 1.1), has supported continuous mining activities for over a century. Seventeen significant mineral deposits have been discovered on the field. The locations of fourteen of these deposits are shown in Figure 1.2. The field's mining history commenced in 1883 with the working of alluvial gold in the Linda Valley and the consequent discovery of The Blow massive sulphide gossan in 1884. Following mergers and takeovers of its major competitors on the field, the Mount Lyell Mining and Railway Company became the sole mining producer in 1933.

Early mining was centred on the high grade copper deposits in the North Lyell area and on The Blow where gold and occasional bonanza silver shoots were also worked. Subsequently, in the forty years prior to 1971, the majority of ore from the Mount Lyell field was extracted from the West Lyell open cut, comprising the Prince Lyell, 'A' Lens and Royal Tharsis copper orebodies. Since 1971, underground mining of the Prince Lyell orebody has been the major source of production from the field. Production and ore reserves figures for the Prince Lyell orebody and the entire Mount Lyell field are given in Table 1.1.

1.2 BACKGROUND AND AIMS OF THIS STUDY

In recent years, underground mining and diamond drilling has made accessable much deeper parts of the Prince Lyell deposit than have been previously studied. More selective mining methods have also necessitated more detailed delineation of the copper orebody and a better understanding of the controls on mineralisation. In addition, considerable debate has been rekindled on the origin of the Mount Lyell mineralisation since the mid 1980's when a post - Cambrian, possibly metamorphic origin for the mineralisation was revived by consultant and mine geologists (eg: Bird, 1982; Sillitoe, 1984; Brook, 1984).

This study aims to describe the deeper exposures of the southern Prince Lyell orebody below 14 Level (zero RL) and relate them to the previously

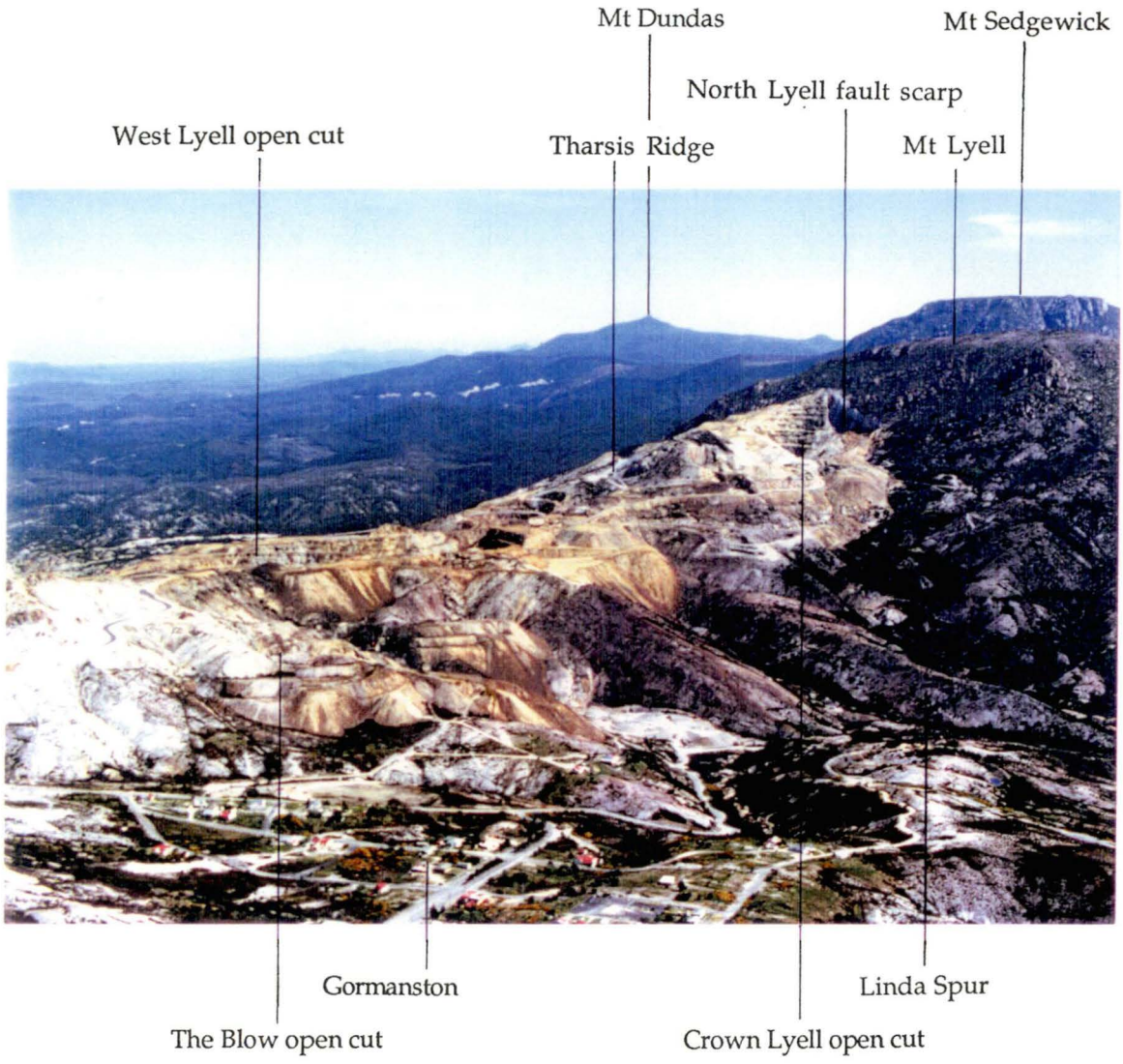

Figure 1.1 The Mt Lyell mining field and West Coast Range viewed north-west from Mt Owen.

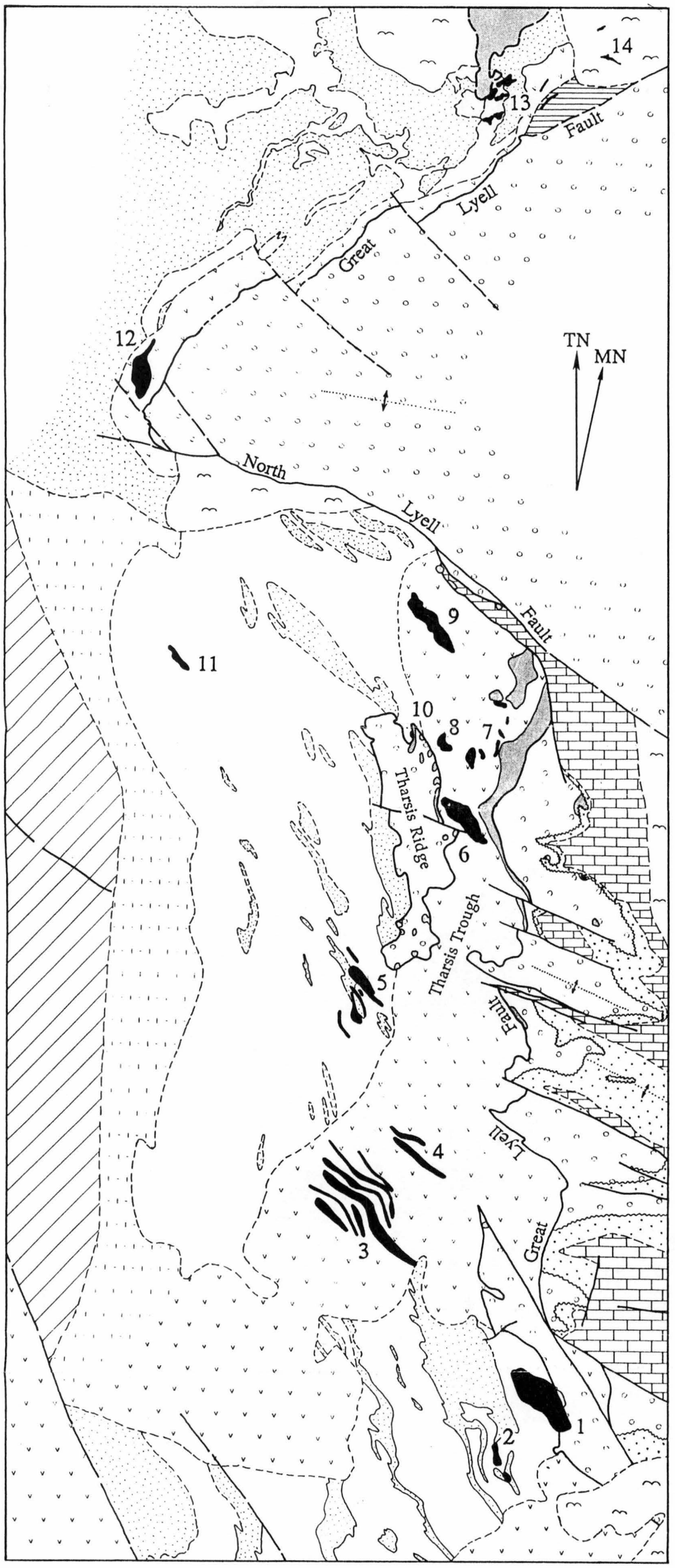

LEGEND

scale

0 200 400 600 800 1000 metres

Quaternary

moraine and recent talus

Ordovician

Pioneer Beds

Gordon Limestone

late Cambrian - early Ordovician

Owen Conglomerate

Cambrian - Mt Read Volcanics

Tyndall Group

Central Volcanic Complex

rhyolitic lavas and pyroclastics

undifferentiated volcanics

altered felsic volcanics

altered intermediate - mafic volcanics

undifferentiated altered volcanics

lithological boundary - position accurate, inferred

unconformity

fault - position accurate, inferred

fold axis

intense hematite-silica-barite alteration

sulphide orebodies - representative subsurface outlines

1 The Blow
2 South Lyell
3 Prince Lyell
4 'A' Lens
5 Royal Tharsis
6 Lyell Tharsis
7 North Lyell
8 Crown 1
9 Crown 3
10 Twelve West
11 Western Tharsis
12 Cape Horn
13 Comstock
14 Tasman

Figure 1.2 Geology of the Mt Lyell mineral field, showing the locations of major sulphide orebodies. (compiled from Mt Lyell Mining and Railway Co. 1 : 5000 scale mapping)

studied shallower parts of the orebody. In particular, it seeks to examine any variation in the style of mineralisation in the deeper parts of the orebody, and to assess the relative importance of volcanic, metamorphic and structural processes on the genesis and subsequent modification of the orebody.

To some extent, it is unavoidable that parts of this study will cover aspects of Prince Lyell studied by previous authors. However, in these cases I have endeavoured to re-evaluate existing models in the light of more recent observations and establish new models where appropriate.

Source	Tonnes ($x10^3$)	% Cu	g/t Ag	g/t Au
Production				
West Lyell (open cut)	58 312	0.72	1.7	0.3
Prince Lyell and 'A' Lens (underground)	24 960	1.26	3.0	0.4
Total Mt Lyell production	105 660	1.19	6.9	0.4
Ore Reserves				
Total Mt Lyell	6 934	1.79	3.0	0.6

Table 1.1 Mount Lyell Mining and Railway Co. Ltd production and ore reserves figures for the West Lyell orebodies and the total Mount Lyell field to June 1990.

1.3 Previous Studies of the Prince Lyell Deposit

Description of the Prince Lyell disseminated and stringer pyrite-chalcopyrite mineralisation has featured in many studies of the Mount Lyell ore deposits. Notable works are those of Markham (1968), McDonald (1968), Walshe (1971, 1977), Hendry (1972, 1981), Walshe and Solomon (1981) and Braithwaite (1985) which described much of the mineralogy, structure and geochemistry of the Prince Lyell deposit at and above the 14 Level underground workings.

Solomon (1964) and Sheppard (1987) studied the alteration geochemistry of surrounding volcanic rocks, while Loftus-Hills and Solomon (1967) and Loftus-Hills (1968) described the trace element distribution in sulphide minerals. Stable isotope variations at Prince Lyell have also been studied by

Solomon *et al.* (1969), Gulson and Porritt (1987) and Solomon *et al.* (1988). The effects of Devonian remobilisation on grade distribution were investigated by Bird (1982).

1.4 Regional Setting of the Mount Lyell Mining Field

1.4.1 Middle to late Cambrian - The Mount Read Volcanics and Dundas Group

The Mount Read Volcanics are an arcuate belt of calc-alkaline, mainly felsic and intermediate volcanics which form the eastern margin of the Dundas Trough, an elongate zone of Cambrian rocks bounded by the Precambrian Tyennan and Rocky Cape Regions (Fig. 1.3). The volcanic belt and laterally equivalent Dundas Group sediments of the Dundas Trough are thought to represent an arc-forearc sequence developed above an easterly dipping subduction zone during the middle to late Cambrian (Corbett and Lees, 1987).

Many authors have described the stratigraphic and structural relationships of the Mount Read Volcanics; most recently Corbett *et al.* (1974), White (1975), Corbett (1979, 1981, 1986), Corbett and Lees (1987) and Corbett and Solomon (1989). The complex structure and facies relationships of the Mount Read Volcanics have so far defied strict stratigraphic definition. The following description uses the nomenclature of Corbett and Solomon (1989). A simplified stratigraphy of the Mount Read Volcanics and associated lithologies is illustrated in Figure 1.4.

The Mount Read Volcanics are obliquely bisected by the NNE trending Henty Fault Zone; a major structure interpreted as the margin to an inter-arc basin (Corbett and Lees, 1987). North and west of the Henty Fault Zone, the belt is divided into a Central Volcanic Complex and overlying correlates of the Dundas Group of mainly andesitic composition. The massive sulphide deposits at Rosebery, Hercules, Que River and Hellyer are contained within this segment of the Mount Read Volcanic belt (Fig 1.3).

South and east of the Henty Fault Zone, the Mount Read Volcanics comprise a slightly younger Central Volcanic Complex of mainly feldspar-phyric rhyolitic volcanics, flanked by a volcano-sedimentary "western sequence". Both these units are overlain by the Tyndall Group arc sequence of quartz- and feldspar-phyric lavas and pyroclastics. In the Queenstown area, the Central Volcanic Complex has been described in detail by numerous authors, most recently Corbett *et al.* (1974), Cox (1981), Corbett (1979, 1981), and Walshe and Solomon (1981).

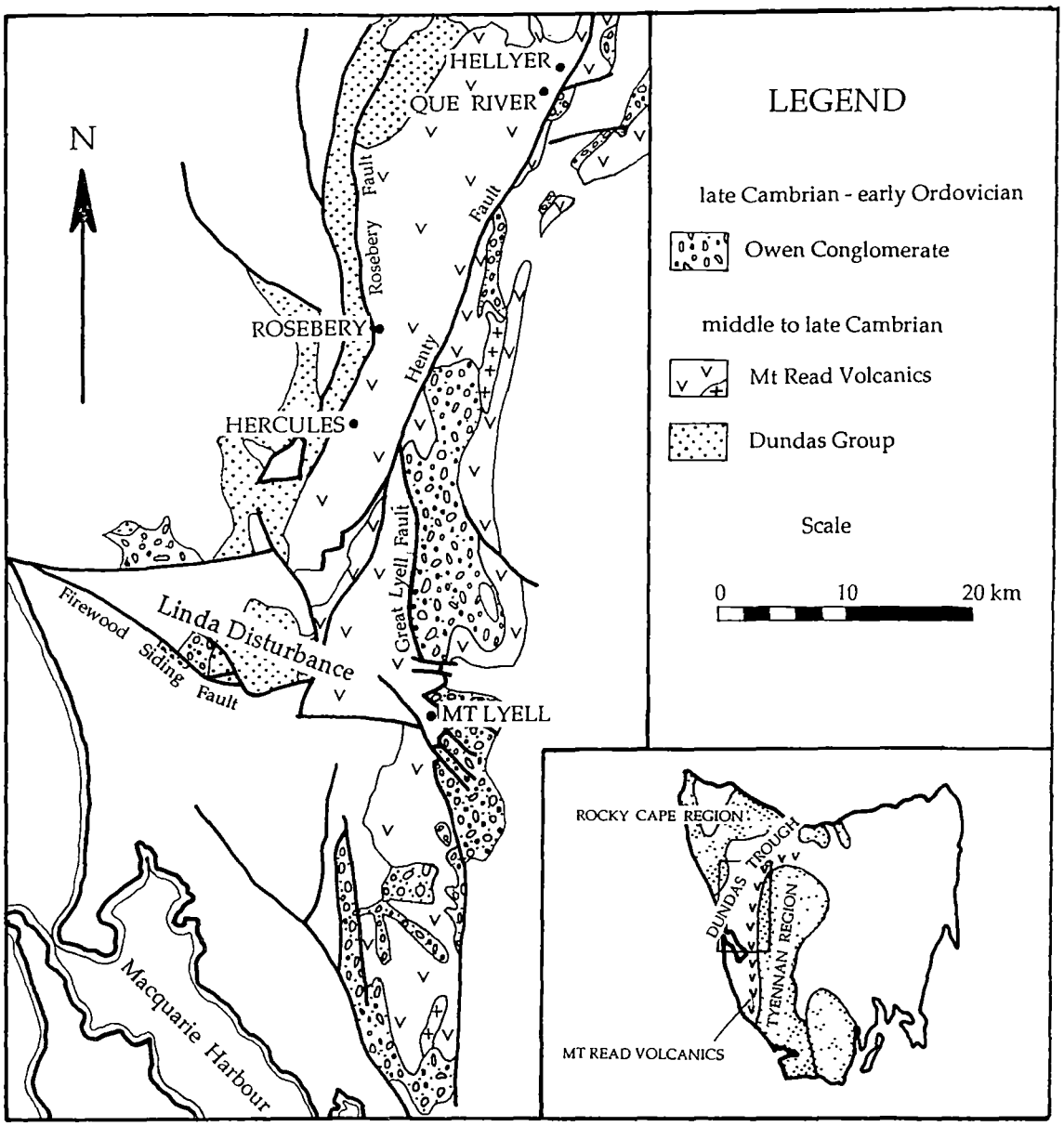

Figure 1.3 Middle Cambrian to early Ordovician lithologies of central western Tasmania, showing major ore deposits in the Mt Read Volcanics. The Devonian Linda Disturbance is marked by the WNW trending fault zone through the Mt Lyell area. Inset shows the location of Precambrian regions (shaded) and the Dundas Trough (modified after Corbett and Solomon, 1989).

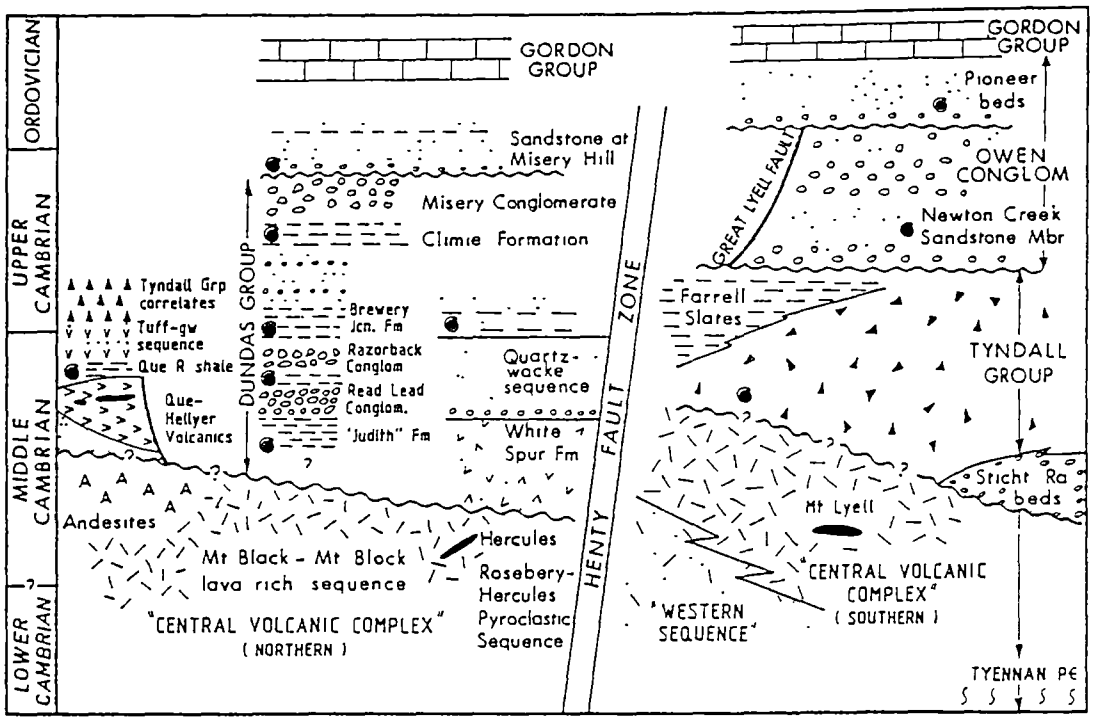

Figure 1.4 Correlation diagram for the Mount Read Volcanics and associated rock units, viewed from north to south across the Henty Fault Zone (after Corbett and Solomon, 1989).

Within the volcanic succession at Mount Lyell, Cox (1981) defined a "mine sequence" of predominantly subaerial origin, containing all the volcanic - hosted sulphide mineralisation at Mount Lyell (Fig. 1.5). It comprises laterally impersistent silicic lavas and volcaniclastics, abundant open framework mass flow breccias and minor intermediate volcaniclastics and intrusives. An extensive zone of hydrothermal alteration around the Mount Lyell deposits occurs over at least eight kilometres of strike length within the mine sequence.

1.4.2 Late Cambrian to early Devonian - structure and sedimentation

The late Cambrian to early Ordovician Owen Conglomerate was deposited in a graben-like basin at the eastern edge of the Mount Read Volcanics. The conglomerate has conformable and unconformable contacts with the underlying Tyndall Group volcaniclastics in the Queenstown area.

The siliciclastic Owen Conglomerate is almost entirely derived from the Precambrian Tyennan Region to the east. However, minor volcanic detritus occurs in the conglomerate adjacent to the Mount Read Volcanics at the

western margin of the graben in which the Owen Conglomerate was deposited. Walshe and Solomon (1981) suggested that erosion of the 'mine sequence' may have occurred prior to Owen Conglomerate sedimentation, removing some of the associated sulphide deposits. It is possible that volcanism was still active during early stages of Owen Conglomerate deposition (Brook, 1984, Berry, 1990b).

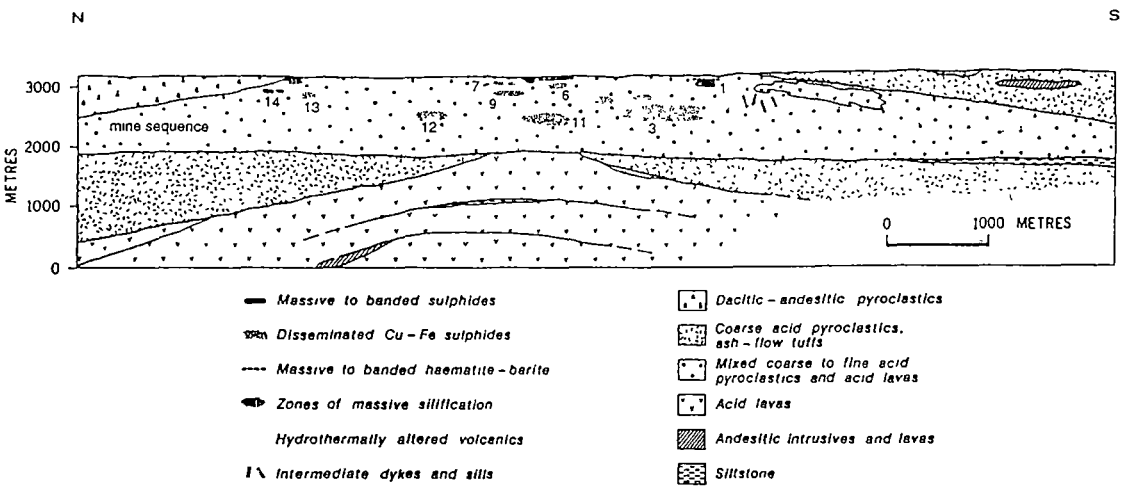

Figure 1.5 Simplified unfolded north-south section of the Mount Lyell volcanic sequence prior to deposition of the Tyndall Group, showing the position of major orebodies within the mine sequence and the extent of hydrothermal alteration (after Cox, 1981). Numbers refer to orebodies in Figure 1.2.

The depositional environment of the Owen Conglomerate is interpreted to be terrestrial grading upwards to shallow marine (Walshe and Solomon, 1981; Banks and Baillie, 1989). The Owen basin thickens towards its western margin which is marked by a probable growth fault, now preserved as the Great Lyell Fault. West of the Great Lyell Fault, the Owen Conglomerate was either not deposited over much of the area or was eroded during the Cambrian. Internal unconformities and rapid thickness variations within the conglomerate reflect depositional control by syn-depositional normal faulting (Berry, 1990b). The inferred maximum thickness of Owen Conglomerate is developed adjacent to the Great Lyell Fault, coincident with a major Devonian east-west trending structure, the Linda Disturbance (Walshe and Solomon, 1981). Walshe and Solomon (1981) suggested that a similar graben structure existed in the late Cambrian, accounting for the thickening of the Owen Conglomerate and the preservation of much of the Mount Lyell mineralisation.

The Owen Conglomerate was succeeded by the marine sediments of the Pioneer Beds. To the west of the Great Lyell Fault, the Pioneer Beds unconformably overlie both the Central Volcanic Complex and Tyndall Group volcanics. East of the Great Lyell Fault, the Owen Conglomerate - Pioneer Beds contact is locally unconformable along the Haulage Unconformity (Fig. 1.2). The origin of the folding of the conglomerate beneath the Haulage Unconformity in a 400 metre wide zone adjacent to the Great Lyell Fault is highly contentious. Wade and Solomon (1958) suggested contemporaneous movement on the Great Lyell Fault, while Solomon (1967) proposed large scale slumping during Owen deposition. Arnold (1985) and Arnold and Carswell (in press) invoked folding due to early Ordovician thrusting along the Great Lyell Fault. However, Berry (1990b) observed no evidence for such thrusting and considered the conglomerate to be upturned by normal drag along the Great Lyell fault acting as a basin margin growth fault.

The Pioneer Beds grade into the overlying Ordovician Gordon Limestone which contains the copper-clay deposits described by Solomon (1969). Both the Pioneer and Gordon sedimentary units contain native copper, possibly derived from erosion of previous volcanogenic mineralisation, although Sillitoe (1984) considered it to be derived from oxidation of primary epigenetic sulphide mineralisation. The Gordon Limestone is in turn conformably overlain by the Siluro-Devonian Eldon Group sandstones and mudstones of shallow marine origin.

1.4.3 Devonian deformation

The middle Devonian Tabberabberan Orogeny is recorded throughout eastern Australia. Williams *et al.* (1989) have summarised the work of previous authors on the effects of the orogeny in Tasmania.

In western Tasmania, an early phase of E-W compression (D_1) resulted in large amplitude N-S trending folds and associated thrusting. The competent behaviour of the Precambrian Tyennan Region largely determined the northerly trending fold pattern. A later phase of generally N-S compression (D_2) produced WNW trending folds and faults. Reactivation of NNE trending Cambrian structures, such as the Henty Fault, also occurred during Devonian deformation (Berry, 1989). Tin-tungsten mineralisation was associated with passive emplacement of post-kinematic granitoids during the late Devonian and early Carboniferous.

The effects of the Devonian deformation and metamorphism in the Queenstown area have been described by many authors including Wade and Solomon (1958), Solomon (1964), Solomon and Elms (1965), Reid (1975), Cox

(1981), Arnold (1985) and Berry (1990b). Metamorphic conditions during the Devonian deformation did not exceed lower greenschist facies, with temperatures below 350°C and confining pressures of around 2 kbar (Cox, 1981).

The geometry of the Central Volcanic Sequence is controlled largely by upright NNW trending D_1 folds with wavelengths of 1 - 5 km. Within the volcanics at Mount Lyell D_1 fold hinges have not been positively recognised and D_1 cleavage is only sporadically developed. The Mount Lyell mineralisation occurs within the steeply west dipping, overturned limb of a large interpreted D_1 anticline (Cox, 1981). A major NNW trending fault zone separates this east facing limb from the apparently west facing lithologies to the west (Cox, 1981; Berry, 1990b). Reactivation of the Great Lyell Fault probably occurred during D_1 due to the marked competency contrast between the altered Central Volcanic Complex and adjacent Owen Conglomerate.

During D_2, the Tyennan Region failed in a narrow zone of faulting and folding, resulting in a fault bounded graben structure in the Queenstown area known as the Linda Disturbance (Fig. 1.3). This WNW-trending zone deformed D_1 structures and the Great Lyell fault. Notable offset of the Great Lyell fault occurred at this time along the North Lyell fault. A regionally penetrative upright WNW-trending cleavage was also imposed throughout the area. Rotation of the cleavage in the volcanics away from the regional WNW direction, occurs around the more competent Owen Conglomerate.

The deformation style in the volcanics contrasts with that in the younger, well layered sedimentary sequences (Berry, 1990b). Movement accommodated by tight upright folds in the Ordovician and Siluro-Devonian sediments is taken up by steep reverse faulting and cleavage-parallel shearing in the altered volcanics. A strong down-dip mineral elongation lineation (L_2) is associated with D_2 cleavage formation in the volcanics. Shortening of up to 60% perpendicular to the cleavage and elongation of up to 150% in the lineation direction are typical, and are responsible for the elongation of many of the sulphide mineral deposits in the L_2 direction (Cox, 1981).

A complex sequence of events is required to explain the structure of the Tharsis Trough; a mineralised corridor of volcanics bounded by the Great Lyell Fault on its east and an outlier of Owen Conglomerate, the Tharsis Ridge, on its west (Fig. 1.2). Solomon (1969) suggested slumping off the Great Lyell Fault during Owen Conglomerate deposition, followed by thrusting along the Great Lyell Fault to explain the structure. Cox (1981) invoked a complex series of fault movements resulting in a fault bounded wedge of volcanics between blocks of Owen Conglomerate. Berry (1990b) suggested the feature was formed by pre-D_1 thrusting offsetting the Great Lyell Fault, followed by D_1 folding.

1.5 MINERALISATION IN THE MT LYELL FIELD

A schematic unfolded cross-section of the Mount Read Volcanics at Mount Lyell is shown in Figure 1.5. Sulphide mineralisation is confined to the extensively altered mine sequence volcanics (Cox, 1981). Volcanics which conformably and disconformably overlie and underlie the mine sequence are not hydrothermally altered, illustrating the grossly stratabound nature of the zone of alteration (Walshe and Solomon, 1981). Four main types of sulphide mineral deposits are recognised in the Mount Lyell field (Walshe and Solomon, 1981) (Fig. 1.2):

a. disseminated and stringer pyrite-chalcopyrite (e.g. Prince Lyell, A lens, Royal Tharsis, Western Tharsis),
b. bornite-chalcopyrite (e.g. North Lyell, 12 West),
c. massive pyrite-chalcopyrite (e.g. The Blow),
d. massive stratiform pyrite-galena-sphalerite-chalcopyrite (e.g. Tasman, Comstock open cut).

In addition to the sulphide mineralisation, several small deposits of native copper-cuprite mineralisation, derived from leaching or erosion of Cambrian sulphides, occur within clay horizons of the Ordovician Gordon Limestone (Markham, 1968; Solomon, 1969).

The massive sulphide deposits (types c. and d.) occur near the top of the mine sequence (Fig. 1.5). Although largely recrystallised, the massive sulphide ores preserve some laminated textures, suggesting a seafloor exhalative origin. The larger but lower grade disseminated pyrite-chalcopyrite deposits are found stratigraphically beneath the massive sulphide mineralisation and the bornite-chalcopyrite ores.

1.6 EVOLUTION OF THEORIES OF MOUNT LYELL ORE GENESIS

The history of ore genesis theories at Mount Lyell is summarised in Table 1.2. Earliest workers on the field considered the Mount Lyell mineralisation to be of epigenetic replacement origin, with fluids focussed along the Great Lyell Fault at its intersection with the Linda Disturbance during Devonian tectonic activity (e.g. Gregory, 1905; Hills, 1927; Nye *et al.*, 1934).

Hall and Solomon (1962) first proposed a possible genetic link between the mineralisation and the host volcanics, with Devonian fluids possibly deriving their ore components from earlier Cambrian mineralisation. By the

1970's to early 1980's, prevailing thought favoured a Cambrian volcanogenic origin for the Mount Lyell orebodies. Petrographic studies recognised the deformation of original sulphide textures, limiting the age of mineralisation to pre-D_2 deformation (e.g. Markham, 1968; Cox, 1981). Recent studies of lead isotope ratios (Gulson and Porritt, 1987) confirmed the Cambrian connection, with ratios from Mount Lyell ores being similar to those from syngenetic Cambrian mineralisation at Rosebery, Hercules and Que River.

Devonian Epigenetic Replacement	Devonian (Remobilisation of Cambrian Ore?)	Cambrian Volcanogenic Mineralisation	Cambrian/Devonian Two-phase Mineralisation	Cambrian Volcanogenic Mineralisation with Significant Devonian Remobilisation
Gregory (1905) Hills (1927) Nye *et al.* (1934) Edwards (1939) Conolly (1947) Carey (1953) Bradley (1956) Wade and Solomon (1958)				
	Hall and Solomon (1962) Solomon (1964) Solomon and Elms (1965)			
		Solomon (1967, 69, 76) Markham (1968) McDonald (1968) Green (1971) Walshe (1971, 77) Jago *et al.* (1972) Reid (1975) White (1975) Bryant (1976) Walshe and Solomon (1981) Hendry (1981) Cox (1981)	Hendry (1972)	
	Bird (1982)			
Brook (1984) Sillitoe (1984, 85)		Gulson and Porritt (1987)		Arnold (1985) Solomon *et al.* (1987) Solomon and Carswell (1989) Hills (1990) Arnold and Carswell (1990)
		Berry (1990b)		

Table 1.2 Summary of ore genesis theories at Mount Lyell.

The massive sulphide bodies were considered to be seafloor exhalative mineralisation, while cogenetic disseminated sulphides formed by replacement of more permeable subsurface horizons (e.g. Reid, 1975; Walshe and Solomon, 1981). The mineralising fluids were circulating seawater leaching metals from the volcanic pile, and localised by the junction of the Great Lyell Fault and a Cambrian precursor to the Linda Disturbance. Sulphur was derived from reduced seawater sulphate with variable contributions from igneous rock sulphur (Solomon, 1976; Walshe and Solomon, 1981).

Extensive hematite-barite and silica-hematite alteration, commonly associated with high grade bornite-chalcopyrite mineralisation adjacent to the Great Lyell Fault (Fig. 1.2), were thought by Solomon (1967) to be fossil gossans, developed from weathering of sulphides prior to Owen Conglomerate

deposition. Reappraisal of the hematitic and siliceous alteration (Solomon, 1976; Walshe and Solomon, 1981) suggested it could also have formed from Cambrain fumarolic siliceous sinter deposits.

However, more recent work by several authors has shown that the alteration extends at least into the Owen Conglomerate and perhaps across the Haulage Unconformity into the Pioneer Beds. Berry (1990b) considered the alteration to be absent above the Haulage Unconformity, constraining the age of the Mount Lyell mineralisation to pre Pioneer Beds, but at the same time invoking volcanogenic mineralisation during deposition of the Owen Conglomerate.[1] However, Sillitoe (1984, 1985) and Brook (1984) argued that the Pioneer Beds and Gordon Limestone were also altered and mineralised. This led to theories of Devonian (or perhaps Ordovician) metamorphic or porphyry copper type ore formation by fluids focussed along the Great Lyell fault. Sillitoe (1984, 1985) did not discount an early Ordovician volcanogenic origin for the mineralisation, but noted that it would require very rapid (~ 2 - 3 million years) accumulation of the Owen Conglomerate. Bird (1982) also suggested Devonian deposition of sulphides, although possibly leached from deep seated pre-existing Cambrian mineralisation.

In order to explain the juxtaposition of pyrite - chalcopyrite and bornite - chalcopyrite ores, authors have invoked substantial *in situ* modification (eg: Arnold, 1985; Arnold and Carswell, in press) or remobilisation (eg: Solomon, 1984) of Cambrian volcanogenic mineralisation by pre-D_2 Devonian metamorphic fluids circulating below the Haulage Unconformity. However, Devonian metamorphic fluids are unlikely to have added components to the Cambrian mineralisation (Solomon *et al.*, 1987).

1.7 Stratigraphic and Structural Setting of the Prince Lyell Deposit

The Prince Lyell deposit occurs within steeply dipping, overturned, altered rhyolitic to dacitic volcanics at the contact with a sequence of altered intermediate to mafic volcanics which form the stratigraphic footwall to the deposit (see Fig. 2.1, Maps 1, 3, 5, 7). The altered felsic volcanic rocks forming the statigraphic hangingwall of Prince Lyell are also the host rocks for the nearby 'A' Lens, Royal Tharsis and Western Tharsis copper deposits.

---

1. Ordovician Mt Read - type igneous activity has been observed in the Dial Range area (Jago *et al.*, 1977), well to the north of Mt Lyell, but has not as yet been reported elsewhere in the Mt Read Volcanics.

The Prince Lyell deposit is composed of a series of mineralised lenses (Maps 1 - 8). The South Lens and Footwall Lens[2] occupy discrete stratigraphic horizons at the southern end of the deposit. The North Lens mineralisation consists of a number of smaller lenses spanning a wider stratigraphic range along strike from the South and Footwall Lenses.

The dominant structural feature of the Prince Lyell volcanic sequence is the strong pervasive D_2 foliation. Although D_1 cleavage is developed in the Owen Conglomerate adjacent to the volcanics, it is rarely observed in the volcanic host rocks. The D_2 foliation in the Prince Lyell area dips steeply to the south-west, parallel to the regional volcanic layering and to the orientation of the Prince Lyell copper mineralisation. The strong down-dip continuity of the orebody parallel to the L_2 lineation direction has resulted from up to 150% elongation in that direction during cleavage formation (Cox, 1981).

Major discrete faults or shears through the Prince Lyell sequence are rare as most of the strain has been accomodated by movement along D_2 cleavage planes. The steeply dipping Footwall Shear is sub-parallel to the cleavage direction and occurs near the structural footwall of the South Lens mineralisation. The Footwall Shear is the only evidence of any possible "steeply dipping planar ..... orebody defining structures" proposed by Bird (1982). However, the Footwall Shear does not coincide with the orebody margin and there is no evidence of a discrete structure on the hangingwall of the orebody. The consistent linear plunge of the orebody may be attributed to the effect of stretching during D_2 rather than mineralisation between confining planar structures.

Discontinuous, post-cleavage, shallowly dipping reverse faults, locally referred to as "flat faults", are common in the Mount Lyell region. The faults occur as a conjugate set, dipping south-east and north-west. The faults are no more than minor flexures and strongly developed joints as very little if any movement occurs along them. Metamorphic quartz + siderite ± chlorite ± chalcopyrite ± flourite ± hematite veins, which occur throughout the altered volcanics, are commonly associated with the "flat faults" indicating that the faults have acted as fluid conduits during the late stages of the Devonian deformation (see Chapter 6).

---

2. The Footwall Lens is named according to current mine terminology which refers to the present structural attitude of the mine sequence (ie: overturned). Unless specifically referred to as 'stratigraphic footwall' or 'stratigraphic hangingwall', footwall and hangingwall locations will refer to the mine terminology of structural position.

CHAPTER TWO

LITHOLOGIES

2.1 INTRODUCTION AND TERMINOLOGY

The distribution of alteration lithologies interpreted from underground mapping and core logging in the southern Prince Lyell area on 115 and 200 Sublevels and Sections 67 and 73 are shown in Maps 1, 3, 5, and 7. Maps 9 and 10 present the geological mapping data from 115 and 200 Sublevels. A list of drill core logged appears in Appendix 2.1.

Previous descriptions of the Prince Lyell host rocks (eg: Walshe, 1977; Braithwaite, 1985) have referred to the highly altered volcanic succession primarily using volcanic terminology. The terms "intermediate - mafic volcanics" and "felsic volcanics" have been used commonly in describing the two main alteration lithologies (eg: Arnold, 1989). In using these terms, previous authors have assumed that the alteration lithologies are representative of the volcanic precursors their names imply. However, relict igneous textures and trace element geochemistry (Chapter 3) support this assumption as a general rule of thumb only. In particular, it is evident that a range of rhyolitic and dacitic lavas or breccias may be the precursors to the alteration lithology referred to as felsic volcanics.

The present study adopts the commonly used terminology in describing the altered rocks at Prince Lyell, but it is stressed that the terms "intermediate - mafic volcanics" and "felsic volcanics" are not strictly interchangeable with andesite - basalt and rhyolite. Other less altered lithologies, such as dacites and volcaniclastic breccias, exhibit primary volcanic textures which permit the use of conventional volcanic terminology in their description.

2.2 DETAILED STRATIGRAPHY

Irregular units of intermediate - mafic volcanics occur throughout the dominantly felsic volcanic pile which hosts the Mt Lyell mineral field (Fig. 1.2). At Prince Lyell, the stratigraphic footwall to the mineralisation is formed by a sequence of altered intermediate - mafic volcanics (Fig. 2.1), which is at least 200 metres thick and is intercalated with minor lenses of felsic

volcanics. A lack of drilling or underground development prevents accurate delineation of the stratigraphic base of the unit.

Copper mineralisation is almost entirely hosted within a sequence of intensely altered felsic volcanics at the contact with the intermediate - mafic volcanics. The stratigraphic hangingwall rocks comprise altered felsic volcanics similar to the mineralised horizon with enclaves of less altered dacitic volcanics, volcanic breccias and very minor fine grained shale or ash units. The felsic volcanics sequence is up to 500 metres thick at the surface and includes the 'A' Lens mineralisation, approximately 100 metres stratigraphically above the Prince Lyell mineralised horizon. At depth, in the study area, the felsic volcanics are a maximum of 250 metres thick as the Great Lyell Fault truncates a large proportion of the stratigraphic hangingwall sequence.

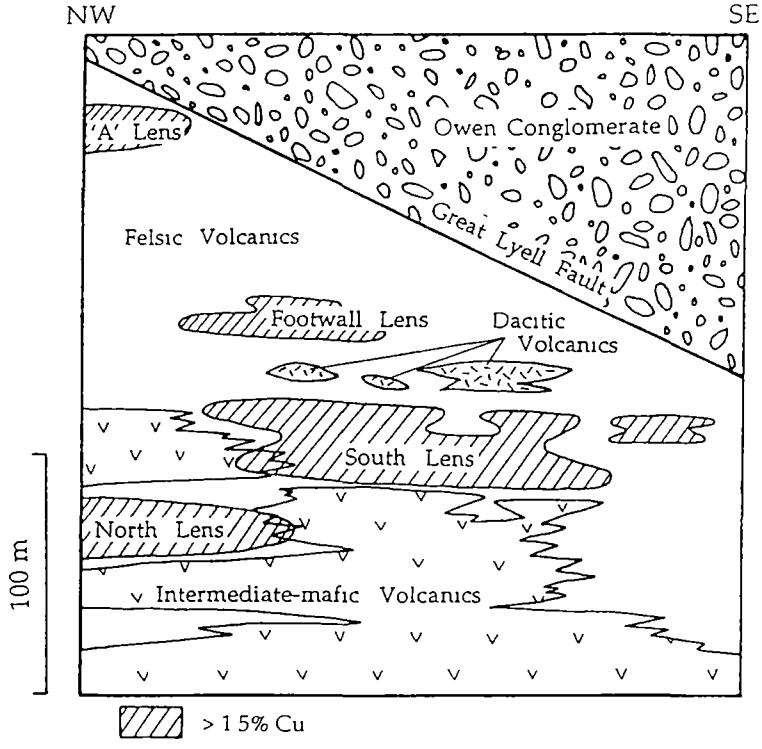

Figure 2.1 Schematic representation of the stratigraphic succession in the southern Prince Lyell area. Lithological units are defined by alteration and are not necessarily directly comparable with the primary igneous lithologies their names imply (see text). Stratigraphic facing is towards the top of the diagram. ($^{V}/_{H} = 1$)

2.3 INTERMEDIATE - MAFIC VOLCANICS

The intermediate - mafic volcanics are a sequence of fine grained, dark green to grey, chlorite-sericite-quartz schists (Fig. 2.2a). They are interpreted to be intensely altered andesitic to basaltic volcanics, mainly from their trace element geochemistry (Chapter 3). Although commonly strongly foliated, large bodies of weakly sheared intermediate - mafic volcanics of similar mineralogy occur possibly in pressure shadows formed adjacent to more competent siliceous felsic volcanics.

In thin section, the intermediate-mafic volcanics predominantly comprise a foliated groundmass of fine grained intergrown chlorite and sericite with disseminated grains of recrystallised quartz and accessory pyrite, magnetite, hematite, monazite and apatite (Fig. 2.2b). The groundmass may be segregated into wispy or crudely lensoidal domains of chlorite-rich or sericite-rich alteration, elongate parallel to the foliation direction. These domains commonly appear as flecks resembling pseudomorphs of phenocrysts or lithic clasts, several millimetres long in hand specimen. Relatively unfoliated intermediate - mafic volcanics consist of an irregular alteration intergrowth of chlorite, sericite and quartz without development of a fleck texture.

The alignment of flecks in the foliated rocks is interpreted to be due to attenuation of areas of more chloritic or sericitic alteration parallel to layering during cleavage development. In thin section, the chlorite or sericite flecks commonly have highly irregular shapes and diffuse boundaries with the groundmass, suggesting that the flecks do not represent original volcaniclastic clasts. It should be noted, however, that diffuse edges of the flecks are not alone diagnostic of an alteration origin, as genuine clastic rocks may have diffusely defined clasts when altered (Allen, 1988).

The disseminated ragged quartz grains in foliated intermediate - mafic volcanics were produced by the fracturing and dispersal of more coherent areas of siliceous alteration during shearing. Pull apart structures of chlorite and sericite developed in pressure shadows between fractured quartz grains are common.

Pyrite occurs as thin planar veinlets, a few millimetres to a few centimetres thick, generally at low angles to the foliation and regional layering (Fig. 2.2a). However, pyrite veinlets also intersect the foliation at high angles. The veinlets are comprised mainly of anhedral pyrite grains separated by metamorphic growth of sericite, chlorite and quartz in pressure shadows between grains. Minor magnetite, apatite and chalcopyrite also occur in the veins. Magnetite more commonly occurs in the intermediate - mafic

Figure 2.2

A. Characteristic stringer pyrite mineralisation and chlorite fleck texture in the intermediate - mafic volcanics. (sample 115003)

B. Photomicrograph of areas of irregular chlorite-rich alteration, or flecks, and brecciated secondary quartz grains (arrowed) in a strongly foliated chlorite - sericite altered intermediate - mafic volcanic. (sample 618010.0, PPL)

C. Photomicrograph of sericite pseudomorphs of plagioclase phenocrysts in an altered, but relatively weakly sheared, probably intrusive body in the intermediate - mafic volcanics. The preservation of such igneous textures in the intermediate - mafic volcanics is unusual. (sample 607013.2, PPL)

D. Repetition of a pyrite - barite - sphalerite vein by shearing along the foliation in the intermediate - mafic volcanics. Foliation and veining are sub-parallel to the regional volcanic layering. Diameter of lens cap is 5 cm. (55/56 crosscut, 115 Sublevel)

E. A massive pyrite - chalcopyrite band with strongly sheared margins within the intermediate - mafic volcanics. Elongate wallrock inclusions in the sulphide band such as the one arrowed may have been included during formation of a volcanogenic massive sulphide band or tectonically emplaced during shearing. Scale rule is 30 cm long. (55/56 crosscut, 115 Sublevel)

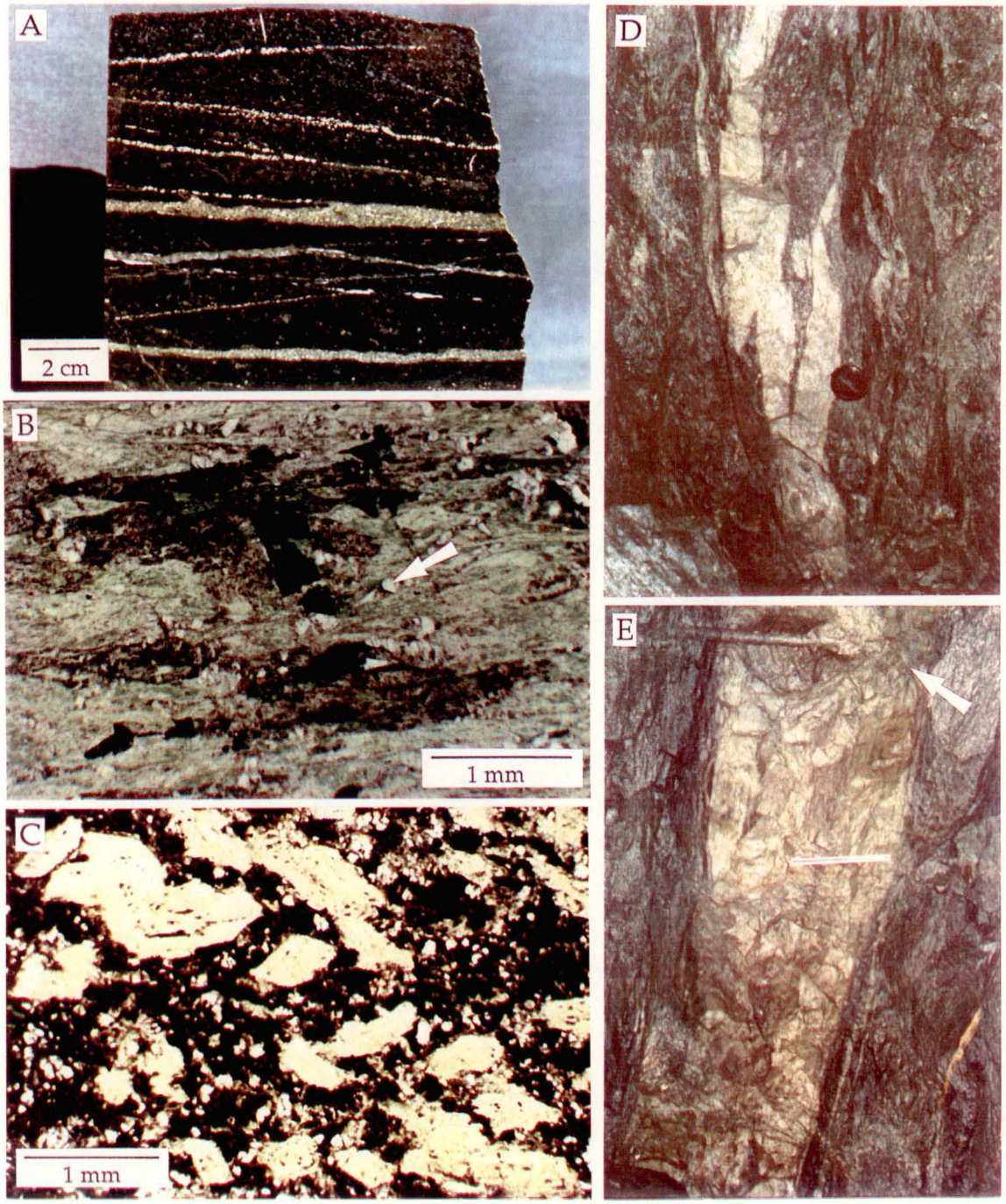
A
2 cm
B
1 mm
C
1 mm
D
E

volcanics as finely disseminated euhedral to subhedral grains in the groundmass. Some poorly defined horizons towards the stratigraphic top of the intermediate-mafic volcanics sequence contain up to 5% disseminated magnetite.

Only one sample of the intermediate - mafic volcanics (sample 607013.2 [1]) was observed to have obvious relict igneous textures. Abundant sericite pseudomorphs of plagioclase phenocrysts, up to 1 mm across, occur in a fine grained chlorite-quartz-sericite groundmass (Fig. 2.2c). The random distribution of euhedral pseudomorphs in the groundmass and their weakly glomeroporphyritic texture suggest that the rock is an altered high level intrusion or lava, rather than an altered volcaniclastic rock. The rock unit was approximately one metre thick, but could have originally been considerably more as its margins graded into more highly altered rock.

The intermediate - mafic volcanics sequence is intercalated with felsic volcanics, described below, and more mildly altered volcaniclastic breccias and conglomerates (section 2.6). Rare, thinly bedded (< 10 cm thick), fine grained altered shale horizons (section 2.7) are also interbedded with the intermediate-mafic volcanics. Individual intermediate-mafic units range from 20 - 30 cm up to tens of metres thick. Felsic volcanics, breccia and conglomerate units range from several centimetres to tens of metres thick. The predominant relationship is for thin felsic and volcaniclastic units to be intercalated with thick units of intermediate - mafic volcanics. However, towards the stratigraphic top of the intermediate - mafic volcanics, complex interfingering of felsic and intermediate - mafic units, each less than one metre thick may occur.

The small scale intercalation of the felsic and intermediate - mafic rocks suggests that the intermediate - mafic volcanics are a sequence of altered bedded fine grained volcaniclastic rocks, either epiclastic or tuffaceous. Thicker units within the sequence may be altered intermediate - mafic lava flows. The presence of intrusive intermediate - mafic rocks is suggested by sample 607013.2 (Fig. 2.2c). However, the intense alteration and layer-parallel shearing (Figs. 2.2d and 2.2e) has masked the internal structure of the intermediate-mafic sequence.

---

1. Sample locations from drill core are denoted by seven digit numbers. The first three digits (607) refer to the drill hole number in the WL series. The last four digits (013.2) refer to the downhole distance in metres. Samples collected from underground workings are denoted by six digit numbers.

2.4 FELSIC VOLCANICS

The felsic volcanics are the host rock for the great majority of Prince Lyell mineralisation and form almost the entire stratigraphic hangingwall succession to the orebody. They also form the stratigraphic footwall to the mineralisation at the south-eastern end of the deposit (Maps 1 and 3).

Within the ore horizon, the felsic volcanics are variably pink to grey, quartz - chlorite - sericite rocks in hand specimen, often with an apparent medium to coarse grained (~1mm - 1cm) fragmental appearance due to the segregation of siliceous and phyllosilicate alteration domains (Fig. 2.3a). Reddening in felsic volcanics is commonly observed in felsic - mafic volcanic sequences, and at Prince Lyell is caused by extremely fine grained (usually submicroscopic) disseminated hematite in the quartz - rich domains. The hematite dusting is usually only visible in the footwall rocks where the felsic volcanics may develop a very deep red colour.

In thin section, the groundmass of the felsic volcanics consists predominantly of very fine grained mosaic textured quartz (with minor disseminated sericite ± chlorite ± siderite) crossed by a network of anastamosing wisps of sericite ± chlorite. Accessory minerals such as pyrite, chalcopyrite, magnetite, monazite and apatite are concentrated in the phyllosilicate zones. Quartz - chlorite - sericite alteration may occur as an intimate intergrowth of very fine grained quartz and sericite, or as well defined rounded siliceous domains separated by interstitial sericite and/or chlorite alteration (Fig. 2.3c). All stages of mineral segregation exist between these extremes (Fig. 2.3b) resulting in varying development of apparent quartz fragments in a phyllosilicate matrix. Some larger planar domains of phyllosilicate alteration have been interpreted as relic fiamme by previous authors (eg: Walshe and Solomon, 1981, Fig. 10a), leading to suggestions of a pyroclastic origin for the felsic volcanics. However, it is regarded as more likely that these are merely larger alteration domains, possibly the result of concentration of phyllosilicate alteration along fractures intersecting at low angles (see discussion of fragmental textures, Fig. 2.6c).

The only definitely primary igneous features preserved in the felsic volcanics are rare, euhedral and embayed quartz phenocrysts, predominantly around 1 mm in diameter (Fig. 2.3d). They are commonly overgrown by thin, optically continuous quartz rims but otherwise appear to have been unaffected by alteration and metamorphism. The crystals appear to be genuine phenocrysts and do not show evidence of fracturing as may be expected if the felsic volcanics were of pyroclastic origin. Instead, it suggests that they may have been passively extruded lavas or shallow intrusives. The

Figure 2.3

A. Characteristic felsic volcanic alteration texture, with a pseudofragmental appearence developed by the segregation of siliceous and phyllosilicate alteration. Disseminated pyrite - chalcopyrite mineralisation occurs predominantly in the chlorite-sericite interstitial areas between pink quartz - rich "fragments". (sample 115004)

B. Photomicrograph of a strongly recrystallised felsic volcanic with an irregular intergrowth of fine grained sericite and mosaic textured quartz, vaguely resembling relic perlitic fractures. The segregation of alteration minerals in this sample occurs on a very small scale and a pseudofragmental texture is not evident in handspecimen. (sample 622171.5, XN)

C. Photomicrograph of well developed pseudofragmental texture in a strongly altered felsic volcanic. Rounded domains of fine grained recrystallised quartz, possibly recrystallised spherulites, are surrounded by wispy growth of sericite. (sample 639116.4, XN)

D. Photomicrograph of two primary volcanic quartz phenocrysts (arrowed), with thin quartz overgrowths, in the irregularly recrystallised quartz-sericite groundmass of an altered felsic volcanic. (sample 618051.8, XN)

E. Photomicrograph of foliated chlorite and sericite developed along a D_2 spaced cleavage in the siliceous matrix of a recrystallised felsic volcanic. The dismembering of siliceous alteration domains by the cleavage has enhanced the falsely fragmental appearance of the rock in handspecimen. (sample 619079.1, PPL)

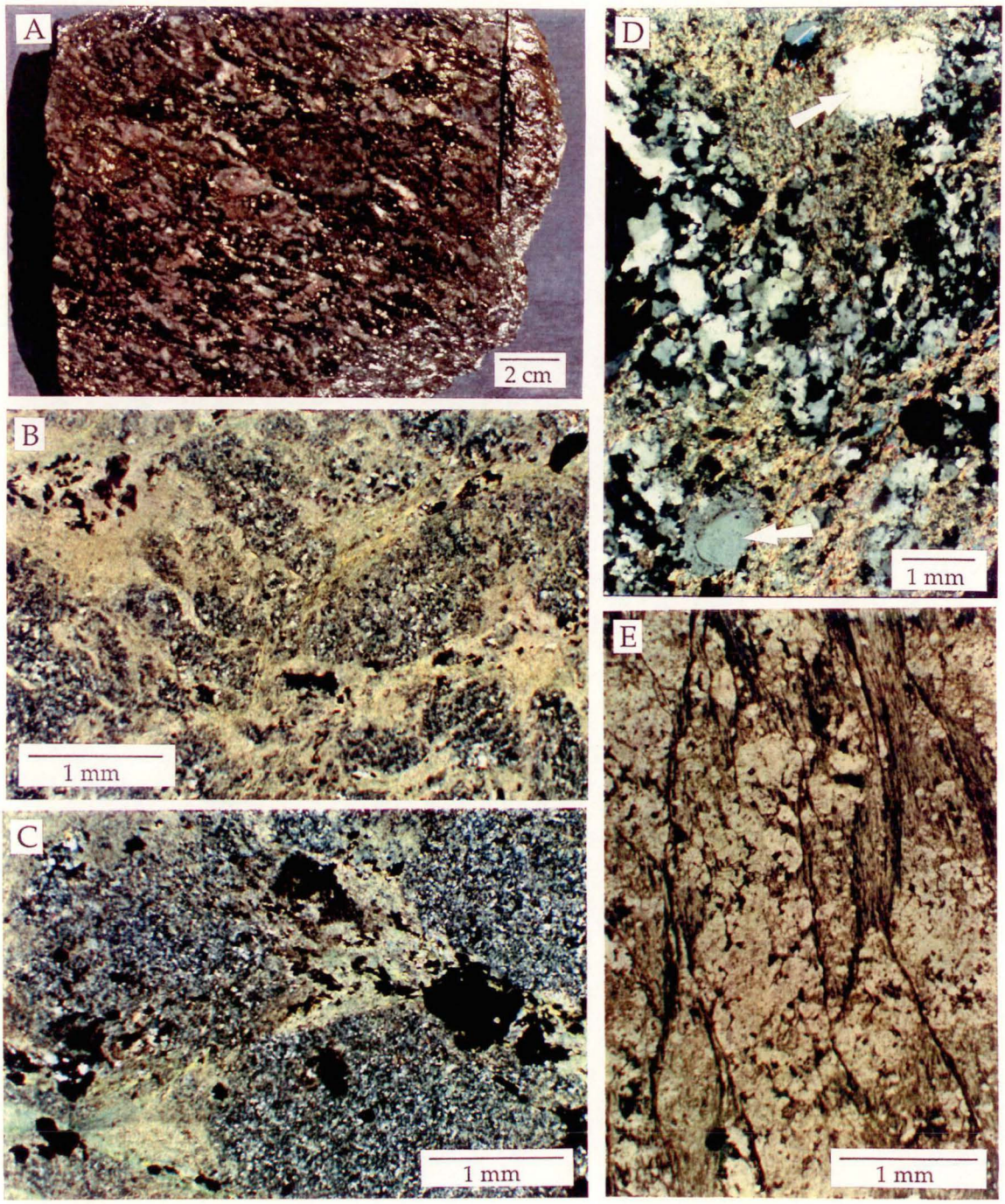
A
2 cm
B
1 mm
C
1 mm
D
1 mm
E
1 mm

small scale interfingering with the intermediate - mafic volcanics further suggests that the felsic volcanics may be bedded volcaniclastic rocks. Further consideration of the origin of the felsic volcanics is given below in the discussion of fragmental textures.

2.5 DACITIC VOLCANICS

Dacitic volcanics are a minor component of the Prince Lyell stratigraphy (<5%) and have not previously been described as a distinct lithology. The preservation of primary igneous textures, combined with geochemical evidence (Chapter 3), indicates that the dacitic volcanics are relatively weakly altered compared to the felsic and intermediate - mafic volcanics. As a result, the term dacitic volcanics accurately reflects the composition of their unaltered precursors.

They occur in discontinuous units, from less than a metre up to twenty metres thick, throughout the stratigraphic hangingwall sequence and also in the ore horizon. Dacitic volcanics units as thin as 10 cm thick were observed in drill core, intercalated with volcaniclastic breccias. However, it is unclear whether these units were in fact interbedded with the breccia or just large clasts in it. The contact relationships between the two rock types were inconclusive.

Least altered dacites are grey, moderately foliated, fine grained rocks containing disseminated 2 - 3 mm sericite pseudomorphs of plagioclase phenocrysts in a mainly quartz-sericite groundmass. The pseudomorphs are evenly distributed throughout and generally have sharp contacts with the groundmass. The euhedral, evenly distributed nature of the phenocryst pseudomorphs suggests that the dacitic volcanics are altered lavas or shallow intrusives rather than clastic volcanic rocks. Shearing has commonly resulted in rhomboidal or more attenuated pseudomorph outlines (Fig. 2.4a). Highly attenuated feldspar pseudomorphs may have a wispy appearance and resemble fiamme.

Rarely pseudomorphs of amphibole phenocrysts have been preserved. Amphibole crystals are replaced by chlorite + magnetite ± siderite ± quartz, with magnetite grains often forming rims around chlorite rich cores (Fig. 2.4b). Very rare rounded volcanic quartz phenocrysts also occur in the dacitic volcanics. Relict euhedral poikolitic biotite phenocrysts, 2 - 3 mm long, were observed in one sample (Fig. 2.4c). The biotite phenocrysts enclosed sericitised plagioclase pseudomorphs and were partially replaced by titaniferous chlorite (displaying brown-green pleochroism) and magnetite along cleavage partings.

Figure 2.4

A. Photomicrograph of sericite pseudomorphs of feldspar phenocrysts in an altered dacitic volcanic. Although shearing has caused marked attenuation of the pseudomorphs, relict euhedral outlines have been preserved. (sample 626129.2, PPL)

B. Photomicrograph of chlorite rimmed by magnetite grains, probably replacing a deformed hornblende phenocryst in an altered dacitic lava. (sample 115001, PPL)

C. Photomicrograph of titaniferous chlorite replacing a primary biotite phenocryst in an altered dacitic volcanic. The altered phenocryst encloses smaller sericite pseudomorphs of feldspar crystals. (sample 622095.5, PPL)

D. Photomicrograph of devitrification spherulites replaced by quartz in the foliated altered sericitic groundmass of an originally glassy dacitic lava. (sample 634017.8, XN)

E. An altered dacitic volcanic, containing sericitic feldspar pseudomorphs (dark flecks), being progressively silicified (pink colouration) from the top of the figure and around fractures. (sample 577124.6)

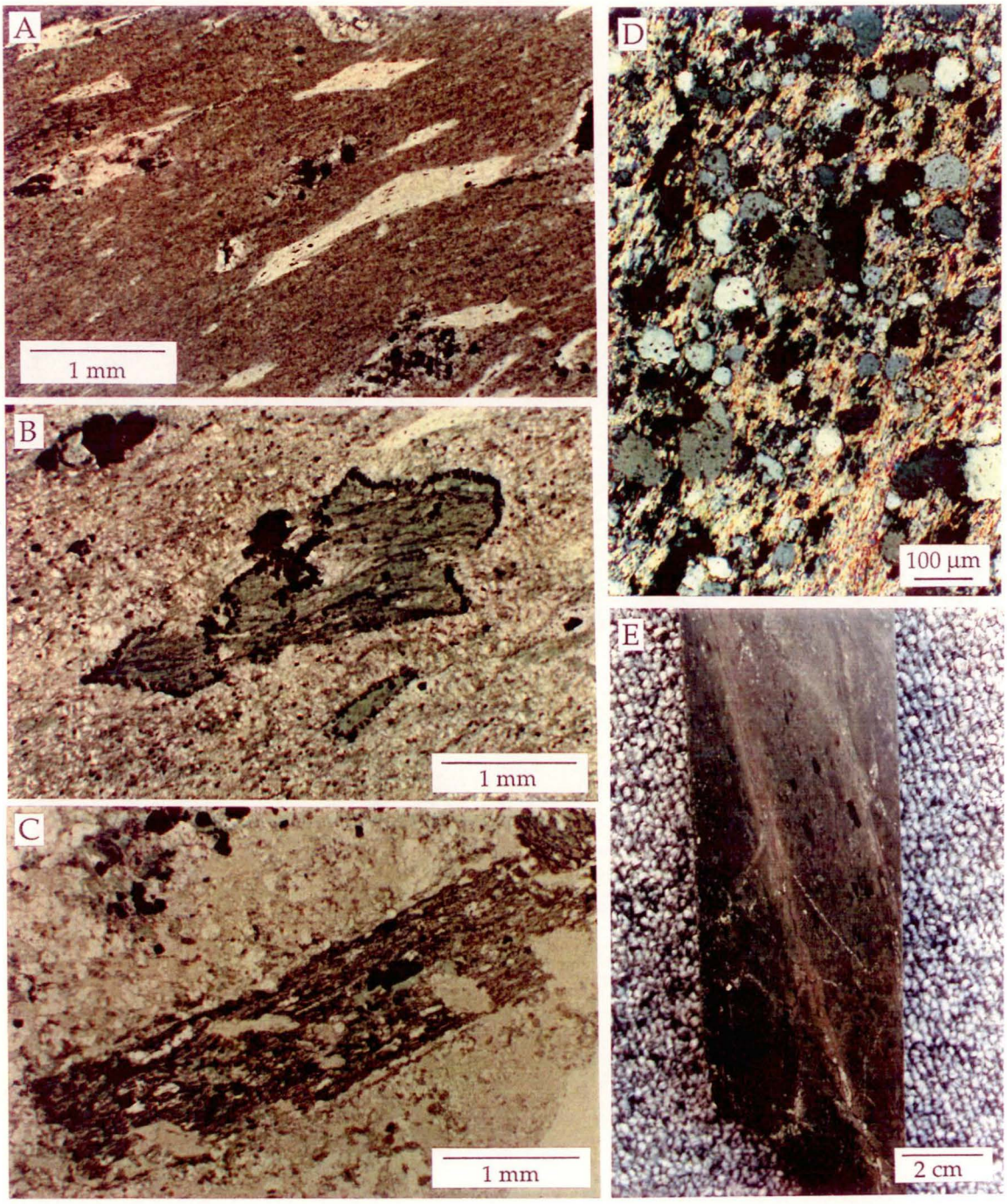
A
1 mm
B
1 mm
C
1 mm
D
100 µm
E
2 cm

The groundmass of the dacitic volcanics comprises equant to ragged quartz grains; predominantly between 10 and 50 μm, but up to 500 μm; with abundant interstitial foliated sericite (Fig. 2.4d). The groundmass minerals are not segregated into domains of quartz-rich or sericite-rich alteration as they are in the more strongly altered felsic volcanics. The equant quartz grains are interpreted to be silica replacement of small spherulites developed from the devitrification of an originally glassy rock (Fig. 2.4d). Coalescing of spherulite pseudomorphs may be seen in some samples.

Contacts with surrounding felsic volcanics range from sharp to gradational. One sharp discordant boundary of an altered dacite was observed in No. 22 Drawpoint on 200 Sublevel. Although the discordance was apparently not sheared or faulted, alteration prevented an interpretation of whether it was of erosional or intrusive origin. Such well defined, sharp boundaries preserved between felsic and dacitic volcanics are not common.

Predominantly, the mildly altered dacitic volcanics exhibit a gradational or irregular transition to the more extensively recrystallised felsic volcanics. Silicification fronts can be seen pervading dacitic volcanics from fractures and veinlets (Fig. 2.4e). As alteration and deformation become stronger, feldspar phenocryst pseudomorphs lose their well defined margins and become incorporated into an increasingly recrystallised siliceous groundmass. This relationship between the felsic and dacitic volcanics strongly suggests that the felsic volcanic style of alteration is texturally destructive and that the felsic volcanics may be derived at least in part from the dacitic volcanics. A horizon of small dacitic volcanic bodies which occur at the stratigraphic hangingwall margin of the South Lens on 115 Sublevel may be interpreted as mildly altered enclaves of an originally continuous dacite body (Map 1).

Very strongly schistose, fine grained quartz + sericite ± chlorite rocks, up to several metres wide, resembling dacitic volcanics but without relict phenocrysts, also occur in the felsic volcanic pile. More chloritic versions of these rocks resemble strongly sheared intermediate - mafic volcanics. The intense pervasive foliation in these units suggests that they were local zones of concentrated shearing during deformation. It is possible that the rocks were originally fine grained dacitic volcanics, but such an interpretation is most tentative.

2.6 VOLCANICLASTIC BRECCIAS AND CONGLOMERATES

Very minor units of polymict volcaniclastic breccias and conglomerates are the only rocks in the Prince Lyell area to preserve undoubted volcaniclastic textures (Fig. 2.5a, 2.5b). These rocks occur throughout the

Figure 2.5

A. Volcaniclastic textures preserved in an altered polymict breccia. Although most sulphide mineralisation is concentrated in the interstitial matrix areas, selective pyritisation of various types of volcanic clasts has occurred. (sample 115002)

B. Matrix supported volcaniclastic breccia showing variable alteration of felsic (fels) and dacitic volcanic (dac) clasts. Pale coloured rims around the dacitic volcanic clasts may reflect primary thermal discolouration from a hot pyroclastic flow or be due to later alteration by later fluids moving through the breccia matrix. (sample 589065.7)

C. Progressive recrystallisation of primary textures observed within a volcaniclastic breccia unit from drillhole WL 605. Textural changes from the original volcaniclastic breccia to the alteration pseudobreccia are entirely gradational.

Top: Relict volcaniclastic textures preserved in a pyritic and chloritic, but weakly recrystallised polymict breccia. (sample 605104.3)

Middle: A pseudofragmental texture develops in a patch of siliceous alteration in the volcaniclastic breccia. (sample 605105.1)

Bottom: Complete destruction of primary textures by quartz-chlorite - sericite alteration and development of chlorite "pseudo-fiamme" within a siliceous matrix. (sample 605106.3)

D. Encroachment of siliceous alteration (bottom of sample) into chloritic, sericite-flecked intermediate - mafic volcanics (top of sample). Although contacts between the intermediate - mafic and felsic volcanics are commonly sharply defined, siliceous recrystallisation is not entirely confined to originally felsic host rocks. (sample 636019.9)

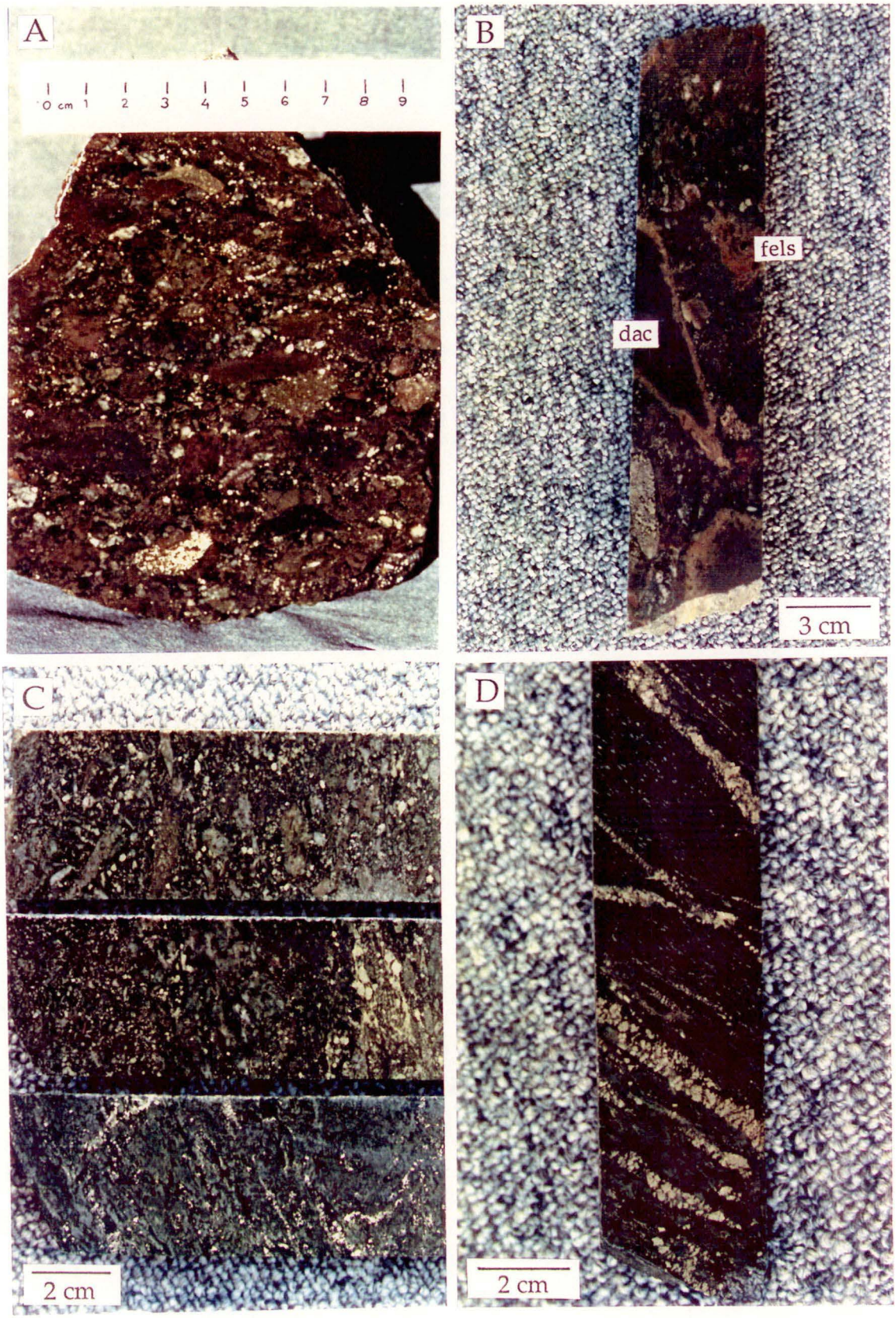
A
0 cm 1 2 3 4 5 6 7 8 9
B
fels
dac
3 cm
C
2 cm
D
2 cm

Prince Lyell sequence in horizons a few centimetres to a few metres thick and may be clast or matrix supported. A single lithic breccia unit over twenty metres thick was intersected in drillhole WL 627. Clasts range in size from 1 mm to at least 50 mm and are predominantly angular to subangular.

The volcaniclastics are laterally very impersistent. Units several metres thick either wedge out or may be destroyed by alteration over less than 10 metres along strike. When intercalated with the felsic volcanics, the breccias occur as mildly altered enclaves which grade into more strongly altered felsic volcanics. Figure 2.5c illustrates the texturally destructive nature of the siliceous felsic volcanic alteration style when imposed on the breccias.

Volcaniclastic breccias and conglomerates also occur throughout the intermediate - mafic volcanics sequence. They are more prevalent towards the stratigraphic top of the intermediate - mafic pile and have sharp contacts with the intervening units. These sharp contacts are commonly due to shearing along lithological boundaries.

Alteration of the breccias and conglomerates ranges from mild recrystallisation with clast textures largely intact to more strongly altered rocks with only ghosts of the original clasts preserved. The matrix of the breccias is the most altered part of the volcaniclastics, comprising a fine grained weakly foliated intergrowth of chlorite, sericite and quartz, preserving none of its primary character. Accessory alteration minerals such as pyrite, magnetite and lesser chalcopyrite, hematite, apatite and monazite are concentrated within the matrix of the breccias, indicating the highly permeable nature of the matrix.

The different alteration styles of individual clast types in the more weakly altered breccias allows interpretation of the primary volcanic clast populations. Varying degrees of alteration of clasts within a single breccia are due to the varying susceptibility of the different primary volcanic clast types to the alteration fluids. Most common breccia clasts are fragments of dacitic and felsic volcanics (Fig. 2.5b). Intermediate - mafic volcanics fragments could not be positively identified. The high relative abundance of dacitic fragments in the breccias is disproportionate to the apparent scarcity of dacitic volcanics in the Prince Lyell sequence overall. The breccias may have been sourced from a particularly dacite-rich area. However, they may indicate that dacites were originally more abundant in the Prince Lyell sequence than is suggested by the distribution of altered rock types. Texturally destructive alteration of dacites may have given a misleading impression of an originally more widespread distribution.

Volcanic quartz phenocrysts and altered fragments of fine grained shale or siltstone also occur in the breccias. Angular fragments of vein quartz,

exhibiting symmetrical crustiform growth were found in one sample of volcanic breccia (sample 115002). In thin section, different clasts within a single breccia have varying degrees of alteration, allowing identification of different clasts. This contrasts with the homogeneous grain size of the mosaic textured quartz of apparent fragmental clasts in the felsic volcanics (Fig. 2.3c).

No evidence was observed of sulphide mineral clasts in the breccias. Sulphide mineralisation of altered volcanic clasts was interpreted to have occurred after deposition of the breccias. Pyrite mineralisation in some clasts extended outside the clast margins and was due to the irregular development of pyrite in a favourable host clast.

The small scale (< 10 cm) intercalation of the volcaniclastic breccias and conglomerates with the intermediate - mafic volcanics suggests that the breccias and conglomerates are epiclastic rocks. Thicker units, up to the 20 metre thick breccia intersected in WL 627 may be of pyroclastic origin, such as hydrothermal explosion breccias or basal breccias from ignimbrite flows (Cas and Wright, 1987). Their strongly heterolithic nature suggests they are not lava-related breccias such as autobreccias. However, as it is impossible to discern whether the altered matrix of the breccias was of a clastic or coherent origin, a more certain picture of the origin of the breccias can not be gained. Thermal discolouration of clasts in a hot pyroclastic flow may be suggested by pale coloured rims around dacitic volcanic clasts in one breccia sample (589065.7, Fig. 2.5b). However, the rims may alternatively be due to later alteration fluids moving through the breccia matrix and leaching the clast rims.

If the breccias were of epiclastic origin, however, it may be expected that some intermediate - mafic fragments would be found in the breccias. The lack of identifiable intermediate - mafic volcanics detritus in breccias which occur in and immediately above a stratigraphic footwall sequence of intermediate-mafic volcanics suggests that the breccias are not of epiclastic origin. Another explanation could be that the entire Prince Lyell sequence is not overturned and that the intermediate - mafic volcanics in fact form the stratigraphic hangingwall of the sequence. However, the regional stratigraphic studies of Cox (1981) do not support this.

The rounded volcanic quartz phenocrysts which occur in the matrix of the breccias are identical to those found in the felsic volcanics. The presence of these phenocrysts in the both rocks and the gradational contacts of the breccias with felsic volcanics (Fig. 2.5c) suggest that, like the dacitic volcanics, the breccias and conglomerates are a precursor to the texturally destructive felsic volcanic style of alteration.

2.7 SHALE OR ASH UNITS

Rare, very thin altered shale or ash units occur as intercalations in the felsic and intermediate - mafic volcanics. The lenses are up to 10 cm thick (commonly < 5 cm) and preserve no internal layering or sedimentary structures. They may extend laterally for at least several metres, but limited drill core and underground exposure prevents more comprehensive description of their extent. Contacts between the shales and surrounding altered volcanics are sharp. However, the lenses are commonly truncated by shearing along foliation, sub-parallel to the primary layering.

The rocks consist of moderately to well sorted, fine to very fine grained (5 - 200 μm) quartz grains with very fine interstitial foliated sericite, probably replacing original interstitial clays. The quartz grains range from rounded to ragged, depending on the degree of dissolution or recrystallisation at the margins of the grains. Rare polycrystalline quartz fragments, up to 4 mm across, also occur in the shale units. Rare highly attenuated or irregular clots of chlorite ± sericite ± siderite ± magnetite ± hematite ± quartz may represent altered lithic fragments or be the product of irregularly developed alteration seen in other altered rocks at Prince Lyell.

The altered shales commonly contain minor or accessory amounts of fine grained (10 - 30 μm) disseminated magnetite mineralisation. Finely disseminated or veinlet pyrite of similar grainsize is developed to a lesser extent. Shale horizons toward the stratigraphic hangingwall of the felsic volcanics sequence contain disseminated hematite, commonly pseudomorphing euhedral or embayed magnetite, imparting a purple-grey colour to the rocks.

Abundant magnetite, and to a lesser extent pyrite, developed in shale lenses enclosed by relatively unmineralised altered volcanics, illustrates a strong focussing of hydrothermal fluid movement at this small scale. Strong pyrite and/or magnetite mineralisation may occur at the margins of shale units suggesting that fluids moved along lithological boundaries which may have dilated due to ductility contrasts between the shales and volcanics during deformation.

2.8 LAMPROPHYRE DYKES

Rare lamprophyre dykes, up to several metres wide, occur in the footwall of the Prince Lyell orebody in both the intermediate - mafic and felsic volcanics. The dykes are of uncertain age, but are at least younger than mid Devonian as they are undeformed and relatively unaltered.

The dykes contain large euhedral olivine phenocrysts up to 8 mm across. Smaller subhedral phenocrysts of augite are abundant in the groundmass. The groundmass comprises mainly fine acicular biotite crystals with interstitial carbonate and quartz. Rare apatite euhedra also occur.

The groundmass carbonate and quartz are probably the result of weak alteration by groundwaters. One dyke sample (627006.7) was strongly affected by carbonate - quartz alteration and also contained an unusual fine grained nodular hematite alteration.

2.9 Owen Conglomerate

Exposure of the Owen Conglomerate was limited to short drill core intersections. The conglomerate consisted of well rounded metamorphic quartz clasts up to several centimetres across in a sandy, siliceous, hematitic matrix, with lesser units of pink hematitic quartz sandstone. Silicification and minor sericite alteration was developed in places adjacent to the volcanics contact.

2.10 Discussion of Alteration Textures

The segregation texture typical of quartz and phyllosilicates in the felsic volcanics has been interpreted by some previous authors as reflecting alteration of a primary volcanic fragmental texture, either pyroclastic or autobrecciated (e.g: Walshe, 1977; Braithwaite, 1985). However, the anastamosing network of sericite-chlorite alteration and the irregular orientation of larger phyllosilicate domains are not consistent with replacement of fiamme. Alteration of irregularly brecciated or devitrified lavas, however, may account for development of the bimodal alteration textures.

Allen (1988) noted that false pyroclastic textures may develop through alteration of a variety of precursor volcanics. Primarily, he recognised devitrification of glassy lavas and welded ash flows as the precursor for many pseudofragmental textures. Nodular devitrification domains may be preferentially replaced by siliceous alteration, while fresher glassy material was replaced by phyllosilicate-rich alteration. The relative proportions of each precursor material would dictate whether the resulting alteration texture resembled siliceous fragments in a chlorite-sericite matrix, or phyllosilicate-altered pumice or lithic fragments in a massive siliceous matrix (Fig. 2.6). Strong foliation may stretch phyllosilicate - rich domains into lenticular

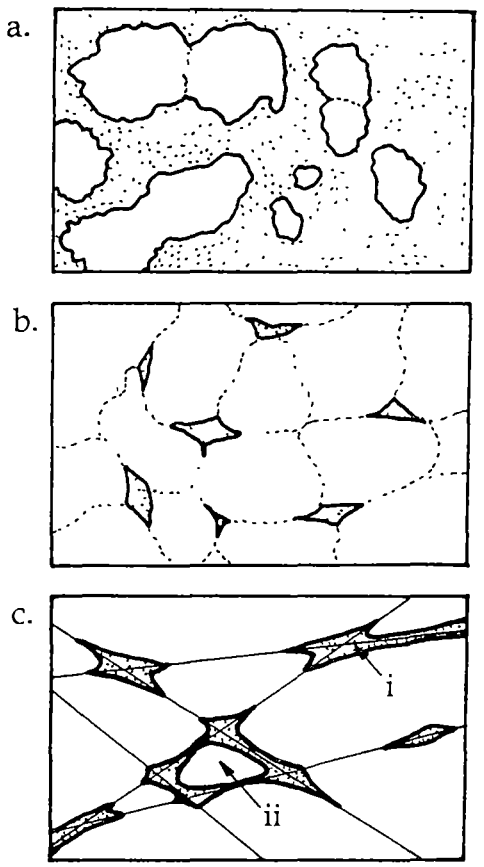

Figure 2.6 Development of pseudofragmental textures by segregation of siliceous (white) and phyllosilicate (dotted) alteration. (Modified after Allen, 1988)

a) Silicification of nodular devitrification domains in a phyllosilicate-altered glassy groundmass. The resulting texture resembles siliceous clasts in a micaceous matrix.

b) Alteration of coalesced devitrification zones as above, giving the appearance of phyllosilicate altered clasts resembling fiamme in a siliceous matrix.

c) Development of phyllosilicate alteration along fractures in a massive siliceous matrix. Fiamme-like features (i) or siliceous "clasts" surrounded by phyllosilicate alteration (ii) may result from this type of alteration.

shapes resembling fiamme, prompting interpretation of previously coherent lavas as pyroclastic rocks.

Two phase alteration controlled by fracturing may also produce pseudofragmental textures. Fluid movement through the volcanics may have been controlled by perlitic fracturing, or on a larger scale, fracturing induced by cooling or deformation (Fig. 2.6c). Pervasive alteration along and out from these fractures may develop textures resembling volcanic breccias or even vitriclastic rocks (Allen, 1988).

Walshe (1977) suggested that the fine granular nature of siliceous alteration may have developed from recrystallisation of devitrification domains. However, the wispy nature of phyllosilicate alteration at Prince Lyell is most likely fracture controlled. Perlitic fracturing of a glassy host, such as a lava or welded tuff, may have led to development of phyllosilicate domains such as in Figures 2.3b and 2.3c. Figure 2.3e shows sericite - chlorite alteration along fractures subparallel to the foliation, developed during the Devonian D_2 deformation event. Development of a tectonic fabric during the Devonian would have resulted in dismembering of earlier alteration domains and further enhancement of the fragmental appearance of the altered volcanics.

At Prince Lyell there is also evidence to suggest the development of pseudofragmental textures from epiclastic rocks as well as glassy lava precursors, suggesting that devitrification domains may not have been an overriding control of alteration domains. Figure 2.5c shows three samples taken one metre apart from drillhole WL 605. They are representative samples from an entirely gradational transition from chloritised volcaniclastic breccia with relict textures clearly defining primary polymict breccia clasts to a typical siliceous, chloritic felsic volcanic. The progressive alteration of the breccia is completely destructive of the volcaniclastic texture. Primary lithic clasts gradually lose their definition as they are progressively recrystallised, with ghosts of original clasts between areas of stronger siliceous alteration. A nodular pseudofragmental texture finally results from segregation of quartz and chlorite alteration. The distribution of quartz - rich and phyllosilicate-rich domains does not appear to have been controlled by pre-existing compositional or textural heterogeneities in the original rock.

Figure 2.5d shows the same felsic - style alteration in an intermediate - mafic volcanic. This type of alteration of the intermediate - mafic volcanics is rare with contacts between the intermediate - mafic and felsic volcanics usually sharp. However, minor quartz and phyllosilicate pseudofragmental alteration textures may develop in the more mafic rocks immediately adjacent to the felsic volcanics.

Figure 2.4e shows the first stage of siliceous alteration of a dacitic volcanic. Transitional textures from dacitic to felsic volcanics showing ghosts of altered feldspar phenocrysts are not uncommon in the contact zones between dacitic and felsic volcanics. Not only is the visual character of the dacitic volcanics destroyed by felsic alteration, but evidence presented in Chapter 3 suggests that the geochemical signature of the original dacites is also lost during this severe alteration. The implications for misinterpretation of the primary distribution of dacites are great.

2.11 CONCLUSIONS

The two main alteration lithologies at Prince Lyell, the intermediate - mafic volcanics and felsic volcanics, are the result of the alteration of two compositionally distinct volcanic precursors. The consistently well defined contacts between the two alteration styles, even when units are thinly intercalated, strongly suggests primary compositional differences between the original rocks. This is supported by geochemical evidence detailed in Chapter 3.

Despite the presence of the two predominant alteration lithologies, it is not clear that the original Prince Lyell volcanic sequence was bimodal. The felsic volcanics may have originated from a wide range of siliceous extrusive or volcaniclastic rocks. The ubiquitous quartz phenocrysts in the felsic volcanics suggests rhyolitic precursors. However, the distribution of relict dacitic volcanic bodies and the relative abundance of altered dacite clasts in breccias suggests that dacite lavas could have composed a significant portion of the Prince Lyell volcanic sequence.

The texturally destructive alteration of the intermediate - mafic volcanics prevents petrographic interpretation of their precursor lithology. The fine scale interfingering relationships of the intermediate - mafic volcanics with felsic volcanics and volcaniclastic breccias suggest that the intermediate - mafic volcanics were fine grained, bedded volcaniclastic rocks with some intrusive bodies.

CHAPTER THREE

ALTERATION GEOCHEMISTRY

3.1 INTRODUCTION

3.1.1 "Immobile" elements

The texturally destructive nature of the alteration around many volcanic hosted ore deposits such as the Prince Lyell makes interpretation of original volcanic facies difficult. Geochemical characteristics which are resistant to alteration may be used to gain a better understanding of primary volcanic chemistry, stratigraphy and environment of deposition. Unlike the major elements, concentrations of trace elements such as Ti, Zr, Nb, Y, Ga, Sc, V and the rare earth elements remain relatively stable during certain processes of seafloor and hydrothermal alteration and low grade metamorphism. These elements have been termed "immobile" elements by previous authors and may be used to interpret original volcanic compositions (eg: Floyd and Winchester, 1978; Morrison, 1978).

The tectonic setting and degree of differentiation of unaltered volcanic rocks may be determined using characteristic ratios of the high field strength elements Nb and Y, and Ti and Zr (Pearce and Cann, 1973; Winchester and Floyd, 1977). The ratios Nb/Y and Ti/Zr increase with increasing degree of alkalinity and differentiation respectively. Winchester and Floyd (1977) also regarded the Ga/Sc ratio as a measure of the degree of differentiation in volcanic rocks. The use of element ratios, as opposed to concentrations of single elements (eg: Ga, Floyd and Winchester, 1978), eliminates the effects of dilution by major elements being added to or leached from the altered rock.

More recently, however, various authors have demonstrated that virtually all elements may become mobile under the most severe alteration conditions. Finlow-Bates and Stumpfl (1981) demonstrated that during intense hydrothermal alteration in Tasmanian and New Brunswick volcanogenic deposits, Y and particularly Sc and Nb were mobile and even prone to complete leaching. Ti exhibited partial mobility, but Zr was immobile and Ti/Zr ratios were relatively stable. The relative immobility of Ti and Zr was also observed by Peterson (1983) in hydrothermally altered, metamorphosed and deformed Precambrian volcanics of New Mexico. Felsic

and mafic precursors of similar chloritic schists were distinguished by their characteristic Ti/Zr ratios.

Although the Ti/Zr ratio appears to be the most reliable of the immobile element ratios in altered rocks, substantial mobility of both Ti and Zr has been observed. Hynes (1980) attributed the mobility of Ti and Zr in metavolcanics to high CO_2 levels in the metamorphic fluid and the formation of weakly bonded complexes of Ti^{4+} and Zr^{4+} with CO_3^{2-} ligands. Ti and Zr transport is also favoured by high concentrations of the ligands B^- (Alderton *et al.*, 1980), F^- (Gieré, 1986; 1990; Rubin *et al.*, 1989) and PO_4^{3-} (Gieré, 1986; 1990) in the fluid. Gieré (1990) concluded that deposition of Ti and Zr minerals was controlled by the lowering of ligand activity in the fluid by crystallisation of hydrous mineral phases. Rubin *et al.* (1989) suggested that hydrothermal zircon at Round Top, Texas was a vapour-phase precipitate from a flourine-rich fluid.

Despite the possibility of mobilisation, Ti and Zr appear to be the most resistant to metamorphic and hydrothermal alteration processes except under the most extreme of fluid compositions and water/rock ratios. However, the mounting evidence for trace element mobility in altered volcanic rocks requires that great care be taken in the interpretation of "immobile" element geochemistry.

3.1.2 Mt Read Volcanics "immobile" element geochemistry

Calc-alkaline volcanics, such as the Mount Read Volcanics, typically show the following range of Ti/Zr ratios, although exact boundaries between ranges are likely to vary between volcanic piles (Large *et al.*, 1986):

rhyolites/rhyodacites	Ti/Zr = 4 to 12
dacites	Ti/Zr = 12 to 20
andesites	Ti/Zr = 20 to 60
basalts	Ti/Zr = 60 to 120 +

Large *et al.* (1986) established typical differentiation trends for the major elements plotted against the Ti/Zr ratio for unaltered Central Volcanic Complex rocks (Fig 3.1). They also illustrated that the Ti/Zr ratio was generally resistant to hydrothermal alteration in the Mt Read Volcanics. By plotting potentially mobile major elements against the Ti/Zr ratio for altered rocks, magmatic differentiation trends could be distinguished from alteration trends (Fig 3.2).

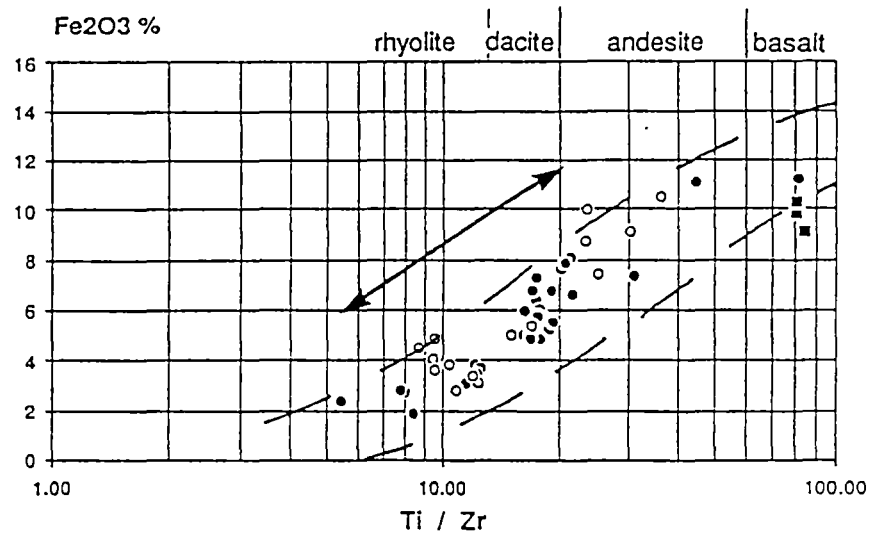

Figure 3.1 A typical example of a major element magmatic differentiation trend vs the Ti/Zr ratio of rhyolite - dacite - andesite - basalt in the Mt Read Volcanics (after Large *et al.*, 1986).

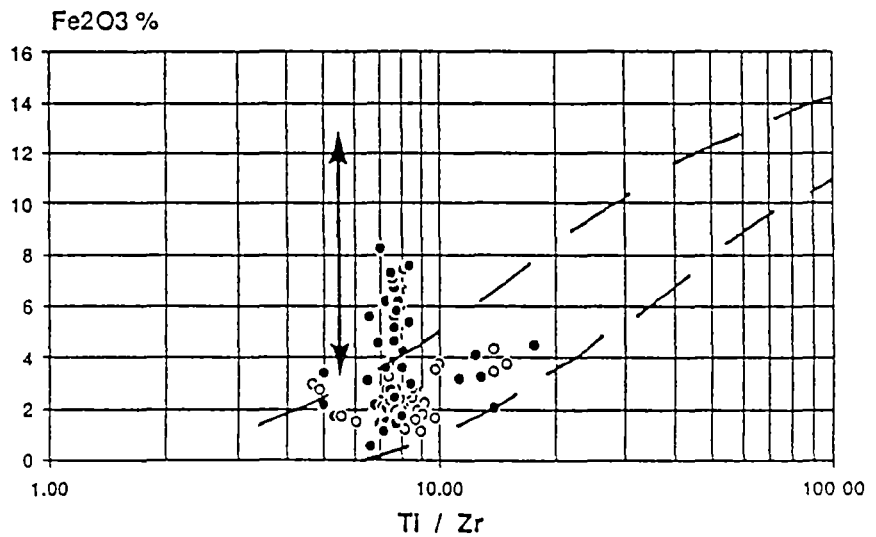

Figure 3.2 A typical example of a hydrothermal alteration trend (enrichment of Fe_2O_3 at constsant Ti/Zr) superimposed on a magmatic differentiation trend of rhyolite - dacite from the Rosebery deposit (from Large *et al.*, 1986).

White (1975) suggested that the ratios V/Sc, V/Ti and V/Y were useful discriminants for relatively unaltered Mt Read Volcanics. White (1975) and Walshe and Solomon (1981) also concluded that these elements had similar concentrations in the altered Mt Lyell volcanics and that the V/Sc and V/Ti ratios were resistant to alteration. Their observations contrast with the reported mobility of Y, V and Sc in altered volcanics at the Que River, Chester and Pinnacles deposits in the northern Mt Read Volcanics (Finlow-Bates and Stumpfl, 1981). Sheppard (1987) observed only minor mobility of Ti, Zr, Y and V in the altered volcanics around the Prince Lyell deposit. However, he concluded that enrichment of Ti occurred in the highly altered ore zone due to concentration of Ti in hydrothermal rutile, magnetite, hematite, sericite and chlorite, making Ti/Zr ratios unreliable.

3.2 Sample Collection and Analytical Methods

WL 636 and WL 637, two diamond drill holes which traverse a large part of the Prince Lyell volcanic succession on section 72, were sampled in two metre intervals and analysed at the Renison Tin Mine x-ray flourescence spectrometry laboratory by Mr I. Barrow for Ti, Zr, Nb, Y, Sc and V. WL 636 was also analysed for Ga. In addition, samples of typical alteration lithologies (samples PL1 - PL32) were collected in 1 - 2 metre half-cores from diamond drill holes throughout the southern Prince Lyell area. These samples were analysed for Ti and Zr at the Renison Mine laboratories.

Major elements concentrations of samples PL1 - PL32 were analysed by x-ray fluorescence spectrometry at the Department of Geology of the University of Tasmania, under the supervision of Mr P. Robinson. Sodium analyses, which were below reasonable detection limits for this method, were repeated by atomic absorption spectrometry (Appendix 3.1).

Clasts and matrix were physically separated and analysed from three polymict volcaniclastic breccias (samples PL42 - PL58 from breccias 115002, 586210.6 and 589065.7). Two altered dacite clasts from sample 589065.7 exhibited highly sericitic alteration rims formed by the dissolution of disseminated hematite from the clast margins by a fluid moving through the breccia matrix. The rims were analysed separately from the interior of the clasts. However, insufficient sample could be gained from one clast to provide meaningful analyses. These samples were analysed for Ti, Zr, Nb, Y, Sc, V and Ga also at the Renison Mine laboratories by Mr I. Barrow.

Detection limits for trace element analyses at the Renison Mine laboratories were 5 ppm for Zr, Nb and Y, and 10 ppm for Sc, Ga and V. Accuracy and precision at Renison Mine (trace elements) and at the

University of Tasmania (major elements) were monitored by check analyses of University of Tasmania standards and by repeat analyses of selected samples (Appendix 3.8). Precision error for Ti analyses at Renison Mine was generally below 5%. However, Zr check analyses showed a wide range of precision error (3 - 40%), highest at Zr levels approaching detection limits. Accuracy errors for Ti, Zr and Nb were around 10%. However, Y, V and Sc check analyses were more variable, especially at low concentrations. A comparison between the Renison Mine and University of Tasmania laboratories of thirty samples for Ti showed an average error of 7% between laboratories.

Two whole rock samples were analysed for a suite of nine rare earth elements (REE) by neutron activation at Bequerel Laboratories Pty Ltd, Lucas Heights, N.S.W. Sample 640063.0 was a typical felsic volcanic and sample 637052.0, a typical intermediate mafic volcanic.

3.3 "IMMOBILE" TRACE ELEMENT RESULTS

3.3.1 Drillholes WL 636 and WL 637

3.3.1.1 Ti, Zr and V

The results of trace element analyses of drillholes WL 636 and WL 637 are presented in Appendices 3.2 and 3.3. Figures 3.3a and 3.3b show the relationships between the various "immobile" element ratios, alteration lithology and magnetite content (measured as magnetic susceptibility, see Appendix 4.1).

The ranges of Ti/Zr ratios for each of the main alteration lithologies (felsic, intermediate - mafic and dacitic volcanics) are generally consistent with the typical ranges of fresh calc-alkaline volcanics outlined by Large *et al.* (1986). The sharp contacts between the felsic and intermediate - mafic volcanics are mirrored by changes in the Ti/Zr ratio. Narrow dacite units in WL 637 also have Ti/Zr ratios slightly higher than the surrounding felsic volcanics and which correspond to unaltered dacitic Ti/Zr ratios.

Anomalously high Ti/Zr ratios in felsic volcanics from WL 636 (~105 - 130 metres) correlate with vein and disseminated magnetite mineralisation and strongly suggest that minor Ti occurs in the magnetite. The corresponding increase in V/Ti ratios also suggests that the magnetite contains minor vanadium. Chemical analyses of the magnetite showed it to contain up to 1.7% TiO_2 (see Chapter 5). Vanadium analyses of the magnetite are not available. Calculations assuming magnetite as the dominant

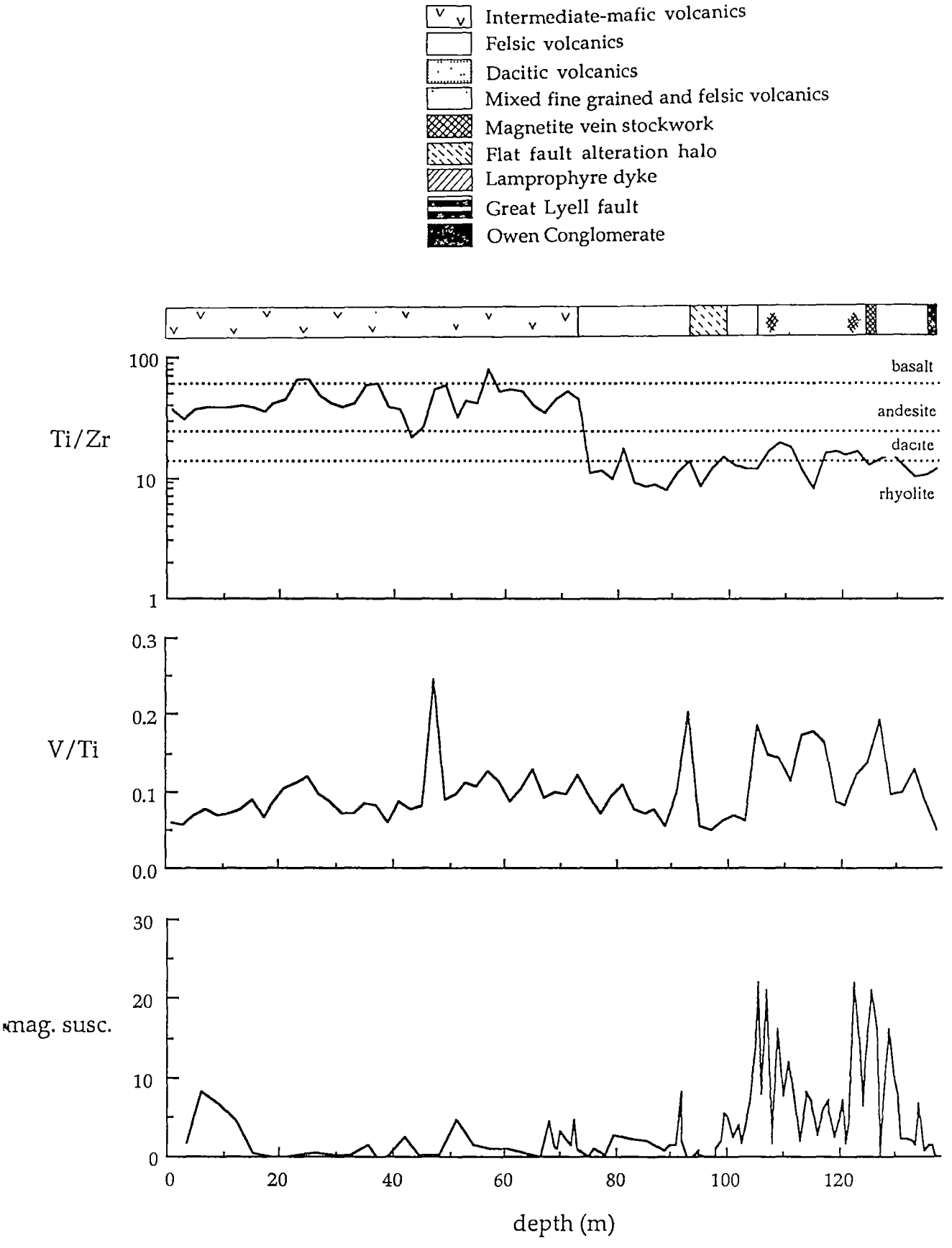

Figure 3.3a Lithologies, trace element geochemistry and magnetic susceptibility of diamond drill hole WL 636. Vanadium peaks correlate well with magnetite vein stockwork mineralisation (90 - 130 metres), but poorly with areas of disseminated magnetite in the intermediate - mafic volcanics (5 - 12 metres).

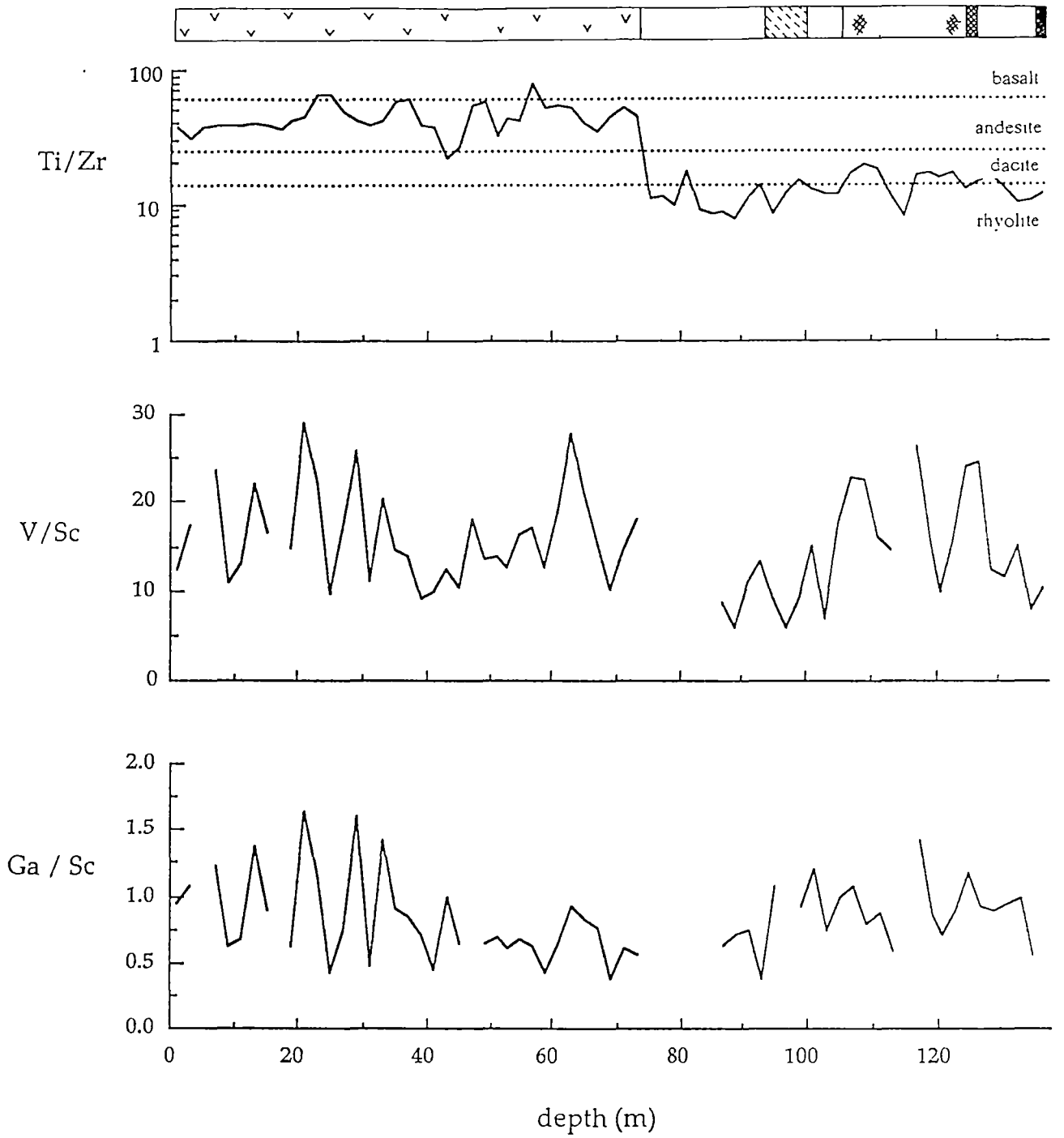

Figure 3.3a continued. Lithologies and trace element distribution in diamond drill hole WL 636. Unlike the Ti/Zr ratio, the V/Sc and Ga/Sc ratios are erratic and show no relation to lithology. Discontinuities in the graphs indicate leaching of Sc and/or Ga to below detection limits.

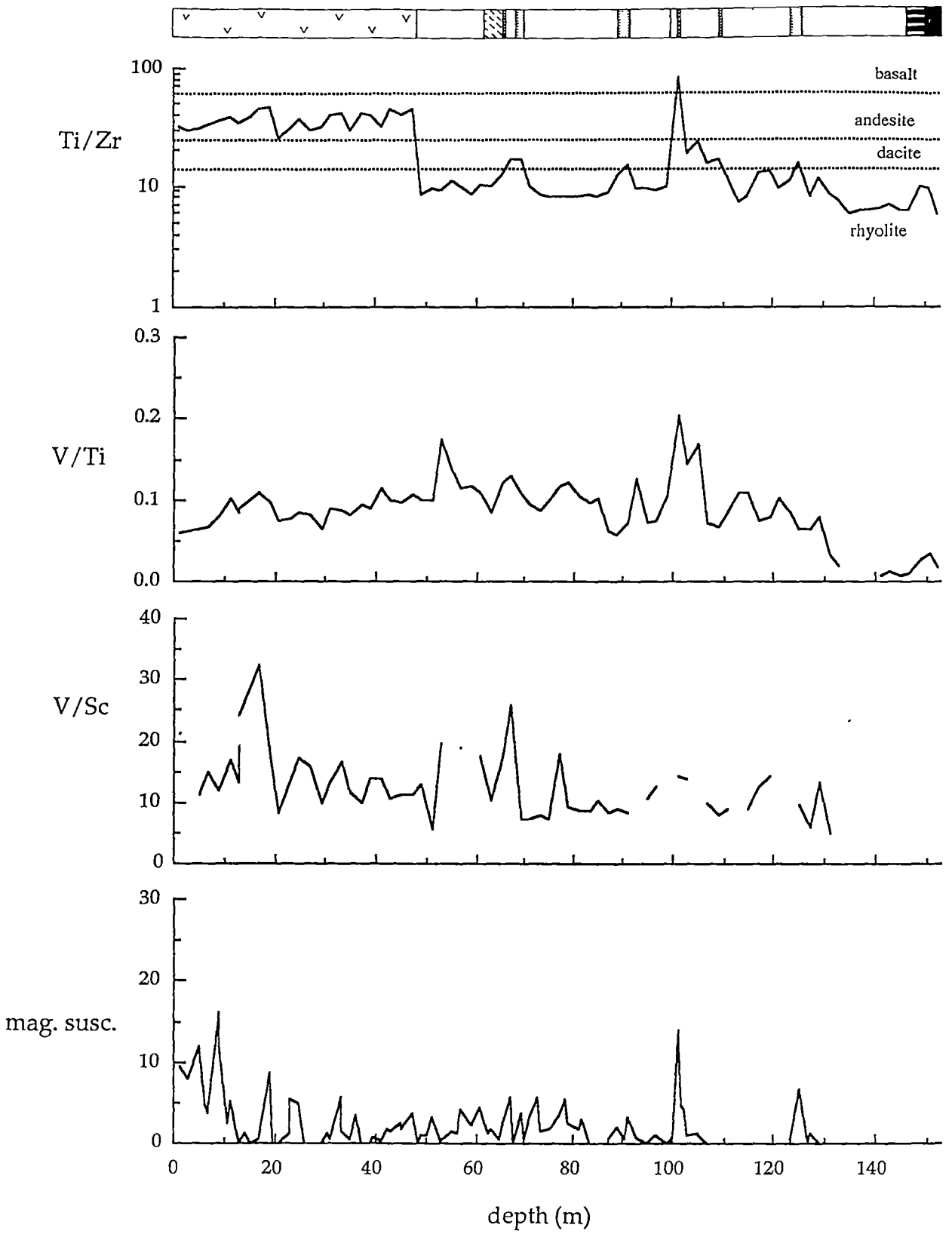

Figure 3.3b Lithologies, trace element geochemistry and magnetic susceptibility of diamond drill hole WL 637. Discontinuities in the V/Ti and V/Sc graphs are due to leaching of V and/or Sc to below detection limits. Lithology key as for Figure 3.3a.

vanadium - bearing phase in the rock suggest levels of around 1% V_2O_5 in magnetite. In contrast, magnetite mineralisation in the intermediate - mafic volcanics does not affect the Ti/Zr or V/Ti ratios (WL 636, 3 - 12 metres; WL 637, 0 - 10 metres). Titanium contents of this magnetite, which occurs as disseminated euhedra, are very low. A more complete presentation and discussion of magnetite geochemistry is given in Chapter 5.

The very high Ti/Zr and V/Ti ratios around 101 metres in WL 637 are due to a combination of magnetite mineralisation and the occurrence of a thin highly carbonate-altered ?lamprophyre dyke. Zr levels are very low and Ti and V levels very high. The very low Zr levels suggest some leaching of Zr as well as the addition of Ti and V from magnetite mineralisation.

Apart from the magnetite-rich areas, Ti/Zr ratios outside the rhyolite - rhyodacite range (4 - 12) are rare in the felsic volcanics. This suggests that in general the felsic volcanics were derived from a rhyolite - rhyodacite precursor. Dacite Ti/Zr ratios (12-20) are confined to the dacitic volcanics and one analysis of mixed felsic and intermediate - mafic volcanics in WL 636. Although the felsic volcanics may have been derived from texturally destructive alteration of dacitic volcanics, it is not implied by the Ti/Zr ratios alone. However, it must be considered that dacite Ti/Zr ratios have been homogenised by the more intense alteration.

Highly sericitic alteration haloes and quartz - siderite veining around "flat faults" and associated veining does not appear to have affected Ti/Zr ratios.

Figure 3.4 compares the concentrations of TiO_2 and Zr in the altered Prince Lyell volcanics with unaltered volcanics from the Central Volcanic Complex (CVC) of the Mt Read Volcanics (Crawford and Berry, 1992; Crawford *et al.*, 1992). The extensive alteration zone of the Mt Lyell field prevents a direct comparison with undoubtedly unaltered volcanics from the immediate vicinity of Prince Lyell.

The altered volcanics have a similar absolute range of TiO_2 and a slightly lower range in Zr compared to the unaltered CVC volcanics. There is considerable overlap of both TiO_2 and Zr in unaltered and altered dacites. This may reflect the fact that the altered dacites are considered to be the least altered rocks at Prince Lyell (Chapter 2).

Diagrams similar to Figure 3.4 have been used to establish immobility or otherwise of Ti and Zr during alteration (eg: Barrett and Maclean, 1991). Variation of Ti and Zr along lines of constant Ti/Zr ratio reflect the immobility of Ti and Zr, diluted or enriched by addition or removal of more mobile elements. Estimates of precursor volcanic compositions may be

gained by projection of these alteration trends back to unaltered volcanic differentiation trends.

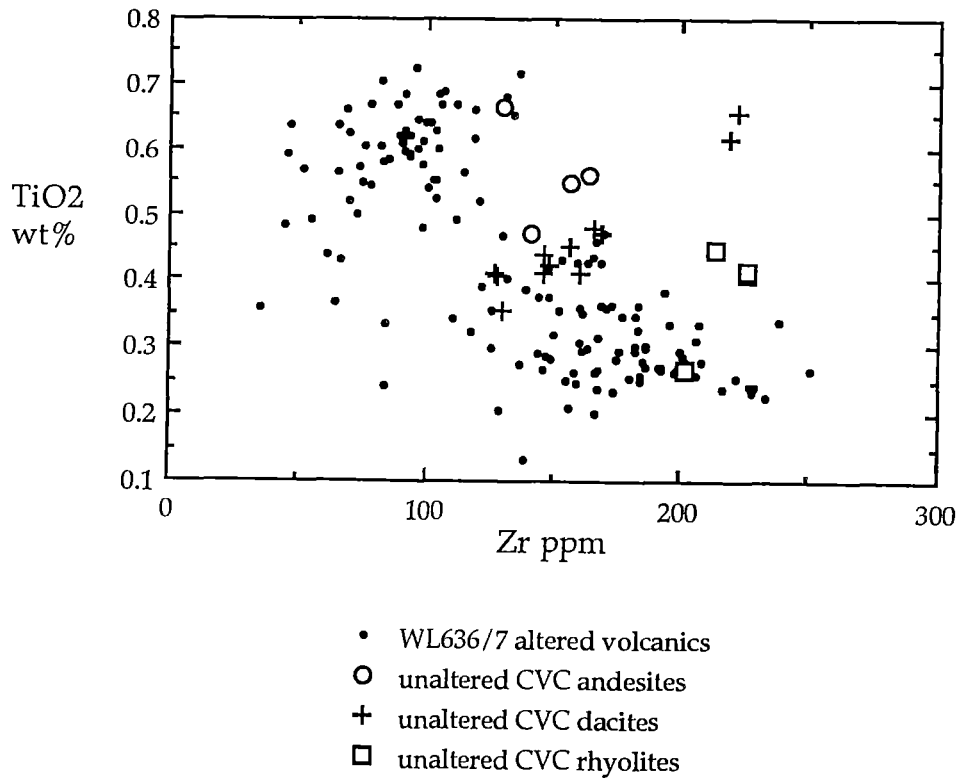

Figure 3.4 Comparison of TiO_2 and Zr concentrations in altered Prince Lyell volcanics from drill holes WL636 and WL637, and unaltered volcanics from the Central Volcanic Complex (CVC) of the Mt Read Volcanics (data from Crawford and Berry, 1992 and Crawford *et al.*, 1992).

However, no linear trends of constant Ti/Zr ratio are observed in the altered Prince Lyell data. In addition, the difference in Ti and Zr between Prince Lyell altered rocks and possible precursor volcanics is small compared to that observed in other massive sulphide deposits (Barrett and Maclean, 1991; Barrett *et al.*, 1991a, b and c), limiting the oppurtunity to define alteration trends at Prince Lyell. The more scattered spread of data at Prince Lyell may indicate some mobility of Ti and/or Zr during alteration. Notably, the low values of some Zr analyses suggests that Zr has been subject to leaching. Alternatively, the spread in the data may be partly caused by primary compositional variation in the precursor volcanics, especially if polymict epiclastic rocks comprised a significant proportion of the volcanic pile (Chapter 2).

3.3.1.2 Sc, Ga and V

Apart from Ti and Zr, "immobile" elements previously applied to less altered Mt Lyell volcanics (White, 1975; Walshe and Solomon, 1981) exhibit considerable mobility in the highly altered Prince Lyell area. Sc and Ga in particular show a narrow range of values at low concentrations in all lithologies and are entirely leached in some cases (< 10ppm, Fig. 3.3). Most leaching occurs in the ore horizon (the felsic volcanics adjacent to the intermediate - mafic contact) and in the footwall felsic volcanics. In contrast to the homogenisation of Sc and Ga, V displays an erratic distribution outside magnetite altered areas, probably due to only partial mobility in areas of intense alteration.

3.3.1.3 Nb and Y

The Nb/Y ratios of WL 636 and WL 637 are illustrated in Figure 3.5. The Nb/Y ratios of the altered volcanics cover a wide range of calc-alkaline to alkaline compositions and illustrate the unreliable nature of the Nb/Y ratio in these severely altered rocks. There is no well defined trend of either enrichment or depletion of Nb or Y. In fact, a large number of the Nb and Y analyses fall within the range of concentrations for unaltered Mt Read Volcanics (Crawford, 1987). This suggests that although the extensive leaching or addition of Nb or Y has not occurred, redistribution of both elements has occurred within the altered volcanics.

3.3.2 Alteration Index and Ti/Zr ratios

The Alteration Index (A.I.) (Ishikawa, 1976; Date *et al.*, 1983) is a measure of the destruction of sodic and calcic feldspars ($Na_2O + CaO$) and the introduction of chlorite and sericite ($MgO + K_2O$) during hydrothermal alteration. The index is defined as:

$$A.I. = \frac{100 \times (MgO + K_2O)}{Na_2O + K_2O + CaO + MgO}$$

Higher A.I. values reflect more intense alteration. In this study, the index was applied to altered Prince Lyell rocks to examine the variation of the "immobile" elements Ti and Zr with increasing alteration. The Ti/Zr ratios and concentrations of Ti and Zr of typical Prince Lyell alteration lithologies (samples PL1 - PL32) are plotted against alteration index in Figure 3.6.

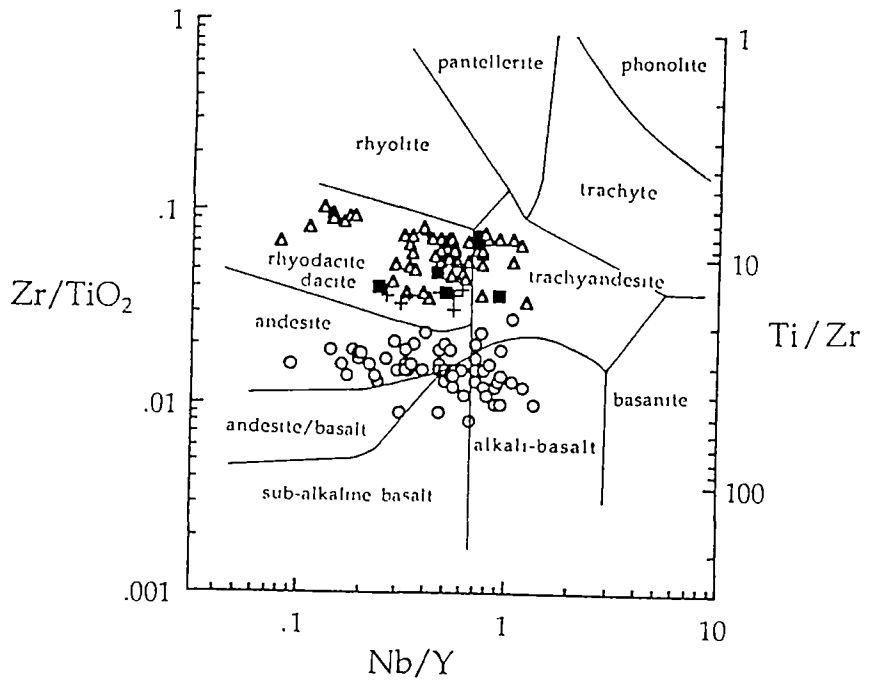

△ felsic volcanics

■ dacitic volcanics

\+ undifferentiated fine grained volcanics, probably dacitic

○ intermediate-mafic volcanics

Figure 3.5 Nb/Y ratios plotted against Ti/Zr ratio for altered volcanics from diamond drill holes WL 636 and WL 637. The Nb/Y ratios span a wide range of alkaline to calc-alkaline compositions, illustrating the unreliability of this ratio in determining the provenance of the altered Prince Lyell volcanic sequence.

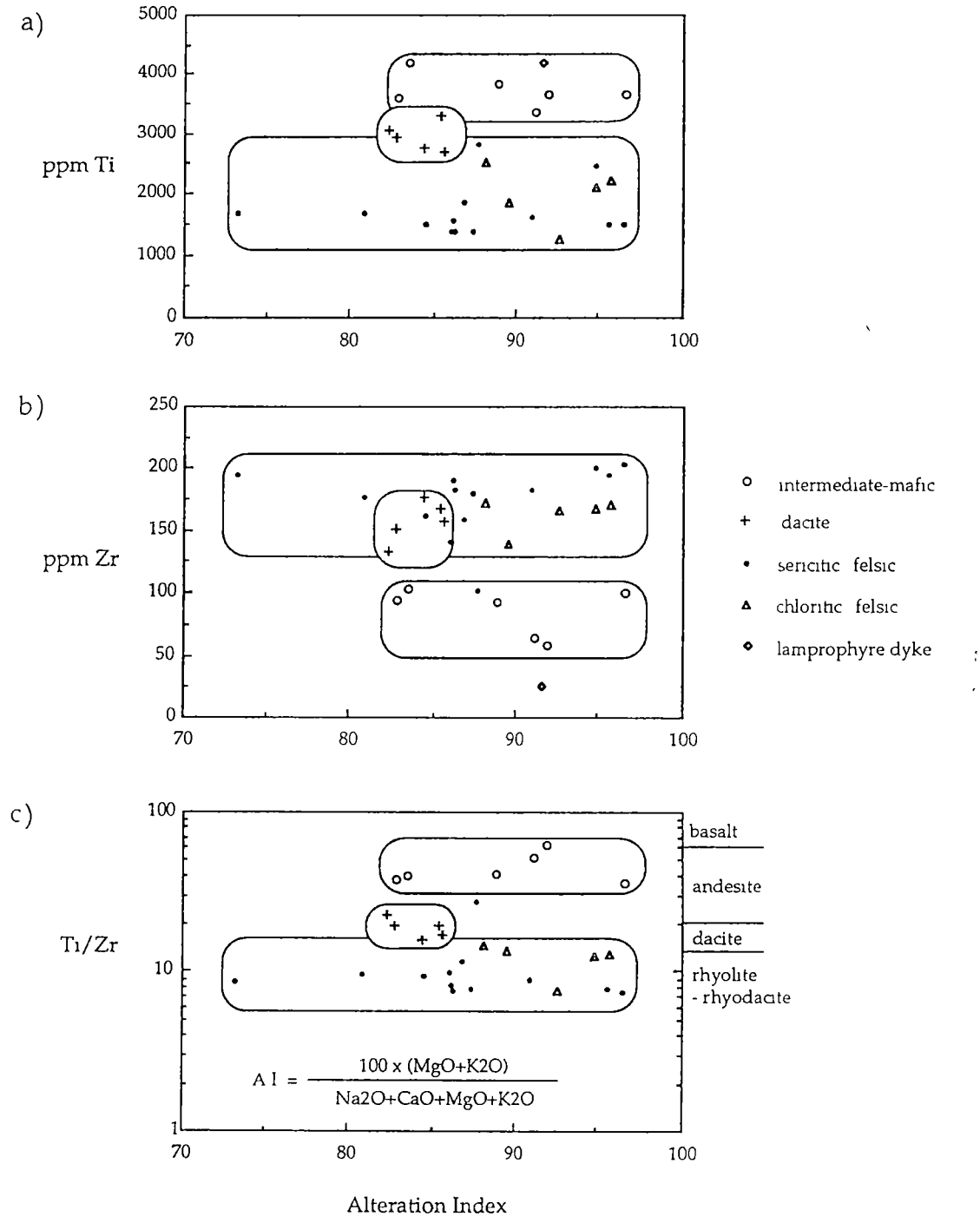

Figure 3.6 Alteration Index plotted against the "immobile" elements, Ti and Zr, and the Ti/Zr ratio for typical Prince Lyell alteration lithologies. The characteristic Ti/Zr ranges for unaltered Central Volcanic Complex rocks (Large *et al*, 1986) are shown at the right of the bottom graph.

The Ti/Zr ratio appears to be largely unaffected by the degree of alteration of the volcanics. Apart from one sericitic felsic volcanic analysis with an anomalously high Ti/Zr ratio, felsic and intermediate - mafic volcanics plot in well-defined fields spanning a range of alteration index values. The Ti/Zr ratios also appear to be largely unaffected by the differing chlorite and sericite alteration of the felsic volcanics, with only marginally higher Ti/Zr ratios in the chloritic felsic volcanics.

The altered dacitic volcanics do not have alteration index values higher than 86. More highly altered rocks only have Ti/Zr ratios within the rhyolite and andesite - basalt ranges. This could imply that dacitic volcanics were less susceptible to hydrothermal alteration. More likely, however, it indicates that texturally destructive "felsic" style alteration of the dacitic volcanics has been accompanied by homogenisation of the original dacite Ti/Zr ratios to rhyolite values. The obvious depletion of Zr in one sericitic felsic volcanic sample and the overlap of many of the dacitic and felsic volcanic Zr concentrations (Fig 3.6) suggests that Zr may have been relatively more mobile during alteration than Ti.

Not shown in Figure 3.6c is the analysis of a strongly carbonate-altered lamprophyre dyke (sample PL25) which has a Ti/Zr ratio of 167.8. This anomalously high Ti/Zr ratio is due to strong depletion of Zr in the sample (25 ppm). The strong carbonate alteration suggests that Zr may have been mobilised by complexing with CO_3^{2-} ligands in the fluid; a mechanism of Zr mobility suggested by Hynes (1980).

3.3.3 Rare Earth elements

The results of rare earth element (REE) analyses of two typical Prince Lyell lithologies are presented in Appendix 3.4. Their REE distribution patterns are compared to unaltered volcanics of the Central Volcanic Complex (Crawford, 1987) in Figure 3.7 (a, b). As only two samples were analysed, interpretation of their REE distributions must be regarded as preliminary only.

Both samples, but especially the felsic volcanic, show enrichment in the light rare earths (LREE) compared to unaltered Mt Read Volcanics. The addition of hydrothermal apatite may account for LREE enrichment. Increased levels of P_2O_5 also suggest this (see Section 3.5). However, a negative Eu anomaly may have been expected with the addition of such apatite.

The heavy rare earth distribution of the felsic volcanic and overall trend of the REE pattern are similar to unaltered Central Volcanic Complex

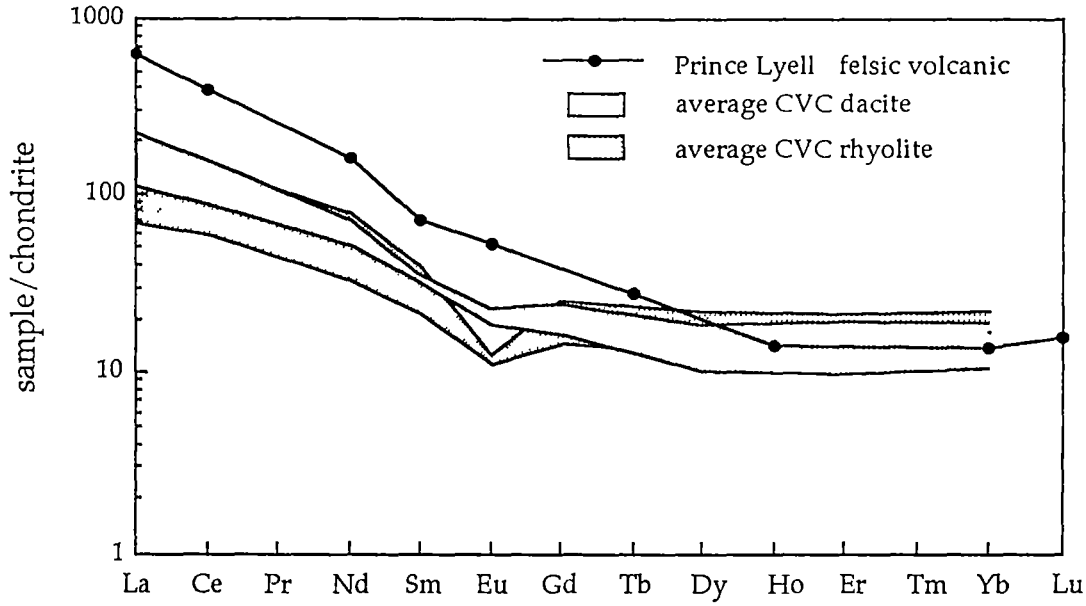

Figure 3.7a Chondrite - normalised rare earth element distribution pattern for a typical Prince Lyell felsic volcanic plotted for comparison against unaltered rhyolites and dacites from the Central Volcanic Complex (Crawford, 1987).

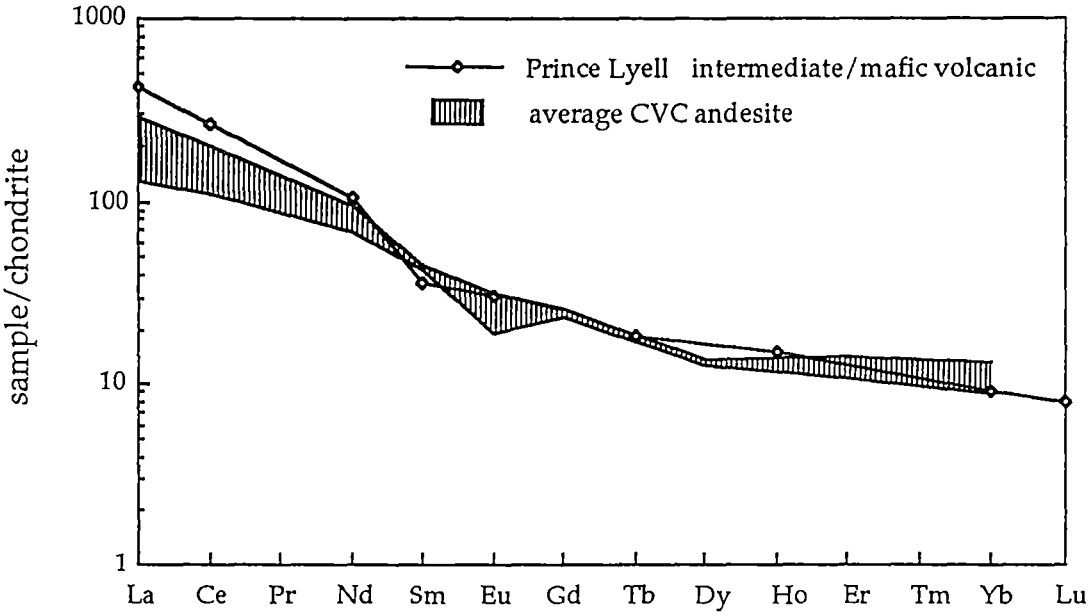

Figure 3.7b Chondrite - normalised rare earth element distribution pattern for a typical Prince Lyell intermediate - mafic volcanic plotted for comparison against unaltered andesites from the Central Volcanic Complex (Crawford, 1987).

felsic volcanics. The intermediate - mafic volcanic shows a remarkable similarity in its REE distribution to average Central Volcanic Complex andesites. The close coincidence of the altered and the two unaltered REE patterns suggest that the rare earth elements have not been significantly leached during Prince Lyell alteration, except for introduction of LREE into the more strongly altered felsic volcanics. This is a little surprising, considering that the extensive alteration at Prince Lyell has remobilised most of the so-called "immobile" elements to differing degrees.

The lack of a negative Eu anomaly in the felsic volcanic sample is in contrast to average Central Volcanic Complex rhyolites (Fig. 3.7a) where the anomaly is caused by magmatic fractionation of plagioclase. The overall felsic volcanic REE distribution pattern is more similar to the average dacitic volcanic pattern, which does not have a negative Eu anomaly and is more LREE enriched. This is supporting evidence for the hypothesis that felsic volcanics may have been derived by alteration of dacitic volcanics (see section 3.3.2 above).

3.3.4 Volcaniclastic breccias

Clasts and matrix of three volcanic breccias were individually analysed to determine whether trace element compositions have been homogenised during alteration or had preserved variations in trace element composition between clasts and matrix. Trace element analyses for the volcaniclastic breccia samples 115002, 58621.6 and 589065.7 are presented in Appendix 3.5.

3.3.4.1 Ti and Zr

The distribution of Ti/Zr ratios in the volcaniclastic breccias is outlined in Table 3.1. The whole rock Ti/Zr ratios of breccias 115002 and 589065.7 have a dacitic composition. The overall dacitic composition of these epiclastic breccias is additional evidence for a wider primary distribution of dacites than is presently preserved (see Section 2.6).

The clasts and matrix have similar Ti/Zr ratios, except for one "felsic" altered clast in sample 589065.7 which has a lower, rhyolitic Ti/Zr ratio. Although appearing to be a rounded volcanic clast, the margins of the felsic clast are diffuse, unlike the sharply defined margins of the dacite clasts. It is possible that the felsic clasts represents a small region of siliceous alteration within a generally less strongly altered rock. Hence, it is uncertain whether the low Ti/Zr ratio represents a primary compositional feature or an alteration feature.

Breccia sample no.	Sample description	Ti/Zr ratio
115002	whole rock	18.5
	dacitic volcanic clast	24.2
589065.7	matrix	17.6
	matrix	18.6
	matrix	19.6
	dacitic volcanic clast	20.3
	dacitic volcanic clast	19.1
	felsic volcanic clast	8.0
586210.6	whole rock	47.9
	dacitic volcanic clast	38.1
	dacitic volcanic clast	68.4
	unidentified strongly altered clast	405.0
	siliceous pyritic matrix	45.0

Table 3.1 Ti/Zr ratios of clasts, matrix and whole rock analyses of volcanic breccias.

The Ti/Zr ratio of the altered rim of the dacite clast in sample 589065.7 is virtually the same as the less altered core. The increase in both Ti and Zr in the clast rim is most likely due to some volume loss during secondary alteration of the rim. However, both Ti and Zr appear to have remained essentially immobile.

In direct contrast to the apparently reliable Ti/Zr ratios of breccias noted above, sample 586210.6 shows considerable depletion of Zr, resulting in Ti/Zr ratios much higher than reasonably expected in both clasts and matrix. For example, clasts with relict dacitic volcanic textures have Ti/Zr ratios of andesites and basalts. The two clasts with highest Ti/Zr ratios also have high Ti concentrations, suggesting limited mobility of Ti in addition to Zr depletion.

3.3.4.2 Nb, Y, Sc, V and Ga

The most obvious feature of these elements shown by the volcanic breccias is the severe depletion of Nb in samples 115002 and 589065.7. Sample 586210.6 also shows irregular depletion of Nb. In the felsic volcanic clast of sample 589065.7, Y is enriched and V depleted relative to dacitic volcanic

clasts. Otherwise, Y, Sc and Ga show little variation at low levels, while V shows irregular variation. The high V and Ti contents of two clasts in breccia 586210.6 suggest fine grained magnetite alteration of those clasts.

3.4 SUMMARY OF "IMMOBILE" ELEMENT GEOCHEMISTRY

It has been shown that the "immobile" trace elements Sc, Ga, V, Nb and Y were significantly mobile during the intense hydrothermal alteration of the Prince Lyell succession. Sc, Ga, V and Nb were all subject to virtually total leaching at times (ie: below detection limits), although severe depletion of one element is not necessarily accompanied by leaching of the others.

The light rare earth elements show some enrichment, especially in the felsic volcanics, compared to average unaltered Mt Read Volcanics. However, concentrations of the heavy rare earths and the overall rare earth distribution pattern are similar to unaltered volcanics, notably in the case of the intermediate - mafic volcanic. The overall felsic volcanic rare earth distribution more closely resembles the average Central Volcanic Complex dacite pattern, suggesting the felsic volcanics may have been derived from a dacitic precursor.

Ti and Zr generally exhibit a good correlation with alteration lithologies, although Zr is prone to leaching, possibly associated with high CO_2 levels in the hydrothermal fluid. Also, late magnetite alteration has introduced Ti and V into some felsic volcanics resulting in higher Ti/Zr ratios. Evaluation of the small scale mobility of Ti and Zr in the volcanic breccias was inconclusive as the clasts and matrix had similar ratios. The apparent immobility of Ti and Zr in altered clast rims suggests that the homogeneity in Ti/Zr ratios is primary and not due to homogenisation during alteration.

Ti/Zr ratios of the intermediate - mafic, dacitic and felsic volcanics suggest andesite - basalt, dacite and rhyolite - rhyodacite precursors respectively. However, the lack of intensely altered dacitic volcanics and the observed mobility of Ti and Zr in some samples suggests that Ti/Zr ratios of dacites have been homogenised to rhyolite levels during the texturally destructive "felsic" style alteration. The presence of epiclastic volcanic breccias of dacitic composition may also indicate a wider primary distribution of dacitic volcanics than previously thought. As a result, the original extent of dacitic volcanics may only be guessed at.

The results of major element analyses of 32 samples of Prince Lyell altered volcanics are shown in Appendix 3.6. Lithological descriptions of these samples are presented in Appendix 3.7. Ti/Zr variation diagrams for nine major elements and combined volatiles (L.O.I.) are presented in Figure 3.8. The differentiation trends of unaltered Mt Read Volcanics for SiO_2, Al_2O_3, total Fe (as Fe_2O_3), MgO, CaO, K_2O and P_2O_5 (Large *et al.*, 1986) are included in Figure 3.8 for comparison with the altered Prince Lyell samples.

Depletion of Na_2O during alteration was extreme, with most samples containing less than 0.2 wt% Na_2O. The leaching of Na is a ubiquitous feature of hydrothermal alteration haloes around volcanogenic ore deposits (eg: Urabe *et al.*, 1983) and reflects the total destruction of feldspar during alteration. The destruction of plagioclase and amphiboles is reflected in the strong depletion of Ca_2O in the intermediate-mafic volcanics and the lesser depletion of Ca_2O in the dacitic volcanics.

Widespread sericite alteration is reflected in the general homogenisation of K_2O values and the enrichment of K_2O in the phyllosilicate-rich intermediate-mafic volcanics. Dominantly chlorite altered felsic volcanics have lower, depleted K_2O levels compared to their more sericitic counterparts. P_2O_5 is enriched in the felsic and dacitic volcanics, indicating the deposition of apatite from mineralising fluids.

Total iron (as Fe_2O_3) and to a lesser extent MnO are both enriched in the altered rocks relative to typical Mt Read Volcanics, reflecting the addition of chlorite, iron-bearing sulphides and siderite to the rocks. Surprisingly, the overall magmatic differentiation trend (increasing Fe_2O_3 in more mafic volcanics) is preserved even though total Fe_2O_3 contents are commonly around 10 wt% above average unaltered values. This indicates a non-selective flooding of iron into the volcanic pile from the hydrothermal fluid during pyritic and chloritic alteration.

The distribution of SiO_2 in the altered volcanics also parallels the average Mt Read Volcanics differentiation trend. Selective addition or removal of SiO_2 in different rock types is not indicated from this distribution. The apparent depletion of SiO_2 across the entire range of altered volcanics may be due to dilution by the addition of large amounts of iron and volatiles to the entire altered sequence. Decreases in SiO_2 concentration are antipathetic to increases in Fe_2O_3 (Fig 3.8) and may indicate that SiO_2 itself may not have been removed from the volcanics during alteration.

MgO and Al_2O_3 display distribution trends similar, but not parallel to unaltered differentiation trends of Mt Read Volcanics. The slight deviation

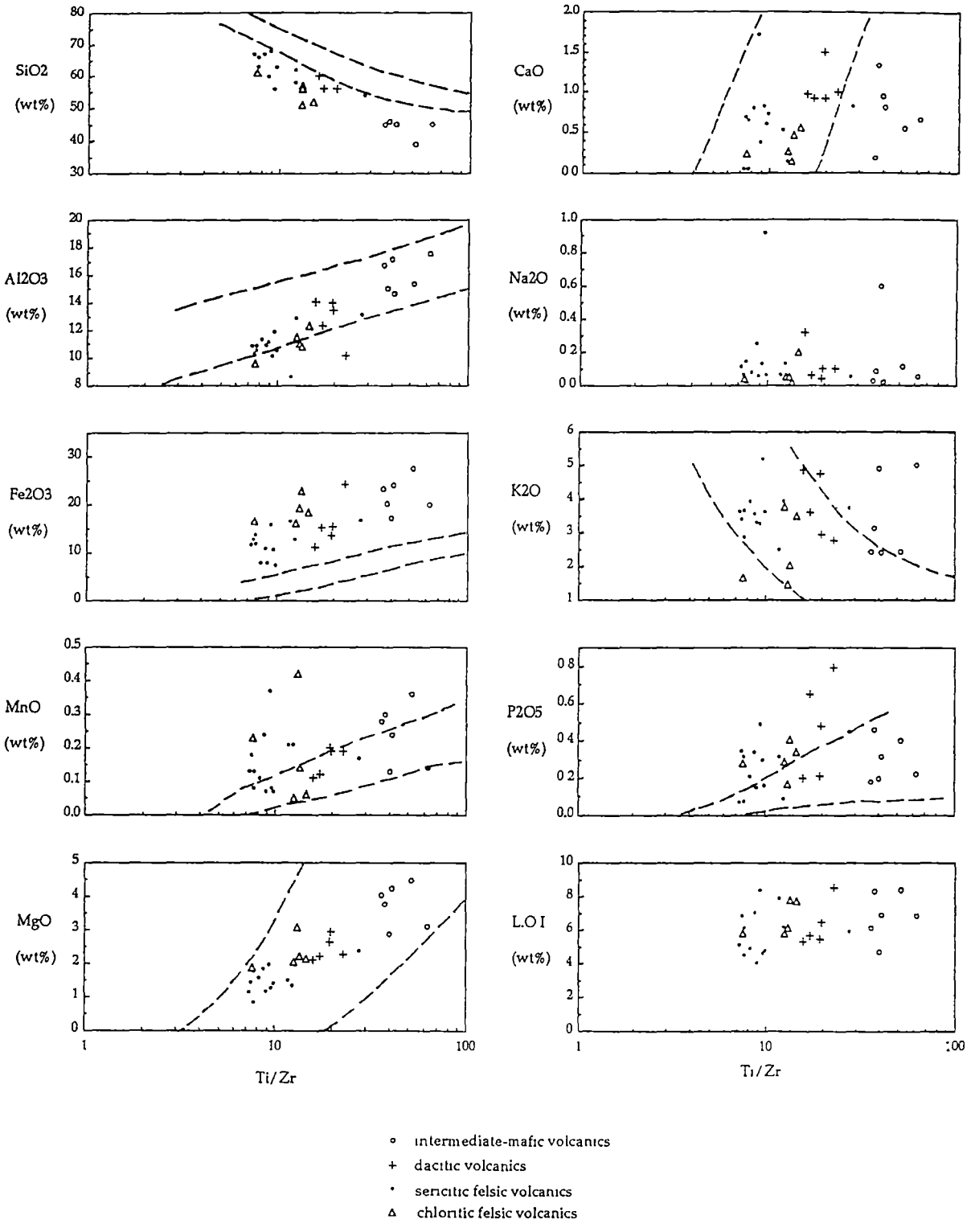

Figure 3.8 Distribution of major element oxides in typical Prince Lyell alteration lithologies plotted against their Ti/Zr ratio. Dashed lines indicate differentiation trends of unaltered volcanic rocks of the Central Volcanic Complex.

of MgO and Al_2O_3 from the unaltered magmatic trends suggests limited mobility of these two elements during alteration. Al_2O_3 appears to be preferentially leached from the felsic volcanics or added to the intermediate - mafic volcanics. The high MgO contents of chlorite - altered felsic volcanics relative to sericite - altered volcanics suggests that MgO was introduced during chlorite alteration. The higher MgO content of the intermediate - mafic volcanics reflects the higher concentrations of chlorite in these rocks. The high volatile content (H_2O, S and CO_2) of all the altered rocks reflects the abundance of hydrous (phyllosilicate), sulphide and carbonate alteration minerals throughout the Prince Lyell alteration zone.

CHAPTER FOUR

MINERALISATION AND METAL DISTRIBUTION

4.1 INTRODUCTION

The southern Prince Lyell orebody occurs as several steeply plunging lenses of disseminated and stringer pyrite - chalcopyrite mineralisation (Fig. 4.1) in quartz - sericite ± chlorite altered felsic volcanics adjacent to the contact with the intermediate - mafic volcanics (Fig. 2.1). The detailed distribution of copper and gold and their relationships to alteration lithologies and magnetite and hematite mineralisation are shown in Maps 1 to 8.

The occurrence of copper mineralisation can be accurately inferred from the extensive close spaced diamond drilling and assaying over 2 metre intervals. However, mine assaying of gold and silver is not as widespread or as detailed. Gold and silver have been routinely assayed over 6 metre intervals and only in areas of significant copper mineralisation. Due to the incomplete nature of this data, the occurrence of gold mineralisation on Sections 67 and 73 is shown as drilling intersections rather than as an interpreted distribution (Maps 6 and 8).

4.2 PREVIOUS STUDIES

The mineral paragenesis and geochemistry of the Prince Lyell deposit has been studied by numerous workers. Markham (1968) carried out a detailed study of the mineral textures of the Prince Lyell deposit, emphasising the strong Devonian structural overprint on the mineralisation. McDonald (1968) described the Prince Lyell mineralisation exposed in the West Lyell open cut. The alteration assemblages of the Prince Lyell orebody were also described by Walshe (1977) and Walshe and Solomon (1981), accompanied by thermodynamic modelling of the conditions of ore formation. Hendry (1972, 1981) and Braithwaite (1985) also studied the geochemistry of the mineralisation, and interpreted the geochemistry of phyllosilicate minerals.

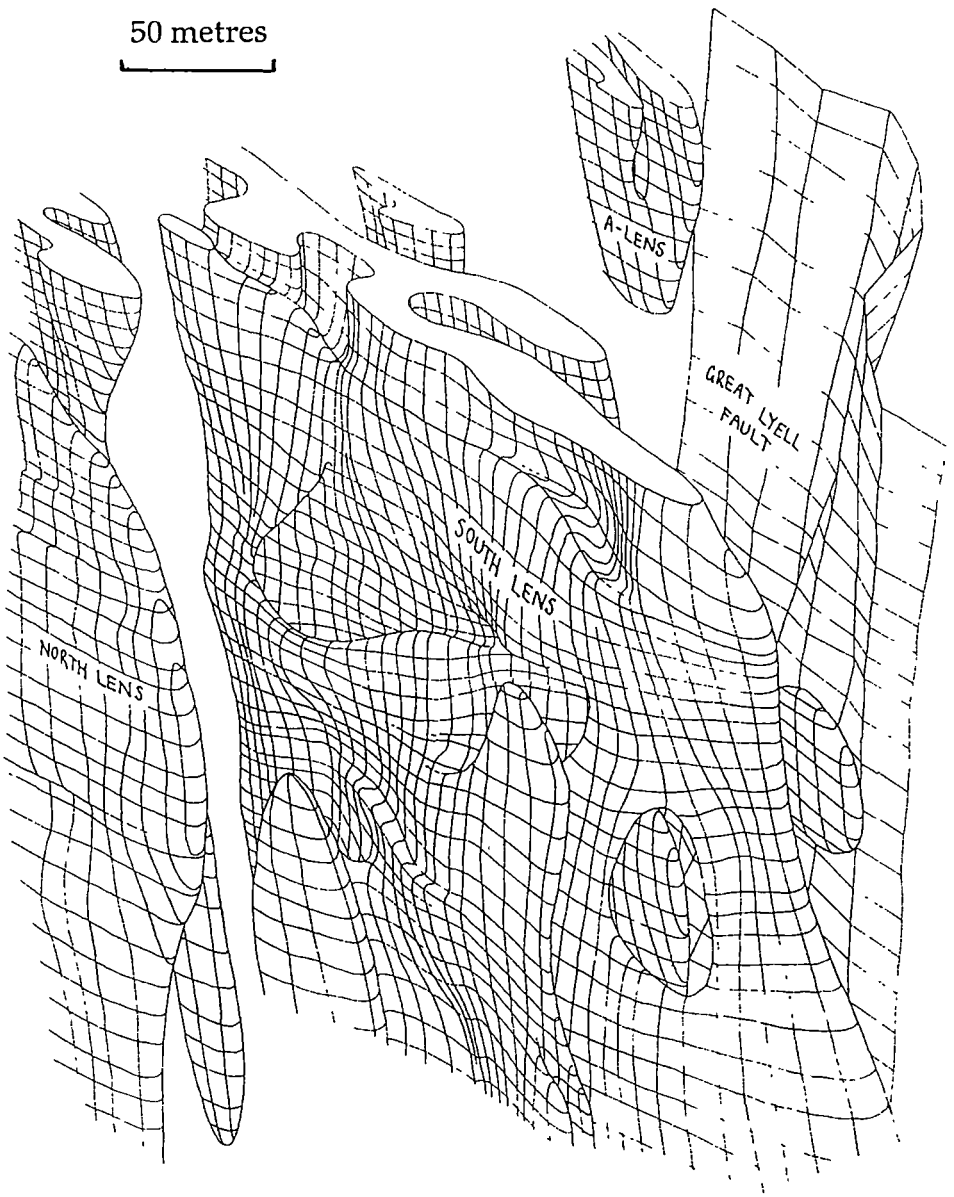

Figure 4.1 Three dimensional projection of the southern Prince Lyell orebody and the 'A' Lens below zero RL, viewed from the south. The North, South and Footwall Lenses (partly obscured behind the South Lens) of the orebody dip west at 75 - 85°, intersecting the shallower dipping Great Lyell fault at depth. Mineralisation is defined by a 1.5% Cu cutoff.

4.3 COPPER - GOLD - SILVER MINERALISATION

4.3.1 Rheological controls on mineralisation

The distribution of copper-gold-silver mineralisation in the southern Prince Lyell orebody is strongly controlled by the host volcanic lithologies. Virtually all chalcopyrite mineralisation occurs within the altered felsic volcanics. The intermediate - mafic, and to a lesser extent dacitic, volcanics rarely contain copper mineralisation. The main body of the intermediate - mafic volcanics forms the stratigraphic footwall margin of the South Lens copper mineralisation. The southern end of the North Lens mineralisation occurs within a unit of felsic volcanics up to 50 metres wide, bounded by intermediate - mafic volcanics at its hangingwall and footwall margins. In interbedded sequences of felsic and intermediate - mafic volcanics, the intermediate - mafic units contain significantly less pyrite than the felsic units and virtually no chalcopyrite mineralisation, with sharp cut-offs between the mineralised and unmineralised units.

The contrasting rheology of each rock type is reflected in the style of pyrite mineralisation in each. Pyrite is common in the felsic volcanics, occurring as disseminations within phyllosilicate alteration domains and veinlets. Fluids have moved through the rock via a highly permeable network of interconnected fractures along which phyllosilicate alteration was developed. Pyrite mineralisation in the intermediate - mafic and dacitic volcanics is much weaker and occurs predominantly as planar veins and stringers. This suggests that mineralising fluids were focussed through the fine grained intermediate - mafic and dacitic volcanics along more discrete planar fractures developed sub-parallel to the volcanic layering compared to the more pervasive fracturing of the felsic volcanics.

The correlation of copper mineralisation and alteration lithology is most likely due to a porosity and permeability contrast between the intermediate - mafic and felsic volcanics. Primary permeability would have been relatively high in coarse grained felsic volcaniclastic breccias and perlitically or hydraulically fractured silicic lavas compared to the fine grained intermediate-mafic volcaniclastics. Lenses of copper mineralisation stratigraphically higher in the felsic volcanic pile (eg: the Footwall Lens, 'A' Lens) may reflect original rock units with very high primary porosity and permeability such as agglomerates and coarse grained debris flows.

Cambrian seismic activity or Devonian deformation may have enhanced permeability near the felsic/intermediate - mafic contact. The less siliceous, more phyllosilicate-rich intermediate - mafic volcanics would have deformed

more easily compared to the more competent siliceous felsic volcanics. The resulting high strain experienced by the felsic volcanics near the intermediate - mafic contact would have resulted in further fracturing of the felsic volcanics and focussing of fluid flow through them.

4.3.2 Quartz - chlorite - sericite - pyrite - chalcopyrite assemblage

Disseminated pyrite - chalcopyrite mineralisation is concentrated within phyllosilicate alteration domains in the quartz-chlorite-sericite altered felsic volcanics, with comparatively little disseminated sulphide mineralisation in siliceous domains (Fig. 4.2a). The anastamosing network of phyllosilicate alteration zones appears to have controlled the movement of mineralising fluids. Sulphides may also be concentrated at the margins of the contrasting alteration domains where fluid flow was further focussed by ductility contrasts on a very small scale.

Pyrite occurs as disseminated, fractured anhedral to subhedral grains up to several millimetres across and as thin veinlets or stringers, most commonly oriented parallel or subparallel to the regional layering and foliation (Fig. 4.2a). Up to 30% disseminated and veinlet pyrite occurs in some areas of the orebody. However, concentrations of less than 10% pyrite are typical. The veinlets consist of strings of typically fractured pyrite grains. In many cases, originally massive pyrite veinlets have been fractured and torn apart by extension in the L_2 stretching direction during D_2 deformation in the Devonian. Margins of pyrite fragments commonly retain a jigsaw fit with their neighbours.

Chalcopyrite most commonly occupies fractures and pressure shadows in and around pyrite grains (Fig. 4.2b). Chalcopyrite also occurs without pyrite as intergrowths with the foliated phyllosilicate groundmass and smeared out along cleavage planes. Rare grains of electrum up to 25 μm were observed associated with chalcopyrite in fractured pyrite (Fig. 4.2c). Huston *et al.* (1992) have reported electrum grains up to 300 μm in pyrite concentrates.

The mineral textures described above are the result of substantial deformation of original depositional relationships during the Devonian D_2 deformation event. Although the predominant orientation of pyrite veinlets is now sub-parallel to the stratigraphic layering, the strong layer parallel shearing during D_2 is likely to have resulted in significant rotation of original veinlet orientations towards the extension (L_2) direction. Typically, pyrite has deformed by brittle fracture, while the highly ductile chalcopyrite and electrum has been remobilised into pyrite fractures and pressure shadows. Rarely, precipitation of secondary pyrite has occurred in the pressure shadows of primary pyrite grains (Fig. 4.2d). Metamorphic recrystallisation has also

Figure 4.2

A. Disseminated and stringer pyrite-chalcopyrite mineralisation in a pink quartz - sericite - chlorite altered "felsic volcanic". Disseminated sulphides are concentrated in phyllosilicate alteration domains, interstitial to the pink siliceous alteration zones. Pyrite stringers are oriented subparallel to the D_2 foliation direction. (sample 200003)

B. Reflected light photomicrograph of characteristic mineral textures of pyrite and chalcopyrite, imparted by Devonian D_2 deformation. Chalcopyrite (cpy) occurs in cracks and pressure shadows of brittly fractured pyrite grains (py). Accessory magnetite (mgt) is partly replaced by hematite. (sample 598307.9)

C. Reflected light photomicrograph of electrum grains (el) associated with chalcopyrite (cpy) in a fractured pyrite grain (py). (sample 618051.8)

D. Reflected light photomicrograph of syntectonic pyrite growth in the pressure shadow of a larger pyrite grain at the top of the figure. Although pressure shadow growth is common among ductile sulphides such as chalcopyrite and sphalerite, this texture is rare in Prince Lyell pyrite. (sample 634017.8)

E. Photomicrograph of apatite (ap) concentrations in chloritic alteration zones (chl) in an altered felsic volcanic rock. An embayed volcanic quartz phenocryst (qtz) occurs in the centre of the figure in a groundmass of fine grained quartz and sericite. (sample 634017.8, PPL)

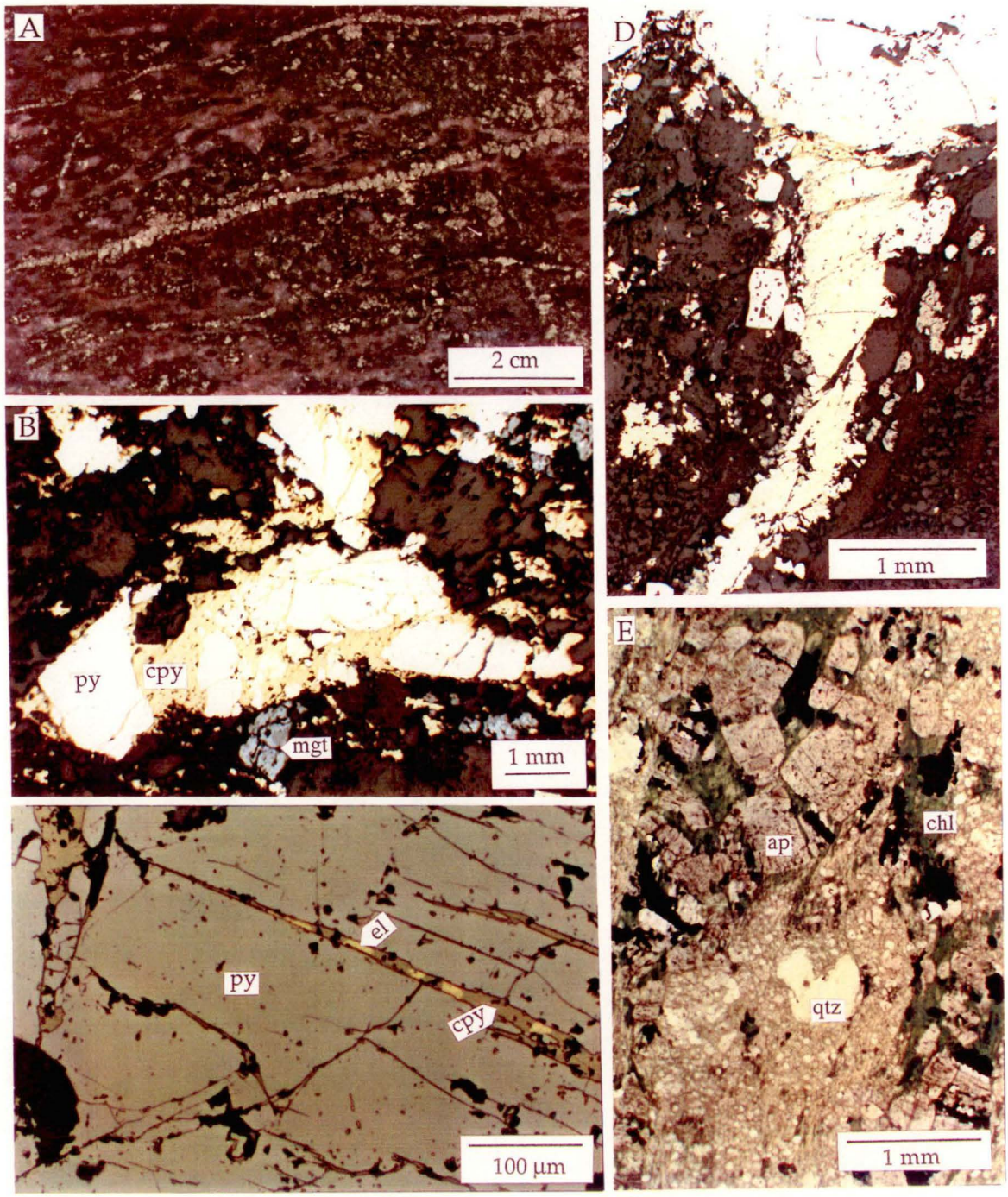
A
2 cm
B
py
cpy
mgt
1 mm
D
1 mm
E
ap
chl
qtz
1 mm
py
el
cpy
100 µm

resulted in a relatively coarse grainsize of electrum (Huston *et al.*, 1990) compared to other Tasmanian sulphide deposits. The interstitial pressure shadows between pyrite fragments are commonly filled by metamorphic growth of quartz, chlorite and siderite. Ribbon quartz, siderite and chlorite, oriented parallel to the cleavage, also emanate from small fractures in the host rock oriented at high angles to the cleavage.

Disseminated magnetite and siderite are common accessory minerals with pyrite - chalcopyrite mineralisation (Fig. 4.2b). Magnetite grains are commonly euhedral or embayed and may contain abundant inclusions of chalcopyrite in areas of copper mineralisation. Like the sulphide mineralisation, magnetite is concentrated in phyllosilicate alteration domains. Magnetite may be partially replaced by hematite. Siderite forms very fine grained disseminated rhombohedra in both the siliceous and phyllosilicate alteration domains.

Minor rounded and fractured grains of pink flourapatite up to several millimetres across also occur in pyritic veinlets and as disseminated grains in phyllosilicate alteration domains of felsic volcanics. The apatite is commonly associated with chlorite and may form remarkable concentrations of closely packed grains in veinlets or irregular clusters (Fig. 4.2e). Anhedral grains of accessory monazite occur as single grains or, less often, as clusters of grains in the phyllosilicate groundmass.

4.3.3 Quartz - sericite - pyrite ± chalcopyrite assemblage

The felsic volcanics in the structural footwall of the orebody and in low grade regions between ore lenses are predominantly composed of a quartz - sericite - pyrite assemblage. Mineral textures are similar to mineralisation in the ore horizon. Weak chalcopyrite mineralisation may occur in these rocks. Accessory chlorite, magnetite, siderite, hematite, apatite and monazite also occur in these rocks as in the ore horizon. One occurrence of molybdenite was observed in the footwall felsic volcanics on 115 Sublevel. Fine grained molybdenite platelets were crudely aligned in the foliation of phyllosilicate alteration domains.

4.3.4 Late quartz - pyrite mineralisation

Extremely siliceous quartz - pyrite - minor sericite alteration intrudes upon the above-mentioned assemblages in minor narrow zones in the northern parts of the study area (Map 1). The study area includes the southern margin of the Prince Lyell North Lens mineralisation which is substantially

affected by this phase of silicification and pyritisation. Contacts of the typical South Lens quartz - chlorite - sericite - pyrite - chalcopyrite mineralisation with narrow quartz - pyrite zones suggest a pervasive quartz - pyrite overprinting of the main chalcopyrite mineralisation phase. Walshe (1977) also concluded that a prograde relationship from quartz - pyrite - sericite to the chloritic mineralisation assemblage was not tenable on geochemical grounds. Outside the main silicification zones, movement of this late fluid along previously existing pyrite veinlets is inferred by the presence of weakly silicified haloes around pyrite veinlets.

4.3.5 Massive sulphide mineralisation

Occasional tabular bodies of massive pyrite ± chalcopyrite ± minor sphalerite ± minor galena up to a metre wide, occur in and around the ore horizon. These massive sulphide bands are variably continuous over a few metres to tens of metres and are parallel or subparallel to the regional foliation and bedding. Boudinage and displacement along bedding - parallel shears has resulted in a highly deformed nature of the bands.

Evidence for the origin of the bands is inconclusive. Although usually entirely recrystallised and annealed, fine internal layering of sulphides, up to several millimetres wide, may occur in the bands. McDonald (1968) and Arnold (1985) suggested that they were the result of syngenetic seafloor exhalation. However, the probability of structurally enhanced layering of a massive vein is high, as a strong layer parallel cleavage is developed in the host volcanics. Cleavage formation in other western Tasmanian massive sulphide ores such as Rosebery has resulted in similar small scale sulphide laminations parallel to cleavage and at high angles to the primary layering (Berry, 1990a). Fine scale laminations (0.1 - 2 mm) were interpreted by Berry to be the result of intense cleavage development, while larger scale layering (10 - 50 mm) reflected primary compositional layering.

Finely laminated, layer-parallel magnetite - pyrite ± hematite bands also occur in the intermediate - mafic and felsic volcanics. Metamorphic quartz, chlorite and siderite infill fracturing of the bands induced by D_2 deformation. The laminations of alternating pyrite and magnetite are only a few millimetres wide and can be continuous over several metres. They are interpreted to be the result of incremental opening of layer-parallel veins, not exhalation. Mirror image repetition of laminations occurs from the centre of bands and laminations may terminate along internal fractures within the veins (Fig 4.3a).

Figure 4.3

A. Photomicrograph of finely laminated magnetite and quartz, produced by cyclic deposition of minerals in a symmetrical, multiply opened vein. Note the termination of some laminations at the centre of the vein. The laminations may be continuous over several metres and comprise pyrite and hematite as well as quartz and magnetite. In veins parallel to the regional volcanic layering the texture resembles sedimentary layering. (sample 623076.6, PPL)

B. Reflected light photomicrograph of the internal structure of massive sphalerite, enhanced by etching, from a sphalerite - barite - pyrite vein. Randomly distributed blebs of chalcopyrite "disease" occur at the boundaries of twinned sphalerite grains. (sample 115012)

C. Massive magnetite vein transected by; a) anastamosing cobaltiferous pyrite veinlets, b) chlorite - filled D_2 tension cracks, and finally c) late D_2 quartz - siderite - chlorite - chalcopyrite veins. (sample 580184.0)

D. Large crystals of pink apatite within a zone of magnetite - chlorite (possibly after actinolite) - pyrite mineralisation. (sample 580181.5)

E. Finely disseminated and veinlet magnetite developed in a fine grained sericite - chlorite altered felsic volcanic rock. (sample 641040.1)

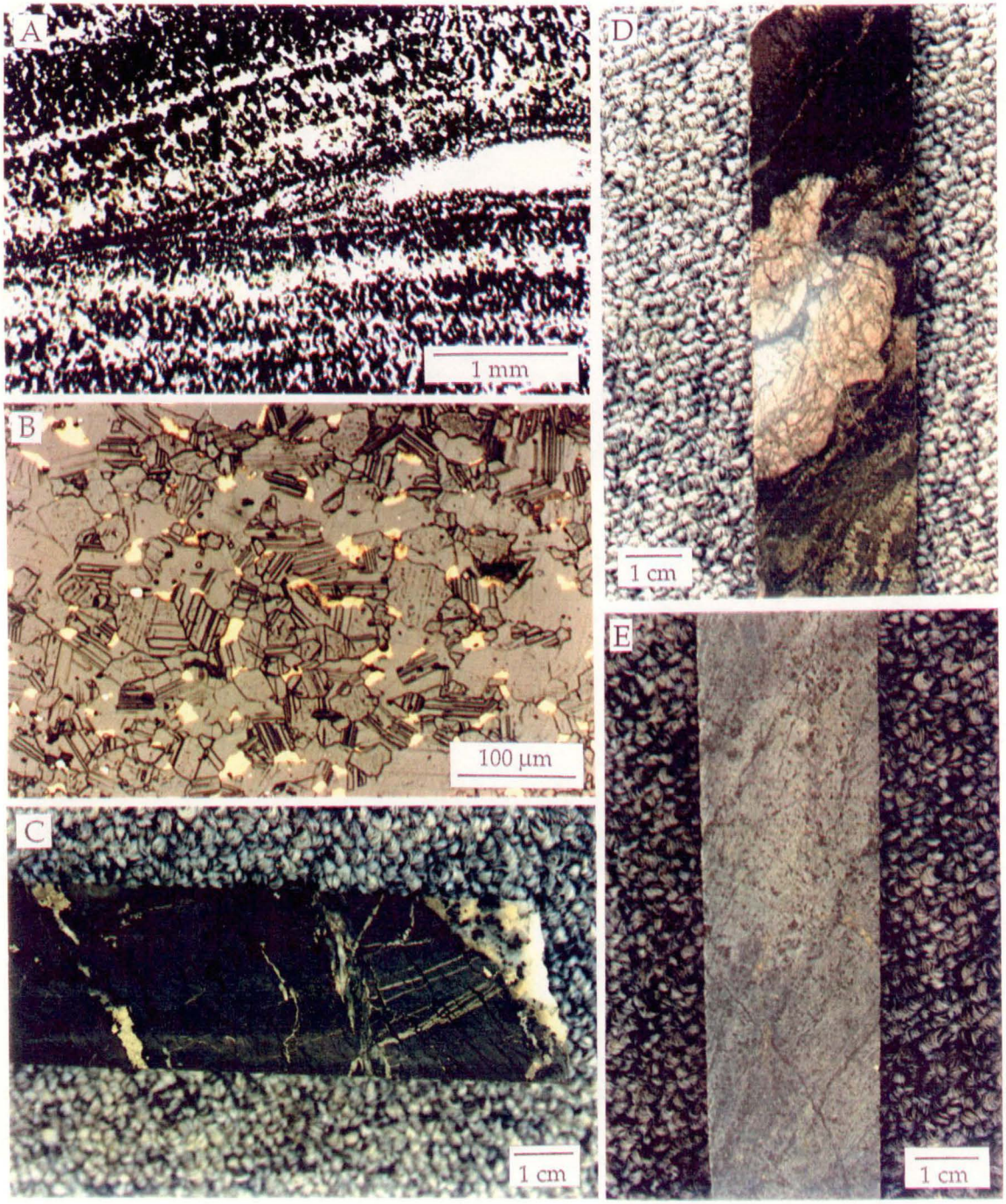
A
1 mm
B
100 µm
C
1 cm
D
1 cm
E
1 cm

4.3.6 Sulphide mineralisation in the intermediate - mafic volcanics

Although chalcopyrite mineralisation is relatively uncommon in the intermediate - mafic volcanics, 10 - 20% pyrite may occur towards the stratigraphic top of the unit in thin stringers generally oriented parallel or subparallel to the regional layering and foliation (Fig. 2.2a). Minor stringers are oriented at higher angles to the layering and foliation. In contrast to the occurrence of pyrite in the felsic volcanics, veinlet mineralisation is by far the predominant style of pyrite mineralisation. The pyrite content increases irregularly towards the stratigraphic top of the intermediate - mafic volcanics from less than 5%, 20 metres below the orebody, up to 20% in some areas adjacent to the ore horizon.

As in the felsic volcanics, previously massive pyrite stringers have been extended and dismembered in the D_2 lineation direction with metamorphic quartz, chlorite and siderite crystallised between pyrite fragments. Accessory magnetite and flourapatite also occur in the pyrite stringers.

Rare baritic veins also occur in the intermediate - mafic volcanics. These veins are up to 15 cm wide and comprise barite, pyrite, sphalerite, magnetite, quartz and apatite. Crude internal laminations of predominantly barite - sphalerite or magnetite - apatite indicate that the veins provided passage for a range of contrasting hydrothermal fluids during their lifetime.

The rapid decrease in sulphide content in the intermediate - mafic volcanics away from the orebody and the bedding-parallel attitude of the pyrite stringers preclude the intermediate - mafic stringer zone from being a Cambrian footwall feeder zone to the orebody. Instead, mineralisation in the intermediate - mafic volcanics probably reflects the lateral passage of fluids through the intermediate - mafic volcanics parallel to the main fluid pathway in the adjacent felsic volcanics.

4.4 Lead and Zinc Mineralisation

4.4.1 Distribution and character of mineralisation

Lead and zinc are a very minor component of the Prince Lyell mineralisation. Elevated lead and zinc values are irregularly distributed in and around the South Lens ore horizon, showing no apparent correlation with copper - gold mineralisation, and are due to two types of thin, discontinuous sphalerite-rich veins. These are:

a) sphalerite-barite-pyrite-siderite-chlorite-quartz veins with accessory magnetite, apatite, galena and chalcopyrite; parallel or subparallel to the regional foliation, and

b) irregular sphalerite-chlorite-siderite veins with accessory galena, pyrite, chalcopyrite and monazite, which post-date both the Devonian cleavage and late D_2 quartz - carbonate veining.

Type a) veins cut across earlier pyrite stringers at low angles. They may contain coarsely crystalline barite and siderite and be up to 10 cm wide. However, more commonly they are highly foliated, fine grained veins only 2 - 3 cm wide. Repetition of a type a) sphalerite-barite vein by cleavage-parallel shearing is shown in Figure 2.2d. Type b) veins are post-D_2, unfoliated veins of virtually massive sphalerite, probably formed by remobilisation of minor quantities of zinc during waning metamorphism.

Irregular blebs of chalcopyrite "disease" occur throughout sphalerite. The chalcopyrite appears to be randomly disseminated throughout regions of massive sphalerite. However, etching of sphalerite for approximately ten seconds in a solution of $KMnO_4$ and 7:1 H_2O:H_2SO_4 (Appendix 5.1) revealed that the sphalerite was composed of a mass of small interlocking, twinned grains with chalcopyrite inclusions occurring at sphalerite grain boundaries (Fig 4.3b). The occurrence of chalcopyrite at grain boundaries, rather than within sphalerite grains, may be the result of expulsion of chalcopyrite from the sphalerite structure during deformation and recrystallisation. Such a process was suggested by Barton and Bethke (1987). One example of fine chalcopyrite inclusions oriented along cleavage planes in sphalerite was observed in a very late vein which transected and partly replaced a D_2 quartz-siderite vein. Although it is apparently the result of dissolution and redeposition of earlier sphalerite mineralisation, the chalcopyrite impurities were apparently not expelled from the sphalerite.

Hendry (1981) and Braithwaite (1985) delineated apparent zinc rich lenses near the footwall margin of the South Lens copper mineralisation from drill hole assay data on 14 Level. In this zone, Hendry (1981) reported that sphalerite occurred as millimetre thick bands parallel to fine scale pyrite, chlorite and sericite banding, although Braithwaite (1985) indicated that sphalerite and galena were not visible. The zone was delineated by very low zinc grades; only $\geq 0.1\%$ (not $\geq 1.0\%$ as reported in Fig. 5, Braithwaite (1985)). In this study, the zone could not be traced in drill core below 14 Level. The lack of continuity of this zinc-rich layer and the observed occurrence of sphalerite as vein mineralisation rather than disseminations or laminated lenses, suggests

that this zinc mineralisation is not of exhalative origin, as proposed by Braithwaite (1985) and Hills (1990).

Hannington and Scott (1989) attempted to relate the geochemistry of sphalerite and gold mineralisation at Prince Lyell. Specifically, the FeS content of sphalerite was used as a guide to temperature of sphalerite and hence gold mineralisation. However, given the lack of sphalerite associated with copper - gold mineralisation, the distinct mineralisation styles of zinc and copper - gold, and the contrasting gangue mineralogy of each, it is suggested that Hannington and Scott may have related two distinctly separate episodes of mineralisation. Furthermore, the large amount of sphalerite remobilisation at Prince Lyell raises the possibility that primary trace element levels in sphalerite have been modified during remobilisation.

4.4.2 The Zinc Ratio

The distributions of lead and zinc in 493 two metre intervals from drill core through the South Lens are presented in Figure 4.4. The histograms show background levels of lead and zinc of around 0 - 0.5% and 0 - 0.2% respectively, with tails of sporadic, higher grade vein mineralisation. The two populations of lead-zinc mineralisation are also reflected in their distinctive zinc ratio patterns.

The ratio 100.Zn/(Zn+Pb), or "zinc ratio", was developed by Huston and Large (1987) as a tool for discrimination of volcanogenic massive sulphide mineralisation from other vein-style or sedimentary-hosted sulphide deposits. They concluded that Tasmanian volcanogenic massive sulphide deposits were characterised by mean zinc ratios between 60 and 77, with low standard deviation of the ratio within each deposit (less than 15). In comparison, other mineralisation styles had a lower, wider range of mean values (39 - 61) with higher standard deviations.

Background lead-zinc mineralisation in the South Lens (< 0.5% Zn) exhibits a distribution close to that of typical lead-zinc rich volcanogenic massive sulphide deposits of western Tasmania (Huston and Large, 1987) with a mean value of 67.1 and a standard deviation of 16.6 (Fig. 4.5a). The similarity is even more marked when it is considered that the histogram peak at zinc ratio = 50 is due primarily to assays of dubious quality at the lower limit of analytical precision (50 ppm).

The tail of low zinc ratio values may reflect higher temperatures of mineralisation at Prince Lyell compared to lead-zinc dominated massive sulphide deposits. Above 200 - 250°C, zinc and especially lead solubility increases with equilibrium zinc ratios decreasing rapidly from around 60 to

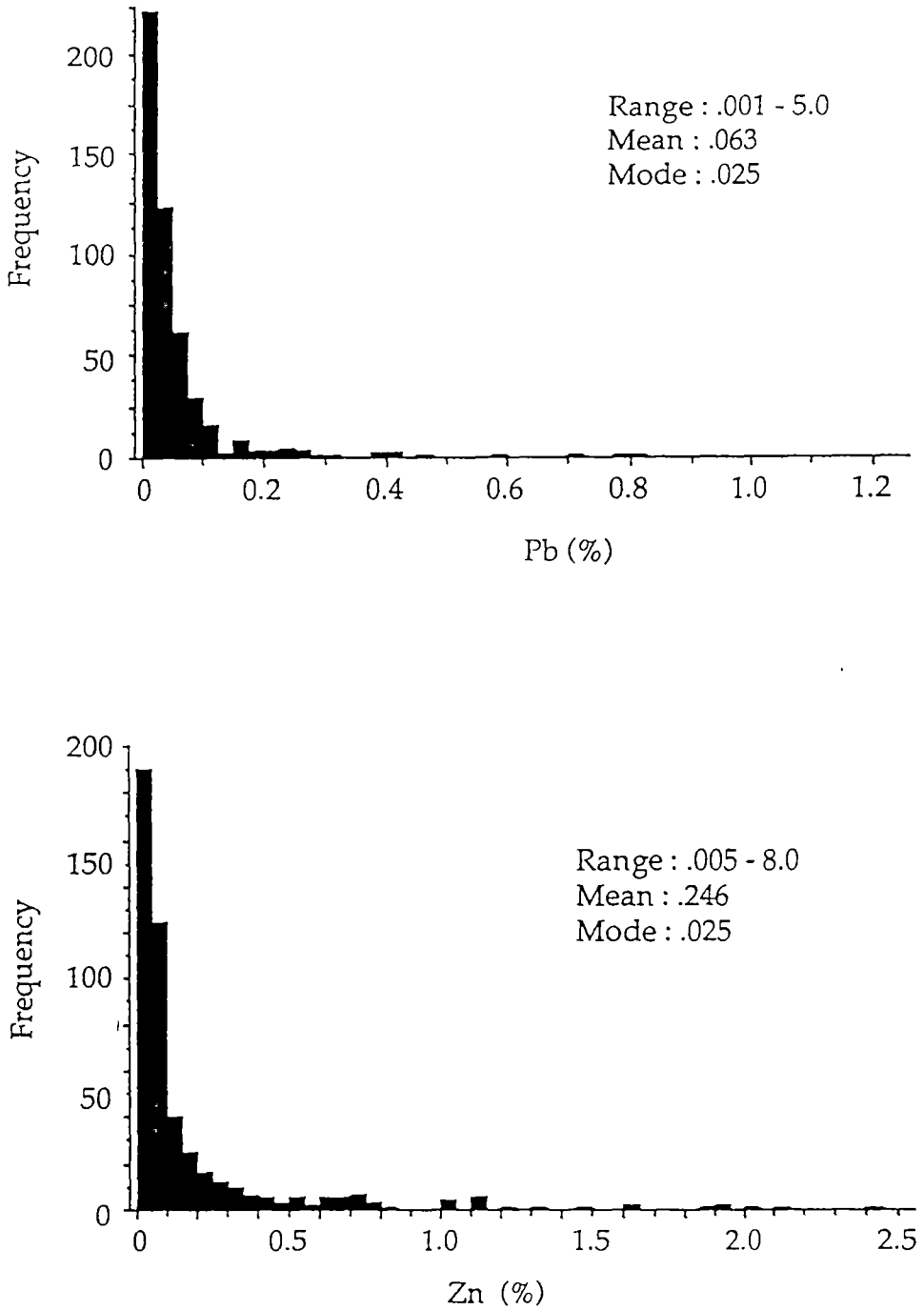

Figure 4.4 Frequency distributions for lead and zinc mineralisation above the detection limit of 0.025%. The great majority of values are less than 0.5%. Sporadic higher values generally represent massive veins developed by remobilisation of lead and zinc late during metamorphism.

A.

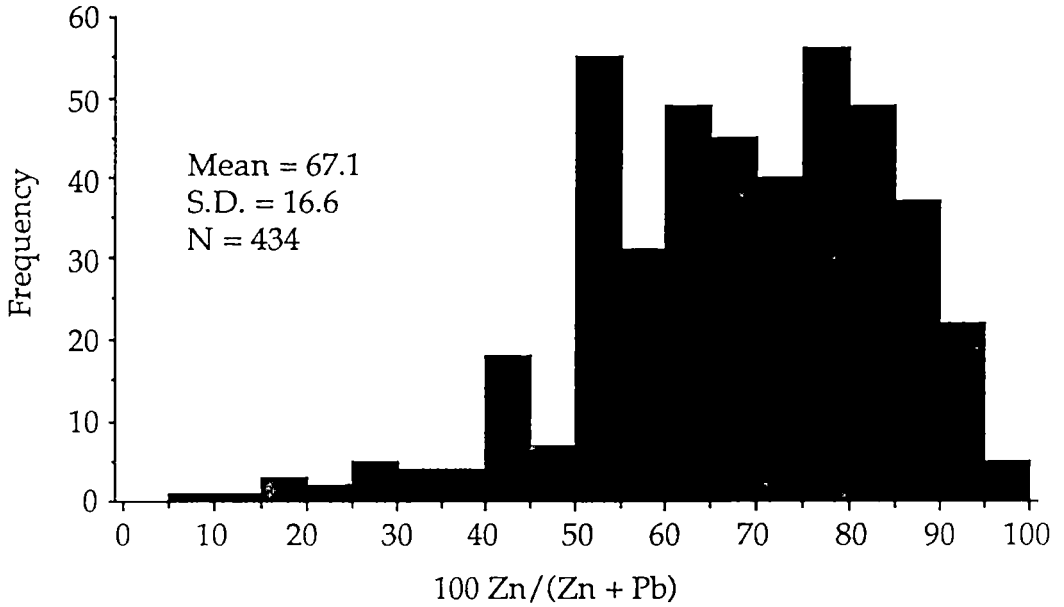

B.

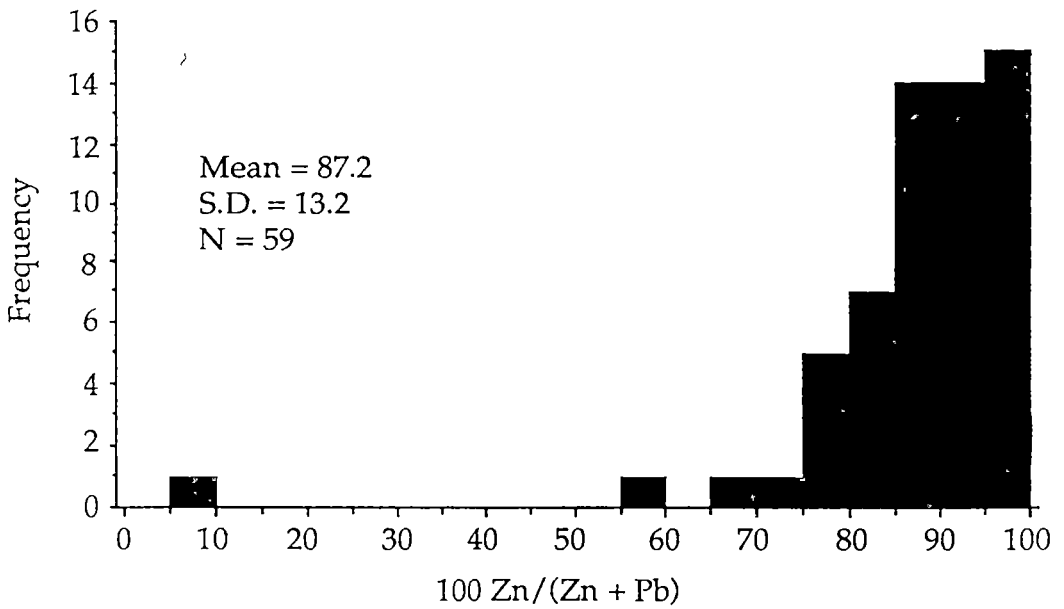

Figure 4.5 Frequency distributions of the 'zinc ratio' at Prince Lyell for (a) background zinc values (< 0.5% Zn) and (b) higher grade, generally remobilised zinc mineralisation (≥ 0.5% Zn).

less than 30 (Huston and Large, 1987). Undersaturation of the fluid with respect to lead and/or zinc would also cause increased variation of the zinc ratio. Huston and Large (1987) concluded that the zinc ratio was not reliable below 1% Zn, due to the likelihood of undersaturation. However, the Prince Lyell data show a very close correlation to massive sulphide deposit patterns, suggesting a link to volcanogenic hydrothermal fluids.

Higher grade mineralisation (≥ 0.5% Zn) shows a contrasting distribution of zinc ratios to the background levels, with a mean of 87.2 and a standard deviation of 13.2 (Fig. 4.5b). The higher mean is caused by the dominant influence of late stage remobilised sphalerite veins which contain only minor galena. The higher zinc ratio illustrates the greater mobility of zinc over lead during metamorphism.

4.5 MAGNETITE - APATITE MINERALISATION

4.5.1 Data collection

Quantitative estimates of magnetite alteration were obtained by measuring the magnetic susceptibility of sawn drill core and assay pulps using a Scintrex SM-5 Digital Magnetic Susceptibility Meter. Magnetic susceptibility was measured in c.g.s. units which approximately convert to volume per cent magnetite by the relationship;

$$\text{susceptibility in c.g.s.} = (2 \times 10^{-3}) \times \text{vol. \% magnetite}$$ [1.]

Measurement of the assay pulp samples were preferred, as a true average reading of the magnetite content over two metres could be gained. Where assay pulps were not available, spot susceptibility measurements of drill core were averaged over 1 - 2 metres. Although measurements from the crushed pulps were marginally lower than for drill core readings, reasonably good correlation existed between the two methods. Spot readings had a wider range as the influence of irregular magnetite mineralisation was greater over the small sample areas.

---

1. Specifications of the Scintrex Magnetic Susceptibility Meter suggest a conversion factor for c.g.s. units to vol. % magnetite of approximately 3×10^{-3}. However, point counting of magnetite in five polished samples of Prince Lyell drill core revealed conversion factors of between 1×10^{-3} and 3×10^{-3}, with an average of around 2×10^{-3} (Appendix 4.1).

4.5.2 Magnetite - apatite alteration in the felsic volcanics

Although magnetite is an almost ubiquitous accessory mineral in the pyrite chalcopyrite mineralisation (Fig. 4.2b) of the felsic volcanics, it is rarely a major component of the mineralisation. However, sporadic zones of strong magnetite - apatite ± chlorite alteration, not associated with copper mineralisation, occur in the felsic volcanics. These zones are lensoidal and highly elongate down dip, parallel to the volcanic stratigraphy and foliation. Tectonic extension, up to 150% during the D_2 metamorphic event (Cox, 1981), has exaggerated the down-dip continuity of the magnetite - apatite lenses with several being over 300 metres in down-dip extent. The magnetite - apatite lenses are between 1 and 30 metres thick and occur at several levels in the South Lens and Footwall Lens ore horizons. Strong magnetite mineralisation is discontinuous along strike and commonly occurs as lenses separated by regions of weaker magnetite mineralisation along discrete horizons.

In order of decreasing intensity, magnetite - apatite mineralisation occurs as:

i) elongate lenses to irregular semi-massive bodies of magnetite, up to 1 - 2 metres wide, with accessory large apatite crystals, chlorite and minor pyrite, (Fig 4.3c, d),

ii) stockworks, veins and veinlets, 1 mm to 10 cm wide, and disseminations of magnetite - apatite ± chlorite (Fig. 4.3e), and

iii) disseminated magnetite and/or apatite and chlorite in the phyllosilicate alteration domains of pseudofragmental rocks.

Larger bodies of massive or vein magnetite commonly grade into disseminated magnetite or a composite of the two types. Apatite is a ubiquitous accessory mineral of the stockwork and massive magnetite mineralisation. It occurs as pink, subhedral to rounded, fractured crystals from 1 mm to at least 5 cm in diameter (Fig 4.3d). Larger apatites have been reported by mine geologists. Qualitative electron microprobe analyses showed the apatite to be of flourapatite composition. The apatites contain fine dustings of many solid and fluid inclusions, including monazite, chalcopyrite, siderite, chlorite and hematite (Walshe, 1977; Hendry, 1981). Concentrations of this same apatite without magnetite are found in some pyrite veinlets and felsic volcanics (Fig. 4.2e).

Chlorite is commonly developed interstitial to magnetite veins and in crack-seal chlorite - quartz fibre veins which were developed when massive magnetite bodies and veins were extensively fractured by the Devonian D_2 cleavage-forming event. Very minor amounts of magnetite were dissolved by the metamorphic fluids and reprecipitated on the edges of the chlorite - quartz fibre veins.

Zones of strong magnetite veining have locally sheared margins, along which late D_2 quartz - siderite veining is commonly developed (Fig 4.3c). The shearing and quartz - siderite veins clearly cross cut and post-date the magnetite and therefore do not represent possible focussing structures for the magnetite alteration fluids as was suggested by Bird (1982). Instead, the deformed margins of magnetite bodies are the result of shearing during D_2 along zones of competency contrast between the more competent magnetite-rich zones and the more ductile phyllosilicate-rich felsic volcanics. Large scale boudinage development during D_2 may account for local discontinuities of massive magnetite alteration zones.

4.5.3 Magnetite mineralisation in the intermediate - mafic volcanics

In stark contrast to the character of magnetite mineralisation in the felsic volcanics, magnetite mineralisation occurs in the intermediate - mafic volcanics as generally diffuse stratabound zones up to 20 metres wide containing up to 5% disseminated magnetite euhedra. The lack of closely spaced drilling in the hangingwall areas does not permit detailed delineation of these zones. Minor magnetite also occurs with pyrite and quartz in finely laminated veins described above in Section 4.3.5

Several features of the hangingwall magnetite suggest that it is related to that found as an accessory to pyrite ± chalcopyrite mineralisation, rather than to the magnetite - apatite zones. Firstly, the disseminated hangingwall magnetite is similar in morphology to the sulphide-associated magnetite, although the abundant chalcopyrite inclusions found in magnetite in the ore horizon are uncommon in the hangingwall volcanics. Secondly, apatite is not present in any more than trace amounts in the hangingwall magnetite zones; and thirdly, whole rock geochemical analyses (see section 3.3) suggest that hangingwall magnetite contains lower levels of Ti and V than magnetite - apatite mineralisation.

4.5.4 The relationship between magnetite - apatite mineralisation and copper - gold mineralisation

Magnetite - apatite mineralisation zones in ore horizons correlate with regions of reduced grades of both copper and gold. Bird (1982) peviously noticed the dispersion of copper into the wallrocks where apatite mineralisation was present. However, it is difficult to establish if pyrite, which is more irregularly distributed (see section 4.7), has been affected by magnetite - apatite mineralisation. The antipathetic relationship between copper and magnetite mineralisation is exemplified by the development of magnetite on Section 73 (Map 8). Below -150m RL, a narrow corridor of reduced copper - gold mineralisation extends through the middle of the South Lens, corresponding in the main to a continuous zone of magnetite alteration. Above -150m RL, the magnetite mineralisation widens into a large body of vein and disseminated magnetite, 50 metres high by 30 metres wide and 80 metres along strike. High grade copper - gold mineralisation drops off sharply directly adjacent to the magnetite alteration zone, resulting in a large low grade hole in the orebody.

The occurrence of narrow copper - depleted magnetite - apatite lenses transecting regions of otherwise continuous copper - gold mineralisation is illustrated in numerous other locations in the Prince Lyell orebody (eg: Section 68) and suggests dissolution and removal of copper and gold by later magnetite mineralising fluids. However, the presence of laminated magnetite - pyrite veins (Fig. 4.3a) and pyrite veinlets cutting across massive magnetite (Fig. 4.3c) indicate that pyrite mineralisation also occurred during and after magnetite mineralisation. Further microtextural evidence of the relationship between magnetite - apatite and pyrite - chalcopyrite mineralisation is discussed in Chapter 5.

4.6 HEMATITE ± SIDERITE ± CHLORITE ALTERATION

4.6.1 Distribution and petrography

Disseminations, clots and veinlets of hematite - siderite ± chlorite ± quartz (Fig. 4.6a, b) occur in much of the stratigraphic hangingwall felsic volcanics. Hematite has a characteristic bladed form, up to 0.5 mm long. Very fine grained disseminated hematite occurs in fine grained shale or ash units, dacitic and felsic volcanics, imparting a distinctly purple colour to the rocks. Siderite commonly occurs as aggregates of anhedral grains or isolated rhombohedra. Strong finely disseminated siderite alteration may impart a buff

Figure 4.6

A. Veinlets and disseminated clots of hematite - siderite alteration in a highly sericitic footwall felsic volcanic. The characteristic buff colour of the rock is due to abundant finely disseminated siderite. (sample 623104.5)

B. Photomicrograph of disseminated rounded clots of siderite, bladed hematite and clear quartz in a footwall felsic volcanic. (sample 622171.5, PPL)

C. Reflected light photomicrograph of hematite pseudomorphs after skeletal magnetite grains in a footwall felsic volcanic. (sample 607130.3)

D. Reflected light photomicrograph of siderite alteration (sid) of massive magnetite (mgt), along cleavage partings and fractures. Accessory apatite grains (ap) are apparently unaffected by the siderite alteration. (sample 200001)

E. Reflected light photomicrograph of extensive siderite alteration of previously massive magnetite. Finely disseminated relict magnetite (light grey) occurs in an almost wholly siderite matrix (mid grey). (sample 200001)

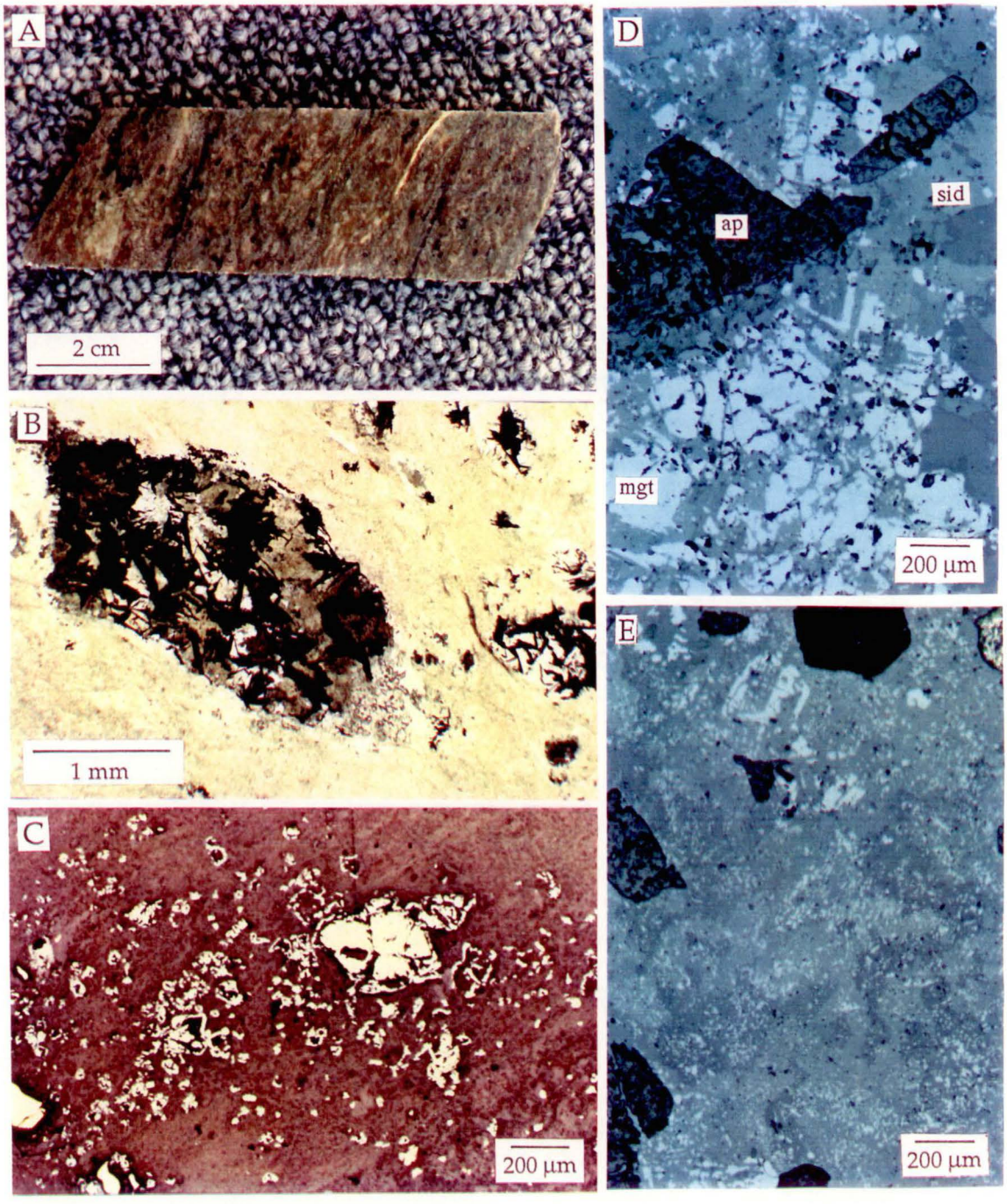
A
2 cm
B
1 mm
C
200 µm
D
sid
ap
mgt
200 µm
E
200 µm

Prince Lyell ore horizon in places, particularly at the southern end of the orebody. The distribution of siderite alteration is more irregular than hematite and is generally confined to regions closer to the Great Lyell fault.

The 'A' Lens orebody, which comprises virtually the same mineralogy as the Prince Lyell mineralisation, occurs entirely within the hematitic alteration zone in the footwall felsic volcanics. Hematite alteration predates the Devonian D_2 deformation, with hematite blades often crudely oriented in the cleavage direction and cleavage wrapping around hematite alteration clots. Magnetite mineralisation within the hematite alteration zone is partly or wholly replaced by hematite ± siderite (Fig. 4.6c). Contrary to Hendry (1972), intergrowths of magnetite and siderite do not represent replacement of a third phase by magnetite and siderite. Instead, siderite ± hematite is developed along magnetite cleavage planes and fractures and probably results from alteration of magnetite by a CO_2 - bearing fluid (Fig. 4.6d). Massive magnetite veins may be almost completely replaced by siderite dusted with fine grained relict magnetite inclusions (Fig. 4.6e).

The origin of rounded clots of hematite, chlorite, siderite and minor quartz, up to several millimetres across, is unclear. The clots may have developed from replacement of ferromagnesian phenocrysts or vesicles. However, the absence of phenocrysts or vesicles in similar felsic volcanics outside the hematite alteration zone suggests the clots are merely the result of sporadic nucleation of hematite, chlorite and siderite alteration.

4.6.2 Origin of the hematite alteration zone

The distribution of hematite alteration adjacent to the Great Lyell fault at Prince Lyell is similar, although much weaker, to that seen in the North Lyell area where massive hematite - barite - silica alteration crops out along the Great Lyell fault. This distribution strongly suggests that the hematite was deposited by fluids focussed by the Great Lyell fault and percolating into the volcanic pile. An immediately apparent source for an oxidised, iron - rich fluid is the adjacent hematitic Owen Conglomerate.

Walshe and Solomon (1981, Fig. 8) and Walshe (pers. comm.) indicate that hematite alteration in the stratigraphic footwall of the Prince Lyell orebody above zero R.L. is separated from the Great Lyell fault by a zone of only weak hematite development. The 'A' Lens horizon above zero R.L. appears not to have suffered significant hematite alteration. The apparent disparate occurrences of hematite alteration above and below zero R.L. may be explained by alteration by a fluid focussed along the Great Lyell fault below zero R.L. but channelled through a permeable layer in the footwall volcanic

orebody above zero R.L. is separated from the Great Lyell fault by a zone of only weak hematite development. The 'A' Lens horizon above zero R.L. appears not to have suffered significant hematite alteration. The apparent disparate occurrences of hematite alteration above and below zero R.L. may be explained by alteration by a fluid focussed along the Great Lyell fault below zero R.L. but channelled through a permeable layer in the footwall volcanic stratigraphy above zero R.L. A similar scenario may account for the development of hematite away from the Great Lyell fault at the Western Tharsis and Cape Horn orebodies (Walshe and Solomon, 1981).

The close relationships of the hematite alteration zone with the Great Lyell fault and Owen Conglomerate below zero R.L. suggest hematite alteration developed after the Cambrian period. However, Walshe and Solomon (1981) concluded that hematite was developed early during Cambrian volcanogenic mineralisation. This would imply that the association of the Great Lyell fault, Owen Conglomerate and hematite alteration in the Prince Lyell deeps is accidental and would necessitate oxidised iron being sourced from the volcanic pile.

Further microtextural evidence of the complex relationship between hematite and sulphides, notably the development of hematite after initial pyrite - chalcopyrite mineralisation, is presented in Chapter 5.

4.7 Copper, Gold, Silver and Pyrite Statistical Associations

4.7.1 Method and results

The statistical relationships of over 1300 six metre drill core assays of copper, gold, silver and pyrite content (recalculated from sulphur analyses) were analysed to gain an understanding of the associations of minerals and metals in the southern Prince Lyell mineralisation. The results are presented in Figure 4.7.

The correlation coefficients between copper and gold (Fig 4.7a) and between copper and silver (Fig. 4.7b) are the most obvious associations in the mineralisation. The correlation between copper and gold increases from 0.53 to 0.70 if the few high grade gold values are omitted. Gold values above 1.3 ppm are increasingly variable due to the nugget effect of high grade gold mineralisation.

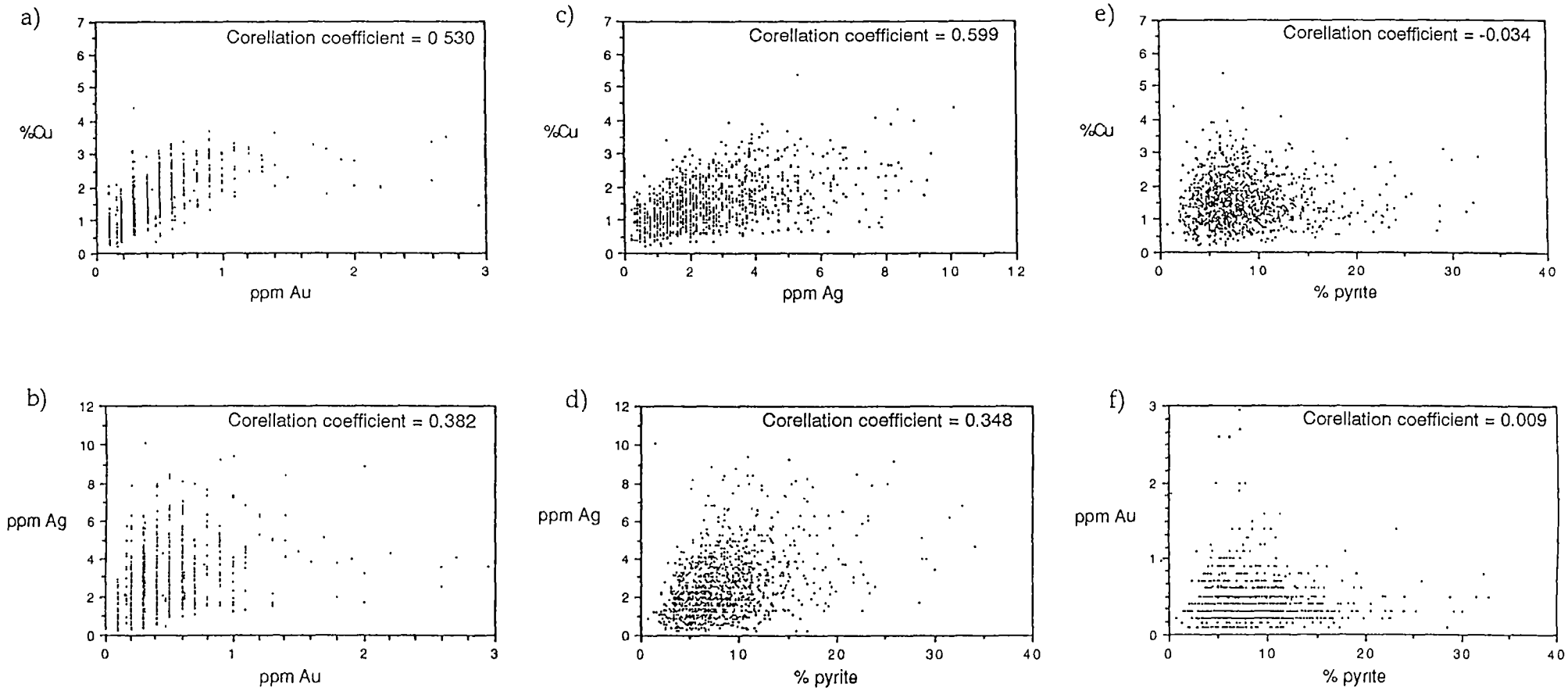

Figure 4.7 Graphs showing the relationships between copper, gold, silver and pyrite mineralisation at Prince Lyell. Pyrite has no significant correlation with any of the economic metals, suggesting possibly more than one phase of pyrite mineralisation. Correlations between copper, gold and silver suggest any remobilisation of ore minerals during metamorphism has not preferentially affected one metal significantly more than another.

4.7.2 Discussion

The sympathetic variation of gold and silver with copper suggests that they may have been associated with the same mineralisation event. Large *et al.* (1988) proposed that the correlation of copper and gold at Prince Lyell was due to chloride complexing of both metals in the hydrothermal fluid at relatively high temperatures (≥ 300°C), similar to other copper-rich volcanic-hosted sulphide deposits such as Mount Chalmers and Mount Morgan in Queensland.

Bird (1982) suggested that silver was more associated with pyrite mineralisation than copper and gold. However, pyrite mineralisation appears to have only a weak correlation with silver (Fig. 4.7d), and none with copper or gold (Fig. 4.7e, f). The poor correlation of pyrite with copper and precious metal mineralisation suggests that pyrite mineralisation has been affected by different depositional processes than copper, gold and silver. The addition or remobilisation of pyrite by late fluids after chalcopyrite mineralisation may account for the poor pyrite correlations.

4.7.3 The Au/Cu ratio

4.7.3.1 Data collection and analysis

The generally strong correlation of copper and gold at Prince Lyell provides a tool for examining variations in the distribution of metals in the orebody. Variations in the Au/Cu ratio within the orebody may indicate variations in conditions of mineralisation or later redistribution of either copper or gold during metamorphism. Remobilisation of copper from the Prince Lyell into higher grade orebodies such as the North Lyell may be reflected in variation of the Au/Cu ratio within the Prince Lyell orebody.

The distribution of Au/Cu ratios was investigated by calculating the average ratios of two metre drill core splits, in blocks of the orebody 60 metres long by 50 metres high, by M. Franks[2] using the Datamine® computer software at the Mt Lyell Mining and Railway Company (Table 4.1). As routine gold assays were not performed in areas of low grade copper mineralisation, Au/Cu ratios could generally only be calculated within areas of significant copper mineralisation (ie: approximately ≥ 1% Cu). The sample populations extracted from the computer database were not ideal, as copper was analysed in two metre splits and gold in six metre splits. The calculation of Au/Cu ratios

2. Mt Lyell Mining and Railway Company geologist

therefore assumed uniform distribution of gold across the entire six metres of each gold assay. Average Au/Cu ratios were not calculated in the deeper parts of the orebody (below -350m RL) which commonly contained only small numbers of gold assays.

RL	Section block					Total ratio for RL block
	67-68	69-70	71-72	73-74	75-76	
0m						
	0.29	0.34	0.33	0.33	0.29	0.31
	(369)	(297)	(172)	(162)	(22)	
-50m						
	0.43	0.35	0.36	0.33	0.36	0.34
	(250)	(210)	(177)	(255)	(37)	
-100m						
	0.31	0.28	0.34	0.49	0.28	0.34
	(244)	(192)	(174)	(173)	(52)	
-150m						
	0.31	0.27	0.26	0.36	0.22	0.29
	(195)	(282)	(185)	(229)	(60)	
-200m						
	0.30	0.24	0.26	0.32	0.37	0.28
	(329)	(250)	(237)	(195)	(46)	
-250m						
	0.31	0.26	0.30	0.35	0.27	0.30
	(200)	(126)	(215)	(109)	(26)	
-300m						
	0.31	0.36	0.28	0.25	0.47	0.30
	(82)	(41)	(99)	(50)	(36)	
-350m						
	0.25	***	0.22	***	***	0.24
	(70)		(39)			
-400m						

Table 4.1 Table representing a NW - SE longsection through the southern Prince Lyell orebody showing the distribution of the Au/Cu ratio (Au in ppm, Cu in %). Values shown are the averages of Au/Cu ratios from all analysed Au - Cu pairs within a block of the orebody 50 metres high and 60 metres along the section. Figures in parentheses are the number of analyses averaged for each block. (*** = insufficient data)

4.7.3.2 Results and discussion

The distribution of Au/Cu ratios is presented as a contoured long section plot of the copper orebody in Figure 4.8. There is no consistent variation in the Au/Cu ratio in the orebody either along strike or down dip. This contradicts Bird's (1982) conclusions (based on preliminary drilling results) that the Au/Cu ratio increased with depth in the orebody. A marked increase in the Au/Cu ratio occurs adjacent to a large body of stockwork magnetite mineralisation around Sections 73 and 74. A smaller increase in Au/Cu ratio also occurs on Section 67, also a site of significant magnetite mineralisation. As routine gold assays were not carried out in the copper - poor magnetite zones, gold levels within the magnetite mineralisation are poorly defined. The Au/Cu ratios refer mainly to the orebody adjacent to the magnetite zones.

Inspection of gold and copper assays adjacent to the magnetite body showed that the higher Au/Cu ratio around Section 73 is caused by a weak depletion in copper relative to gold in the areas immediately surrounding the magnetite mineralisation zones. Additional gold does not appear to have been introduced into the altered volcanics. Although both copper and gold are severely depleted within these zones, copper appears to have been remobilised marginally more, possibly by dissolution by the magnetite mineralisation fluids.

The lack of variation of the Au/Cu ratio on a larger scale either down-dip or along strike suggests that metamorphic fluids have not preferentially mobilised large volumes of either copper or gold. The grade of copper mineralisation also does not vary significantly with depth in the orebody, indicating that dissolution and redistribution of deep copper mineralisation has not occurred on a large scale during metamorphism.

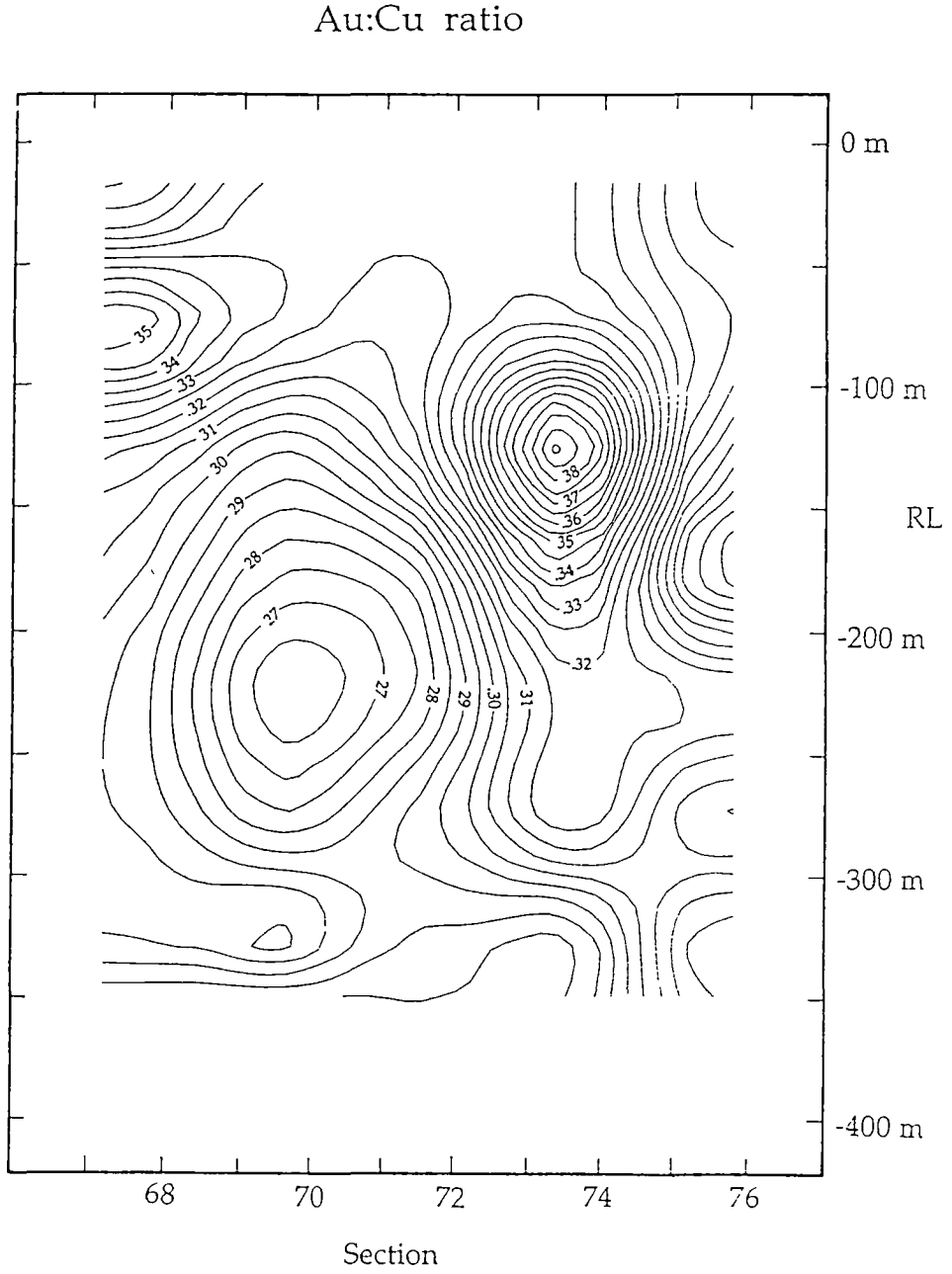

Figure 4.8 Contour plot of the Au/Cu ratio distribution presented in Table 4.1. The pronounced high around -120m RL and section 73 corresponds to the largest development of magnetite mineralisation in the Prince Lyell ore zone.

CHAPTER FIVE

DETAILED STUDIES OF PYRITE AND MAGNETITE MINERALISATION

5.1 PYRITE MINERALISATION

5.1.1 Introduction

Interpretation of Cambrian mineral paragenesis in the Mt Lyell field is often impossible due to the deformation or destruction of original mineral relationships during the major Devonian metamorphic event. Ductile sulphides such as chalcopyrite and sphalerite and silicate gangue minerals exhibit textures imparted by remobilisation and cleavage formation. Pyrite, on the other hand, is one of the few minerals in the Prince Lyell orebody which has not been entirely recrystallised. Although much of the pyrite has been deformed by brittle fracture, minimal movement of pyrite fragments has occurred and internal structures are preserved. As a result, pyrite is the only sulphide which preserves a record of pre-deformation sulphide paragenesis, in addition to subsequent mineralisation events.

5.1.2 Previous studies

Loftus-Hills and Solomon (1967) and Loftus-Hills (1968) were the first to investigate the geochemical characteristics of Prince Lyell pyrite in a regional study of the cobalt, nickel and selenium contents of western Tasmanian sulphides. Their work revealed contrasting trace element signatures of sulphides, especially pyrite, in a range of ore deposits and suggested that Cambrian volcanogenic and Devonian metamorphic deposits could be fingerprinted by their pyrite geochemistry. White (1975) also analysed trace elements in pyrite from the Mt Read Volcanics and associated ore deposits.

Walshe (1971, 1977) investigated cobalt and nickel abundances in pyrite from the Prince Lyell and other orebodies in the Mount Lyell field. A positive correlation between the cobalt content of pyrite and copper grade was established and thermodynamic modelling of pyrite mineralisation was attempted using trace element compositions. Walshe (1977) also noted some zoned pyrite and suggested that cobalt was not homogeneously distributed in pyrite.

The above mentioned works were carried out using wet chemical analyses of pyrite flotation separates. Analyses were not selective of any trace element variation within pyrite grains. As a result, many samples included multiple generations of geochemically distinct pyrite. The present study has sought to combine the results of previous work with a detailed investigation of pyrite paragenesis and the chemistry of individual growth stages.

5.1.3 Analytical methods

Polished sections of pyritic ore were etched for 30 to 60 seconds in a solution of sulphuric acid and $KMnO_4$ (modified after Ineson, 1989; Appendix 5.1) to highlight the internal structure of pyrite grains previously masked by the high polish imparted on reflected light sections.

Trace element analyses of pyrite generations were performed on a Cameca SX-50 electron microprobe at the Central Science Laboratories of the University of Tasmania under the supervision of Mr W. Jablonski. Although individual generations and growth zones of pyrite could be analysed in this way, detection limits were far higher than for the earlier bulk pyrite studies which employed wet chemical methods. Progressive modification of the operating conditions of the microprobe reduced detection limits for the majority of analyses to 100 ppm for Co, Ni and Cu; 150ppm for Ag; and 350 ppm for Zn and Se (Appendix 5.2).

Arsenic and lead in pyrite were also analysed on the electron probe but with very limited success. Corrections applied to the lead results were unable to correct for the large overlap of the sulphur K_α peak on the lead M_α peak at trace lead levels. The range of lead values obtained (~ 800 - 1600 ppm) was significantly higher than those obtained by wet chemical methods by Gulson and Porritt (1987) and were regarded as unreliable data. Arsenic results were affected by the overlap of the lead L_α peak on the arsenic K_α peak. However, the trace levels of lead in pyrite did not have the major affect on arsenic that sulphur had on lead. The lack of arsenic values below 300ppm strongly suggested that the lead overlap inflated the arsenic data by around 300 ppm. Consequently the arsenic data may be regarded as of semi-quantitative value only.

5.1.4 Background to pyrite trace element geochemistry

Trace elements occur in pyrite in isomorphous substitution for either iron or sulphur, or in discrete mineral inclusions and exsolutions (Fleischer, 1955). Of vital importance in interpreting the substitution of trace elements in

the pyrite structure is to establish that the trace elements are in solid solution and not included as foreign mineral inclusions. This may be done by comparison of stoichiometric ratios of substituting elements (Fleet *et al.*, 1988), x-ray diffraction analysis of the variation in pyrite lattice spacings (Riley, 1968), and detailed *in situ* analysis of trace element distribution.

Cobalt and nickel are the most common trace elements found in pyrite, exhibiting extensive isomorphous solid solution with iron (Fleischer, 1955; Hawley and Nichol, 1961; Riley, 1968). Both cobalt, and to a lesser extent nickel, are strongly chalcophile and are preferentially incorporated into the pyrite structure relative to iron (Springer *et al.*, 1964). Complete substitution of cobalt for iron (pyrite - cattierite series) is not achieved at temperatures below 700°C. However, up to 9 wt% Co can be accommodated in the pyrite structure at 400°C under equilibrium conditions (Klemm, 1962). Almost all ratios of Co:Ni:Fe occur in nature (Springer *et al.*, 1964). Brown and Bartholmé (1972) observed up to 20 wt% Co in Zambian copper belt pyrite. They suggested that such very high cobalt levels were metastable and the result of disequilibrium conditions during deposition.

The Co/Ni ratio in pyrite has been used by many authors as an empirical indicator of the environment of pyrite deposition. Although regarded by some as of dubious value to ore genesis interpretation (eg: Campbell and Ethier, 1984), Co/Ni ratios of less than one with a low standard deviation are accepted to represent pyrite of sedimentary origin. Low cobalt and nickel concentrations are also characteristic of such pyrite. Conversely, highly variable Co/Ni ratios, usually greater than one, are thought to be the result of hydrothermal mineralisation (Bralia *et al.*, 1979).

The isomorphous substitution of other metals for iron in pyrite is limited. Although copper and zinc both have ionic radii similar to iron, these elements are most commonly included in pyrite in discrete chalcopyrite and sphalerite inclusions (Bartholmé, *et al.*, 1971; Branov *et al.*, 1972). Branov *et al.* (1972) suggested that copper and zinc may enter the pyrite lattice in solid solution up to 630 and 170 ppm respectively. Mineral inclusions may be submicroscopic in size and in such cases may only be inferred by the presence of erratic microprobe analyses within single pyrite grains.

Elements such as arsenic, selenium and lead may substitute for sulphur in the pyrite lattice. Arseniferous pyrite is commonly associated with gold mineralisation (eg: Bradinskaya *et al.*, 1980; Fleet *et al.*, 1988). From experimental studies, Clark (1960) concluded that arsenic solid solution in pyrite was only of the order of 0.53 wt% As up to 600°C, but that arsenic was more commonly present as inclusions. However, more recently, Fleet *et al.* (1988) have recorded up to 8 wt% As in pyrite from three gold deposits in

Canada and South Africa. They regarded the arsenic to be incorporated in the pyrite as a metastable solid solution.

The amount of selenium substitution for sulphur in pyrite has been used as an empirical indicator of sedimentary and hydrothermal environments of deposition (Fleischer, 1955; Loftus-Hills and Solomon, 1967). Selenium solid solution in sulphides is largely controlled by depositional processes rather than availability (Loftus-Hills, 1968), and Suzuoki (1964) suggested that it was proportional to the temperature of deposition.

Lead and silver, like copper and zinc, exhibit only limited solid solution in the pyrite structure (Brett and Kellerud, 1967), and are more commonly found as inclusions and admixtures. Gulson and Porritt (1987) at Prince Lyell, and Ryall (1977) at Woodlawn, N.S.W., reported up to 800ppm Pb in pyrite, but Ryall regarded the highest levels to be due to galena inclusions in the pyrite. Branov *et al.* (1972) suggested a possible limit of 340 ppm Pb in solid solution in pyrite.

5.1.5 Internal structure of Prince Lyell pyrite

Etching of pyrite revealed a complex paragenesis of growth zoning, dissolution and multiple overgrowths within individual pyrite grains, not previously described (Fig. 5.1). As the rate of etching of pyrite is dependant on the crystallographic orientation of the etched surface (Ramdohr, 1969), different pyrite generations could not be correlated on the basis of the amount of pitting or the depth of etching in a given time (Fig 5.1a).

Composite pyrite grains commonly consist of a finely zoned core with corroded margins. Up to five subsequent generations of unzoned, anhedral to euhedral pyrite overgrowths can occur around the core, often separated by dissolution boundaries. Fine grained disseminated pyrite euhedra with no internal zoning or other structures are also common. Rarely, incremental widening of pyrite veins can be observed with symmetrical growth of pyrite generations along the edges of the veins. Rarely, healing of brecciated pyrite grains by later pyrite and growth of pyrite in pressure shadows has occurred. By far the majority of pyrite mineralisation is pre-tectonic, with many grains being fractured but not recrystallised by Devonian deformation.

Figure 5.1

Textures highlighted by etching of southern Prince Lyell pyrite mineralisation.

A. Reflected light photomicrograph of intergrown pyrite grains in a thin pyrite veinlet, illustrating the different responses of grains to the etching process which is dependent on the crystallographic orientation of the etched surface. The many small etching pits in the upper grain probably represent dislocations in the pyrite lattice (Ramdohr, 1969). The lower right grain is comprised of an inner core with a highly corroded rim and rich in cobalt and nickel (Pyrite I), overgrown by an inclusion-rich, anhedral, cobalt-poor generation of pyrite (Pyrite II). (sample 115003)

B. Reflected light photomicrograph of disseminated, partly corroded pyrite euhedra. Pyrite of this type (Pyrite II) typically contains very low levels of trace elements and displays no internal zoning. This sample is from the Great Lyell fault zone. (sample 639121.3)

C. Reflected light photomicrograph of multiple stages of pyrite growth in a fractured massive pyrite band. A relict corroded and zoned core (Pyrite I) is overgrown by an embayed euhedral pyrite and a later massive generation (both Pyrite II). The jigsaw fit of fractured pyrite fragments is a common feature of the brittle deformation style of pyrite at Prince Lyell. (sample 605050.2)

D. Reflected light photomicrograph of a strongly fractured pyrite grain which has been recemented by later post- or syn-deformational pyrite. Such textures are strong evidence for the remobilisation of pyrite during the Devonian. Fragments of other brecciated pyrite grains occur below and to the right of the recemented grain. (sample 636126.8)

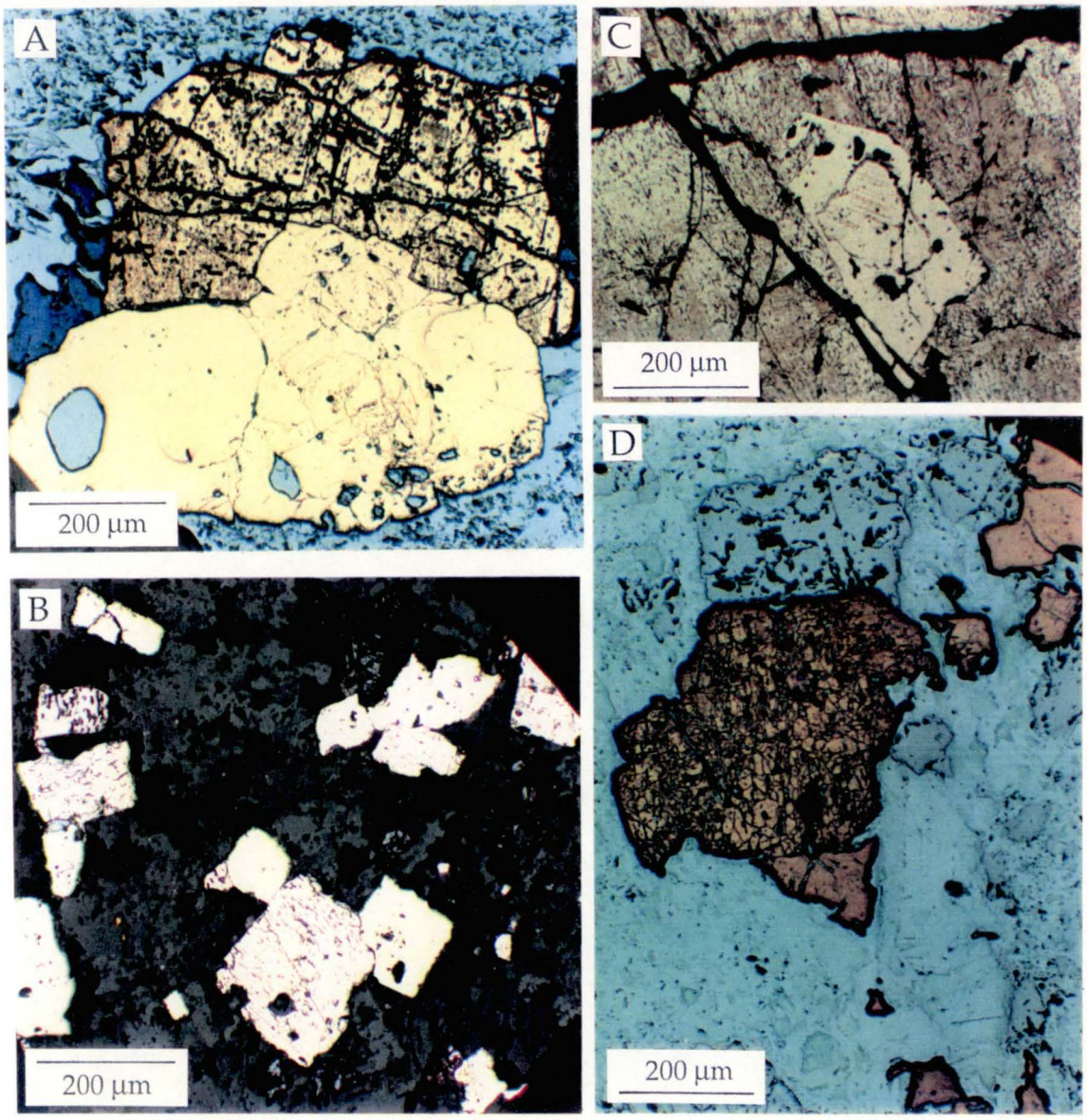
A
200 µm
C
200 µm
B
200 µm
D
200 µm

5.1.6 Trace element distribution in Prince Lyell pyrite

5.1.6.1 Copper, Zinc, Silver, Selenium and Arsenic

Trace element abundances for all pyrite microprobe analyses are shown in Figure 5.2. A table of analyses is given in Appendix 5.3. Most of the data for zinc, silver and selenium and a high proportion of the copper data were below the detection limits for this study. The distributions of zinc and copper above the detection limits were highly erratic. In most cases, these isolated high values were interpreted to be due to submicroscopic inclusions of sphalerite and chalcopyrite in the pyrite. However, highest zinc levels were recorded in pyrite from a sphalerite - barite vein (sample 605100.6) where it is probable that zinc has diffused into the pyrite lattice from the enclosing sphalerite.

Pyrite with levels of copper consistently above detection limits was observed only in one sample (626037.0). The host rock did not contain significant chalcopyrite mineralisation. The unusual pyrite composition may have been due to local high concentration of copper in the mineralising fluid, although not associated with the main chalcopyrite mineralisation event.

The lack of silver and selenium data above detection limits prevents a meaningful interpretation of their distribution. No rock samples contained pyrite with consistent levels above detection limits. As a result, no further consideration of these data will be given.

Pyrite containing high levels of arsenic was observed within a zone of silicification on Section 68. The pyrite contained up to 1% As, with levels of all other analysed trace elements below detection limits. The consistently high arsenic analyses within grains suggested that arsenic was contained in solid solution in the pyrite lattice and not as inclusions of arsenopyrite.

5.1.6.2 Cobalt and Nickel

Cobalt and nickel are by far the most abundant and useful trace elements for discerning chemically distinct generations of pyrite at Prince Lyell. These elements exhibited even distribution within growth zones and individual pyrite overgrowths, indicating their inclusion in the pyrite structure in solid solution rather than mineral inclusions. However, levels of cobalt and nickel do not show sympathetic variation (Fig. 5.3). The highly irregular relationship between the two elements indicates that equilibrium partitioning did not occur, due to undersaturation of one or both of the elements with respect to pyrite. This undersaturation meant that buffering of

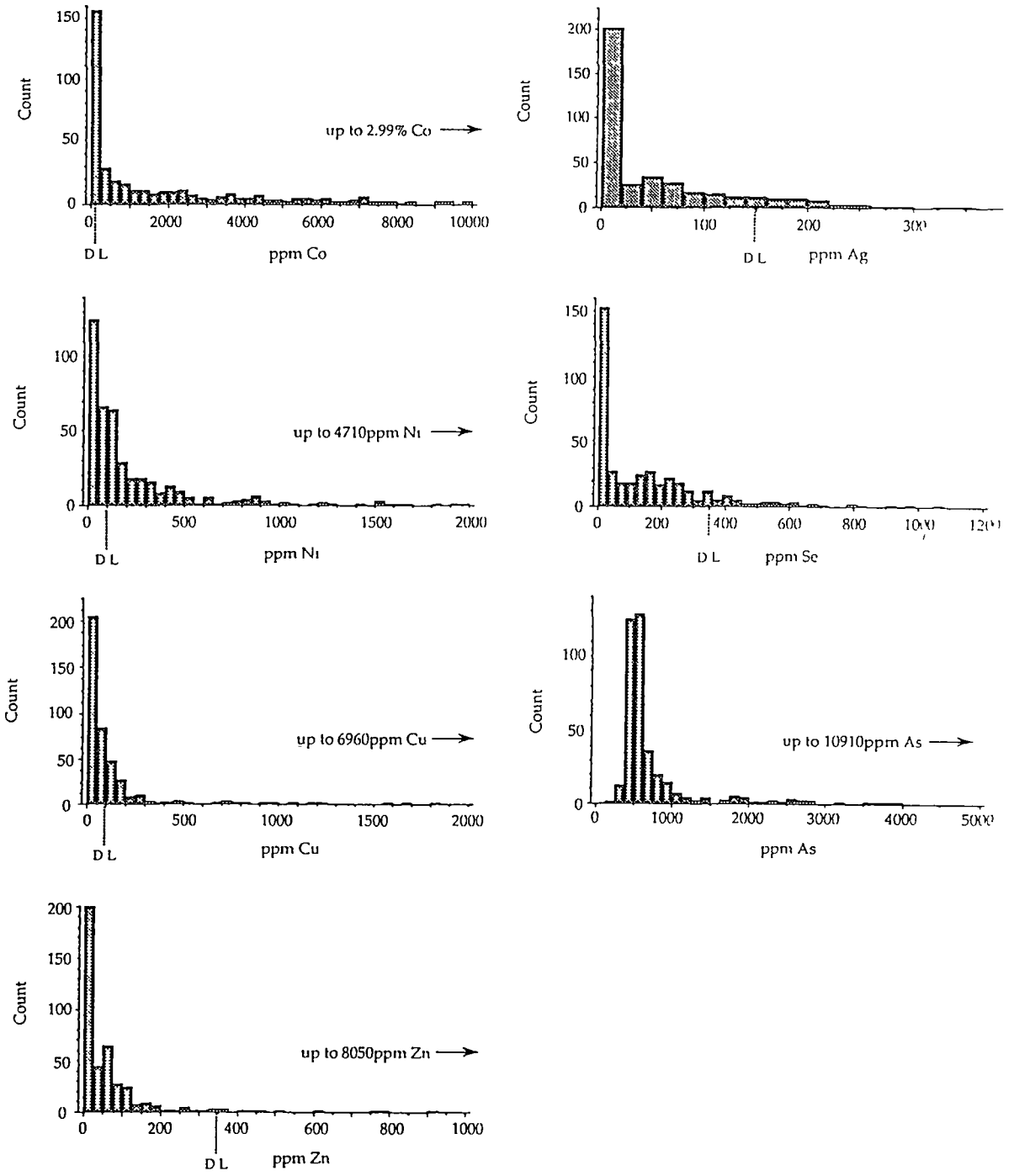

Figure 5.2 Distributions of trace elements in pyrite from the southern Prince Lyell area. A small number of erratic very high values are indicated in most histograms. Only cobalt and nickel have a significant number of analyses above the detection limits of the electron microprobe (D.L.). Interference of the lead and arsenic x-ray signatures has probably increased measured arsenic levels by around 300 ppm.

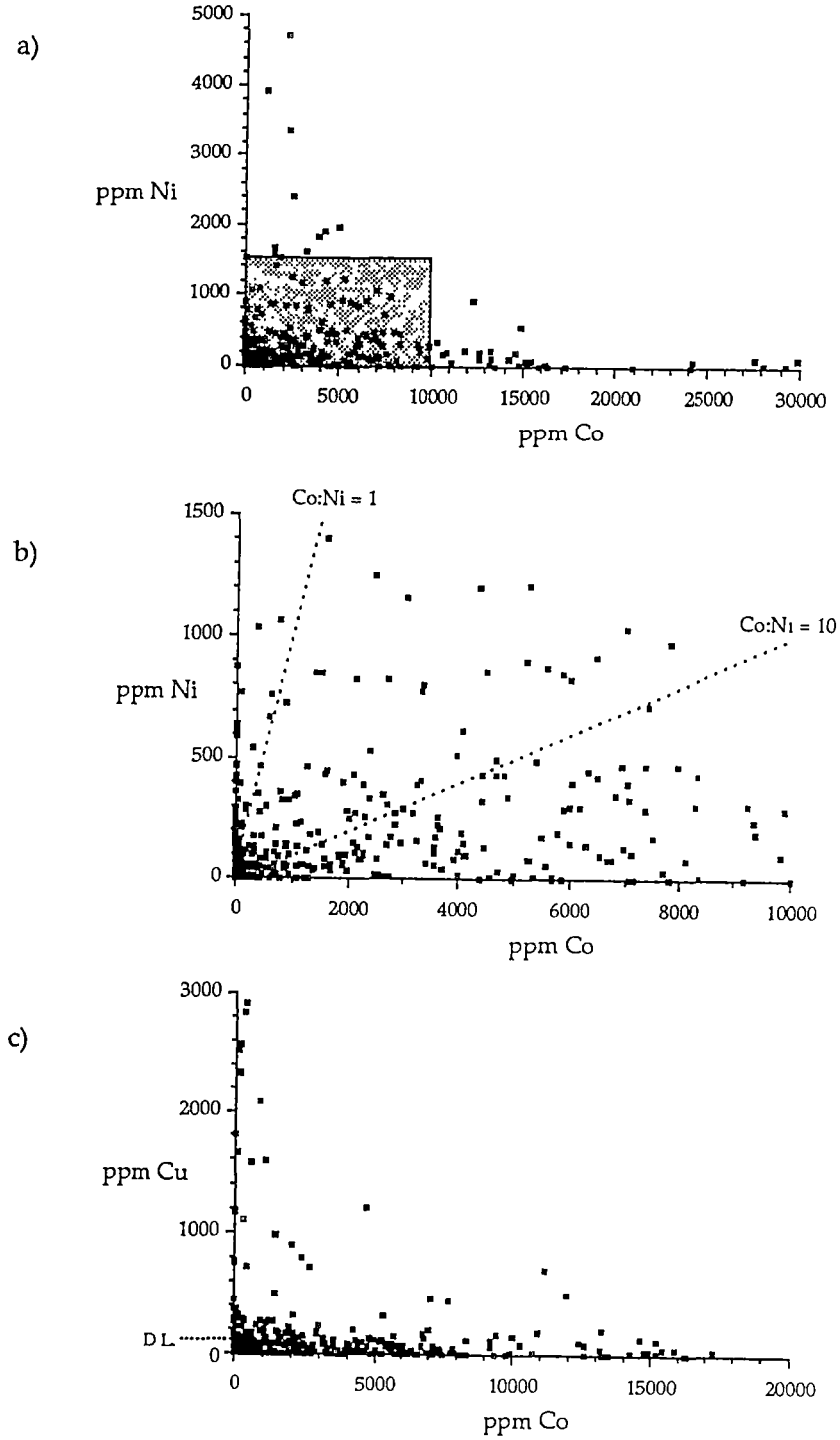

Figure 5.3 a) Plot of cobalt and nickel concentrations in all pyrite analyses.

b) Enlargement of the shaded area in a), illustrating the lack of correlation between cobalt and nickel levels in pyrite. Note that the majority of Co:Ni ratios are greater than one and are highly variable.

c) A poor correlation is also shown between cobalt and copper, an element more likely to be included in pyrite as minute mineral inclusions rather than in solid solution.

the cobalt and/or nickel concentration in the fluid could not take place, resulting in rapid variation of cobalt and nickel as new pulses of hydrothermal fluid were introduced or physiochemical conditions varied. Equilibrium concentrations of cobalt in pyrite under saturation conditions (~ 9% Co at 400°C; Klemm, 1962) would also be significantly higher than those observed at Prince Lyell.

Despite the poor correlation between the elements in solid solution, the concentration of cobalt, and to a lesser extent nickel, exhibits the most consistent relations of all the trace elements with different pyrite morphologies. As a result, three main groups of pyrite mineralisation have been defined on the basis of cobalt content and morphology and are described below.

5.1.7 Pyrite types

5.1.7.1 Pyrite I

Pyrite I, forming the cores of many pyrite grains, exhibits concentric idiomorphic growth zoning (Fig. 5.4, 5.5). Individual growth zones may be as narrow as 0.5 μm. The margins of Pyrite I are characteristically corroded and euhedral outlines are very rarely preserved. Grains which show only a small degree of dissolution have complex finely zoned cores followed by simpler wider growth zones nearer the margins.

The zoning is oscillatory and contains cobalt at levels generally between 1000 and 10,000 ppm, although some zones may have as low as 300-500 ppm cobalt. In the few specimens observed where the outer, wider zones have not been corroded, there is a poorly defined trend towards lower cobalt values in the outer zones. Nickel concentrations in Pyrite I are variable, ranging from below detection limits (<100 ppm) to almost 5000 ppm. They exhibit no correlation with accompanying cobalt levels (Fig. 5.3). The majority of Pyrite I contains very little arsenic. Elevated arsenic levels were observed in some inner zones of Pyrite I which were also very high in cobalt, however, no overall correlation of arsenic and cobalt was observed.

Pyrite I rarely contains small inclusions of pyrite with very high cobalt levels, up to 3% cobalt. These inclusions are the remnants of a very early stage of cobaltiferous pyrite mineralisation which has been almost entirely corroded away by later fluids. Pyrite I is usually free of gangue mineral inclusions. However, gangue inclusions do occur clustered around the margins of Pyrite I cores within later pyrite overgrowths.

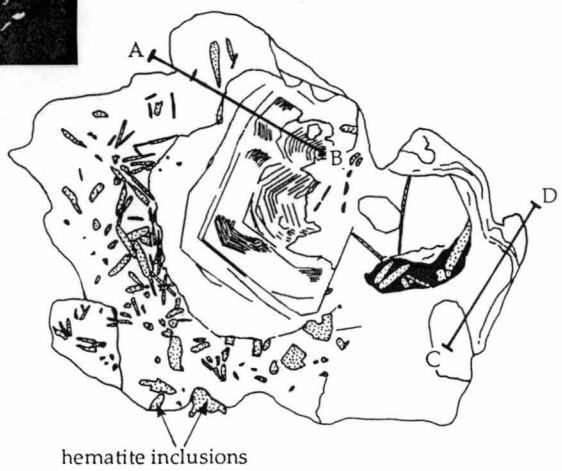

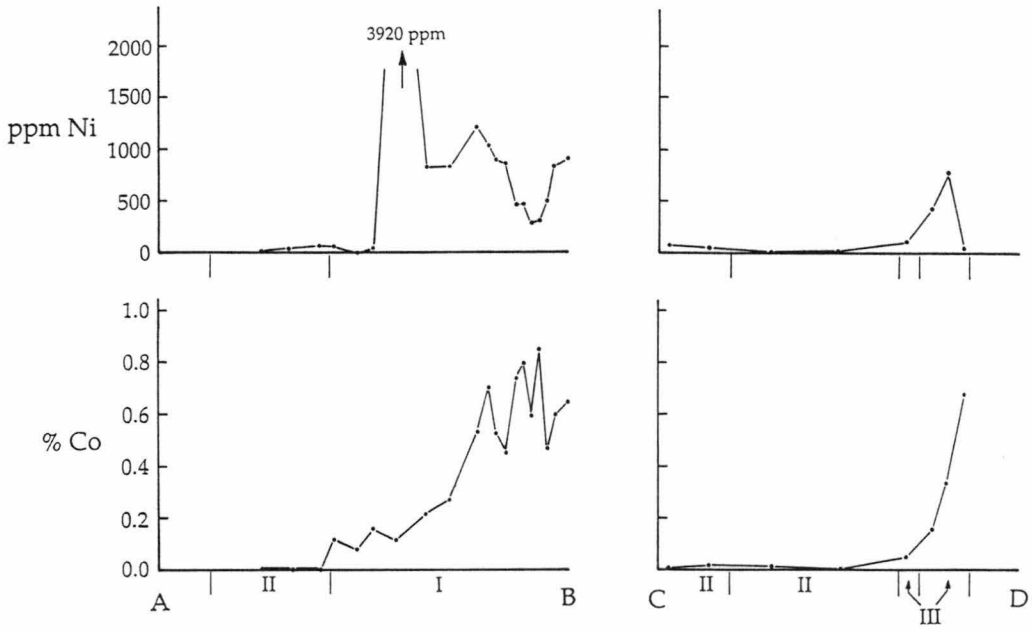

Figure 5.4 Distribution of cobalt and nickel from two electron microprobe traverses across a complex pyrite grain (sample 599377.3). Corroded, oscillatory zoned Pyrite I (at B) is overgrown by anhedral Pyrite II (at A and C) containing hematite inclusions. Thin overgrowths of cobalt-rich Pyrite III occur around Pyrite I and II.

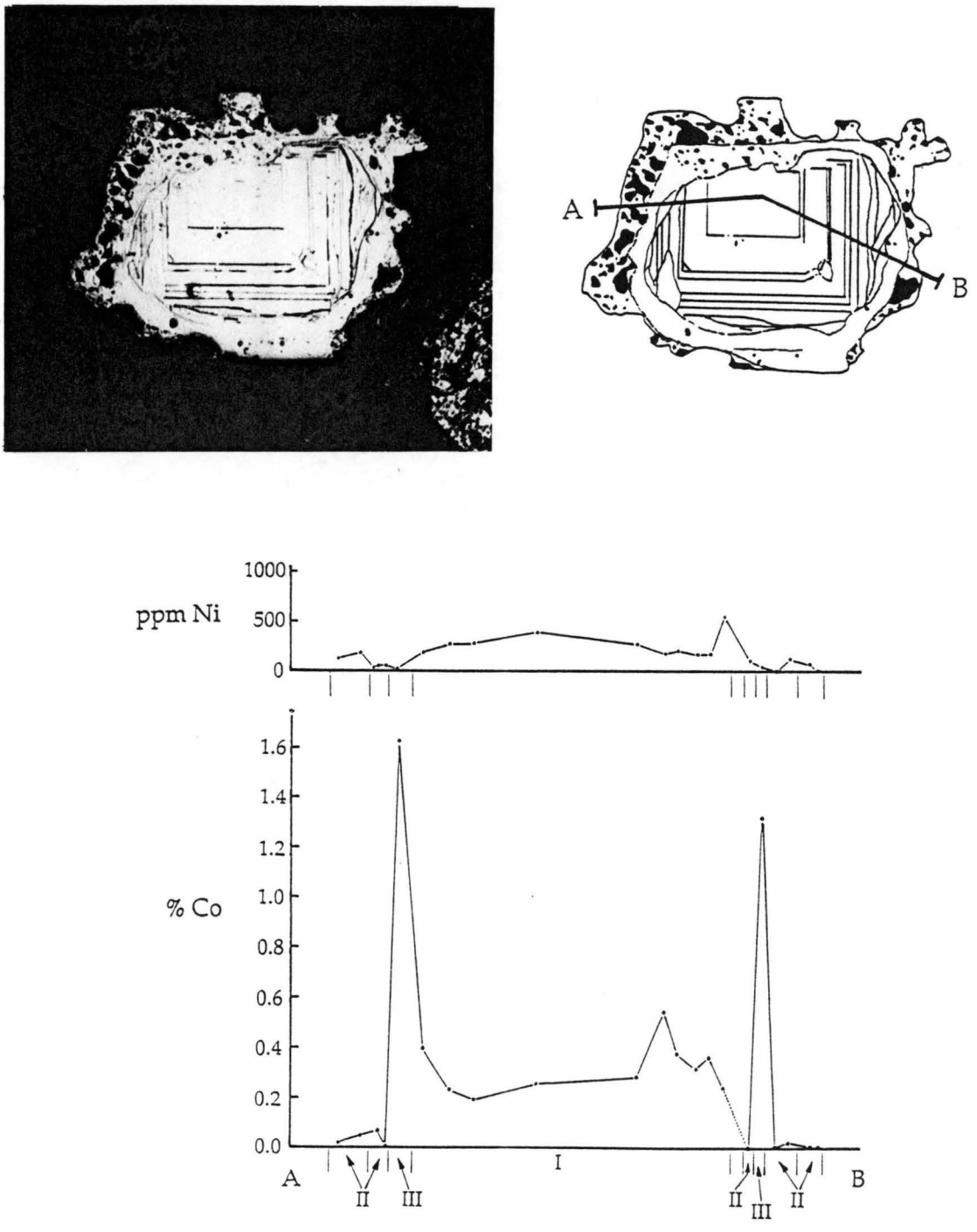

Figure 5.5 Distribution of cobalt and nickel from an electron microprobe traverse across a complex pyrite grain (sample 618051.0). Etching has revealed at least five generations of pyrite mineralisation in the grain, with dissolution along corroded margins between each generation.

The absence of hematite inclusions in Pyrite I, but their common occurrence around Pyrite I grain margins, indicates that Pyrite I was an earlier phase of mineralisation than hematite. This is in contrast to Walshe and Solomon's (1981) suggestion that the bulk of hematite alteration was an early pre-sulphide phase.

5.1.7.2 Pyrite II

The term "Pyrite II" does not refer to a single generation of pyrite mineralisation as several overgrowths of Pyrite II may occur within a single composite pyrite grain (Fig. 5.4, 5.5). Pyrite II does not have internal zoning and typically contains cobalt and nickel at levels below the detection limits for this study (<100 ppm). Pyrite II is volumetrically the most common type of pyrite in the southern Prince Lyell mineralisation.

Pyrite II forms euhedral to anhedral overgrowths on Pyrite I cores and discrete disseminated pyrite euhedra (Fig 5.1b), with varying degrees of dissolution around its margins. No evidence was observed of any Pyrite II predating Pyrite I. Fractured grains of Pyrite II occur where previously continuous veinlets have been dismembered by extension along the Devonian cleavage. Distinct generations of Pyrite II may be defined by etching or by lines of inclusions aligned along overgrowth boundaries (Fig. 5.4, 5.5). Pyrite II contains all types of gangue mineral inclusions, including quartz, sericite, chlorite, siderite, apatite, magnetite, hematite, monazite, rutile and a calcium alumino-silicate, tentatively identified as epidote. Inclusions of sphalerite and galena were also observed in samples of Pyrite II from the Great Lyell fault zone.

5.1.7.3 Pyrite III

Pyrite III is a small but important pyrite population at Prince Lyell. It occurs as thin unzoned, anhedral overgrowths on Pyrite I and II, and minor veinlets. It typically contains cobalt above 5000 ppm, but rarely as low as 500 ppm (Fig. 5.4, 5.5). As with all the cobaltiferous pyrite at Prince Lyell, nickel contents are variable, ranging from < 100 to 800 ppm. Repeated thin rims of Pyrite II and Pyrite III may overgrow each other within a single pyrite grain, illustrating the highly variable trace element chemistry of the mineralising fluids.

A variation of Pyrite III was found in one sample from sheared volcanics in the Great Lyell fault zone (sample 639121.3). Disseminated euhedra contained high levels of nickel but no cobalt. Although the chemical

characteristics of this pyrite were similar to Pyrite III, its morphology was that of Pyrite II euhedra.

5.1.8 Metamorphic effects

Homogenisation of compositional zoning in pyrite occurs by the diffusion of trace elements such as cobalt and nickel under moderate to high metamorphic temperatures and pressures (Brown and Bartholmé, 1972). Although Rose (1967) regarded the process of solid diffusion in sulphides as ineffective, the diffusion of trace elements in pyrite is generally well documented. However, the interpretation of the effects of metamorphism on trace element distribution varies.

Roscoe (1965) noted that trace element levels in pyrite from the Matagami district of Canada, which has been subjected to upper greenschist metamorphism, were less erratic than those of the weakly metamorphosed Noranda district. He suggested that the trace element distribution of Matagami pyrites had been homogenised during metamorphic recrystallisation. Cambel and Jarkovsky (1966) observed that the cobalt content of pyrite increased and the nickel content decreased with increasing metamorphic grade in pyritic ores from Czechoslovakia. Loftus-Hills (1968) suggested that this could represent equilibrium partitioning of cobalt into and nickel out of the pyrite structure during metamorphism.

On the other hand, Itoh (1973) observed that cobalt was expelled from pyrite towards the margins of grains in southern Honshu ore deposits subjected to lower amphibolite grade metamorphism. Carrollite ($CuCo_2S_4$) can be formed at the edges of pyrite grains as a result of the metamorphic reaction of chalcopyrite with cobalt expelled from the pyrite structure (Brown and Bartholmé, 1972; Itoh, 1973). The same process of cobalt redistribution may account for the cobalt-rich rims found in some Zambian copper belt pyrites (Bartholmé *et al.*, 1971).

Under metamorphic conditions of lower - middle greenschist facies or less, primary compositional heterogeneities in pyrite appear to be preserved (Brown and Bartholmé, 1972; Itoh, 1973; Fleet *et al.*, 1988). However, an increase in the Co/Ni ratio of pyrite with increasing grade of metamorphism in the Japanese deposits suggests that nickel is more easily diffused from the pyrite structure during metamorphism (Itoh, 1973).

No diffuse zoning of trace elements was observed in Prince Lyell pyrites (Fig. 5.4, 5.5), although the behaviour of trace elements at very low levels (< 100 ppm) could not be examined. The lower greenschist metamorphic grade and the sharply defined compositional boundaries within Prince Lyell

pyrite imply that redistribution of trace elements in pyrite has not occurred during Devonian metamorphism.

However, in a study of the West Lyell pyritic ores, Loftus-Hills (1968) noted that pyrite from remobilised quartz veins of Devonian age contained far less cobalt and marginally less nickel than pyrite from the mineralised volcanics (Fig. 5.6). The depletion of cobalt and nickel in associated chalcopyrite was more poorly defined. As the ductile chalcopyrite has been highly deformed during Devonian deformation, redistribution of cobalt and nickel in the disseminated chalcopyrite mineralisation is likely prior to remobilisation into the quartz veins. This may account for the small difference between disseminated and vein chalcopyrite.

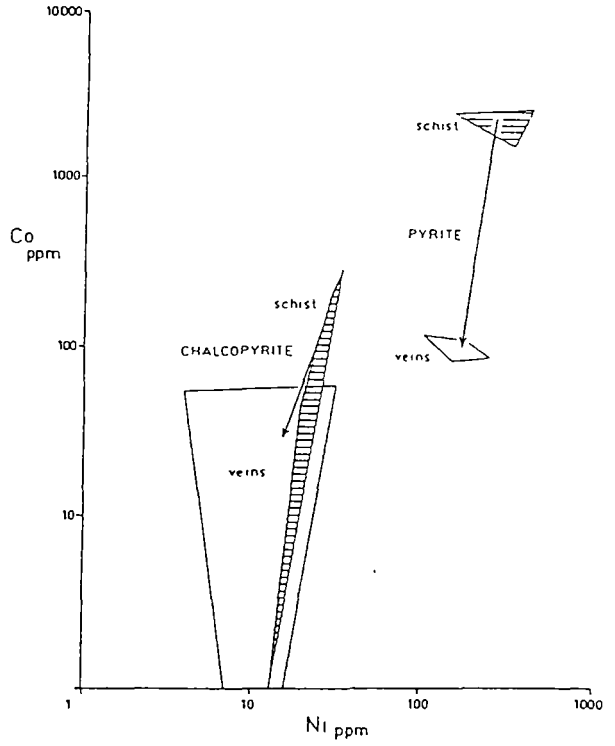

Figure 5.6 Depletion of cobalt, and to a lesser extent nickel, in pyrite and chalcopyrite remobilised from the altered volcanics (schist) into Devonian metamorphic quartz veins (from Loftus-Hills, 1968).

5.1.9 Trace element geothermometry

The extent of cobalt and nickel solid solution in the pyrite structure is temperature dependent (Klemm, 1962; Springer *et al.*, 1964). However, if the trace elements are undersaturated with respect to the host pyrite, the fundamental availability of the elements in the ore fluid will probably have a controlling influence on the concentration of the elements in the pyrite (Fleischer, 1955; Barton, 1970). Unlike the sphalerite geothermometer, for which the minor element iron is commonly in excess, the pyrite geothermometer is severely limited in its use by the typically undersaturated concentrations of cobalt and nickel in ore fluids (Fleischer, 1955). It has been demonstrated earlier that both cobalt and nickel were probably undersaturated with respect to pyrite in the Prince Lyell ore fluid. Thus, thermodynamic calculations based on equilibrium partitioning of cobalt and nickel into pyrite (eg: Walshe, 1977), may be affected more by the varying composition of the fluid than by physiochemical conditions.

Attempts to establish partitioning relationships of trace elements between coexisting sulphides have met with limited success (Rose, 1967; Gosh-Dastidar *et al.*, 1970), due to problems with establishing equilibrium at the time of deposition. However, Bezmen *et al.* (1978) reported that below 1 wt% Co in pyrite and chalcopyrite, temperature was the main controlling factor on partitioning of cobalt between the two minerals. The application of such a two-mineral geothermometer is dependent on equilibrium between the two phases at the time of deposition and does not require saturation levels of the trace element in the fluid.

The partitioning of cobalt between pyrite and chalcopyrite is governed by the reaction:

$$CuFeS_2 + CoS_2 \rightarrow FeS_2 + CuCoS_2 \qquad (1)$$

Bezmen *et al.* (1978) concluded that cobalt partitioning was related to temperature by the equation:

$$T\,(K) = 100 / [1.2921 \log K_D^{ccp\text{-}py} + 2.382] \qquad (2)$$

and considered that for practical purposes, a simplified formula for the cobalt distribution factor, $K_D^{ccp\text{-}py}$, could be used in temperature calculations:

$$K_D^{ccp\text{-}py} = (\%Co_{ccp} / \%Co_{py}) \times 1.53 \qquad (3)$$

Measurements of cobalt concentrations in chalcopyrite using the electron microprobe were below detection limits of the instrument. In their place, cobalt levels in Prince Lyell chalcopyrite from Loftus-Hills (1968) and Walshe (1977) were used for comparison with Pyrite I cobalt concentrations. Cobalt concentrations in chalcopyrite from these studies ranged from 1 to 135 ppm with one outrider of 465 ppm Co.

At 250 - 300°C, the calculated Co_{ccp}/Co_{py} ratio ranges from 0.28 to 0.21 (from equations 2 and 3). Thus, chalcopyrite deposited in equilibrium with Pyrite I (1000 - 10,000 ppm Co) would be expected to contain approximately 250 - 2500 ppm Co. Only one chalcopyrite analysis falls within this range, with the majority of cobalt analyses requiring unrealistic temperatures of formation.

These results suggest that Pyrite I and chalcopyrite did not form in equilibrium; a fact supported by sulphur isotope partitioning described in Chapter 7. If Pyrite I and chalcopyrite did precipitate under equilibrium conditions, then *in situ* impoverishment of cobalt in chalcopyrite may have occurred during metamorphism, in contrast to the more chemically resistant pyrite.

5.1.10 Discussion of pyrite paragenesis

5.1.10.1 Cambrian volcanogenic mineralisation

The volcanogenic association of cobaltiferous pyrite in western Tasmania was established by Loftus-Hills (1968). Green *et al.* (1981) also noted a zone of cobaltiferous pyrite in altered footwall volcanics of the Rosebery massive sulphide deposit and interpreted it as a feeder for volcanogenic hydrothermal fluids. These associations strongly suggest a volcanogenic origin for Pyrite I and III (Fig. 5.7). It is supported by the highly variable Co/Ni ratios of Prince Lyell cobaltiferous pyrite which are generally greater than one (Fig. 5.3) - typical of volcanogenic pyrite mineralisation. Bogush (1983) regarded compositional zoning as displayed by Pyrite I to be uncharacteristic of pyrite of metamorphic origin. Fluctuations in fluid chemistry may not be expected from a regional metamorphic fluid which has evolved in equilibrium with the host rocks.

A correlation of cobaltiferous pyrite with copper mineralisation at Prince Lyell (Fig. 5.8) was established by Walshe (1977). This correlation is consistent with numerous studies in Tasmania and world-wide which have documented the association of cobaltiferous pyrite with copper mineralisation of varying origins (eg: Loftus-Hills, 1968; Bartholmé *et al.*, 1971; Itoh, 1973). Although at Prince Lyell petrographic evidence linking any pyrite generation

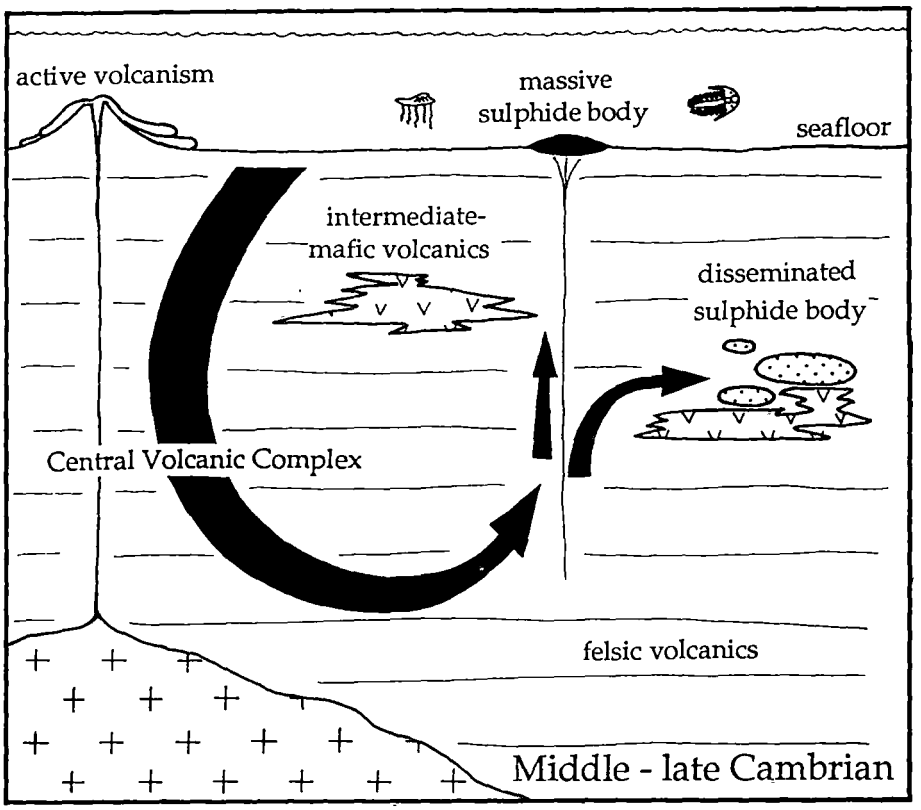

Figure 5.7 Schematic representation of the initial Cambrian volcanogenic stage of mineralisation in the Mt Lyell field.

At Prince Lyell, circulating heated seawater deposited disseminated Pyrite I and chalcopyrite by replacement of favourable subsurface horizons, having derived metals from the volcanic pile. Similar fluids may have deposited massive sulphide mineralisation at the seafloor.

to chalcopyrite mineralisation is lacking due to metamorphic remobilisation of chalcopyrite, the geochemical correlation of cobaltiferous pyrite and copper grade strongly suggests chalcopyrite was deposited with cobaltiferous pyrite.

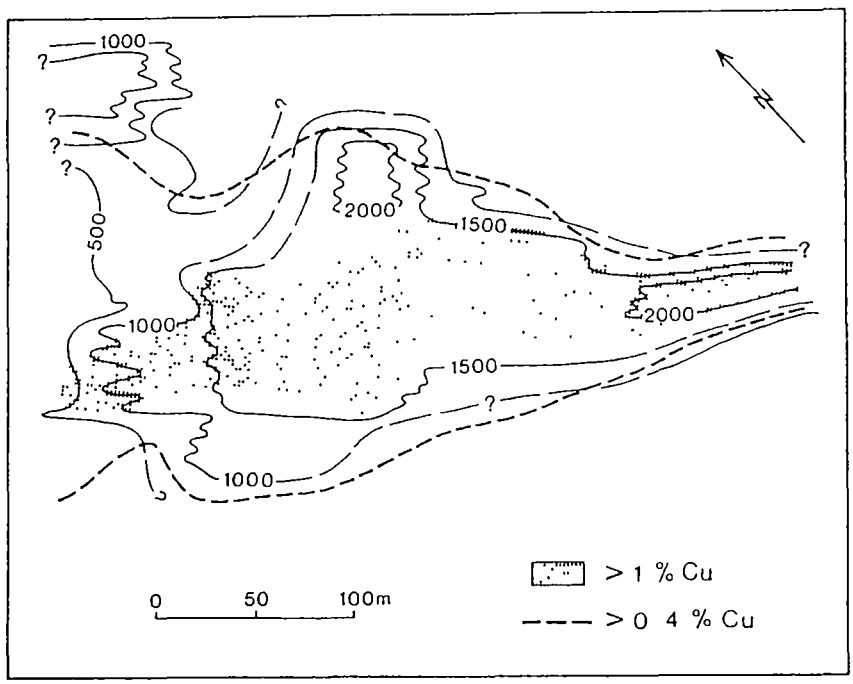

Figure 5.8 Contours of cobalt concentration (ppm) in bulk pyrite samples from the 830' Level at Prince Lyell, shown in relation to copper mineralisation (from Walshe and Solomon, 1981).

The fine scale oscillatory zoning of Pyrite I is most probably due to variations in physiochemical conditions of the hydrothermal fluid during mineralisation. Cobalt concentration in pyrite varies with temperature, pH and fO_2 (Klemm, 1962, Walshe, 1977). Thus the fine scale compositional zoning displayed by Pyrite I may reflect fluctuations in fluid temperature, or pH and fO_2 due to fluid - host rock interaction.

If the cobalt - poor Pyrite II is also of Cambrian volcanogenic origin, it marks a phase of mineralisation probably not associated with chalcopyrite mineralisation. The timing of this phase of pyrite mineralisation is in contrast to that proposed by Walshe (1977) which suggested deposition of cobalt - poor pyrite followed by cobalt - rich pyrite in response to a drop in fO_2 and increase in pH and a move into the chalcopyrite stability field.

Pyrite II may have been deposited due to a significant drop in temperature or pH, resulting in a lesser amount of cobalt partitioning into pyrite. However, it is more probable that the major compositional change

between Pyrite I and II was due to a decrease in the absolute concentration of cobalt (and probably copper) in the fluid (Fleischer, 1950; Loftus-Hills, 1968; Barton, 1970). This may have reflected a decrease in temperature or salinity which suppressed the solubility of metals such as cobalt and copper in the hydrothermal fluid. Alternatively, it may reflect the influx of a poorly mineralised volcanogenic fluid deriving little copper and cobalt from an already strongly leached volcanic pile. Sporadic recharging of the fluid or temperature increases may have resulted in the deposition of cobaltiferous Pyrite III.

5.1.10.2 Devonian metamorphic mineralisation scenario

The close association of hematite alteration in the footwall of Prince Lyell and the Great Lyell fault suggests that hematite may well have been deposited by an oxidised Devonian metamorphic fluid emanating from the Owen Conglomerate. This scenario (Fig. 5.9) would also imply that Pyrite II and III, which enclose hematite, are of metamorphic origin. The association of cobalt - poor pyrite with Devonian mineralisation and granitoids in western Tasmania (Loftus-Hills, 1968) also suggests that Pyrite II may be of Devonian metamorphic origin.

There is ample evidence of dissolution of early volcanogenic pyrite to provide a source for Devonian pyrite. Corrosion and remobilisation of Cambrian pyrite during metamorphism would probably have resulted in the redistribution of trace elements out of pyrite and the redeposition of cobalt-poor pyrite. This scenario is suggested by the lack of cobaltiferous pyrite in Devonian metamorphic mineralisation elsewhere in western Tasmania.

However, the repeated overgrowths of Pyrite II and Pyrite III in some pyrite grains during metamorphism would require the deposition of both cobaltiferous and cobalt-poor pyrite from the metamorphic fluid. This could have resulted from local concentrations of remobilised cobalt occurring in the metamorphic fluid, but it would oppose the trend of cobalt depletion observed in Devonian sulphide mineralisation (Fig. 5.6). The presence of nickel-rich pyrite euhedra in the Great Lyell fault zone may also represent a local concentration of remobilised nickel in the metamorphic fluid.

5.1.10.3 Early Ordovician mineralisation scenario

In the Cambrian mineralisation scenario, hematite alteration in the stratigraphic hangingwall would have been deposited from an oxidised fluid derived from the volcanic pile. However, the paragenetic relationship

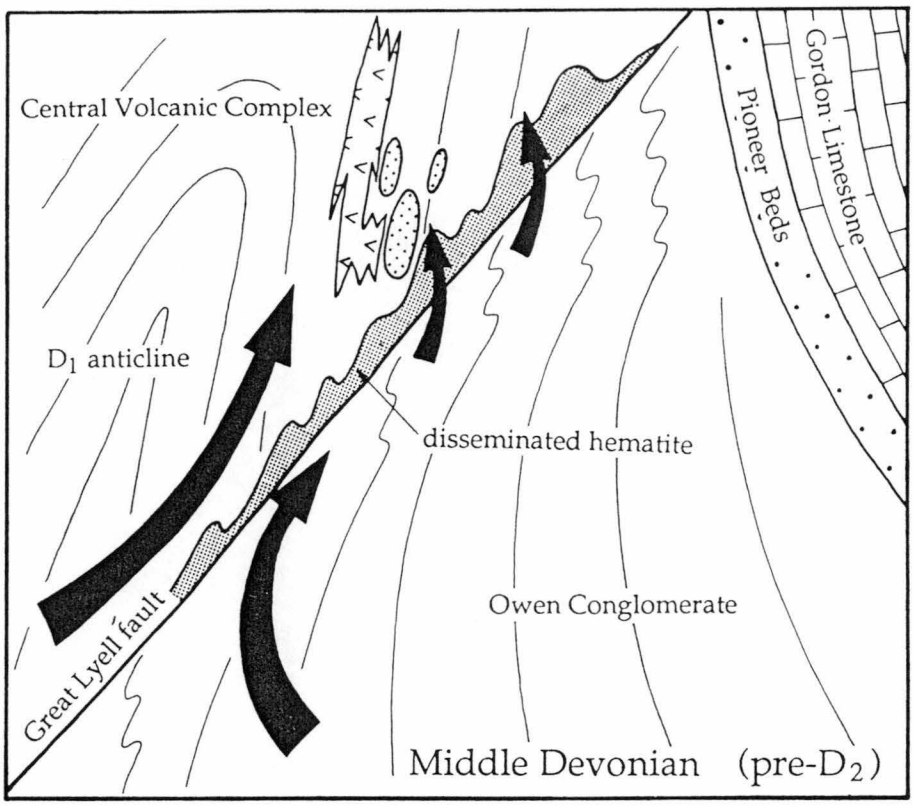

Figure 5.9 Schematic diagram of a Devonian metamorphic scenario for the deposition of Pyrite II and III at Prince Lyell.

During the Devonian metamorphic event, prior to D_2 cleavage formation, metamorphic fluids derived from the relatively oxidised Owen Conglomerate migrated across the Great Lyell fault, depositing disseminated hematite close to the volcanics contact.

Meanwhile, Pyrite I was dissolved by metamorphic fluids and reprecipitated as Pyrite II, enclosing hematite laths in footwall regions of the orebody. Cobalt expelled from the dissolved pyrite was locally concentrated in small amounts of cobalt-rich Pyrite III.

between hematite and pyrite may be explained by considering that the last stages of volcanic activity were active during deposition of the Owen Conglomerate in the early Ordovician. In this scenario (Fig 5.10), an unmineralised Owen Conglomerate formation water was introduced into the hydrothermal system across the Great Lyell fault which formed the western growth - faulted margin of the sedimentary basin.

It must also be considered that the small amount of volcanic detritus in the Owen Conglomerate suggests that volcanic activity had finished by the time sedimentation commenced. This may indicate that volcanic activity was restricted only to circulation of fluids through the volcanic pile heated by cooling subvolcanic plutons [1].

An oxidised connate fluid, derived from dewatering of the compacting hematitic Owen Conglomerate, may have migrated across the fault into the reduced environment of the altered pyritic volcanics. The reactive, sulphur-poor fluid dissolved pre-existing volcanogenic pyrite and deposited hematite in response to the abrupt redox change. It is unlikely that the two fluids mixed or that Pyrite II or III was deposited from an oxidised formation water. Sulphur isotope ratios of all generations of Prince Lyell pyrite are similar (5.6 - 11.1‰, see Section 7.3), and there is no evidence of very low or negative $\delta^{34}S$ values which may expected of pyrite deposited in equilibrium with hematite (Ohmoto and Rye, 1979). However, if their was only a minor influx of oxidised fluid relative to the volcanogenic fluid, it is possible that under essentially closed system conditions, the oxidised fluid may have locally dissolved and reprecipitated Pyrite I as Pyrite II with similar $\delta^{34}S$ ratios (J.L. Walshe pers. comm.).

Given that pyrite and hematite are unlikely to have been deposited in equilibrium, it is somewhat surprising that no evidence of pyrite replacing hematite was found in this study. Although Walshe (1977) and Walshe and Solomon (1981) documented apparent pyrite replacement of hematite in the upper parts of the Prince Lyell orebody, the present study only observed Pyrite II and III rimming or including hematite with no evidence of reaction between the two minerals.

---

1. The notion of Cambrian volcanism and hydrothermal activity continuing into the early Ordovician has been suggested by several authors (Jago *et al*, 1977; Sillitoe, 1985; Bird, 1985; Berry, 1990b). However, Sillitoe (1985) noted that if observed alteration of the Owen Conglomerate were of volcanogenic origin, it would require very rapid accumulation of the conglomerate in the typical life time of a hydrothermal system (~ 2 - 3 million years).

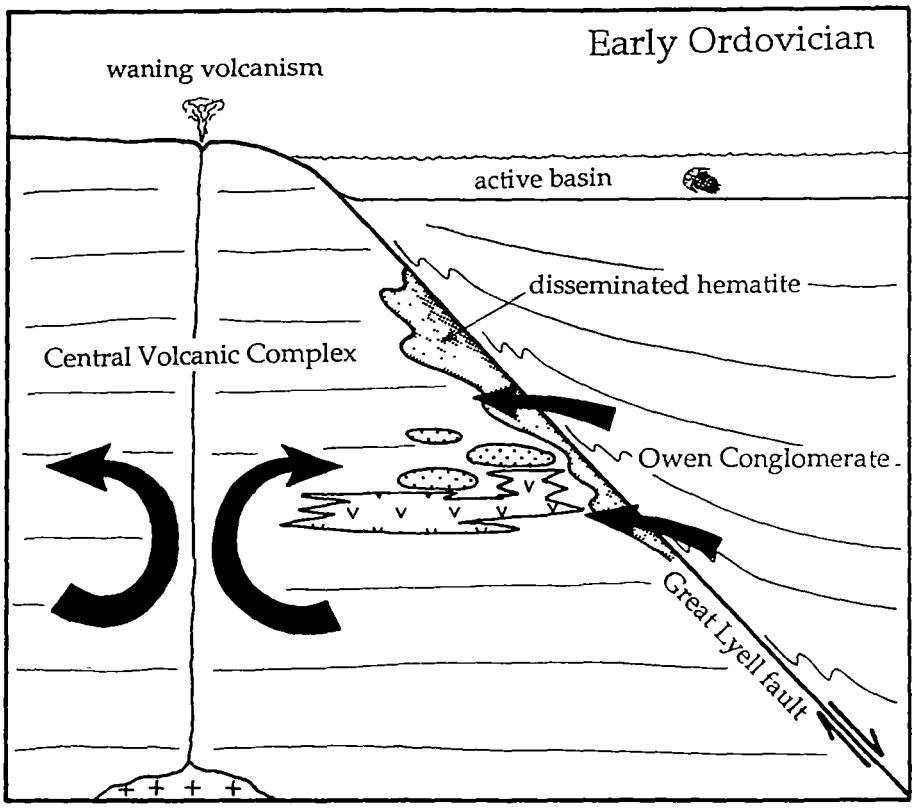

Figure 5.10 Schematic diagram of an early Ordovician scenario for the deposition of Pyrite II and III at Prince Lyell.

In the latest Cambrian and early Ordovician period, development of the Owen basin proceeded during the last stages of volcanism in the Mt Read Volcanics. The Great Lyell fault acted as an active growth fault margin.

Oxidised fluids from dewatering of the Owen Conglomerate migrated across the basin margin into the more reduced volcanic pile, depositing disseminated hematite near the contact.

Volcanogenic fluids circulating in the volcanic pile dissolved Pyrite I and deposited cobalt - poor Pyrite II with minor amounts of cobaltiferous Pyrite III.

5.1.11 Conclusions

It is most likely that the zoned, cobalt-rich Pyrite I is of Cambrian volcanogenic origin and is closely associated with chalcopyrite mineralisation at Prince Lyell. However, the origins of later pyrite overgrowths, Pyrite II and III, are not certain. The relict Cambrian pyrite cores and similar sulphur isotope signatures of all Prince Lyell pyrite (see Chapter 7) strongly suggest that sulphur for Pyrite II and III mineralisation was locally derived from pre-existing sulphides. The predominance of cobalt-poor pyrite at Prince Lyell and throughout the altered volcanics and deposits of the Mt Lyell field (Walshe, 1977 and pers. comm.) suggests the involvement of large volumes of a sulphur- and iron-rich fluid, not associated with the copper mineralising event.

If Pyrite II is of Devonian metamorphic origin, as suggested by its chemical affinity with Devonian vein pyrite elsewhere in western Tasmania, then it implies that the bulk of pyrite mineralisation in the Mt Lyell field is also metamorphic. It would also follow that the cobaltiferous Pyrite III is of metamorphic origin. The deposition of such cobalt-rich pyrite by a metamorphic fluid is probably possible, but anomalous given the evidence gathered in Tasmania and other metamorphic terranes world wide.

The alternative option - that Pyrite II and III are of volcanogenic origin - entails a simpler paragenesis for the various generations of pyrite deposited from a volcanogenic fluid or fluids with physiochemical conditions and trace element composition varying over time in a single hydrothermal system.

However, even this volcanogenic mineralisation option may have significant ramifications for the timing of volcanism and sedimentation at Mount Lyell. If the hematite alteration zone at Prince Lyell is derived from the adjacent Owen Conglomerate, which is the most obvious readily available source of oxidised iron, then volcanogenic mineralisation was continuing during the early Ordovician. This scenario for the Prince Lyell area also implies that the bornite - chalcopyrite mineralisation adjacent to the Great Lyell fault in the North Lyell area may be the result of mineralisation by an Ordovician volcanogenic fluid as it mixed with more oxidised connate waters near the fault. The lower pyrite $\delta^{34}S$ ratios of the North Lyell mineralisation (Walshe and Solomon, 1981) are more consistent with re-equilibration of a volcanogenic fluid with and a more oxidised environment. The contact of an oxidised sedimentary basin with the altered volcanics along an active growth fault would have provided a prime chemical trap for mineralisation right along its length.

5.2 MAGNETITE - APATITE MINERALISATION

5.2.1 Relationships of magnetite - apatite mineralisation to pyrite generations

Macroscopic evidence suggests pyrite mineralisation occurred both before and after magnetite - apatite mineralisation. The apparent remobilisation of copper and gold from magnetite zones into the adjacent parts of the orebody suggests magnetite -apatite mineralisation occurred after Pyrite I - chalcopyrite mineralisation. Microscopic textures show that inclusions of magnetite occur in Pyrite II overgrowths, but not in the Pyrite I cores of composite pyrite grains (Fig. 5.11c, d). Euhedral apatite also occurs as inclusions in Pyrite II overgrowths around the margins of inclusion - free Pyrite I (Fig. 7.3a).

On the other hand, later cobaltiferous veinlets, probably Pyrite III, cut across earlier massive magnetite veins (Fig. 4.3c). Haloes of magnetite and hematite dissolution also occur around some fractures and Pyrite II veinlets (Fig. 5.11a, b), suggesting dissolution of magnetite and hematite by later pyrite - bearing fluids. Pyrite II also occurs interstitial to subhedral apatite and massive magnetite (Fig. 5.11e). These textures indicate that magnetite - apatite mineralisation occurred after Pyrite I - chalcopyrite mineralisation, but prior to Pyrite II and III.

5.2.2 Magnetite geochemistry

5.2.2.1 Data collection

The contrasting responses of whole rock trace element distributions to different styles of magnetite mineralisation (see Chapter 3) prompted a more detailed study of the geochemistry of magnetite alteration. Forty-six analyses for titanium in various types of Prince Lyell magnetite were performed on a Cameca SX-50 electron microprobe at the Central Science Laboratories, University of Tasmania under the supervision of Mr W. Jablonski. Although whole rock analyses suggested that stockwork vein magnetite contained minor vanadium (~ 1.0% V_2O_5; see Chapter 3), this could not be pursued on the electron probe as no standards were available for vanadium.

Figure 5.11

A. Dissolution of finely disseminated magnetite alteration (dark grey colouration) around fractures containing Pyrite II in an altered dacitic volcanic rock. (sample 641101.8)

B. Dissolution of finely disseminated hematite (dark purple), leaving pink siliceous haloes around Pyrite II stringers and fractures in a footwall felsic volcanic. (sample 525135.3)

C. Reflected light photomicrograph of an etched pyrite grain containing magnetite inclusions (light grey). The zoned Pyrite I core is free of magnetite inclusions which occur in the Pyrite II overgrowths. (sample 596459.1)

D. Reflected light photomicrograph of disseminated magnetite around an etched pyrite grain. Note the magnetite grains (mgt) occurring in the corroded embayments of Pyrite I and in the Pyrite II overgrowth. (sample 596459.1)

E. Reflected light photomicrograph of Pyrite II developed interstitial to subhedral, fractured apatite grains in a zone of magnetite mineralisation. (sample 2000001)

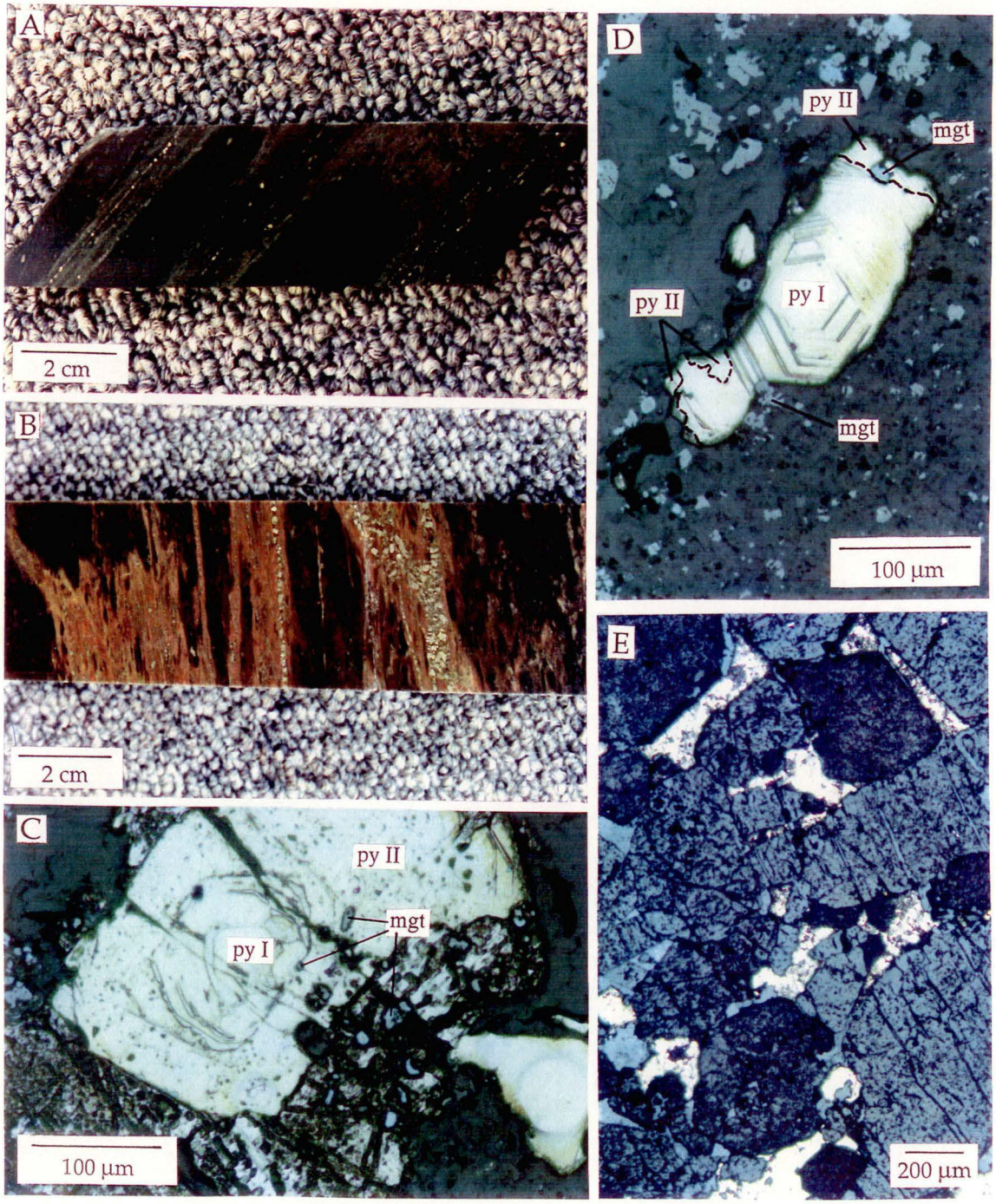
A
2 cm
B
2 cm
C
py II
mgt
py I
100 µm
D
py II
mgt
py I
py II
mgt
100 µm
E
200 µm

5.2.2.2 Results

A histogram of titanium concentrations in the various magnetite types are presented in Figure 5.12. A full list of TiO_2 analyses is given in Appendix 5.2. Disseminated magnetite euhedra and embayed magnetite grains occurring with pyrite-chalcopyrite mineralisation and in the intermediate - mafic volcanics had characteristically low levels of TiO_2; an average of 0.06% TiO_2, but up to 0.26% TiO_2. Vein magnetite from stockwork zones in the felsic volcanics had higher TiO_2 concentrations, between 0.37 and 1.74%. One sample (618051.8) contained grains of highly titaniferous magnetite (up to 7.50% TiO_2) with ilmenite exsolution lamellae.

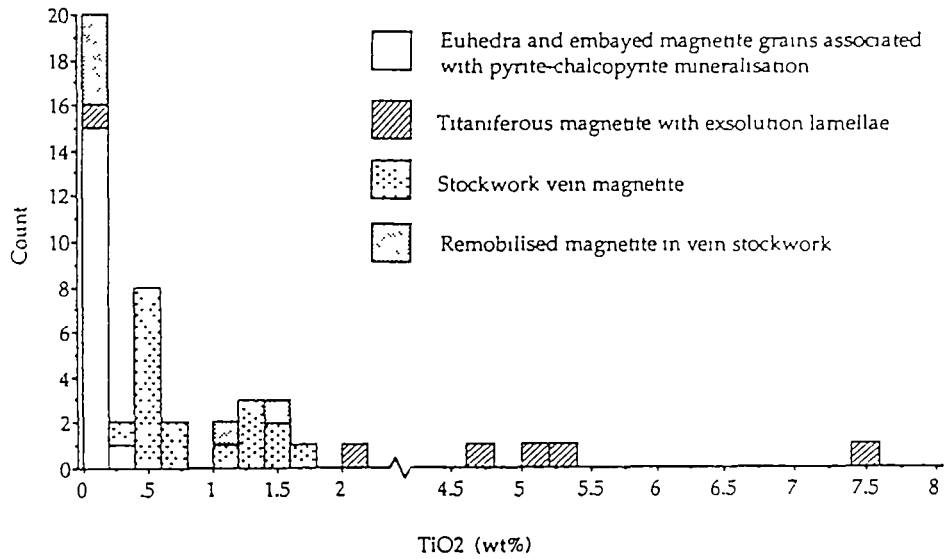

Figure 5.12 Distribution of titanium in various forms of magnetite mineralisation at Prince Lyell. Typical accessory magnetite associated with the main phase of pyrite - chalcopyrite mineralisation is distinctly poorer in titanium than the later vein magnetite.

Very minor amounts of magnetite which has been dissolved and reprecipitated on the margins of chlorite-filled fractures in the magnetite stockworks contained variable amounts of TiO_2; most commonly less than 0.2%, but up to 1.57%. These irregular low concentrations of titanium in the recrystallised magnetite suggest that some titanium may have been released from the magnetite lattice during metamorphic recrystallisation.

5.2.2.3 Discussion

The different trace element geochemistry of the vein stockwork magnetite compared to the disseminated magnetite associated with copper mineralisation and in the intermediate - mafic volcanics suggests that magnetite may have been precipitated from two mineralising fluids of different origins. The relatively enriched titanium and vanadium levels of the vein magnetite are consistent with a magmatic origin, which is discussed below.

Primary magmatic magnetite is relatively enriched in elements such as titanium, vanadium and chromium. Concentrations of TiO_2 and V_2O_5 in magnetite in some New Zealand and Chilean andesites and dacites ranges from 3.4 - 12.1% TiO_2 and 0.2 - 1.1% V_2O_5 (Duncan and Taylor, 1968; Frutos and Oyarzún, 1975). Titaniferous and vanadiferous magnetite is also commonly associated with magmatic magnetite deposits in mafic layered intrusions such as the Bushveld Complex in South Africa, the Barrambie anorthosite-gabbro complex in Western Australia (Ward, 1975) and at Boreumdo, Korea (So, 1978). Typical concentrations of TiO_2 in such magnetite are around 2.9% at Boreumdo and up to 20% TiO_2 at Barrambie. Approximately 2 - 3% V_2O_5 occurs in the Barrambie magnetite.

However, in some magnetite deposits associated with volcanic rocks, TiO_2 can be much lower. Parak (1975) reported only 0.03 - 0.13% TiO_2 in magnetite ores associated with felsic volcanics in the Kiruna district of Sweden. Oyarzún and Frutos (1984) reported approximately 0.02 - 0.2% TiO_2 (and < 0.1% V_2O_5) in Chilean magnetite ores associated with predominantly andesitic volcanics. These low titanium levels were regarded by the above authors as not supportive of a primary magmatic origin for the magnetite. Remobilisation of iron from older sedimentary rocks or the presence of a hydrous fluid phase during magmatic segregation of the magnetite were invoked to explain the anomalously low titanium and vanadium values.

5.2.3 Apatite Geochemistry

5.2.3.1 Sample collection and analysis

Analyses for a suite of nine REE were carried out by Bequerel Laboratories Pty Ltd, Lucas Heights, N.S.W. on three apatite samples from massive magnetite veins at Prince Lyell. Apatite separates were obtained by careful drilling of coarse grained crystals in magnetite veins. Two

representative whole rock samples of altered felsic and intermediate - mafic volcanics were also analysed for comparison with the apatites.

5.2.3.2 *Introduction to the Rare Earth Element chemistry of apatite*

The Lanthanide or Rare Earth Element (REE) chemistry of apatites has been used as an aid to interpretation of magnetite-apatite mineralisation by many researchers (eg: Parak, 1973; Helvaci, 1984). The REE have very similar chemical and physical properties, displaying a small steady increase in ionic radius with increasing atomic number for a given coordination state (Henderson, 1984). As a result, the REE occur in nature as a group rather than singly. Although the REE mainly occur in the 3^+ ionic state, Eu^{2+} and Ce^{4+} are the most common variants due to the enhanced stability of these particular configurations. These variations and the wide variety of coordination states of the REE mean that petrogenetic processes can fractionate them (Henderson, 1984).

Fractionation of the REE between minerals and igneous melts increases as the melts become more silicic, with granitic accessory minerals such as apatite commonly concentrating the light Rare Earth Elements (LREE) (Clark, 1984). In apatite, the REE are incorporated into the Ca site in their normal 3^+ state in 7- and 9-fold coordination sites (Clark, 1984). The divalent Eu ion is not admitted into the apatite structure, resulting in a natural degree of Eu depletion in most apatites. Large negative Eu anomalies may indicate low fO_2 conditions of formation (Puchett and Emmerman, 1976). However, negative Eu anomalies in late-formed igneous minerals are more commonly due to the removal of Eu^{2+} in plagioclase earlier fractionated from the magma. In marine apatites, negative Ce anomalies may occur due to the removal of Ce^{4+} from oxidised seawater by concentration in manganese nodules (Clark, 1984).

5.2.3.3 *Results and discussion*

The REE distributions of Prince Lyell apatites, normalised against chondrite values (Boynton, 1984), are shown in Figure 5.13. A full list of analyses is given in Appendix 3.4. The Prince Lyell apatites have high total REE concentrations ($\geq$ 2.2% RE_2O_3) compared to other examples of apatite associated with magnetite ores (Fleischer, 1983) and are very light rare earth enriched. The REE distributions of the three apatites are tightly constrained and have significant negative Eu anomalies. There is no Ce depletion, suggesting REE have not been derived from seawater.

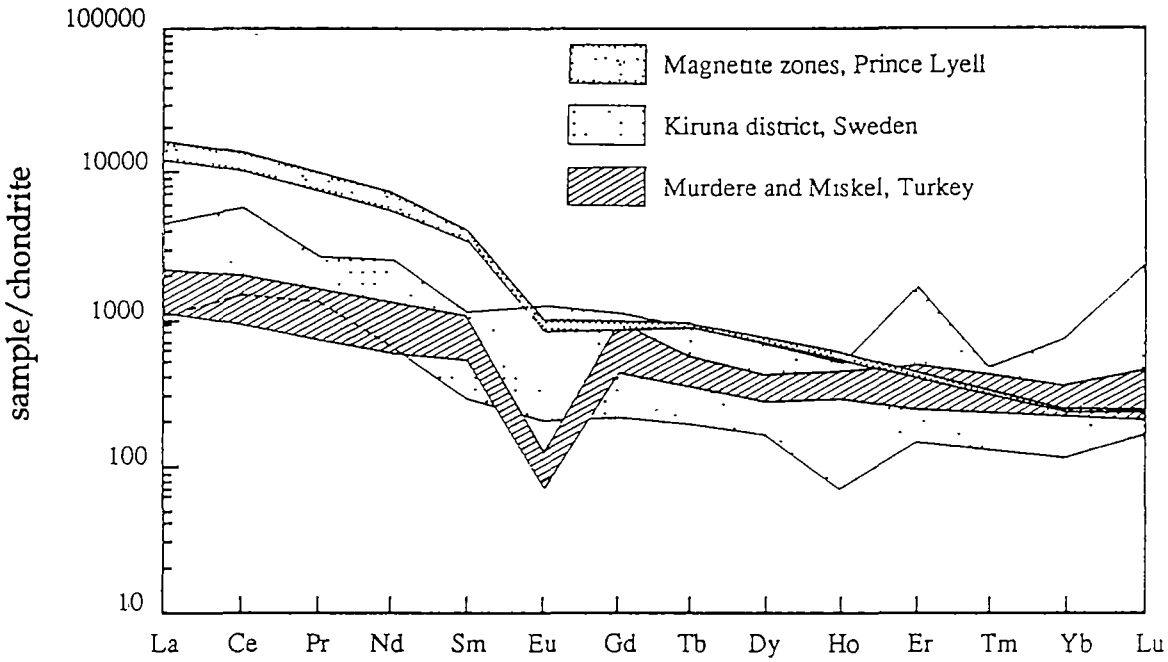

Figure 5.13 Chondrite - normalised rare earth element distribution patterns for apatites from magnetite mineralisation at Prince Lyell compared to apatites in some Swedish and Turkish magnetite iron ores.

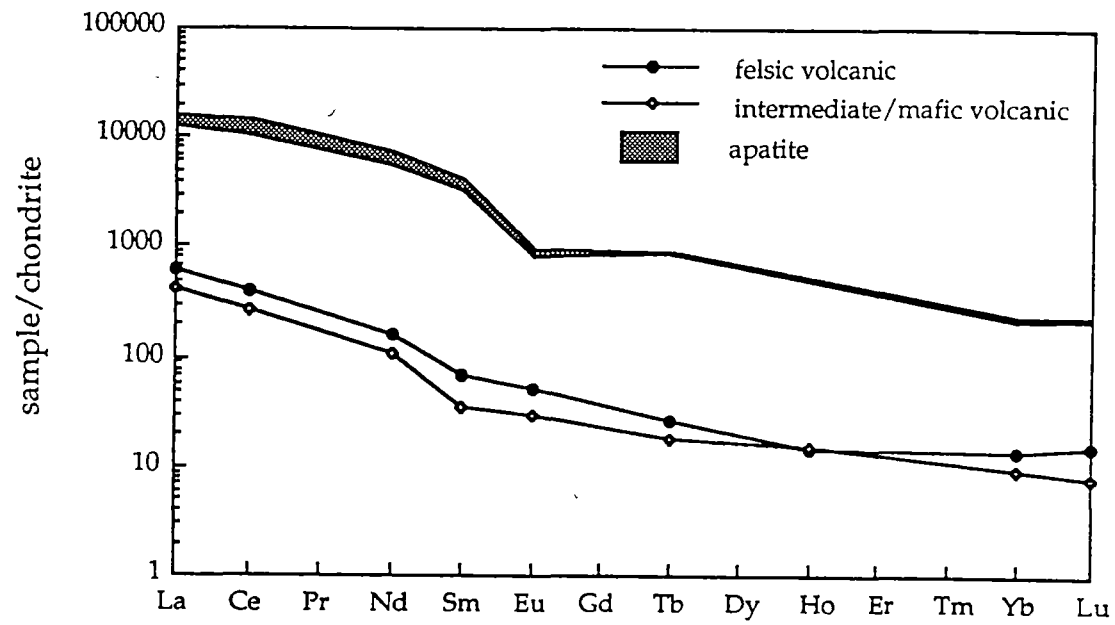

Figure 5.14 Chondrite - normalised rare earth element distribution patterns for a Prince Lyell felsic volcanic and intermediate - mafic volcanic compared with apatite from magnetite - apatite mineralised zones.

The strong LREE enrichment in Prince Lyell apatites is similar to that found in numerous examples of magnetite-apatite mineralisation associated with felsic and intermediate volcanics such as at Durango, Mexico (Young *et al.*, 1969) and Abovyan, U.S.S.R. (Fleischer, 1983). The Kiruna district apatites (Fig 5.13) show a wider spread of REE distribution and do not show a pronounced Eu depletion. These apatites are regarded to be of magmatic origin (Frietsch, 1978; Nystrom, 1985) despite conclusions to the contrary by Parak (1973, 1975).

The negative Eu anomaly of the Prince Lyell apatites is similar to that observed in apatites from the Murdere and Miskel magnetite deposits in Turkey (Helvaci, 1984) (Fig. 5.13). The shape of the Prince Lyell Eu anomaly is masked somewhat due to Gd not being analysed. Helvaci (1984) considered the Turkish apatites and magnetite to be derived from an immiscible fluid separated from a very fractionated felsic magma. The even stronger LREE enrichment in the Prince Lyell apatites suggests that an extreme degree of fractionation would have taken place during derivation of the apatite - magnetite mineralising fluid at Prince Lyell. A potential source magma for this fluid is suggested by Crawford *et al.'s* (1992) documentation of high - potassium volcanics in the southern Mt Read Volcanics (Suites 2 and 3) with high to very high P_2O_5 contents and which are strongly LREE enriched.

Helvaci (1984) regarded the apatites at Murdere and Miskel to be derived from the same magma as the host volcanic sequence, as their REE patterns were similar. Prince Lyell volcanics have similarly LREE enriched patterns to their associated apatite, but do not show a similar Eu depletion (Fig. 5.14). It is difficult to say whether the negative Eu anomaly in the Prince Lyell apatites is due to normal exclusion of Eu^{2+} from the apatite structure or whether the anomaly is also due to fracionation of plagioclase from the magma between eruption of the volcanics and separation of the magnetite - apatite fluid. The differing REE patterns of the apatites and volcanics suggests that the apatites were not originally part of a phosphatic tuff unit (c.f. Hendry, 1981).

The negative Eu anomalies of the Prince Lyell apatites suggest they have not been deposited from a hydrothermal fluid typical of volcanogenic sulphide mineralisation. Graf (1977) observed large positive Eu anomalies in hydrothermal fluids venting on the seafloor and in associated iron formations. These anomalies were apparently derived from the addition of Eu to the fluids from dissolution of feldspars in the volcanic substrate. The lack of Eu depletion in the host volcanics suggests that leaching of Eu by hydrothermal fluids did not occur.

5.2.4 Thermodynamic modelling of magnetite - apatite mineralisation

The physiochemical conditions and character of the hydrothermal fluid which deposited magnetite - apatite mineralisation may be inferred by thermodynamic modelling of the process of magnetite deposition at the expense of earlier chalcopyrite mineralisation. Thermodynamic data used in the calculations was from Ohmoto *et al.* (1983), Bowers *et al.* (1984), Huston and Large (1989) and Sverjensky *et al.* (1991) (Appendix 5.3).

Conditions of the hydrothermal system prior to magnetite mineralisation were assumed to be the conditions of pyrite - chalcopyrite mineralisation as concluded by Walshe and Solomon (1981); i.e:

T = 270 - 310°C	ΣS = -2.5 - 3.0
log fO_2 = -32 - 34	mCl^- = 1
pH = 4.0 - 4.5	mK^+ = 0.1

These conditions are typical for copper - gold volcanogenic sulphide deposits (Huston and Large, 1989). Figures 5.15a and c show the stability fields of iron and copper sulphides and oxides at these initial conditions. The shaded areas in each diagram represent the initial conditions of pyrite - chalcopyrite mineralisation at 300°C.

With the change to magnetite deposition at the expense of chalcopyrite, the conditions of mineralisation would have moved into the magnetite stability field. Chalcopyrite dissolution would have necessitated increased solubility of copper in the fluid. Although some iron would have been released into the hydrothermal fluid from chalcopyrite dissolution, significantly more iron was deposited in magnetite veining, possibly reflecting an overall decrease in iron solubility in the hydrothermal fluid.

Alternatively, a second hydrothermal fluid may have been introduced into the system. This fluid may have introduced large amounts of iron to form the magnetite while dissolving chalcopyrite, overriding the need for a decrease in iron solubility in a closed hydrothermal system.

It can be seen from Figure 5.15a that the solubilities of copper and iron in pH - fO_2 space vary similarly (ie: subparallel contours) in the fields of pyrite, magnetite and chalcopyrite. Both iron and copper are more soluable with decreasing pH. , With increasing temperature, the sympathetic relationship of iron and copper solubilities does not change (Fig. 5.15b). This similar behaviour of copper and iron suggests that magnetite deposition and chalcopyrite dissolution in a closed system is unlikely through variations in pH - fO_2 - T space.

Figure 5.15

Thermodynamic models of magnetite - apatite mineralisation

Log fO_2 - pH and log fO_2 - ΣS diagrams showing solubility contours for iron and copper at 300°C and 350°C. The conditions of pyrite - chalcopyrite mineralisation (log fO_2 ~ -33, pH ~ 4.5, ΣS ~ -2.5 at 300°C; after Walshe and Solomon, 1981) are indicated by the shaded areas in diagrams A and C. These initial log fO_2, pH and ΣS conditions are similarly indicated on diagrams B and D (projected to 350°C).

A. A decrease in pH at constant temperature and ΣS may account for dissolution of chalcopyrite (increasing solubility of copper) by the magnetite - apatite mineralising fluid. A corresponding drop in fO_2 would be required to move the fluid into the magnetite stability field (arrow). The solubilities of iron and copper behave similarly in the fields of pyrite, magnetite and chalcopyrite, indicating that magnetite deposition and chalcopyrite dissolution were unlikely in a closed system.

B. At 350°C, the magnetite field is enlarged and at higher fO_2 compared to 300°C. The initial fO_2 - pH conditions (shaded area) lie in the magnetite field at a temperature between 300 and 350°C. The increase in the solubility of copper with increasing temperature provides a ready mechanism for dissolution of chalcopyrite by a magnetite - bearing fluid. Introduction of a hot, iron - rich, higher fO_2 fluid at similar or lower pH to initial conditions may have dissolved chalcopyrite and deposited magnetite (arrow).

C. At 300°C, a decrease in the sulphur content of the fluid accompanied by an increase in the fO_2 (arrow) may have resulted in an increase in copper solubility and decrease in iron solubility while moving the fluid into the magnetite stability field.

D. A decrease in ΣS and increase in fO_2, as outlined in C, may not have been accompanied by an increase in temperature for magnetite mineralisation in a closed system . Although the solubility of copper is increased with rising temperature, the solubility of iron similarly increases.

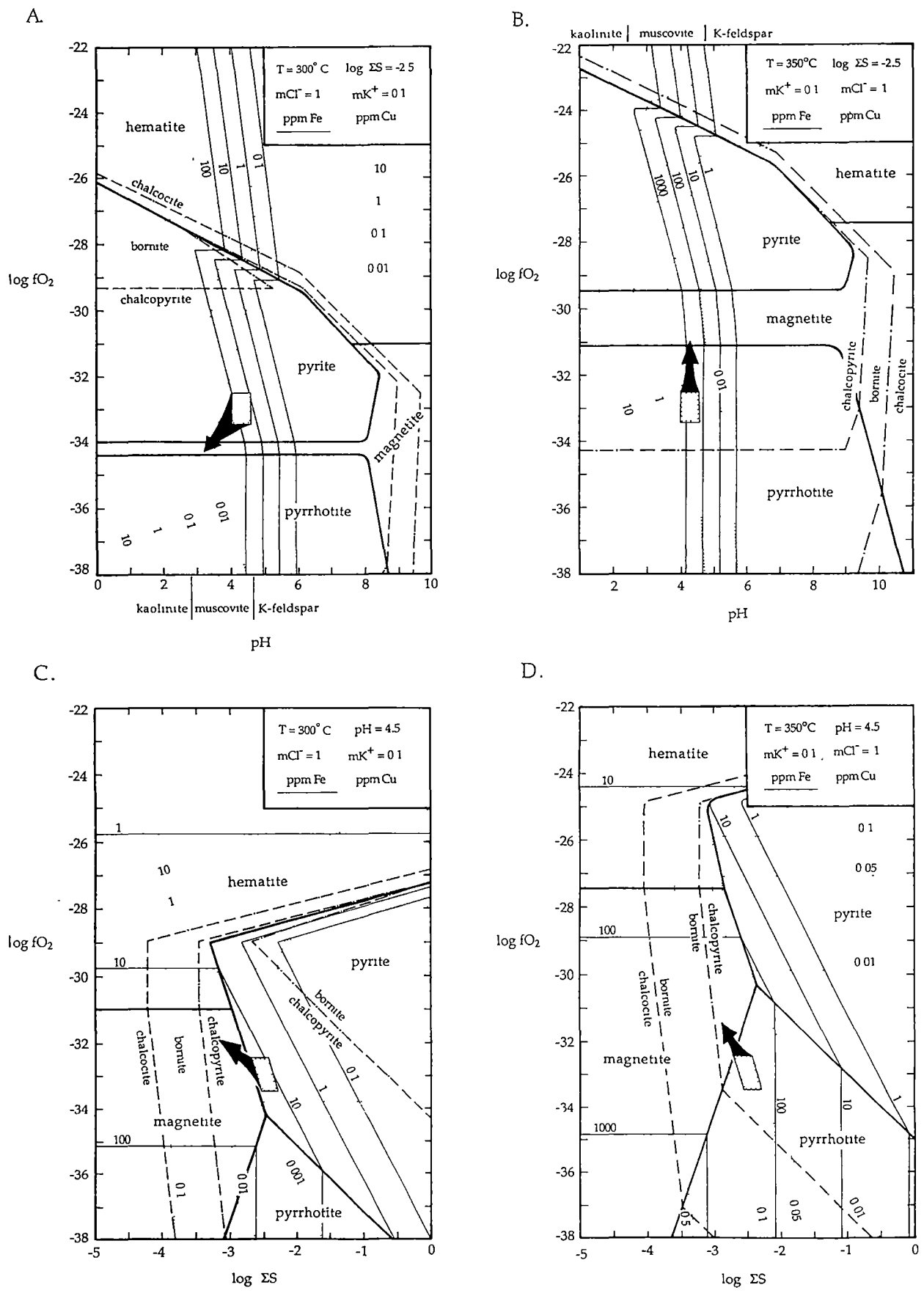
A.
T = 300° C log ΣS = -2 5
mCl⁻ = 1 mK⁺ = 0 1
ppm Fe ppm Cu
10
1
0 1
0 01
hematite
chalcocite
bornite
chalcopyrite
pyrite
magnetite
pyrrhotite
log fO2
pH
kaolinite
muscovite
K-feldspar
B.
kaolinite | muscovite | K-feldspar
T = 350°C log ΣS = -2.5
mK⁺ = 0 1 mCl⁻ = 1
ppm Fe ppm Cu
hematite
pyrite
magnetite
pyrrhotite
chalcopyrite
bornite
chalcocite
log fO2
pH
C.
T = 300° C pH = 4.5
mCl⁻ = 1 mK⁺ = 0 1
ppm Fe ppm Cu
hematite
pyrite
magnetite
pyrrhotite
chalcocite
bornite
chalcopyrite
log fO2
log ΣS
D.
T = 350°C pH = 4.5
mK⁺ = 0 1 mCl⁻ = 1
ppm Fe ppm Cu
hematite
pyrite
magnetite
pyrrhotite
chalcopyrite
bornite
chalcocite
log fO2
log ΣS

However, the introduction of a hot and/or low pH, iron - rich fluid may account for chalcopyrite dissolution while depositing magnetite (Fig. 5.15b). The drop in pH or increase in temperature would dissolve chalcopyrite, while magnetite was deposited from the new fluid as it cooled or became less acidic through reaction with the host rocks. At higher temperatures, the fluid in equilibrium with magnetite would also have a higher fO_2 than pyrite - chalcopyrite conditions (Fig. 5.15b).

Figure 5.15c illustrates that, at 300°C, a decrease in the total sulphur content of the system with a commensurate increase in fO_2 could have resulted in the conditions of the hydrothermal fluid moving into the magnetite field with an increase in the solubility of copper and a decrease in the solubility of iron in the fluid. Figure 5.15d shows that, under closed conditions, an increase in temperature could not have accompanied the change in ΣS and fO_2. Although the solubility gradients of iron and copper vary widely with ΣS and fO_2, both iron and copper become more soluble with increasing temperature.

The ΣS content of the hydrothermal fluid may have been decreased by precipitation of sulphide species. However, no increase in sulphide minerals is associated with zones of magnetite mineralisation and it is unlikely that the progressive precipitation of pyrite - chalcopyrite mineralisation should denude the fluid of sulphur in the restricted areas where magnetite is the overwhelmingly dominant iron - bearing mineral. More likely, the sulphur content of the system would have been diluted and its fO_2 increased by mixing with a second sulphur - poor, oxidised fluid which deposited magnetite and dissolved chalcopyrite.

The thermodynamic data indicate that the most efficient mechanism for dissolving chalcopyrite while depositing magnetite is the introduction of a hot (> 300°C), iron - rich, acid, low sulphur, relatively oxidised fluid into the hydrothermal system. This fluid was strongly focussed along layer - parallel conduits where it mixed with the cooler, more reduced sulphide mineralising fluid.

5.2.5 Conclusions on the Origin of Magnetite - Apatite Mineralisation

The vein style of much of the magnetite suggests that the magnetite-apatite mineralisation is of subsurface origin, not exhalative as proposed by Hendry (1972). No sedimentary layering or structures consistent with an exhalative origin were observed and thinly laminated textures in some magnetite - rich bands were derived from multiple opening of crack - seal veins.

However, the overall layer - parallel shape of the magnetite lenses indicates that the magnetite bearing fluid was very strongly focussed along narrow bedding - parallel fluid pathways. The strong magnetite - apatite mineralisation on Section 73, 115 Sublevel (Maps 2 and 8) suggests that an undefined structure may have acted as a trap for a large volume of the magnetite mineralising fluid between -100m and -150m RL, producing the largely discordant mineralisation adjacent to predominantly concordant magnetite - apatite lenses.

The high titanium and vanadium contents of the magnetite and the character of the apatite REE geochemistry suggest that the mineralising fluid was derived from a magmatic source, possibly a highly fractionated derivative of the source magma of the host volcanics, similar in composition to Crawford *et al.'s* (1992) Suite 2 or 3 volcanics of the Mt Read Volcanics. (Oxygen isotopic evidence in Chapter 8 provides further evidence of a magmatic origin for magnetite.)

Thermodynamic modelling suggests the magmatic fluid was relatively sulphur - poor and more oxidised than the pyrite - chalcopyrite hydrothermal fluid. The dissolution of chalcopyrite in magnetite zones also suggests the magmatic fluid was high temperature and saline, especially given the association of magnetite and apatite with high temperature (> 500°C), hypersaline fluids in the potassic alteration zones of porphyry copper systems (Beane and Titley, 1981).

CHAPTER SIX

THE GREAT LYELL FAULT ZONE AND "FLAT FAULTS"

6.1 THE GREAT LYELL FAULT ZONE

6.1.1 Introduction

A major role of the Great Lyell fault zone in Mt Lyell ore genesis has been proposed by advocates of both Devonian and Cambrian mineralisation. The proximity of many sulphide orebodies in the field to the faulted Owen Conglomerate contact led early researchers to conclude that the Great Lyell fault was the major conduit for hydrothermal fluids and epigenetic mineralisation on the Mt Lyell field (eg: Gregory, 1905). Later, when a Cambrian volcanic origin for the ores was proposed (eg: Walshe and Solomon, 1981), a deep seated precursor to the present Great Lyell fault was envisaged as a large scale focus of volcanogenic fluids. The fault zone has also been envoked as an oxidation - reduction front at which mineralisation occurred during either Devonian metamorphism (Sillitoe, 1985; Arnold and Carswell, 1990) or Owen Conglomerate sedimentation (Berry, 1990b).

6.1.2 Petrography

The Great Lyell fault zone adjacent to the the Prince Lyell orebody generally comprises a zone of intensely sheared and altered volcanics up to several metres wide. However, this is only one of many variable expressions of the volcanics/conglomerate contact in the Mt Lyell mineral field which have been historically termed the Great Lyell fault. The contact may appear as a variably sheared zone (Arnold, 1985) or an unfaulted onlapping contact between the Owen Conglomerate and altered volcanics in places (Berry, 1990b). The fault has been active through several phases of sedimentation and deformation from the Cambrian to the Devonian.

Exposure of the fault zone in the Prince Lyell study area was limited to drill core intersections. The fault varies in character from a sharply defined, narrow shear zone displaying a laminated, almost mylonitic texture (Fig. 6.1), to a zone several metres wide of gradually increasingly sheared and altered volcanics towards the conglomerate contact. Rounded conglomerate

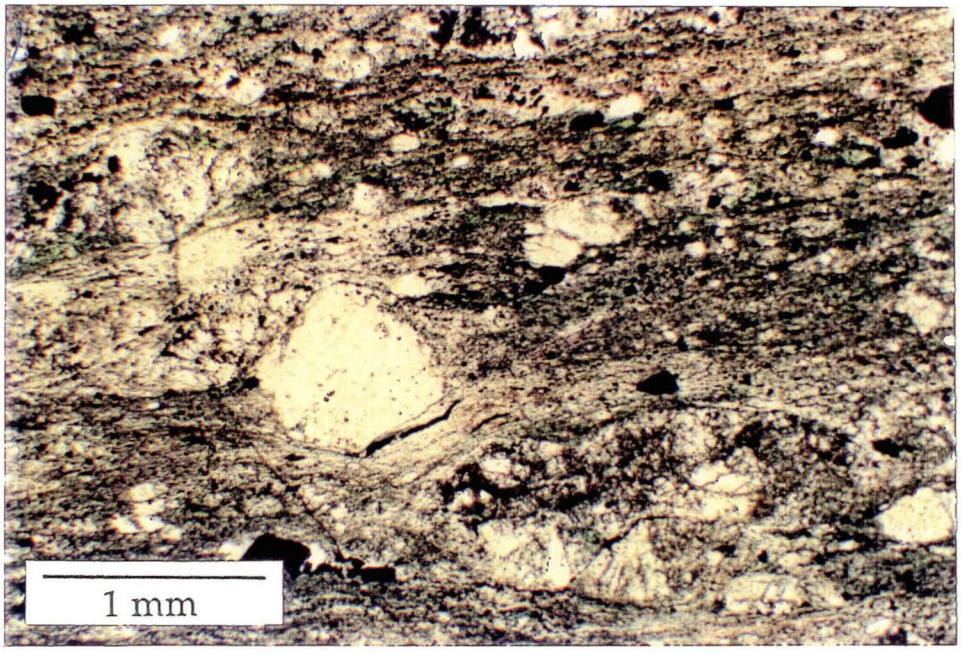

Figure 6.1 Photomicrograph of a strongly sheared and sericitised volcanic rock in the Great Lyell fault zone adjacent to the Prince Lyell orebody. Augens of siliceous rock fragments and strongly brecciated pyrite grains give the rock an almost mylonitic appearance. (sample 639121.3, PPL)

fragments up to several centimetres across and larger coherent fault slivers of Owen Conglomerate have been included in the fault zone.

Altered volcanics within the fault zone are most commonly highly foliated, fine grained sericite - quartz schists with variably weak to intense hematite + siderite alteration. Less commonly, massive sericite exhibiting little foliation may be developed in the fault zone. Rounded augens of fragmented quartz, pyrite and country rock, several millimetres across, are common. Minor chlorite and trace amounts of galena, sphalerite and chalcopyrite occur within augens and rock fragments in the fault zone.

6.2 "FLAT FAULTS"

6.2.1 Introduction

"Flat faults" is a locally derived term used to describe late-D_2, post cleavage, shallowly dipping reverse faults which are common in the Mt Lyell area. The faults occur as a conjugate set, dipping south-east and north-west (c.f. Fig. 1; Bird, 1982), consistent with the local stress regime of the D_2 deformation event (Fig. 6.2). In many cases the "flat faults" may be regarded as no more than strongly developed joints as minimal movement has occurred across them. The faults appear to have generally acted as localised zones of stress relief during D_2 and are commonly discontinuous. Underground mapping revealed that many "flat faults" die out over only a few tens of metres and are not the major continuous structures envisaged by Bird (1982).

Bird (1982) also proposed that metamorphic fluids focussed along "flat faults" resulted in the remobilisation of chalcopyrite into high grade ore lenses within and adjacent to the primary ore horizon. Evidence for this theory were the apparent discontinuities in the primary copper lenses and small high grade lenses outside the main orebody. However, Bird's interpretation of the distribution of copper mineralisation and of large continuous "flat fault" structures was based on limited preliminary drilling information, and has not been substantiated by more recent detailed drilling.

6.2.2 Associated veining

Metamorphic quartz + siderite ± chlorite ± chalcopyrite ± flourite ± specular hematite veins occur in the altered volcanics, but are commonly associated with the "flat faults" (Fig. 6.3). The veins are not planar, but commonly occur as masses of irregular veins oriented along the direction of

the "flat faults". The veins are comprised of minerals leached from the altered volcanics and represent the most mobile components during metamorphism (Reid, 1975). The concentration of veining along "flat faults" indicates that the faults have acted as foci of fluid movement during the late stages of Devonian deformation.

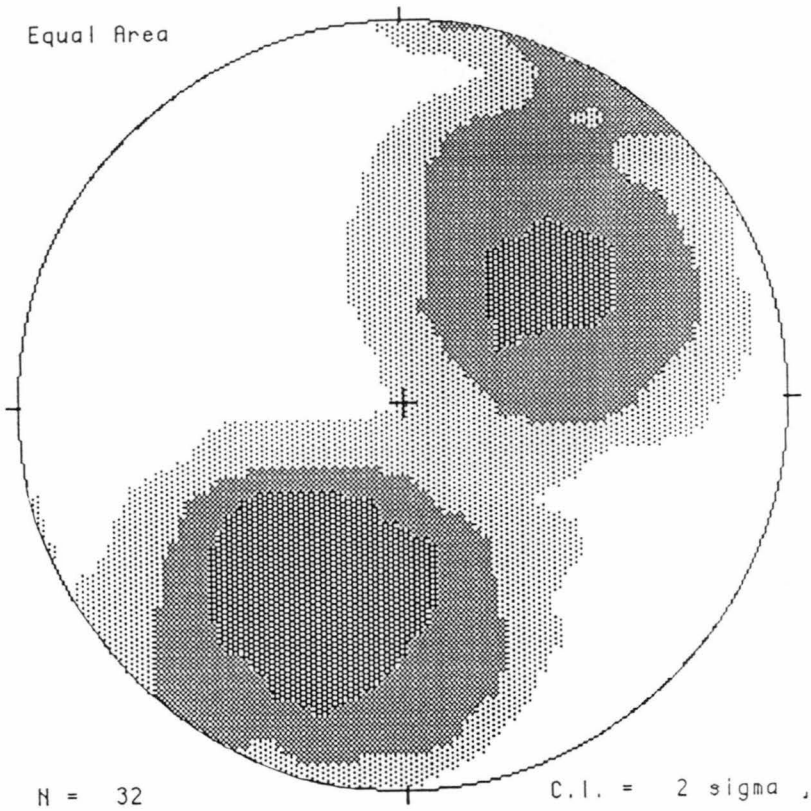

Figure 6.2 Contoured stereoplot of poles to planes of "flat faults" from mapping on 115 and 200 Sublevels.

Similar quartz - carbonate veins occur throughout the Mt Lyell field and at other deposits in the Mt Read Volcanics such as Rosebery where they are also associated with D_2 reverse faulting. At Rosebery, there is strong evidence that Devonian quartz - carbonate veins have not transported metals (Berry, 1990a). In areas of Cambrian lead - zinc and copper ore, the veins contain respectively galena - sphalerite and chalcopyrite, indicating the local derivation of sulphides in the veins.

"Flat faults" and their associated veins are commonly enveloped by haloes of sericitic alteration up to several metres wide, reflecting the dissolution of quartz, chlorite and chalcopyrite from the altered wallrocks into the veins. Intensely sericitised zones impart a bleached appearance on the

Figure 6.3

Examples of quartz (qtz) - siderite (sid) veining associated with "flat faults" in the southern Prince Lyell area.

A. Minor chlorite (chl) and chalcopyrite (cpy) developed with extensive quartz - siderite veining around a shallowly dipping "flat fault". (57 crosscut, 115 sublevel)

B. Offset of the steeply dipping pyritic band (py) indicates minor apparent reverse movement along a "flat fault" with associated quartz - siderite veining. (No. 13 drawpoint, 200 sublevel)

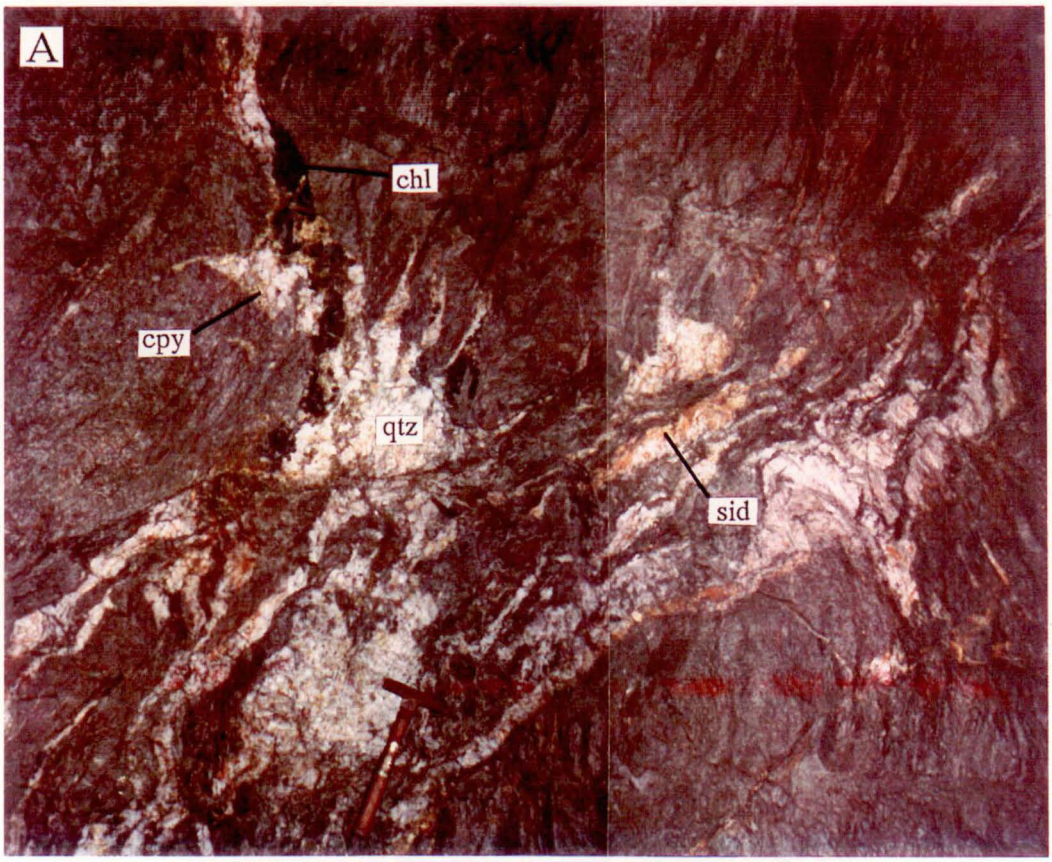
A
chl
cpy
qtz
sid

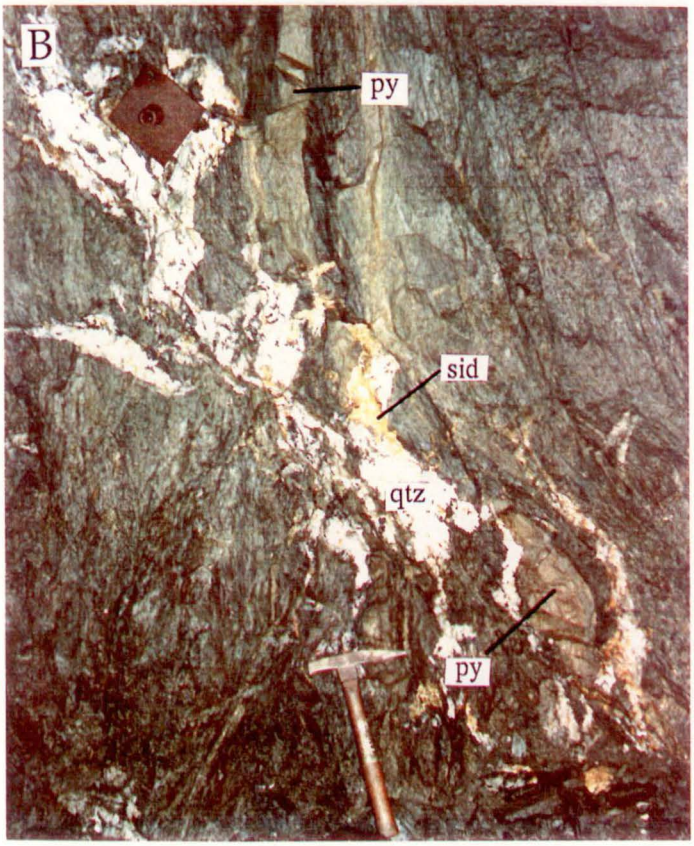
B
py
sid
qtz
py

wallrocks. However, alteration around "flat faults"in general is variable and may be very weak.

6.3 GEOCHEMISTRY OF THE GREAT LYELL FAULT ZONE

6.3.1 Sample collection and analysis

Samples were collected of twenty-four drillcore intersections of the Great Lyell fault zone adjacent to the Prince Lyell orebody (Fig. 6.4). These samples were analysed for gold by fire assay by the Mt Lyell Mining and Railway Company, Queenstown. The samples were also analysed by the Renison Tin Mine laboratories by atomic adsorption spectrophotometry for copper, lead and zinc, and by x-ray flourescence for tin, molybdenum and arsenic (samples LF 1 - 18 and 19 - 25). As a comparison for the fault zone samples, thirty samples of typical Prince Lyell lithologies from throughout the altered volcanic sequence were analysed for the same elements (samples PL 1 - 19, 21 - 25, 27 - 32; see Chapter 3).

Detection limits were 1 ppm for Pb, Cu and Ag; 5 ppm for Sn and Mo; and 10 ppm for As. Controls of analytical precision and accuracy were kept by repeat analyses of selected samples and by analysis of University of Tasmania standards (Appendix 3.8). Check analyses, notably for Cu, Sn and Pb, produced variable errors especially at low concentrations of these elements, suggesting that reliable detection limits may have been higher than quoted.

6.3.2 Results

Histograms of the distribution of Cu, Pb, Zn, Au, Ag, As, Mo and Sn in the Great Lyell fault zone and Prince Lyell altered volcanics are presented in Figure 6.5. Full tables of analytical results are given in Appendices 6.1 and 3.1. The spatial distribution of metals in the Great Lyell fault zone is presented in longsections of the fault zone in Figure 6.6.

As expected, the Great Lyell fault zone is depleted in copper and gold relative to the adjacent highly mineralised volcanics. The fault zone, however, is also depleted in the trace metals arsenic, molybdenum and tin relative to the volcanic sequence. The fault zone contains similar levels of silver and zinc and higher levels of lead compared to the volcanics (Fig. 6.5).

The spatial distribution of metals in the Great Lyell fault zone (Fig. 6.6) is slightly erratic but shows a general increase in all analysed metals towards the south-east. This trend correlates with increasing proximity of the fault zone to the Prince Lyell South Lens mineralisation (Fig. 6.7). Where the

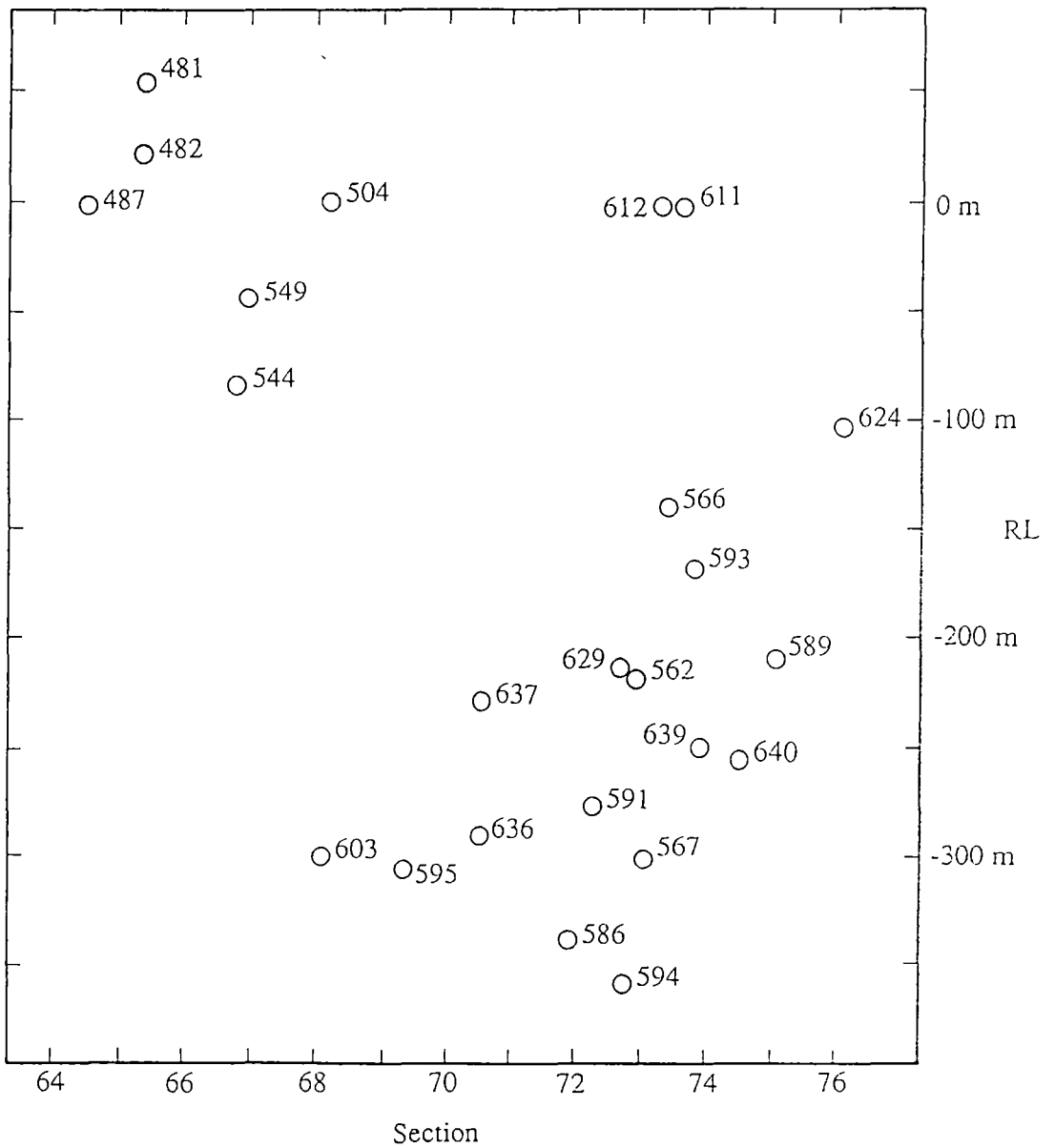

Figure 6.4 Longsection of the Great Lyell fault zone looking east showing sample locations used for the contour plots in Figure 6.6

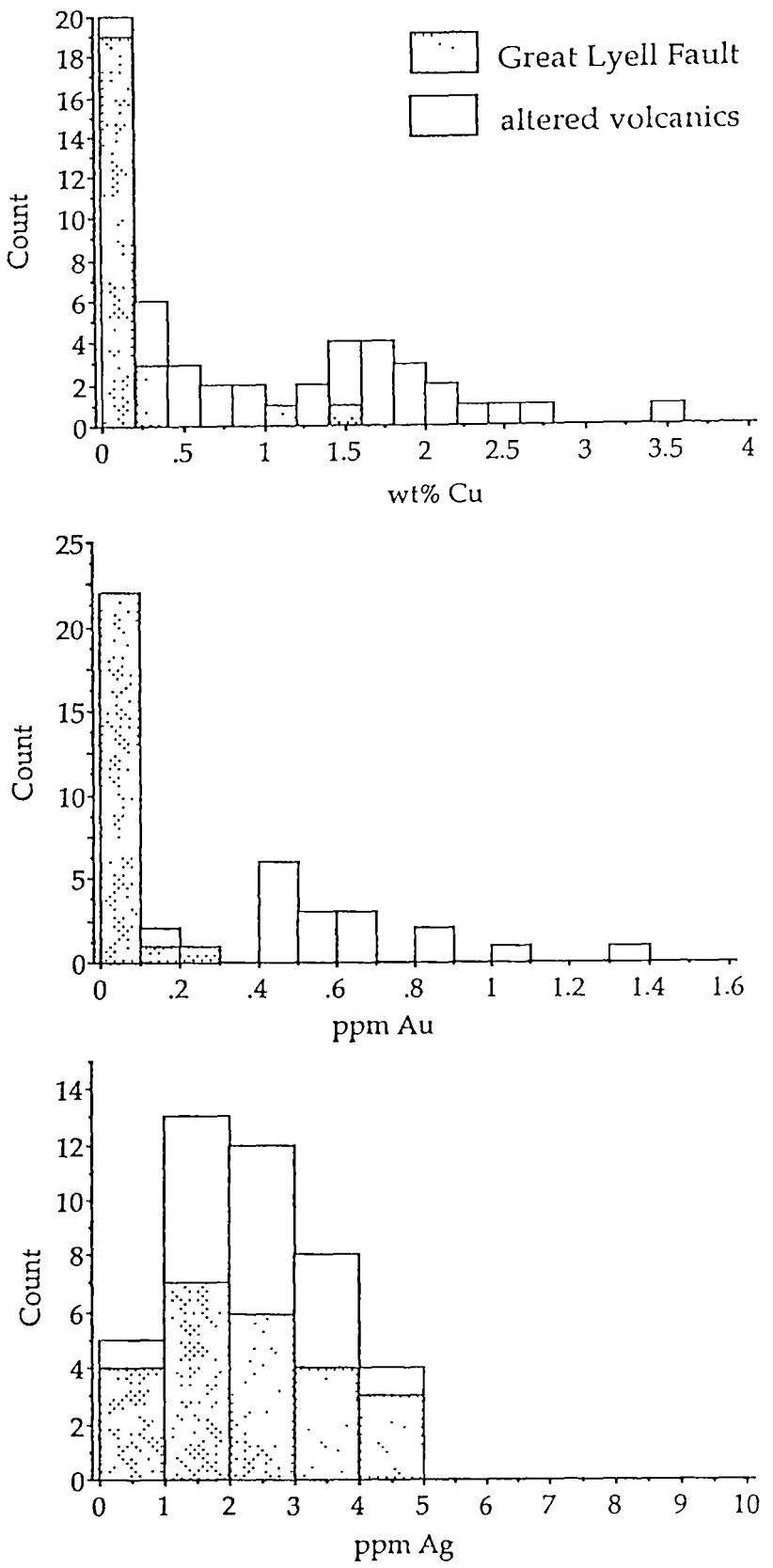

Figure 6.5a Histograms showing the distribution of copper, gold and silver in the Great Lyell fault zone compared to typical Prince Lyell altered volcanics.

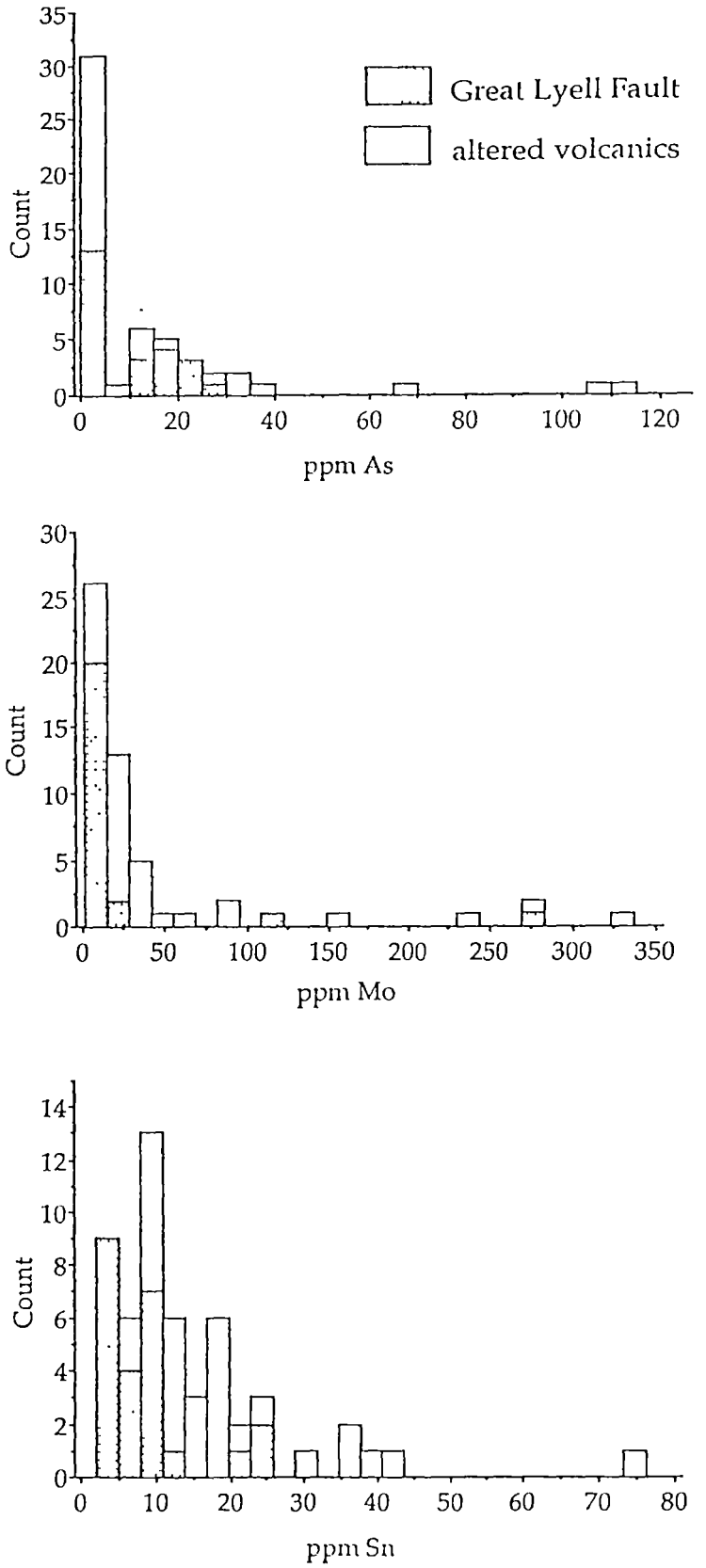

Figure 6.5b Histograms showing the distribution of arsenic, molybdenum and tin in the Great Lyell fault zone compared to typical Prince Lyell altered volcanics.

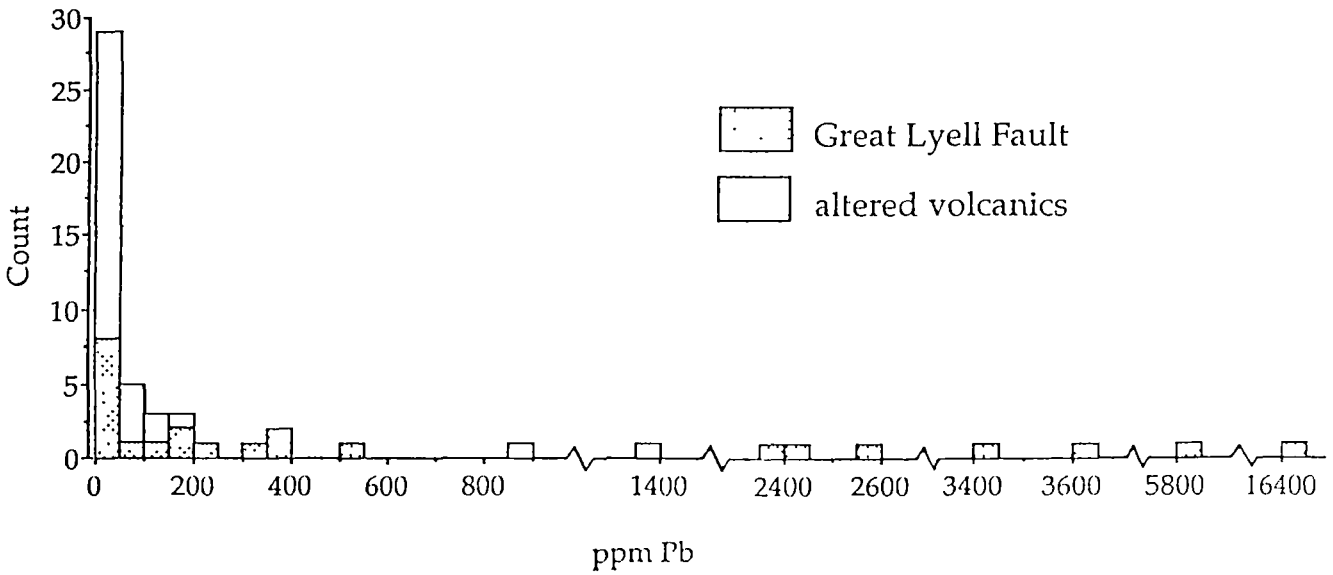

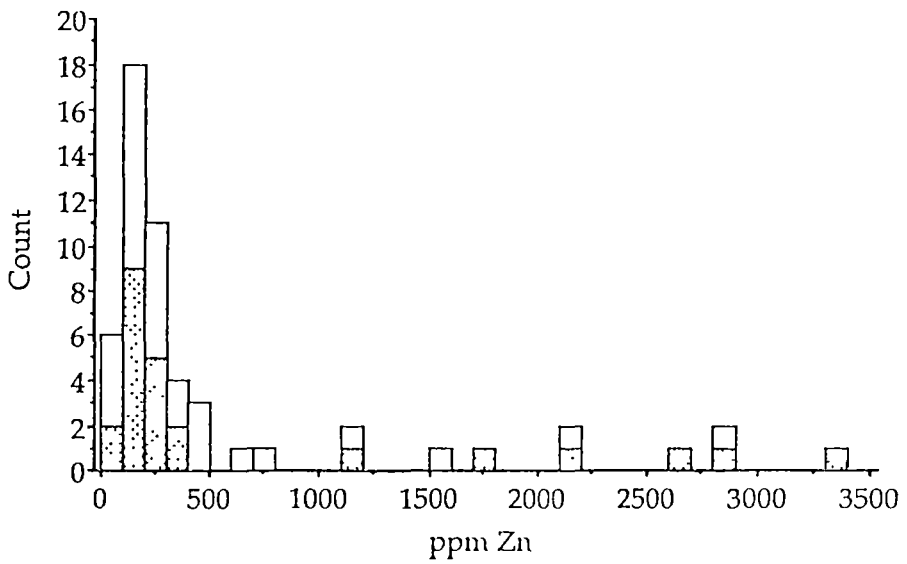

Figure 6.5c Histograms showing the distribution of lead and zinc in the Great Lyell fault zone compared to typical Prince Lyell altered volcanics.

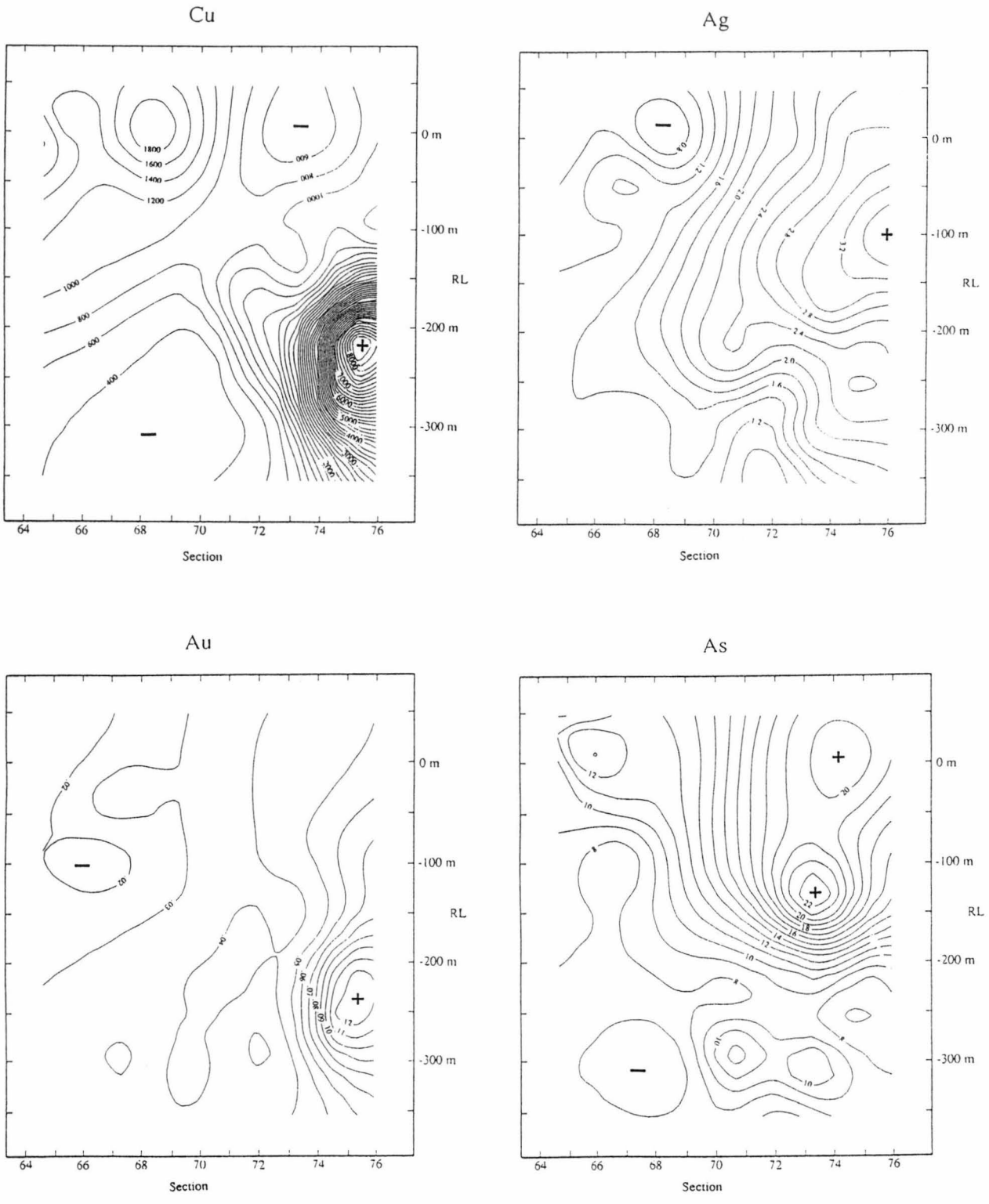

Figure 6.6a Longsection of the Great Lyell fault zone looking east showing the distribution of copper, silver, gold and arsenic. All contours are in ppm.

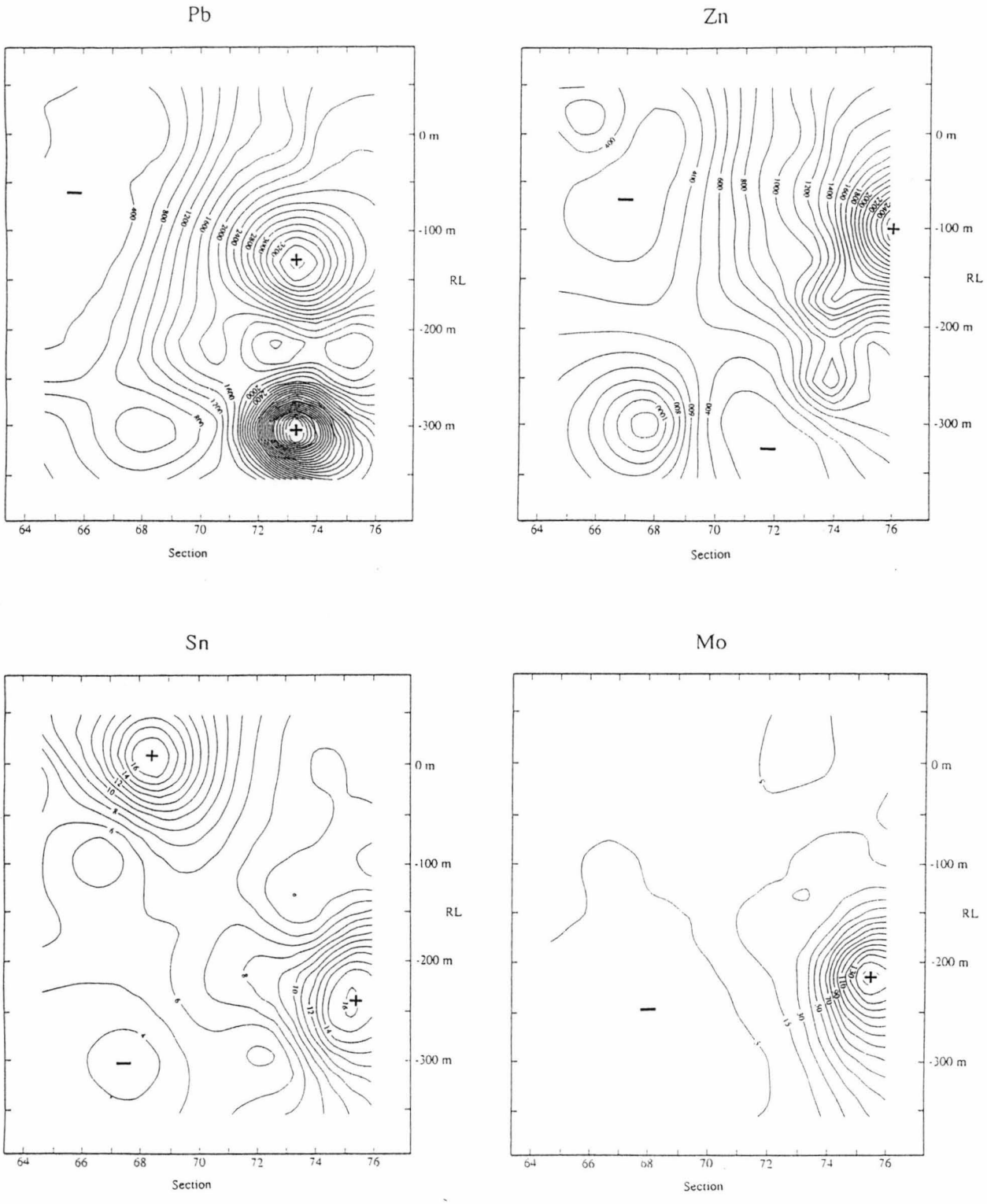

Figure 6.6b Longsection of the Great Lyell fault zone looking east showing the distribution of lead, zinc, tin and molybdenum. All contours are in ppm.

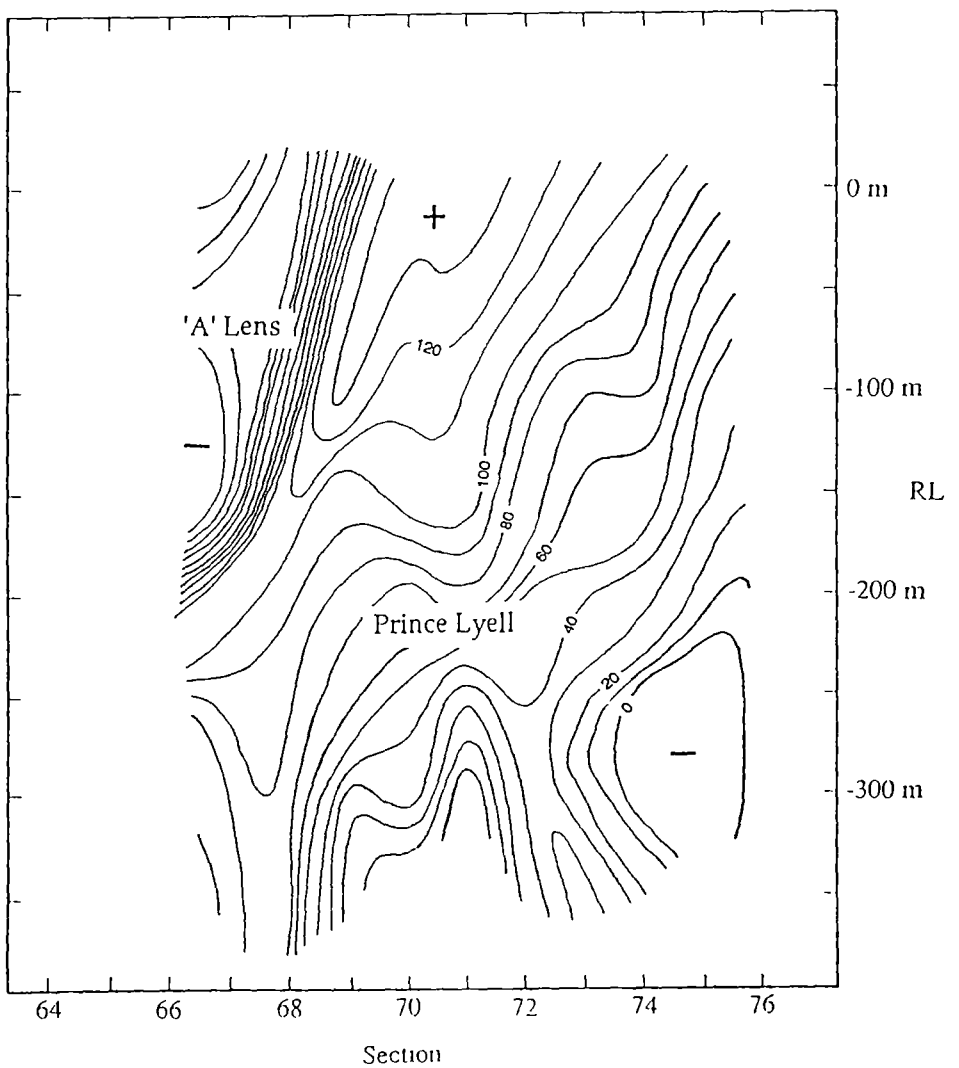

contour interval = 10 metres

Figure 6.7 Contoured longsection looking east showing the distance in metres from the Great Lyell fault zone to the footwall of the Prince Lyell and 'A' Lens orebodies.

orebody is in contact with the Great Lyell fault zone (chiefly below 200m RL on sections 74 and 75), copper, gold, tin, molybdenum and lead all have marked concentrations in the fault zone. Tin, and to a lesser extent arsenic and copper, have increased levels in the fault zone adjacent to the 'A' Lens orebody (above 0m RL, sections 66 to 68). Lead, zinc, silver and arsenic show significant enrichment upwards, away from the intersection of the orebody and the fault zone.

6.3.3 Discussion

The generally low levels of metals in the Great Lyell fault zone adjacent to the Prince Lyell orebody suggests that the fault zone has not acted as a major conduit of hydrothermal metal-bearing fluids. The higher concentrations of metals in the fault zone appear to be strongly related to the proximity of the Prince Lyell, and to a lesser extent the 'A' Lens orebodies. A more widespread and zoned distribution of metals may have been expected had the fault zone been a major pathway for mineralising fluids.

The distributions of copper, tin, molybdenum and gold in the Great Lyell fault appear to be the result of localised leaching of the Prince Lyell and 'A' Lens orebodies where they are very close to or intersected by the fault zone. On the other hand, lead, zinc, silver, arsenic and to a lesser extent gold appear to have been more susceptible to mobilisation by late fluids moving up the fault zone, forming dispersion trails above the intersection of the fault with the orebody. The mobility of lead and zinc in the Great Lyell fault is mirrored in the volcanics by the presence of irregular post-cleavage sphalerite + minor galena veins formed by the remobilisation of zinc and lead during the late stages of metamorphism.

The apparent preferential mobilisation of lead and zinc relative to copper in the fault zone suggests that the late fluids were relatively low-temperature (< 300°C). The distribution of copper in the fault zone is tightly constrained by the proximity of mineralised volcanics and shows no evidence of substantial dispersion by later fluids. The apparent lack of copper mobility in late fluids suggests that the deformation and remobilisation of chalcopyrite in the Prince Lyell orebody during Devonian deformation was not accompanied by substantial redistribution of the pre-metamorphic copper mineralisation. The greater remobilisation of silver relative to copper and gold in the fault zone also offers an explanation for the poorer correlation of silver with copper (relative to gold with copper) within the orebody itself.

6.4 GEOCHEMISTRY OF "FLAT FAULT" ZONES AND QUARTZ-SIDERITE VEINS

6.4.1 Sample collection and analysis

A study was undertaken to examine the extent of copper, gold and silver remobilisation by late metamorphic fluids focussed along "flat faults". Distributions of copper, gold and silver were analysed across seven drill core intersections of altered volcanics cut by zones of "flat faults" and associated quartz - siderite veining.

An additional twelve samples of quartz - siderite ± chlorite ± chalcopyrite veining were analysed to examine if copper, gold or silver were preferentially mobilised into the veins during metamorphism. All analyses were carried out by the Mt Lyell Mining and Railway Co. assay laboratories at Queenstown by fire assay and atomic adsorption spectrophotometry.

6.4.2 Results

6.4.2.1 "Flat fault" zones

Figure 6.8 shows the distribution of copper, gold, silver and the copper/gold ratio across "flat fault" zones from the seven drill holes. A full list of analyses is given in Appendix 6.2. Redistribution of copper, gold and silver by fluids moving through "flat faults" is suggested by the irregular depletion or enrichment in and adjacent to the "flat fault" zones.

The majority of the "flat fault" zones are depleted in copper, gold and silver relative to the surrounding altered volcanics. However, the metals also show virtually unchanged or increased levels in some fault zones (eg: WL 599, WL 640). Zones of metal leaching around "flat faults" may be well defined and extend several metres either side of the fault zone (eg: WL 621, 74 - 83 metres; WL 591, 193 - 191 metres). In contrast, a fault zone in less mineralised volcanics in WL 624 is accompanied by a very weak zone of leaching.

A significant feature of some "flat fault" zones is the enrichment of copper, gold and silver in the wall rocks on the hangingwall side of the faults (eg: WL 607, 126 m; WL 633, 70 m; WL 591, 190 m) which may be up to several metres wide. These hangingwall enrichment zones suggest that remobilisation of primary mineralisation from "flat fault" zones has resulted in relatively localised redistribution of metals rather than wholesale removal of metals from the orebody.

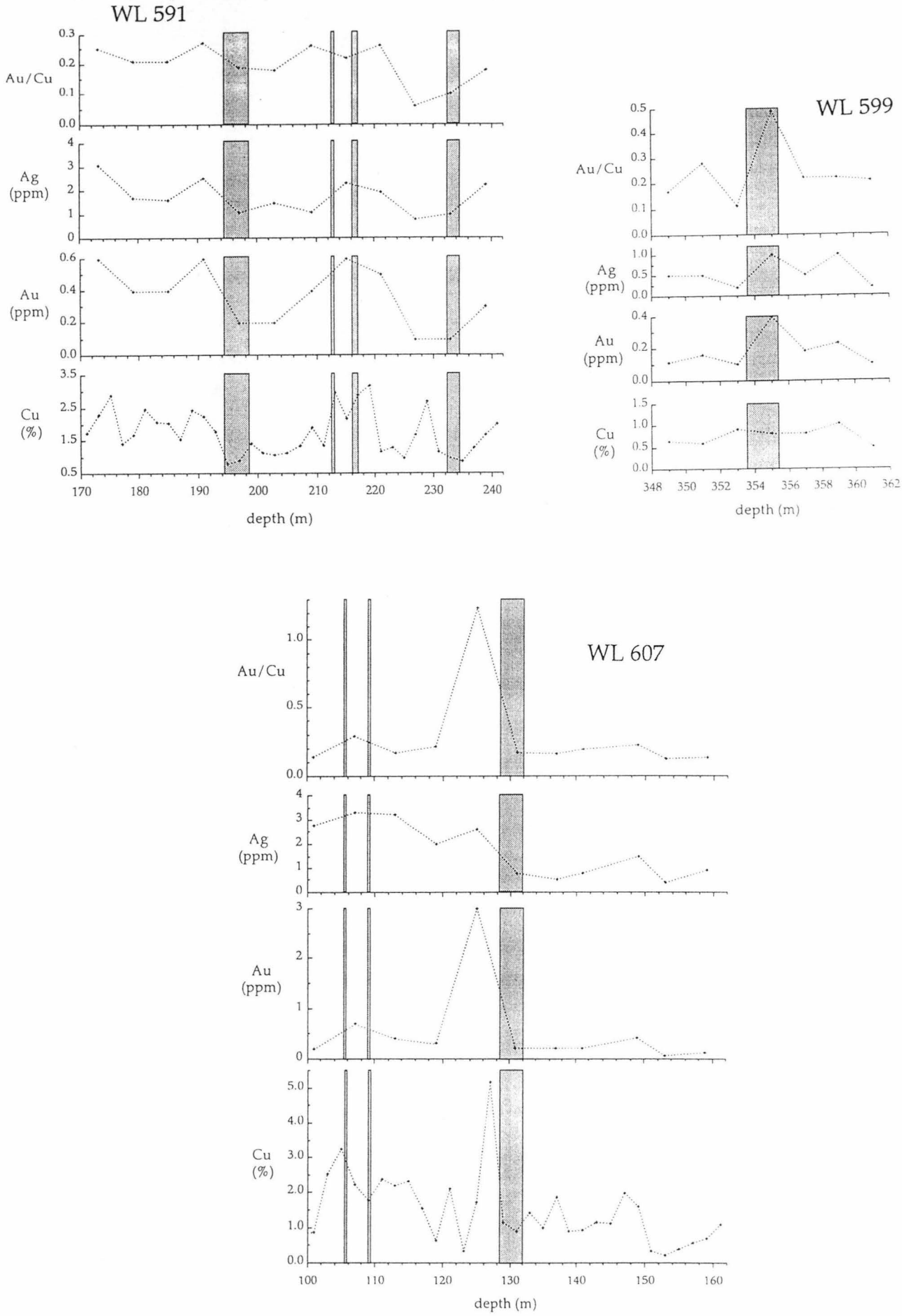

Figure 6.8a Graphs showing the variation in copper, gold, silver and Au/Cu ratio across zones of "flat faults" and associated quartz - siderite veining (shaded areas) in drill holes WL 591, WL 599 and WL 607.

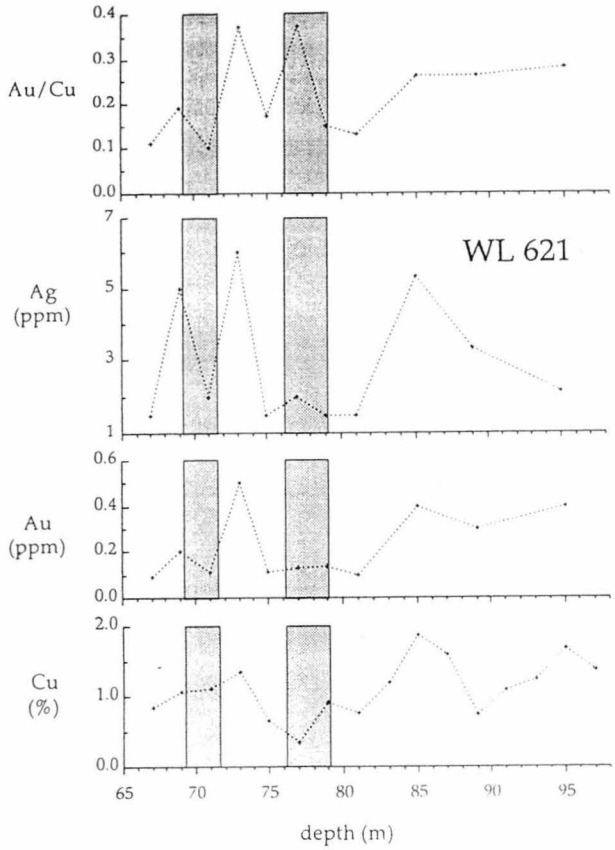

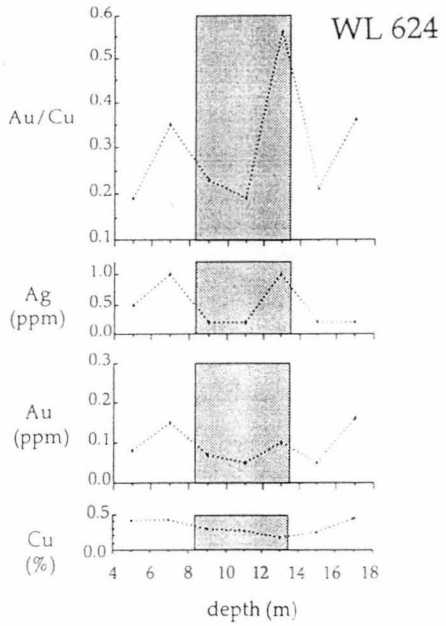

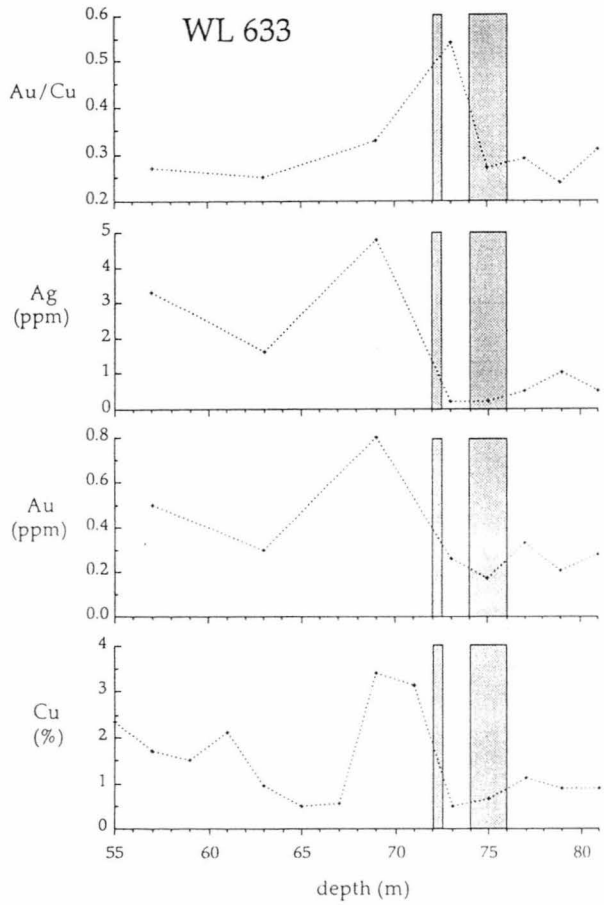

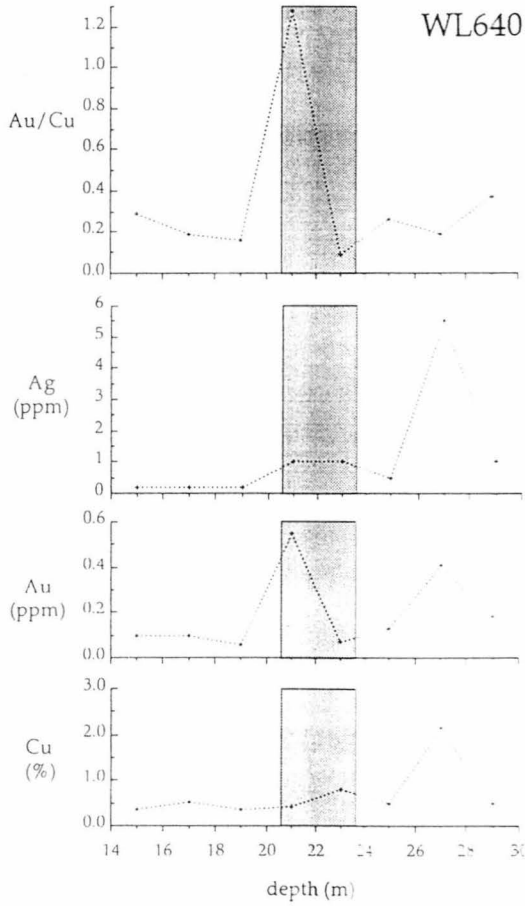

Figure 6.8b Graphs showing the variation in copper, gold, silver and Au/Cu ratio across zones of "flat faults" and associated quartz - siderite veining (shaded areas) in drill holes WL 621, WL 624, WL 633 and WL 640.

6.4.2.2 Quartz - siderite veins

Analyses of the twelve quartz - siderite veins are presented in Table 6.1. All but two of the veins sampled (525108.0 and 574030.4) contained visible chalcopyrite. The veins also commonly contained 0 - 5% massive felted chlorite, although two veins (580165.5 and 591150.0) contained over 10% chlorite. Trace galena occurred in sample 573186.8.

Table 6.1 illustrates that the sympathetic variation in the grade of copper, gold and silver displayed within the mineralised volcanics also occurs in the quartz - siderite veins. Highest grades of copper are generally accompanied by highest grades of gold and silver. However, the Au/Cu ratios of the analysed quartz - siderite veins are on the whole lower than average Au/Cu ratios of the orebody (0.24 - 0.34; see Chapter 4). The Au/Cu ratio of only two samples (573186.8 and 581195.3) fell within the general range of mineralised volcanics, indicating that copper has to some extent been mobilised into the veins preferentially to gold.

Sample number	% Cu	g/t Au	g/t Ag	Au/Cu
525108.0	0.09	< 0.1	0.2	-
526161.6	0.91	< 0.1	0.3	-
573186.8	0.29	0.1	1.2	0.34
573239.2	1.26	0.1	3.6	0.08
574030.4	0.09	< 0.1	0.2	-
577241.0	1.07	0.1	2.5	0.09
580165.5	0.15	< 0.1	1.1	-
581195.3	1.83	0.3	2.3	0.16
591150.0	0.18	< 0.1	1.0	-
591216.5	2.60	0.1	1.9	0.04
593148.2	3.91	0.3	9.6	0.08
679090.4	2.61	0.2	3.1	0.08

Table 6.1 Results of copper, gold and silver analyses of quartz - siderite veining in the Prince Lyell orebody.

6.4.3 Discussion

This study of metal mobility in and around "flat faults" has only partly substantiated the findings of Bird (1982). Although many "flat faults" appear to be the sites of leaching of copper, silver and gold, the extent to which leaching of metals has occurred is irregular. This may be expected considering that bleached alteration haloes around "flat faults" range from non-existent to wide zones of intense sericitisation.

Bird (1982) suggested that copper was remobilised preferentially to gold by metamorphic fluids. Analyses of quartz - siderite veins having lower Au/Cu ratios than average mineralised volcanics support this theory. However, examples of remobilised ore adjacent to "flat faults" shown in Figure 6.8 exhibit increased levels of gold and higher Au/Cu ratios in the remobilised ore than in the surrounding rocks. This apparently variable affect of late fluids on gold and copper mobility is mirrored within the "flat fault" zones themselves. Au/Cu ratios are both increased and decreased within "flat fault" zones compared to the surrounding wall rocks (Fig. 6.8).

6.5 FLUID INCLUSIONS

6.5.1 Introduction

A study of fluid inclusions in the quartz - siderite veins was undertaken to attempt to characterise the metamorphic fluid. Quartz and accessory interstitial flourite were the only minerals in the veins to contain inclusions large enough for quantitative examination ($\geq$ 5 μm). Siderite was clouded by many tiny inclusions characteristic of regional metamorphic environments (Reynolds, 1990). As only secondary inclusions were observed, a robust interpretation of the parent fluid of the veins could not be made.

Several populations of secondary inclusions were observed along fracture planes in quartz and flourite. The most common inclusions in both quartz and flourite were rounded to negative crystal shaped inclusions (Type I) commonly < 5μm in diameter but up to 50μm, with a small vapour bubble (~5 - 10%). Liquid : vapour ratios were generally constant within fractures, indicating healing of fractures prior to the homogenisation temperature (T_h) of the inclusions. Type II inclusions were more irregular in shape than Type I, but were otherwise similar in character to Type I. Rarely, these inclusions contained a small birefringent daughter mineral, probably a carbonate such as siderite or calcite.

The presence of some CO_2 in Type I and II inclusions was inferred by the bubbles commonly becoming very active upon heating. Rarely, a CO_2 bubble was observed in some inclusions (Type III) of similar shape to Type I and II. Flourite also commonly contained large (up to 50μm) highly irregular inclusions (Type IV) with highly variable liquid : vapour ratios. These inclusions were probably the result of low temperature necking of fractures and were not studied further.

6.5.2 Results

The distributions of homogenisation temperatures (T_h) and salinities for Type I and II inclusions are shown in Figure 6.9. A full table of measurements is given in Appendix 6.3. Homogenisation temperatures ranged from 110 °C to 204 °C with maxima of around 120°C and 150°C for flourite and quartz respectively. The pressure correction for a lower greenschist metamorphic environment at Prince Lyell (~2 kb; Cox, 1981) is around 170°C for 5 - 10 wt% NaCl inclusions (Shepherd *et al.*, 1985). This indicates that the inclusions probably formed at around 290 to 320°C.

Salinities of Type I and Type II inclusions ranged from 2.2 to 8.1 wt% NaCl equivalent, with a maxima of around 6 wt% NaCl. Flourite inclusions were on average marginally less saline than quartz inclusions.

6.5.3 Discussion

Homogenisation temperatures suggest that the secondary inclusions were trapped close to peak metamorphic conditions (~ 300°C). The generally low salinities of the fluid inclusions are consistent with the fluid being derived from regional dewatering of the volcanic pile without contributions from Devonian granitoids which characterise metamorphic environments north of Mt Lyell (Solomon *et al.*, 1988). Fluid inclusions also indicate that the metamorphic fluid contained minor amounts of dissolved CO_2.

6.6 CONCLUSIONS

"Flat faults" acted as conduits for metamorphic fluids during the late stages of the regional Devonian D_2 metamorphic event. The faults do not occur as continuous structures and as such provided only localised pathways for fluid movement. Quartz, siderite, chlorite, copper, gold and silver were all remobilised to varying degrees by these fluids. However, wallrock alteration

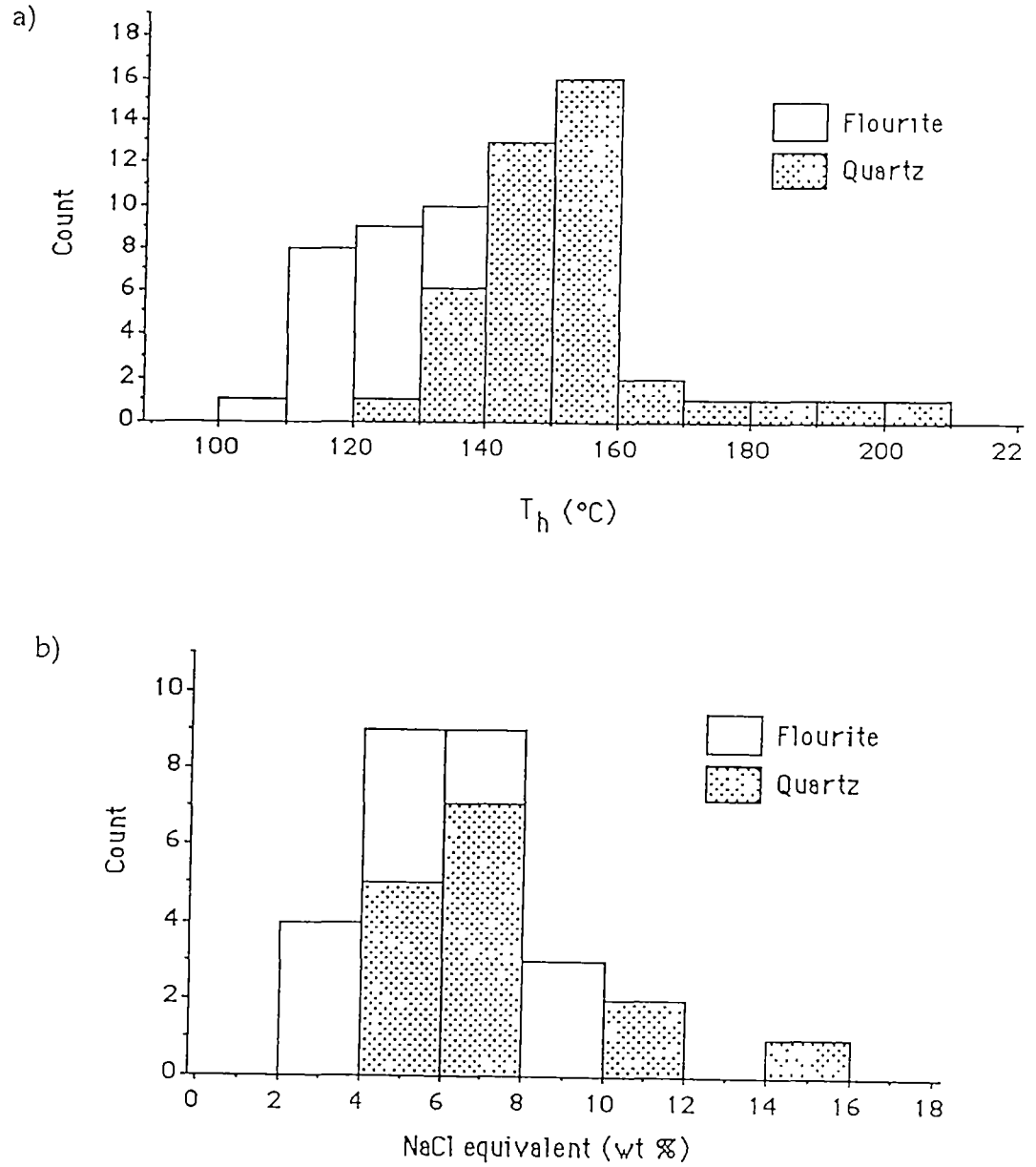

Figure 6.9 Distributions of (a) homogenisation temperatures and (b) salinities of Type I and Type II inclusions in quartz and flourite from D_2 veins associated with "flat faults".

adjacent to "flat faults" was variable and there was no overall preferential dissolution of one metal relative to another. Certainly, the metamorphic fluid does not appear to have been a highly reactive fluid capable of substantial dissolution and redistribution of the primary orebody. This may be expected of a regional metamorphic fluid which was derived from and in equilibrium with the host volcanic pile. There is no evidence to suggest that there was a magmatic contribution to the metamorphic fluid which may have added or removed metals from the system.

Some redistribution of copper, gold and silver has occurred adjacent to "flat faults". However, remobilisation appears to be limited to minor concentrations of chalcopyrite in quartz - siderite veins and enriched zones up to several metres wide on the hangingwall or up dip sides of the fault zones. It is unlikely that there has been a net loss of metals from the orebody due to metamorphic fluids. However, the unpredictable nature of the extent of metal remobilisation and the discontinuity of "flat fault" structures make detailed interpretation of the distribution of metals in the Prince Lyell orebody difficult.

CHAPTER SEVEN

SULPHUR ISOTOPES

7.1 PREVIOUS WORK AND BACKGROUND TO THIS STUDY

Sulphur isotope variation in the Mt Lyell field, including the Prince Lyell deposit, was initially studied by Solomon *et al.* (1969) and Walshe (1977). Walshe and Solomon (1981) summarised and interpreted the work of both previous studies. Solomon *et al.* (1988) collated all previous data as well as providing additional analyses in a regional study of sulphur isotope systematics in western Tasmania.

Walshe and Solomon (1981) suggested that the Prince Lyell mineralisation was deposited from a reduced, Cambrian fluid with $\delta^{34}S_{\Sigma S}$ between +4 and +11‰, and that pyrite and chalcopyrite were not deposited in equilibrium. They considered that the siliceous bornite - bearing North Lyell ores could have been deposited from the same fluid under cooler, more oxidizing conditions. Subsequently, Solomon *et al.* (1987, 1988) concluded that a temperature increase rather than decrease would be necessary to produce the bornite ores, and proposed bornite precipitation during Devonian remobilisation of Cambrian sulphides.

This study is aimed at discriminating between the contributions, if any, of Cambrian and Devonian fluids and sulphur to mineralisation, and the extent of Devonian modification of the original Cambrian isotopic distribution.

7.2 CONVENTIONAL BULK SAMPLE COLLECTION AND PREPARATION

Pyrite, chalcopyrite and sphalerite samples were collected from relatively coarse grained disseminations and veins from drill core and underground sampling. Three chalcopyrite samples were obtained from D_2 quartz-carbonate veins for comparison with disseminated mineralisation. One sphalerite sample was collected from a baritic vein in the hangingwall intermediate volcanics, while the other was from a late post-cleavage massive sphalerite vein.

An effort was made to collect samples across the entire stratigraphic section in the southern Prince Lyell area. Section 68, below zero RL, was chosen for detailed study of down-dip and across-dip $\delta^{34}S$ variation.

Sulphide separates were obtained by drilling from polished blocks after microscopic inspection to eliminate samples with contaminant inclusions. Sphalerite samples, however, could not be separated in this manner from small amounts (~ 10%) of intergrown chalcopyrite and lesser galena. Great care was taken to avoid any barite contamination.

SO_2 gas was extracted from the sulphides by the method of Robinson and Kusabe (1975) and analysed in a VG Micromass 602D spectrometer under the supervision of M. Power (snr) at the Central Science Laboratory of the University of Tasmania. Samples were calibrated against university standard galena from Broken Hill, N.S.W. ($\delta^{34}S$ = 3.2‰) and Tullah, Tasmania ($\delta^{34}S$ = 15.3‰). Analytical precision from five repeated samples ranged from 0.05‰ to 0.73‰.

7.3 'SHRIMP' ION PROBE $\delta^{34}S$ ANALYTICAL METHOD

In situ microanalysis of sulphur isotope ratios in pyrite from six samples was carried out by Dr C. S. Eldridge at the Australian National University, Canberra, using the SHRIMP ion microprobe. The analytical technique is outlined in detail by Eldridge *et al.* (1989). The $\delta^{34}S$ values of sulphur ions, liberated from a site 30 - 40 μm wide and 10 μm deep on a polished pyrite sample, were analysed with an analytical error of ± 2‰.

The study investigated possible $\delta^{34}S$ variations between generations of pyrite growth, and was prompted by the observation of complex internal structures and geochemistry within pyrite grains. The small range of isotopic variation seen in the conventional bulk pyrite analyses (5 - 11‰) suggested that the SHRIMP technique's precision (± 2‰) may not be able to distinguish between the closely spaced $\delta^{34}S_{py}$ values. However, the multiple growth stages of geochemically distinct pyrite suggested that the bulk pyrite values may have represented averages of wider spread values of individual pyrite generations.

7.4 CONVENTIONAL ISOTOPE STUDY

7.4.1 Results

Results of sulphur isotope analyses from the southern Prince Lyell area, from this and previous studies, are given in Appendix 7.1. Sample locations

Figure 7.1 Sulphur isotope sample locations and pyrite δ34S values (‰)

southern Prince Lyell area

(including data from Solomon et al.,1969 and Walshe and Solomon,1981)

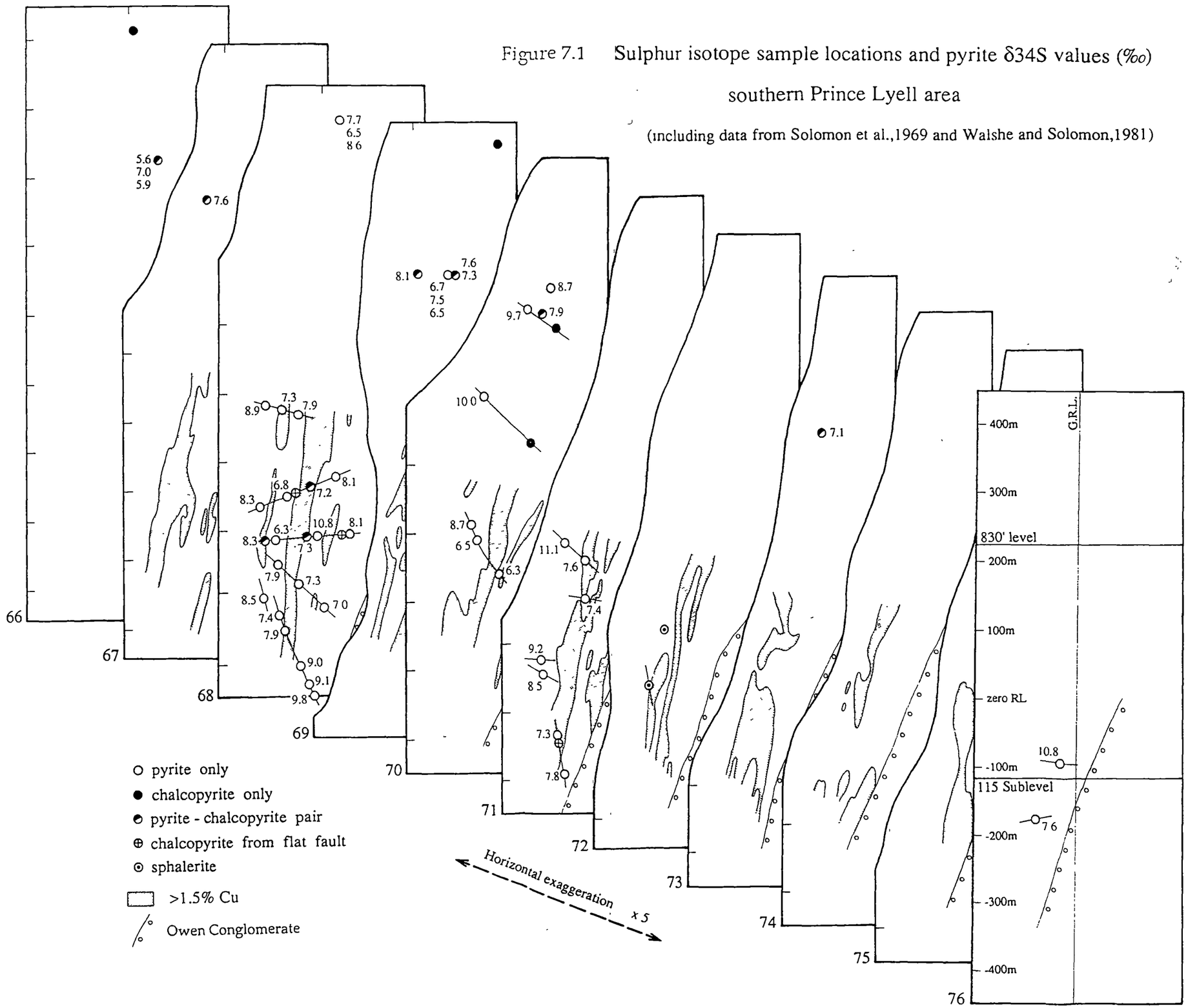

and $\delta^{34}S_{py}$ ratios are shown in Figure 7.1. The distribution of pyrite $\delta^{34}S$ ratios is tightly constrained around a maximum at 7 - 8‰, with a range from + 5.6 to + 11.1‰ (Fig. 7.2). The range of new data is close to those from previous work (Solomon *et al.*, 1988). However, the heaviest $\delta^{34}S$ values are marginally higher than those previously reported, with three values greater than 10‰.

The $\delta^{34}S_{py}$ data show no systematic zonation either down dip or along the strike of the orebody (Fig. 7.1). However, a central core of lighter values ($\delta^{34}S_{py} \leq 8‰$), may be defined, corresponding to the copper mineralised zone. Values above 8‰ generally occur in the hangingwall and footwall rocks to the ore horizon. However, sporadic values greater than 8‰ occur in mineralised areas and occasional values less than 8‰ occur in the footwall felsic volcanics. Analysis of samples of unmineralised felsic volcanics beyond

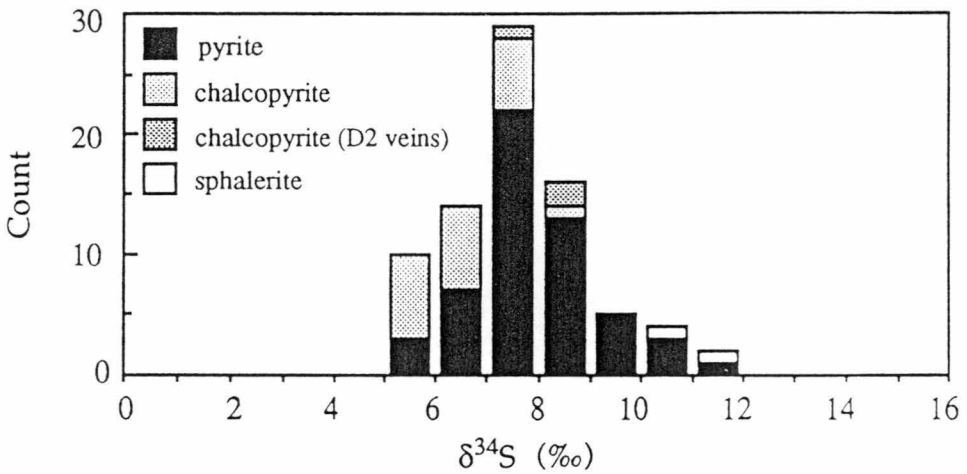

Figure 7.2 Distribution of pyrite, chalcopyrite and sphalerite $\delta^{34}S$ ratios from the Prince Lyell orebody, from this and previous studies.

the southern margin of the orebody (samples 624096.9 and 698100.4 on section 76) produced $\delta^{34}S_{py}$ values of 10.8‰ and 7.6‰ respectively. It is unclear from these samples whether a > 8‰ halo also extends around the southern end of the orebody.

Chalcopyrite $\delta^{34}S$ values range from + 5.2 to + 8.5‰ with D_2 vein chalcopyrite data falling in the upper part of that range. $\Delta^{34}S_{py\text{-}cpy}$ values from the present study (-1.1 - 0.7‰) generally concur with previous studies, suggesting a lack of equilibrium between pyrite an dchalcopyrite (Walshe and Solomon, 1981).

Sphalerite $\delta^{34}S$ values (+ 10.3 to + 11.3‰) reflect minimum values only, as any chalcopyrite or galena present in equilibrium with the sphalerite would reduce the true sphalerite $\delta^{34}S$ ratio.

7.4.2 Discussion

7.4.2.1 *Devonian effects on $\delta^{34}S$ distribution*

Several Cambrian sulphide deposits in western Tasmania show evidence of interaction with Devonian fluids, with varying effects on $\delta^{34}S$ distribution. In the F(J) Lens of the Rosebery massive sulphide deposit Solomon *et al.* (1987) noted Devonian replacement of base metal sulphides by pyrite and pyrrhotite by a post-deformation, reduced, granite-derived fluid. Solomon *et al.* concluded that the fluid had not introduced magmatic sulphur and replacement had not resulted in a significant alteration of the original Cambrian $\delta^{34}S$ distribution. However, a more detailed study by Zaw (1991) showed that the pyrite - pyrrhotite replacement did result in homogenisation of the original isotopic distribution. In contrast, Devonian metamorphic recrystallisation of Cambrian sulphides at the South Hercules deposit did not significantly affect the isotopic composition of the ore.

The lack of obvious replacement textures similar to Rosebery at Prince Lyell suggests that Devonian magmatic fluids have not affected the Prince Lyell mineralisation. Such effects would most likely be seen in the deeper parts of the orebody and adjacent to the Great Lyell fault. These parts of the orebody would be the first to be encountered by a rising hydrothermal fluid focussed by the combined structural conduits of the major D_1 anticline, and the Great Lyell and Linda fault zones. The lack of vertical zonation in $\delta^{34}S$ values in the southern Prince Lyell pyrite, over the 800 metres shown in Figure 7.1, suggests that large scale redistribution of Cambrian $\delta^{34}S$ values by later fluids has not occurred. The lateral persistence of the $\delta^{34}S$ zonation away from the mineralised horizon also suggests that substantial homogenisation of original $\delta^{34}S$ values has not occurred.

A possible minor effect on Cambrian $\delta^{34}S$ values by later fluids is shown at Prince Lyell by the variation in $\delta^{34}S$ between disseminated chalcopyrite and remobilised chalcopyrite in quartz - siderite veins. The veins were formed by the precipitation of minerals sweated out of the wallrocks by metamorphic fluids in tensional fractures, late during D_2 (see Chapter 6). Chalcopyrite in these veins has $\delta^{34}S$ values between 7.5 and 8.5‰ compared to the disseminated chalcopyrite range of 5.2 to 8.3‰. The slightly higher average $\delta^{34}S$ ratio of the remobilised chalcopyrite may reflect re-equilibration

of the Cambrian sulphur with a metamorphic fluid during the waning stages of D_2 deformation. However, the overlap of the two data sets suggests such adjustments in $\delta^{34}S$ would be minor.

A similar lack of variation in the $\delta^{34}S$ of remobilised sulphides is shown by the sphalerite samples. The $\delta^{34}S_{sph}$ of the highly foliated baritic vein of probable Cambrian age (sample 115012, 11.3‰) is virtually identical to the $\delta^{34}S_{sph}$ of the remobilised post-cleavage massive sphalerite vein (sample 586201.3, 10.3‰).

7.4.2.2 *Cambrian $\delta^{34}S$ distribution*

Having assessed that Devonian fluids have probably not caused significant redistribution of Cambrian sulphur isotope patterns, an assessment of the $\delta^{34}S_{py}$ zonation across the southern Prince Lyell orebody is possible. Isotopic variation of the small magnitude seen at Prince Lyell may be due either to absolute changes in the mean $\delta^{34}S_{\Sigma S}$ of the hydrothermal fluid or to changes in physiochemical conditions within a fluid of fairly constant mean isotopic composition. Without detailed temperature information, distinguishing between the two processes is difficult (Walshe and Solomon, 1981). However, on the basis of the inferred evolution of hydrothermal solutions in volcanogenic systems, outlined by Solomon *et al.* (1988), certain observations about the Prince Lyell mineralising fluid may be made.

Reduced seawater sulphate is regarded to be the source of the majority of sulphur in volcanogenic massive sulphide deposits. The complete reduction of seawater sulphate to sulphide, by reducing agents such as ferrous iron from ferromagnesian minerals in the volcanic substrate, is suggested to occur for up to one kilometre below the sea floor (Green *et al.*, 1981; Walshe and Solomon, 1981). Sulphides precipitated from Cambrian seawater ($\delta^{34}S$ = 30‰) would have $\delta^{34}S$ values ranging upwards from about 10‰ assuming complete sulphate reduction and equilibrium fractionation of sulphur species (Solomon *et al.*, 1988).

Dissolution of trace amounts of iron and copper sulphides and igneous sulphate from the host rocks, will progressively modify the isotopic composition of the circulating fluid (Shanks *et al.*, 1981). Mafic volcanics contain some twenty times more sulphur, on average, than felsic volcanics with the resulting hydrothermal systems dominated by rock sulphur (Solomon *et al.*, 1988). Sulphur contents of circulating fluids in felsic volcanics are more likely reflect combinations of reduced seawater sulphate and average felsic igneous rock sulphur ($\delta^{34}S = 0 \pm 3$‰, Ohmoto and Rye, 1979).

The contribution of rock sulphur to the composition of the mineralising fluid is likely to vary with time, as suggested by Solomon *et al.* (1988) at the Rosebery massive sulphide deposit. There, increasing $\delta^{34}S$ values higher in the orebody are thought to reflect a decreasing contribution with time of rock sulphur to the circulating fluid, as the rock sulphur source is depleted by leaching. Previous studies have not recognised $\delta^{34}S$ zonation in the Prince Lyell orebody. Walshe and Solomon (1981) and Solomon *et al.* (1988) concluded that the hydrothermal system was isotopically homogeneous, being dominated by sulphur sourced from the host rocks. This implies the host volcanic pile at Mt Lyell is rich in sulphur, possibly from basalts at depth.

The zonation from lighter to heavier isotopic values, outwards from the central ore horizon, may be explained by a scenario similar to that proposed at Rosebery by Green *et al.* (1981). There, later formed sulphides had higher $\delta^{34}S$ ratios as igneous rock sulphur contributed less to a seawater-derived hydrothermal fluid over time. By this process, later formed isotopically heavier sulphides at Prince Lyell may have been deposited as the fluid permeated further into the wallrocks. Alternatively, the heavier $\delta^{34}S$ values may have been produced by mixing of the hydrothermal fluid with cooler, more oxidised seawater in the volcanic pile on the periphery of the mineralised horizon.

The slightly heavier $\delta^{34}S$ values of sphalerite at Prince Lyell indicate lack of equilibrium with pyrite or chalcopyrite and suggest sphalerite deposition from a cooler, more oxidised fluid. This is supported by the association of sphalerite with a barite gangue. The late stage barite - sphalerite veins at Prince Lyell are probably analogous to barite-sphalerite mineralisation deposited at the top of the Rosebery, Hellyer and other volcanogenic massive sulphide deposits.

The deposition of baritic mineralisation from a fluid containing only partially reduced seawater sulphate has been proposed at Rosebery by Solomon *et al.* (1988). As reducing agents in a hydrothermal cell are gradually exhausted by continued reaction with the circulating fluid, incomplete reduction of seawater sulphate in the mineralising fluid may result. The oxidation state of the fluid under these conditions increases rapidly and usually occurs towards the end of the circulation cycle, when the temperature is falling. Consequent $\delta^{34}S$ values of precipitated minerals are significantly higher than earlier formed sulphides (Solomon *et al.*, 1988).

7.5 SHRIMP $\delta^{34}S$ STUDY

7.5.1 Results

Sample descriptions and results of the SHRIMP analyses are summarised in Table 7.1 and Figure 7.3. Four analyses fall outside the lower limit of values obtained by the conventional method, as may be expected for the reasons outlined above. However, due to the analytical error (± 2‰) of the ion probe, these values may fall within or close to the range of bulk pyrite analyses. There are no values either at or above the upper limit of conventional analyses.

No consistent $\delta^{34}S$ variation is observed between pyrite generations within individual grains. Isotopic variation appears to follow neither trace element geochemical trends nor paragenetic sequence. Sample 115003 shows a decrease in $\delta^{34}S$ from cobalt-rich core to cobalt-poor rim, whereas sample 599377.3 shows the reverse trend. Pyrite generations within samples 598259.7 and 639121.3 are isotopically identical, considering analytical error.

Sample 619098.6, from a silica-pyrite alteration zone within the South Lens,shows no internal variation and exhibits the heaviest $\delta^{34}S$ values of all the samples (8 - 9‰). Samples 624096.9 and 639121.3, from the Great Lyell fault zone, have isotopic compositions similar to pyrite from the host volcanics.

7.5.2 Discussion

The lack of high $\delta^{34}S$ values (> 8‰) from individual pyrite grains is surprising, especially considering several samples were taken from footwall and hangingwall volcanics where conventionally analysed $\delta^{34}S_{py}$ values were highest. The reason for this anomaly is unclear. The small number of analysed grains may represent a very incomplete sample, accounting for the absence of higher $\delta^{34}S_{py}$ values. Alternatively, it may indicate that the zonation in $\delta^{34}S_{py}$ values across the orebody is a perceived rather than real zonation.

The narrow range of sulphur isotope ratios analysed by the SHRIMP technique is not supportive of hydrothermal fluids of distinctly different character being responsible for the different generations of pyrite deposition. In particular, the data do not support the scenarios suggested in Section 5.1.10 whereby Pyrite II was deposited by a fluid in equilibrium with hematite. Distinctly lower $\delta^{34}S_{py}$ values would have been expected from pyrite deposited in equilibrium with such an oxidised fluid (Ohmoto and Rye, 1979).

Sample #	Location	Pyrite description	Trace element composition	Pyrite type	δ34 S	Figure reference
115003 A	Section 71 - Hangingwall intermediate-mafic volcanics	Zoned and corroded core	550ppm Co 700ppm As	I	7 ‰	Fig 7.3a
115003 B		Euhedral overgrowth	4 500ppm Co 1 500ppm Ni 650ppm As	I	7 ‰	
115003 C		Anhedral overgrowth with apatite inclusions	600ppm As	II	4 ‰	
598259.7 A	Section 70 - Footwall Lens horizon	Zoned and corroded core	4 900ppm Co 750ppm Ni 600ppm As 700ppm Se	I	6 ‰	Fig 7.3b
598259.7 B		Anhedral overgrowth	11 200ppm Co 700ppm Cu 2 000ppm As	III	7 ‰	
599377.3 A	Section 75 - Hangingwall hematitic felsic volcanics	Zoned core	6 200ppm Co 850ppm Ni 900ppm As	I	3 ‰	Fig 7.3c
599377.3 B		Anhedral overgrowth with hematite inclusions	500ppm As	II	7 ‰	
599377.3 C		Thin rim around previous overgrowth	2 400ppm Co 450ppm Ni 450ppm As	III	7 ‰	
619098.6 A	Section 68 - Silicified zone between North and South Lens	Early euhedral grain	2 700ppm As	II	9 ‰	Fig 7.3d
619098.6 B		Massive overgrowth	550ppm Co 9 500ppm As	III	8 ‰	
619098.6 C		Massive overgrowth	500ppm As	II	9 ‰	
624096.9 A	Section 76 - Great Lyell fault zone	Finely disseminated zoned grain	500ppm Co 3 000ppm As	I	6 ‰	Fig 7.3e
624096.9 B		Finely disseminated euhedral grain	450ppm As	II	6 ‰	Fig 7.3f
639121.3 A	Section 74 - Great Lyell fault zone	Zoned and corroded core	1 500ppm Ni 450ppm As 650ppm Se	I	4 ‰	Fig 7.3g
639121.3 B		Euhedral overgrowth	250ppm Ni 500ppm As	II	5 ‰	

Table 7.1 Description and chemical composition of pyrite samples analysed by the SHRIMP ion microprobe.

Figure 7.3

Reflected light photomicrographs of SHRIMP Ion Microprobe sulphur isotope sites. All samples are etched to highlight internal growth structures in pyrite.

A. Pyrite from a thin stringer in hangingwall intermediate-mafic volcanics. Euhedral inclusions in the last pyrite overgrowth are apatite. (sample 115003)

B. Disseminated pyrite and chalcopyrite (heavily tarnished) from weakly mineralised felsic volcanics in the Footwall Lens horizon. (sample 589259.7)

C. Disseminated pyrite grain with abundant hematite blades included in later pyrite generations, from weakly mineralised felsic volcanics in the southern hangingwall. (sample 599377.3)

D. Massive pyrite and interstitial chalcopyrite from late stage silica-pyrite alteration. (sample 619098.6)

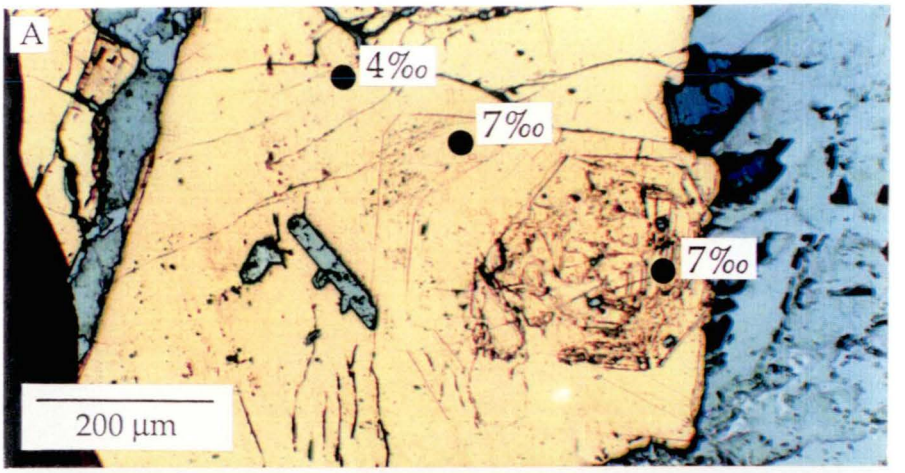
A
4‰
7‰
7‰
200 µm

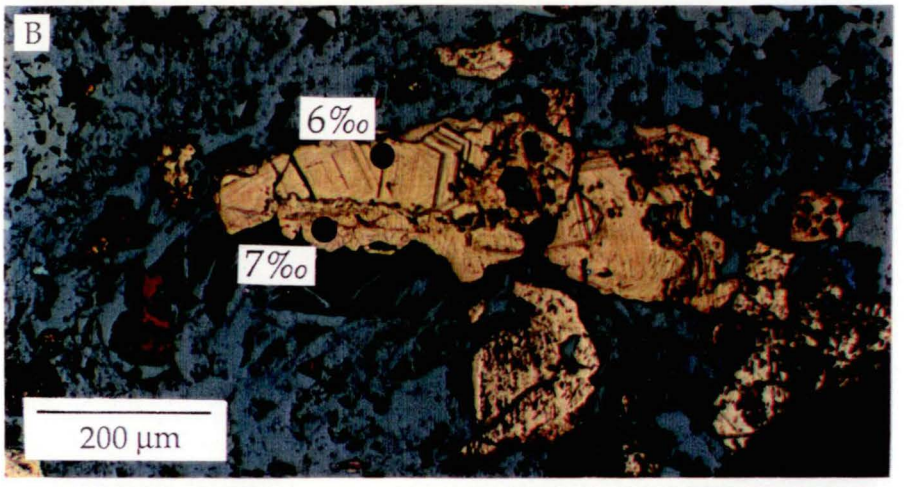
B
6‰
7‰
200 µm

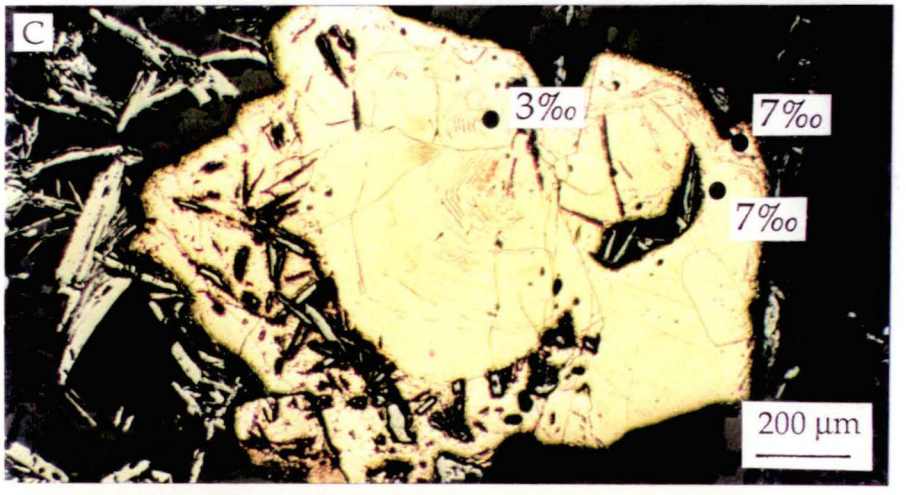
C
3‰
7‰
7‰
200 µm

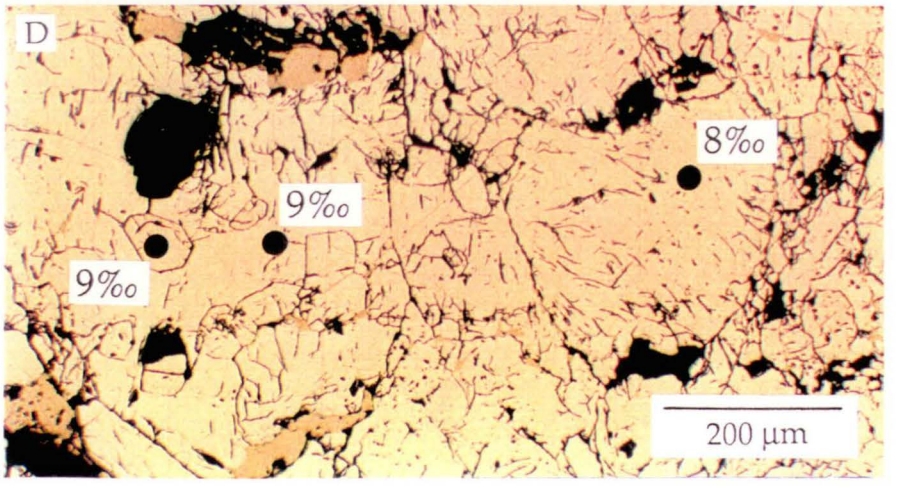
D
8‰
9‰
9‰
200 µm

Figure 7.3 continued

E. Disseminated corroded and zoned pyrite euhedra in the Great Lyell fault zone. (sample 624096.9)

F. Disseminated pyrite euhedra in the Great Lyell fault zone. (sample 624096.9)

G. Euhedral pyrite overgrowth on a zoned and corroded core, from the Great Lyell fault zone. (sample 639121.3)

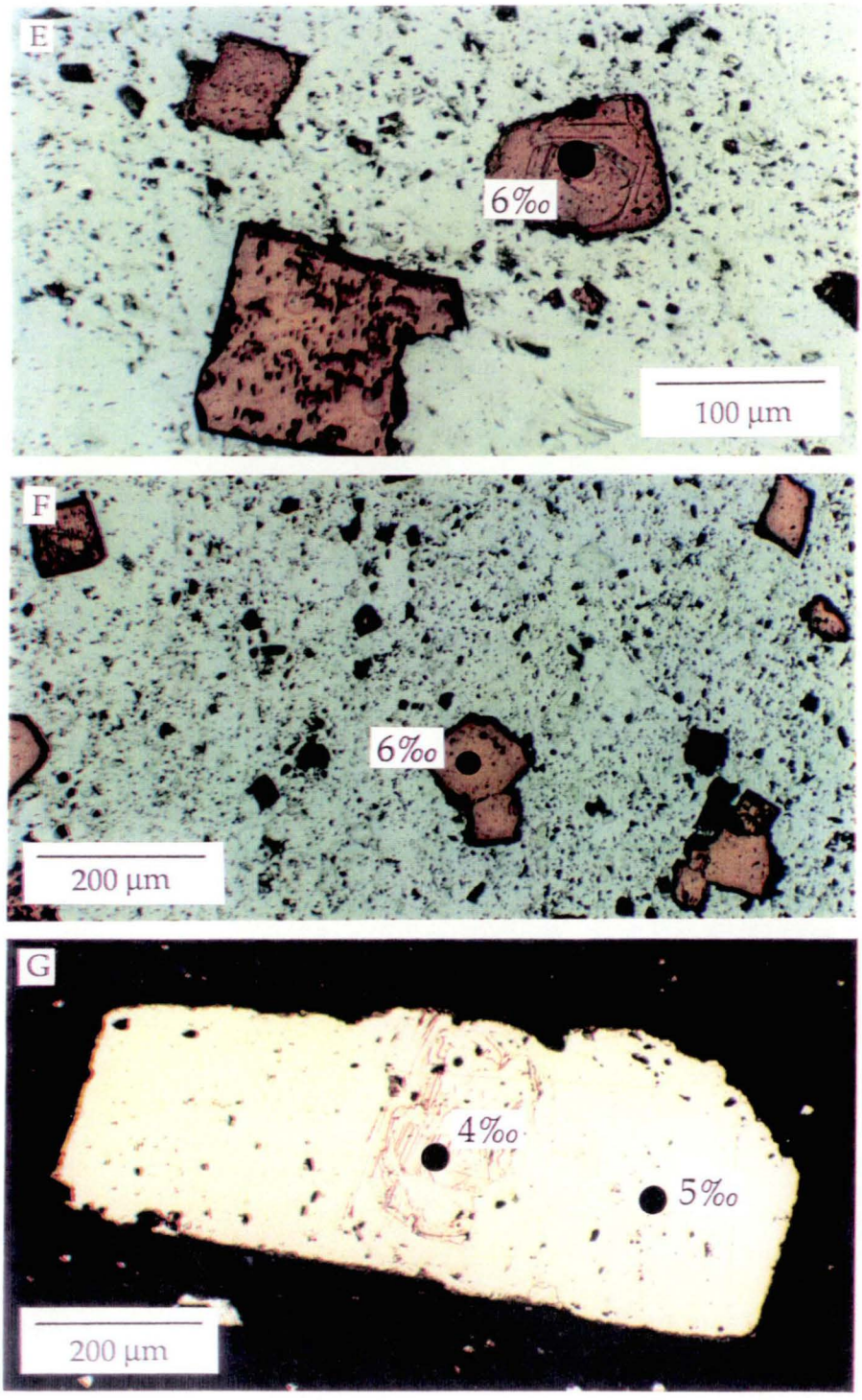
E
6‰
100 µm
F
6‰
200 µm
G
4‰
5‰
200 µm

Examples of very low to negative $\delta^{34}S_{py}$ ratios that may be expected from oxidised conditions occur in the hematitic North Lyell orebodies (Walshe and Solomon, 1981).

The tightly grouped, irregularly variable $\delta^{34}S_{py}$ values obtained from individual pyrite grains suggest that the mineralising fluid (or fluids) was relatively homogeneous and that variations in isotopic composition were caused by local fluctuations in physiochemical conditions at the site of pyrite deposition. Irregularities in mixing of leached rock sulphur with a seawater derived fluid may also have caused small scale aberrations in the $\delta^{34}S_{\Sigma S}$ of the fluid.

The late overprinting silica - pyritic alteration zone (sample 619098.6) is likely to have been at a lower temperature relative to the main mineralisation event. These conditions are suggested by the slightly higher $\delta^{34}S_{py}$ values (8 - 9‰), and low grade of chalcopyrite mineralisation due to the reduction in copper solubility at low temperatures (Crerar and Barnes, 1976).

The similarity of $\delta^{34}S$ values of pyrite in the Great Lyell fault zone to those in the host volcanics indicates addition of sulphur of a different origin by later fluids moving up the fault zone has not occurred. The small range of $\delta^{34}S_{py}$ values (4 - 6‰) is not the result of homogenisation by processes such as metamorphic recrystallisation, as the preservation of small scale structures within the pyrite grains indicates recrystallisation has not taken place.

7.6 CONCLUSIONS

Interpretation of the combined results of conventional sulphur isotope study and *in situ* microanalysis generally concurs with that of previous workers from conventional sulphide analyses (e.g. Walshe and Solomon, 1981; Solomon *et al.*, 1988). Although the zonation in $\delta^{34}S_{py}$ values across the orebody was not previously described, its interpretation does not significantly alter theories of sulphur source and isotopic evolution of the mineralising fluid.

The main mineralising fluid is regarded to be seawater-derived, but modified by igneous rock sulphur leached from the host volcanics during circulation. The mixing of entirely reduced seawater sulphate ($\geq$ 10‰) with the rock sulphur ($\sim$ 0‰), resulted in a relatively homogeneous fluid, with $\delta^{34}S_{\Sigma S}$ = 3 - 11‰. Weak isotopic zonation was probably due to a declining contribution of igneous rock sulphur to the hydrothermal fluid over time, or mixing of the hydrothermal fluid with seawater on the periphery of the mineralised zone. Variations in the overall zonation trend may have been

caused by local irregularities in physiochemical conditions or uneven mixing of sulphur sources.

Waning temperatures and possible incomplete reduction of seawater sulphate in the fluid resulted in an increase in the oxidation state and $\delta^{34}S_{\Sigma S}$ of the fluid, and an increase in sphalerite solubility relative to chalcopyrite. Consequent late sphalerite - barite mineralisation had elevated $\delta^{34}S_{sph}$ values, reflecting the changing conditions of the ore fluid.

CHAPTER EIGHT

OXYGEN ISOTOPES

8.1 WHOLE ROCK ANALYSES

8.1.1 Introduction

A study of the whole rock oxygen isotope distribution in the southern Prince Lyell area has a dual purpose. The first aim is to establish the effect, if any, of metamorphic fluids on a hydrothermal alteration isotopic signature and to gain an insight into the role of the metamorphic fluid in ore remobilisation. Secondly, the character of the original hydrothermal fluid may be estimated if metamorphic effects are negligible or may be accounted for.

Reduction-oxidation (redox) boundaries suggested by previous authors may also be reflected by variations in whole rock oxygen isotope values across the Prince Lyell sequence. Walshe and Solomon (1981) suggested that deposition of early fine grained hematite in the footwall felsic volcanics, causing their characteristic pink colouring, may have acted as a redox front at which later sulphide mineralisation took place.

Arnold (1985) and Arnold and Fitzgerald (1986) suggested that the volcanics - Owen Conglomerate contact is likely to have acted as a chemical boundary or redox front. Fluids derived from the Owen Conglomerate would have been buffered by the abundant primary or diagenetic hematite in the conglomerate, while volcanics-derived fluids would have been more reduced, being buffered by pre-existing pyrite. The precipitation of hydrothermal hematite in the volcanics adjacent to the Great Lyell fault is testimony to circulation of an oxidised fluid in the volcanics near the contact. Oxygen isotope distribution in the volcanics may provide a clue to the nature of this late oxidised fluid.

8.1.2 Sample Preparation and Analysis

Thirty-one samples of altered volcanics across the Prince Lyell sequence were collected from the diamond drill holes WL634 and WL637, on Sections 68 and 71 respectively. In addition, one sample of highly sheared volcanics

from the Great Lyell fault zone and one sample of Owen Conglomerate were collected from WL637.

The samples were crushed and pyrite separated from them to avoid contamination of the oxygen extraction procedure by sulphur-based compounds. A first pass pyrite separation was completed by agitation of the 75 - 106 μm fraction in water and the pyrite float skimmed off the top. Further purification to ≤1% pyrite was performed by gravity separation using an automatic panner (Muller, 1977). Oxygen separation and mass spectrometry were carried out by M. Power (jnr) at the Department of Geology and Central Science Laboratories, University of Tasmania.

8.1.3 Results

Distribution of whole rock $\delta^{18}O$ values and sample descriptions are presented in Table 8.1 and Figure 8.1. The $\delta^{18}O$ range of southern Prince Lyell altered volcanics is fairly small, ranging from 6.6‰ to 10.6‰. The one sample of Owen Conglomerate analysed has a $\delta^{18}O$ ratio of 12.6‰.

Variation of $\delta^{18}O$ values is independent of copper mineralisation. There is no consistent isotopic zonation centred on the mineralised horizon. There is, however, a good correlation of $\delta^{18}O$ values with alteration lithology. Lowest values in the sequence are found in the chloritic intermediate - mafic volcanics with higher values in the felsic volcanics. Highest $\delta^{18}O$ values occur in the sericitic footwall felsic volcanics adjacent to the Great Lyell fault. Samples in or near magnetite alteration zones have lower $\delta^{18}O$ values than the surrounding rocks.

8.1.4 Discussion

8.1.4.1 Comparison with other volcanic hosted deposits

The range of $\delta^{18}O$ values of the altered Prince Lyell volcanics is very similar to that of the most altered zones surrounding other volcanic-hosted sulphide deposits in Japan and Australia. $\delta^{18}O$ values are 5 - 8‰ in the sericite-chlorite altered core of the Fukazawa Kuroko deposit in Japan (Green *et al.*, 1983). The strongly altered footwall volcanics of the Hercules deposit in Tasmania have $\delta^{18}O$ ratios between 7 and 10‰ (Green, 1986, 1990). Both these districts show a consistent relationship between increasing alteration and decreasing whole rock $\delta^{18}O$ values. $\delta^{18}O$ values increase to around 14 - 20‰ in weakly altered rocks on the peripheral alteration zones (Green *et al.*, 1983; Green, 1986, 1990).

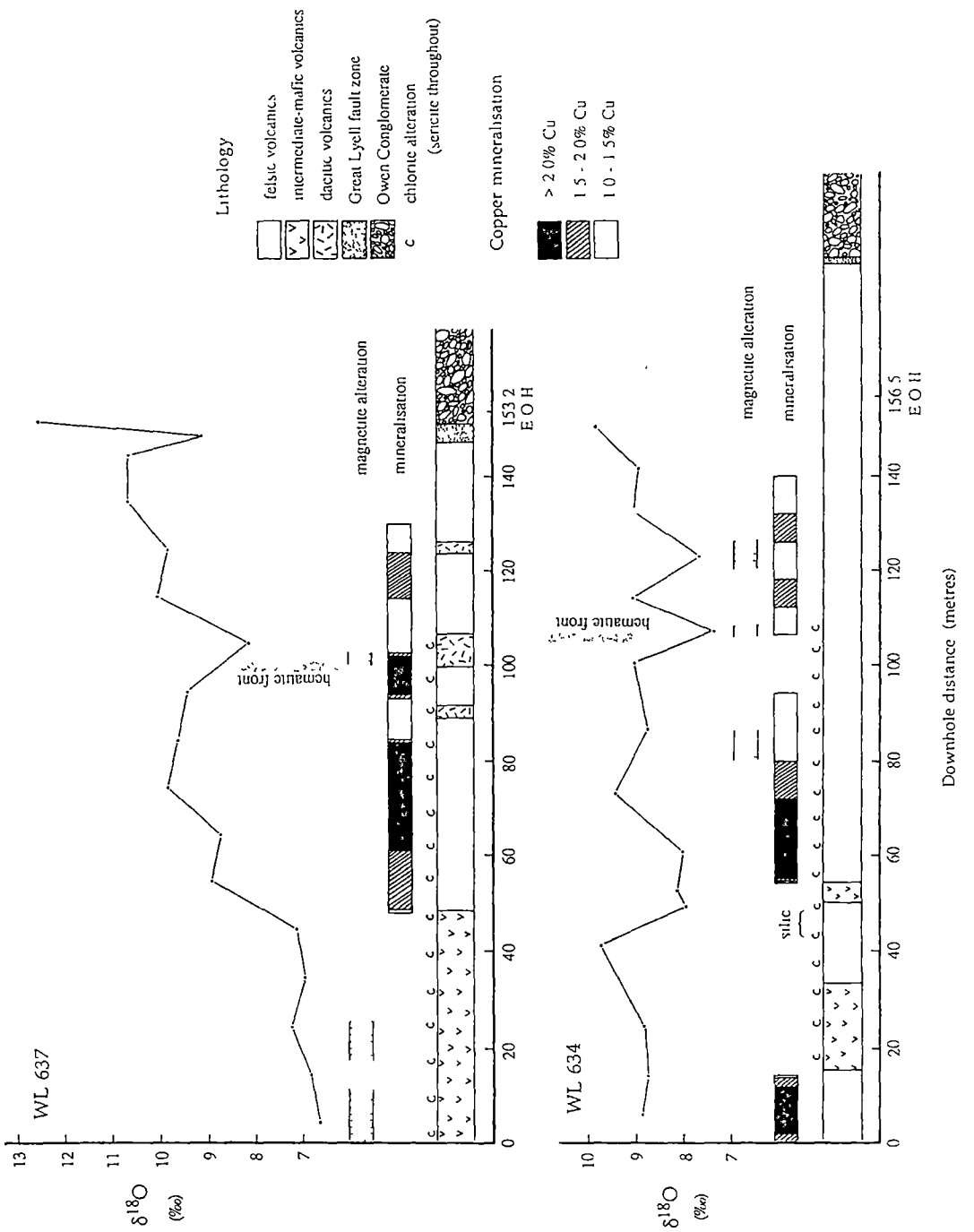

Figure 8.1 Distribution of whole rock $\delta^{18}O$ ratios in the southern Prince Lyell area. Variations in the isotope ratios show no relationship to sulphide mineralisation. However, the $\delta^{18}O$ ratios largely reflect relative abundances of alteration minerals in the altered volcanics.

Green *et al.* (1983) interpreted the $\delta^{18}O$ values of the sericite-chlorite alteration at Fukazawa to be produced by interaction of seawater with the volcanic sequence at between 200°C and 400°C under water-dominated conditions (water/rock ratio > 1).

Drill hole and depth	Lithology	$\delta^{18}O_r$ (‰)
WL637, 0 - 10 m	intermediate-mafic volcanics; disseminated mgt	6.6
WL637, 10 - 20 m	intermediate-mafic volcanics	6.8
WL637, 20 -30 m	intermediate-mafic volcanics	7.2
WL637, 30 - 40 m	intermediate-mafic volcanics	6.9
WL637, 40 - 50 m	intermediate-mafic volcanics	7.1
WL637, 50 - 60 m	chloritic felsic + intermediate-mafic volcanics	8.9
WL637, 60 - 70 m	chloritic felsic + dacitic volcanics	8.7
WL637, 70 - 80 m	weakly chloritic felsic volcanics	9.8
WL637, 80 - 90 m	chloritic felsic volcanics	9.6
WL637, 90 - 100 m	weakly chloritic felsic + dacitic volcanics	9.4
WL637, 100 - 110 m	chloritic felsic volcanics; minor mgt	8.1
WL637, 110 - 120 m	weakly chloritic felsic volcanics	10.0
WL637, 120 - 130 m	sericitic felsic + dacitic volcanics	9.8
WL637, 130 - 140 m	sericitic, hematitic felsic volcanic	10.6
WL637, 140 - 147 m	sericitic, hematitic felsic volcanic	10.6
WL637, 147 - 150.9 m	highly sericitic volcanics; Great Lyell fault	9.1
WL637, 150.9 - 153.2 m	Owen Conglomerate	12.6
WL634, 0 - 13.4 m	weakly chloritic felsic volcanics	8.8
WL634, 16.1 - 34.0 m	chloritic felsic + intermediate volcanics; minor mgt	8.8
WL634, 34.0 - 48.7 m	silicified, weakly chloritic felsic volcanics	9.7
WL634, 48.7 - 50.5 m	weakly chloritic felsic volcanics	7.9
WL634, 50.5 - 54.9 m	intermediate-mafic volcanics	8.1
WL634, 54.9 - 67.0 m	chloritic felsic volcanics	8.0
WL634, 67.0 - 80.0 m	chloritic felsic volcanics	9.4
WL634, 80.0 - 94.0 m	chloritic felsic volcanics; minor mgt	8.7
WL634, 94.0 - 106.1 m	chloritic felsic volcanics	9.0
WL634, 106.1 - 108.1 m	very chloritic felsic + mgt alteration	7.3
WL634, 108.1 - 120.5 m	weakly chloritic felsic	9.0
WL634, 120.5 - 126.2 m	very chloritic felsic + mgt alteration	7.6
WL634, 126.2 - 139.7 m	sericitic, hematitic felsic volcanic	9.0
WL634, 139.7 - 144.3 m	sericitic, hematitic felsic volcanic	8.9
WL634, 144.3 - 156.5 m	sericitic, hematitic felsic volcanic	9.8

Table 8.1. Sample descriptions and results ($\delta^{18}O_r$) of whole rock oxygen isotope analyses.

8.1.4.2 Metamorphic Effects

The effects of isotopic exchange between a metamorphic fluid and the Mt Read Volcanics have been modelled by Green (1990). He indicated that a Devonian regional metamorphic fluid in equilibrium with the Mt Read Volcanics would have had a $\delta^{18}O$ value of 7 - 10‰, assuming average $\delta^{18}O$

values of 6.5 - 9.5‰ for rhyolitic to dacitic volcanics and 5.5 - 8.5‰ for andesitic to basaltic volcanics (Taylor and Sheppard, 1986).

Isotopic exchange during alteration by this metamorphic fluid would have increased the $\delta^{18}O$ values of the volcanic rocks to around 11.5 - 16.5‰ (Green, 1990). This is in contrast to the low $\delta^{18}O$ values of the Prince Lyell altered rocks and to the trend of decreasing $\delta^{18}O$ values with increasing alteration of Hercules altered rocks (Green, 1986). This suggests that a metamorphic fluid did not play a significant role in the formation of the alteration assemblages at Prince Lyell.

The $\delta^{18}O$ ratio of the Great Lyell fault zone sample ($\delta^{18}O$ = 9.1‰), corresponds to the general range of altered volcanics and suggests that the rock has not undergone metamorphic re-equilibration. A fault zone such as the Great Lyell may be expected to focus any metamorphic fluid and yet it preserves a $\delta^{18}O$ ratio which does not appear to be affected by metamorphism. This suggests further that a regionally derived fluid phase did not have a major role in the Devonian metamorphic event.

8.1.4.3 Variation of $\delta^{18}O$ values within the altered volcanics

Due to variable fractionation of oxygen isotopes between different minerals and a fluid, whole rock $\delta^{18}O$ values are dependant on the relative proportions of minerals in the rock. Most of the variation in $\delta^{18}O$ values across the Prince Lyell volcanic sequence can be accounted for by the varying mineralogy of the altered rocks. Common alteration mineral fractionation factors ($\Delta_{mineral\text{-}water}$), which are inversely proportional to temperature (°K), are summarised below:

$$\Delta_{quartz\text{-}water} = 3.38 \times 10^6/T^2 - 3.40 \quad \text{(Clayton et al., 1972)} \quad \ldots\ldots 8.1$$

$$\Delta_{chlorite\text{-}water} = 1.56 \times 10^6/T^2 - 4.69 \quad \text{(Wenner and Taylor, 1971)} \quad \ldots\ldots 8.2$$

$$\Delta_{sericite\text{-}water} = 2.38 \times 10^6/T^2 - 3.89 \quad \text{(O'Neil and Taylor, 1967)} \quad \ldots\ldots 8.3$$

$$\Delta_{magnetite\text{-}water} = -0.13 \times 10^6/T^2 - 6.38 \quad \text{(Wenner and Taylor, 1971)} \quad \ldots\ldots 8.4$$

Wenner and Taylor's (1971) magnetite - water data has been challenged more recently by the theoretical calculations of Becker and Clayton (1976) and Zheng (1991). They suggest that magnetite $\delta^{18}O$ ratios are significantly lighter (by around 1.6‰) than Wenner and Taylor's values at 300°C.

Prince Lyell rocks may be closely approximated by combinations of the above mentioned minerals and their whole rock-water fractionation factors

($\Delta_{r\text{-}w}$) calculated by combination of the component mineral fractionation factors,

$$\text{ie:} \quad \Delta_{r\text{-}w} = \Sigma\, X_{mineral} \cdot \Delta_{mineral\text{-}water} \qquad \ldots\ldots\ 8.5$$

where $X_{mineral}$ is the proportion of a mineral in the rock. Calculated fractionation factors for average compositions of intermediate - mafic, chloritic felsic and sericitic felsic volcanics at various temperatures are shown in Table 8.2.

A commonly used approximation for igneous rock $\Delta_{r\text{-}w}$ values is plagioclase-water fractionation ($\Delta_{plag\text{-}water} = 2.68 \times 10^6/T^2 - 3.53$) (eg: Taylor, 1979; Green *et al.*, 1983). However, only the fractionation factor for chloritic felsic volcanics approaches this value at Prince Lyell (Table 8.2). The range of fractionation factors of the three alteration rock types accounts for the range of $\delta^{18}O_r$ values at Prince Lyell. For example, the approximately 3‰ difference in fractionation factors of intermediate and sericitic felsic volcanics ($\Delta_{r\text{-}w}$, Table 8.2) matches the 3‰ difference in their average $\delta^{18}O_r$ values. Isotopic variation within each rock type may be due to either departures of mineralogical composition from average values or local fluctuations in water/rock ratio and temperature.

Rock type	average %			$\Delta_{r\text{-}w}$			average $\delta^{18}O_r$
	quartz	chlorite	sericite	270°C	300°C	330°C	
intermediate-mafic	12	45	43	3.0	2.3	1.7	7 - 8 ‰
chloritic felsic	55	20	25	5.6	4.6	3.8	8 - 10 ‰
sericitic felsic	55	-	45	6.3	5.3	4.4	9 - 11 ‰
Owen conglomerate	95	-	5	7.9	6.7	5.7	12 - 13 ‰

Table 8.2. Average calculated $\Delta_{r\text{-}w}$ and measured $\delta^{18}O_r$ values for Prince Lyell lithologies.

Units of felsic volcanics with magnetite mineralisation (ie: 102 metres, WL 637; 108 and 123 metres, WL 634) are isotopically lighter than the surrounding rocks by between 0.3 and 1.9‰. Superficially, this appears due to the presence of relatively isotopically light magnetite veining. 5 to 10% of magnetite in equilibrium with the quartz - sericite - chlorite assemblage would lower the whole rock $\delta^{18}O$ ratios by approximately 1 to 1.5‰ (equations 8.4 and 8.5). However, analyses of the vein magnetite (see Section 8.2 below) show that the magnetite is isotopically heavier than would be

expected in equilibrium with the whole rock alteration fluid, requiring 10 to 20% magnetite to achieve the same decrease in whole rock $\delta^{18}O$ ratio. As these levels of magnetite are much more than are present in the rocks, a further, as yet unknown, explanation for the decrease in whole rock $\delta^{18}O$ is required.

The inclusion of minor hematite in the whole rock calculations would also lower the calculated $\delta^{18}O$ values. Bertenrath *et al.* (1973) and Zheng (1991) suggested that hematite Δ_{r-w} = -10 to -10.5‰ at 300°C. The generally small amounts of hematite in the sericitic felsic volcanics would have little effect on the calculations. However, the addition of 5% hematite would lower by almost 1‰ the calculated $\delta^{18}O$ value of an Owen Conglomerate in equilibrium with the altered volcanics.

8.1.4.4 Redox boundaries

Redox or chemical boundaries within the volcanic sequence are not indicated by the whole rock $\delta^{18}O$ values. Isotopic equilibrium appears to have been approached within the volcanic pile.

However, the higher $\delta^{18}O$ value of the Owen Conglomerate ($\delta^{18}O$ = 12.6‰) may indicate a chemical shift across the Great Lyell fault. Calculations from Table 8.2 indicate that Owen Conglomerate in isotopic equilibrium with the observed altered volcanics would have a $\delta^{18}O$ value of around 10‰ (based on a quartz - sericite - hematite assemblage). The higher measured $\delta^{18}O$ value for the conglomerate suggests that isotopic equilibrium was not reached across the Great Lyell fault and may reflect a sedimentary isotopic signature of the oxidised Owen basin and its Precambrian basement source material. A chemical discontinuity at the Great Lyell fault is a likely trigger for precipitation of enriched copper mineralisation along the fault at North Lyell. However, mineralisation more removed from the fault, such as Prince Lyell, is unlikely to have been controlled by this process.

8.1.5 Origin of the hydrothermal fluid

The initial $\delta^{18}O$ of the hydrothermal fluid may be estimated by considering isotopic fractionation between the rocks and the fluid under assumed water/rock (W/R) ratios and temperature conditions (eg: Green *et al.*, 1983). Interpretation of the origin of the fluid may then be made.

Estimation of the W/R ratio is dependant upon the type of fluid circulation system considered. Taylor (1979) considered the extreme examples of entirely closed and open systems for a circulating fluid. In the closed

system, a single packet of water attained equilibrium at a fixed temperature with a volume of rock, with no isotopic exchange outside it. In the open system, a volume of water was introduced to a rock, allowed to attain equilibrium with it and replaced by successive pulses of water. The W/R ratios for the two systems vary according to the equations below,

$$W/R = \frac{\delta^{18}O_{rf} - \delta^{18}O_{ri}}{\delta^{18}O_{wi} - \delta^{18}O_{rf} + \Delta_{r\text{-}w}} \qquad \text{(closed system)}$$

$$W/R = \ln \frac{\delta^{18}O_{rf} - \delta^{18}O_{ri}}{\delta^{18}O_{wi} - \delta^{18}O_{rf} + \Delta_{r\text{-}w}} \qquad \text{(open system)}$$

where $\delta^{18}O_{ri}$ and $\delta^{18}O_{rf}$ are the initial and final rock $\delta^{18}O$ values, and $\delta^{18}O_{wi}$ is the initial water $\delta^{18}O$ value.

Taylor (1979) considered natural systems to lie between the two extreme cases. However, Ohmoto (1986) suggested that natural open systems are heated gradually, with isotopic exchange increasing with temperature, in contrast to Taylor's fixed high temperature model. Given this consideration, Taylor's estimates of the W/R ratio are minimum values only.

Despite the problems of applying these models directly to natural systems, open and closed systems have been modelled for the southern Prince Lyell to consider the relationship between the W/R ratio and the initial $\delta^{18}O$ of the fluid (Fig. 8.2). Average $\delta^{18}O$ and Δ_{rw} values for the chloritic felsic volcanics were taken as representative of the altered volcanics in the ore horizon. An initial value of 7.5‰ for the felsic volcanics was taken from average isotopic compositions of rhyolitic and dacitic lavas and pyroclastics (Taylor and Sheppard, 1986).

Studies on volcanogenic mineralising systems (eg: Beaty and Taylor, 1982; Ohmoto, 1983; Green *et al*, 1983; Michard and Albarede, 1986) suggest that W/R ratios are greater than 1, and commonly much greater. If this constraint is applied to the southern Prince Lyell data an estimate of the initial fluid $\delta^{18}O$ value may be made from Figure 8.2, as the open and closed system lines converge at W/R ratios > 1. At 300°C, the $\delta^{18}O_{wi}$ value lies between 4.5 and 6.0‰.

This $\delta^{18}O_{wi}$ ratio is several per mil higher than the value estimated by Green *et al.* (1983) for Japanese volcanogenic deposits, where seawater ($\delta^{18}O \approx$ 0‰) was invoked as the hydrothermal fluid. Assuming that the $\delta^{18}O$ ratio of

seawater has remained essentially constant at 0‰ since the Cambrian (Muehlenbachs, 1986), the Prince Lyell $\delta^{18}O_{wi}$ ratio could be consistent with

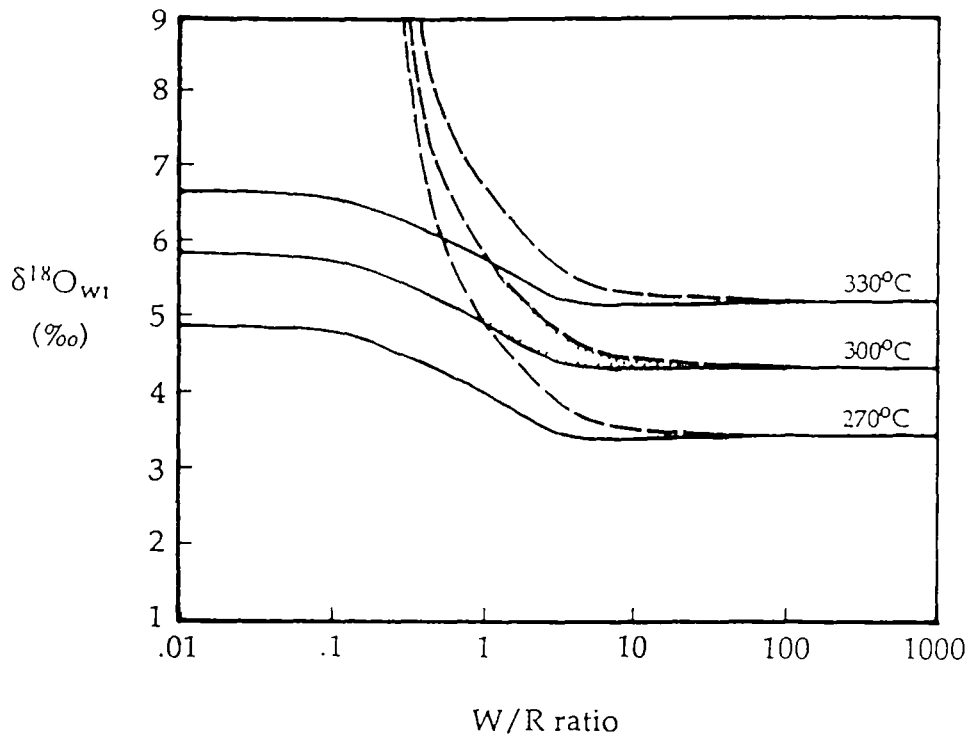

Figure 8.2 Variation of initial fluid $\delta^{18}O$ values with water-rock ratio and temperature, for the case of a chlorite - sericite altered felsic volcanic. Lines for Taylor's (1979) open (full line) and closed (broken line) systems are shown. The shaded area represents the probable range of $\delta^{18}O_{wi}$ values for the fluid at 300°C in the Prince Lyell ore zone.

the fluid being derived from seawater, but with increased $\delta^{18}O$ due to low temperature interaction with the volcanic pile prior to Prince Lyell mineralisation. Such a scenario was suggested by Ohmoto (1986) who stated that calculated $\delta^{18}O_{wi}$ values reflect only the initial conditions of the fluid at the fixed high temperature required by Taylor's (1979) models, and do not take into account evolution of the fluid during previous, lower temperature isotopic exchange.

An alternative explanation of the calculated $\delta^{18}O_{wi}$ value could involve the mixing of seawater with another fluid, resulting in an increased initial fluid $\delta^{18}O$ ratio. Magmatic fluids from a subvolcanic pluton, typically 7 - 13‰ (Ohmoto, 1986), may have been a source of isotopically heavier oxygen.

The calculated initial $\delta^{18}O$ value of the Prince Lyell fluid may not be directly compared to the estimated value of a Devonian metamorphic fluid (Green, 1990) as the water/rock ratio of a metamorphic environment is likely to be less than in fluid-dominated volcanogenic sulphide deposits. A water/rock ratio less than 1 would result in an unconstrained estimate of the initial fluid $\delta^{18}O$ value (Fig. 8.2).

8.2 MAGNETITE VEIN $\delta^{18}O$ ANALYSES

8.2.1. Sample preparation and results

Pure magnetite separates were obtained by drilling massive veins from magnetite alteration zones, after careful inspection to ensure the absence of silicate gangue contamination. The results of analyses by M. Power jnr at the University of Tasmania are presented in Table 8.3.

Sample location	$\delta^{18}O_{magnetite}$ (‰)
Drill hole WL580, 184.0 metres	3.8
Drill hole WL582, 279.4 metres	4.0
Drill hole WL633, 68.9 metres	4.0

Table 8.3. Results of magnetite $\delta^{18}O$ analyses.

8.2.2 Discussion

As the massive magnetite veins were precipitated directly from a hydrothermal fluid, the $\delta^{18}O$ of the fluid may be determined directly from magnetite - water fractionation factors, without consideration of fluid - rock ratios. At 300 - 400°C [1.], the $\delta^{18}O$ of the magnetite vein fluid would have been around 10.5‰ using Wenner and Taylor's (1971) data (equation 8.4), or around 12‰ according to the theoretical calculations of Zheng (1991) and Becker and Clayton (1976). These values are significantly higher than the calculated $\delta^{18}O$ value of the whole rock alteration fluid ($\delta^{18}O$ = 4.5 - 6.0‰) and an absurdly high temperature would be required to precipitate magnetite with $\delta^{18}O$ = 4.0 from this alteration fluid.

The inferred magnetite fluid $\delta^{18}O$ values are, however, consistent with a magmatic origin. Ohmoto (1986) quoted typical magmatic water values in

1. Apppoximate temperature assuming deposition of magnetite from a hot magmatic fluid, as suggested by thermodynamic modelling in Chapter 5.

the range 7 - 13‰. Pulses of an isotopically heavier magmatic fluid may have been injected into the zone of circulating seawater in the volcanic pile to produce the magnetite alteration zones. A magmatic origin for the magnetite mineralisation is supported by trace element compositions of the magnetite and associated apatite (see Chapter 5). The chemical disequilibrium suggested by oxygen isotopes between the magnetite mineralisation and earlier mineralisation assemblages is also supported by the dissolution of earlier chalcopyrite mineralisation around magnetite zones.

8.3 CONCLUSIONS

The Prince Lyell altered volcanic pile appears to have approached isotopic equilibrium. However, a relatively high $\delta^{18}O$ value of the Owen Conglomerate suggests that isotopic equilibrium did not extend across the Great Lyell fault.

$\delta^{18}O$ ratios for the Prince Lyell host rocks are lower than may be expected if significant isotopic exchange had occurred with a metamorphic fluid phase (Green, 1990). Even the Great Lyell fault zone, which may have been expected to have focussed a metamorphic fluid retains a relatively low whole rock oxygen isotope ratio. The $\delta^{18}O$ ratios of the Prince Lyell host rocks are similar to other Tasmanian and Kuroko volcanogenic deposits.

The whole rock $\delta^{18}O$ ratios are consistent with an initial fluid $\delta^{18}O$ of 4.5 - 6‰. This is significantly higher than Cambrian seawater, which would require some degree of low temperature interaction with the volcanic pile to raise its $\delta^{18}O$ ratio to the calculated initial value prior to mineralisation. It is most unlikely that magnetite mineralisation zones were precipitated from the same fluid which altered the Prince Lyell volcanic pile. However, magnetite $\delta^{18}O$ ratios suggest that a magmatic fluid with a $\delta^{18}O$ ratio of 10.5 - 12‰ may have been responsible for magnetite mineralisation.

CHAPTER NINE

CONCLUSIONS AND PARAGENETIC SUMMARY

9.1 ORIGIN AND ALTERATION TEXTURES OF THE HOST VOLCANICS

The southern Prince Lyell orebody occurs within a steeply plunging, overturned sequence of quartz - sericite - pyrite ± chlorite altered volcanics. The host volcanics underwent intense pervasive and texturally destructive alteration in the mid to late Cambrian volcanism as heated seawater circulated through the sequence. Textures previously interpreted as "fragmental" in the strongly altered felsic volcanics (eg: Braithwaite, 1985) are the product of heterogeneous development of siliceous and phyllosilicate alteration. Only minor relict enclaves of less strongly altered dacitic lavas and polymict mass flow breccias have preserved primary magmatic and volcaniclastic textures. Hence, terminology such as "intermediate - mafic" and "felsic volcanics" refer to highly altered rocks of which the precursor volcanic lithology can only be inferred.

At Prince Lyell, an irregular lens of altered intermediate - mafic volcanics, at least 200 metres thick, occurs within a predominantly felsic volcanic pile and forms the stratigraphic footwall to the mineralisation. Near the top of the lens, the intermediate - mafic volcanics are intercalated with the felsic volcanics in beds as thin as a few centimetres, indicating a probable volcaniclastic, even epiclastic, origin for both these lithologies. Resorbed igneous quartz phenocrysts in the felsic volcanics may be derived from either primary lavas or volcaniclastic rocks. Trace relict igneous porphyritic textures are preserved in altered basaltic dykes within the intermediate - mafic volcanics.

9.2 ROCK GEOCHEMISTRY

The intense alteration resulted in the mobilisation and leaching of most elements generally regarded as relatively immobile during metamorphism and hydrothermal alteration (eg: Sc, V, Ga, Nb, Y). Chemically, the felsic and intermediate - mafic volcanics are characterised only by their Ti/Zr ratios which have ranges typical of unaltered rhyolitic and andesitic - basaltic volcanics of the Mt Read Volcanics. Less altered dacitic

volcanics, with relatively low Alteration Indices, have relict porphyrytic textures and have preserved primary dacite Ti/Zr ratios. However, more intense alteration of dacites was texturally destructive and resulted in the development of felsic volcanic pseudofragmental alteration textures and homogenisation of Ti/Zr ratios to rhyolite values.

From whole rock oxygen isotope analyses, an initial fluid $\delta^{18}O$ ratio of 4.5 - 6.0‰ is inferred, assuming a water /rock ratio greater than 1 at 300°C. This initial value is higher than may be expected for Cambrian seawater (~ 0‰). However, the fluid still may have been derived from seawater modified by low temperature isotopic exchange with the volcanic pile prior to alteration at Prince Lyell. Alternatively, some input from a relatively isotopically heavy magmatic water may have raised the initial $\delta^{18}O$ ratio of a seawater - derived alteration fluid. Some input from a magmatic fluid source is implied by the presence of magmatic - derived magnetite - apatite mineralisation zones.

The range of oxygen isotope ratios of the altered volcanics (6.6 - 10.6‰) is comparable to that of the most altered zones of volcanogenic sulphide deposits in variably metamorphosed terranes in Japan and Tasmania. The lack of higher $\delta^{18}O$ ratios suggests that isotopic exchange with a low grade Devonian regional metamorphic fluid at Prince Lyell was not significant and that Cambrian $\delta^{18}O$ ratios have been preserved. Isotopic equilibrium was approached within the intensely altered sequence which may suggest a high fluid - rock ratio during alteration. Variation in the amounts of alteration minerals between alteration lithologies accounts for almost all the range in the whole rock $\delta^{18}O$ values.

9.3 MINERALISATION

9.3.1 Movement of the hydrothermal fluid

Disseminated and veinlet pyrite mineralisation was deposited throughout the altered Prince Lyell sequence from subsurface circulation of volcanogenic fluids. Evidence of seafloor deposition of massive or laminated sulphides is minimal and has been subjected to strong layer - parallel cleavage formation which has masked possible primary laminations. There is no evidence for a vertical feeder zone for the fluids. Pyrite and especially chalcopyrite mineralisation was concentrated in the felsic volcanics adjacent to the contact with the intermediate - mafic volcanics. The strong lithological control of mineralisation is epitomised by the partitioning of mineralisation in thinly interbedded sequences of felsic and intermediate - mafic volcanics.

A network of interconnected phyllosilicate alteration domains in the felsic volcanics and fracturing in the finer grained, less permeable intermediate - mafic volcanics provided fluid pathways for mineralising fluids. Seismic activity resulting in deformation along the ductility contrast between the phyllosilicate-rich intermediate - mafic and siliceous felsic volcanics may have enhanced porosity and permeability near the contact.

9.3.2 Pyrite I - chalcopyrite mineralisation

Earliest sulphide mineralisation was from volcanogenic fluids and comprised cobaltiferous pyrite (Pyrite I) and chalcopyrite (Fig. 9.1). It was accompanied by chloritic alteration of the host felsic volcanics adjacent to the intermediate - mafic volcanics. Pyrite I contained fine oscillatory zoning, high levels of cobalt (100 ppm - 3 %) and sporadic high levels of nickel (up to 5000 ppm). Such cobaltiferous pyrite is associated with copper mineralisation worldwide and volcanogenic mineralisation in western Tasmania (Loftus-Hills, 1968; Walshe, 1977).

9.3.3 Magnetite - apatite mineralisation

Two generations of chemically distinct magnetite mineralisation were deposited in the Prince Lyell orebody. Accessory disseminated Ti- and V-poor magnetite mineralisation occurred with volcanogenic Pyrite I - chalcopyrite mineralisation. A second magnetite generation occurred after Pyrite I in veins and disseminations in narrow, highly elongate, layer parallel zones, along highly permeable rock horizons or layer - parallel structures. Although many of these zones appear grossly concordant, the strongest development of magnetite mineralisation, on Section 73, is clearly discordant in part.

The magnetite was deposited with accessory apatite and actinolite (now metamorphosed to chlorite) and contained up to 1.7% TiO_2 and around 1% V_2O_5. This mineralogical association, the trace element geochemistry and oxygen isotope ratio of the magnetite (~4‰) suggest that it was deposited from a magmatic fluid with initial ratio 10.5 - 12‰. High concentrations and distribution of rare earth elements in associated apatites are also suggestive of a highly fractionated magmatic origin for this mineralisation.

The magmatic fluid was iron -, P_2O_5 - and REE - rich, and was derived from a strongly fractionated magma, possibly similar in composition to P_2O_5. - and LREE - enriched volcanics which occur in the southern Mt Read Volcanics (Suites 2 and 3 of Crawford *et al.*, 1992). The relatively hot, low sulphur, oxidised and probably saline fluid dissolved and remobilised pre-

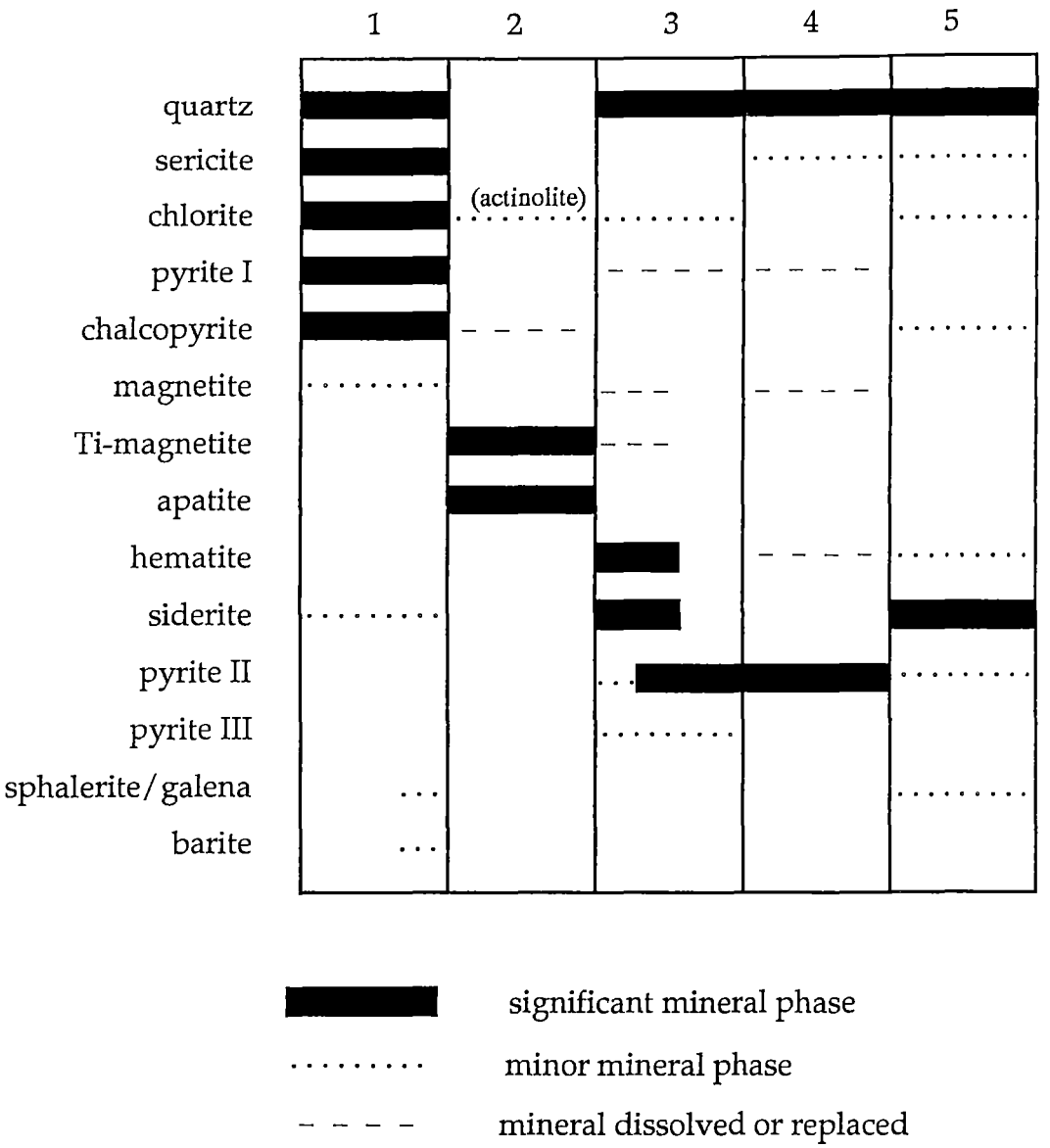

Figure 9.1 Paragenetic summary of mineralisation in the southern Prince Lyell orebody. Mineralisation stages are as follows:

1. Base metal bearing volcanogenic fluid deposits Pyrite I - chalcopyrite mineralisation.
2. Magmatic sulphur-poor fluid deposits magnetite - apatite mineralisation, locally remobilising chalcopyrite.
3. Oxidised fluid derived from the Owen Conglomerate deposits hematite alteration in footwall volcanics. Concurrent volcanogenic fluids deposit Pyrite II and III.
4. Silica - pyrite alteration overprint (more prevalent in northern Prince Lyell). Magnetite/hematite dissolution haloes around some pyrite veins.
5. Devonian D_2 metamorphic remobilisation and veining.

existing copper - gold mineralisation. Notable discontinuities in the orebody coincide with significant magnetite mineralisation. Gold was remobilised marginally more than copper, forming local increases in the Au/Cu ratio in the orebody adjacent to large magnetite bodies.

9.3.4 Pyrite II and III, and hematite alteration

Most of the original Pyrite I mineralisation was dissolved by a later unmineralised hydrothermal fluid or fluids and reprecipitated as unzoned, trace element poor Pyrite II. Pyrite II commonly overgrew the corroded remnants of Pyrite I. Small amounts of a second generation of cobalt - rich pyrite (Pyrite III) were deposited concurrently with Pyrite II in the rims of composite pyrite grains.

Pyrite II and III contain inclusions of bladed hematite which was deposited with associated siderite alteration in the stratigraphic hangingwall of the orebody, adjacent to the Great Lyell fault. This hematite may have been deposited by an oxidised volcanogenic fluid, with iron derived from leaching of the volcanic pile. However, the close spacial association of hematite alteration with the adjacent hematitic Owen Conglomerate strongly suggests that the hematite alteration was deposited from an oxidised fluid derived from the conglomerate migrating along the Great Lyell fault contact. Similar hematite alteration, more removed from the Great Lyell fault in the upper parts of Prince Lyell and Western Tharsis (Walshe and Solomon, 1981), may have been controlled by fluid movement along permaeble rock layers or layer - parallel structures intersecting the Great Lyell fault

The presence of hematite inclusions in Pyrite II would indicate that Pyrite II mineralisation occurred after or during Owen Conglomerate sedimentation. It is possible that the fluid responsible for the deposition of Pyrite II was of Devonian metamorphic origin. Certainly, the cobalt - poor Pyrite II is geochemically similar to Devonian metamorphic pyrite mineralisation in other western Tasmanian mineral deposits (Loftus-Hills and Solomon, 1967). The low cobalt levels in Pyrite II indicate that it is not associated with the copper mineralisation event. However, the contrasting cobalt - rich chemistry of Pyrite III suggests that Pyrite III was deposited from a base metal - rich, possibly volcanogenic fluid. Cobaltiferous pyrite is not associated with Tasmanian Devonian metamorphic mineralisation and it is probable that trace elements such as cobalt are preferentially excluded from the pyrite structure during metamorphism (Brown and Bartholmé, 1972; Itoh, 1973).

A second scenario may better explain the relationship between Pyrite II and III and hematite alteration. This scenario requires that Mt Lyell volcanic activity extended into the earliest Ordovician and that volcanogenic and Owen Conglomerate formation waters interacted along the Great Lyell fault margin of the Owen Conglomerate basin. Hematite alteration in the volcanics near the fault was caused by an unmineralised connate fluid, highly oxidised and low in sulphur, derived from the dewatering of the hematitic conglomerate. As the fluid migrated into the reduced volcanic pile, it precipitated hematite in response to the marked redox change across the faulted contact.

The similar sulphur isotope ratios of different pyrite generations (see below) suggest that pyrite was not deposited from this oxidised fluid. Instead, Pyrite II and III were deposited from variously unmineralised and mineralised volcanogenic fluids circulating about the time of the hematite alteration fluid but not mixing with it.

Latest alteration involved a highly siliceous and pyritic quartz - Pyrite II - sericite alteration overprint. This alteration occurs in very minor amounts in the southern Prince Lyell orebody, but is more prevalent in the northern parts of the orebody and in many other parts of the Mt Lyell field. The low base metal content of this pyrite suggests that it was not associated with copper - gold mineralisation, but was the result of the widespread circulation of a poorly mineralised volcanogenic fluid.

The paragenetic relationships between pyrite and hematite have significant implications for the age of mineralisation in the Mount Lyell field. Hematitic bornite - chalcopyrite mineralisation along the Great Lyell fault in the North Lyell area has been regarded as being of Devonian metamorphic origin by many authors (eg: Brook, 1985; Solomon *et al*, 1987). However, the second scenario described above suggests that the hematite alteration zones along the fault are not Devonian in age but early Ordovician. The high grade North Lyell mineralisation may be the result of the mixing of large volumes of Cambrian volcanogenic fluids with Owen Conglomerate formation waters near the Great Lyell fault.

9.3.5 Sulphur isotopes

The range of pyrite $\delta^{34}S$ ratios (+3 - 11‰) is consistent with that of Cambrian volcanogenic mineralisation in western Tasmania. *In situ* sulphur isotope analyses showed that there is no consistent isotopic variation between pyrite generations. They suggest that sulphur for all pyrite mineralisation was

derived from a Cambrian volcanic source and that pyrite generations were not deposited under substantially different physiochemical conditions.

A poorly defined zonation of lighter to heavier $\delta^{34}S$ values occurs away from the centre of the ore horizon. The zonation may have been due to an increased influence of relatively cool, more oxidised wall rocks on the hot, reduced hydrothermal fluid further from the centre of fluid flow. Alternatively, the zonation may reflect a decreasing contribution over time of relatively isotopically light sulphur from the host volcanics to the seawater - derived hydrothermal fluid.

9.4 METAMORPHIC EFFECTS

Mid Devonian deformation of the Prince Lyell orebody resulted in its significant elongation parallel to the volcanic layering. Original mineral textures were modified by brecciation of brittle minerals such as pyrite and magnetite and plastic flow of more ductile minerals such as chalcopyrite and sphalerite. However, the role of mid Devonian fluids and structures in remobilisation of the Prince Lyell orebody appears to have been limited.

The grade and character of copper - gold mineralisation and the Au/Cu ratio do not vary substantially with depth in the orebody, indicating that large scale remobilisation of metals within the orebody has not occurred. Although it is likely that metamorphic fluid movement would be focussed along the Great Lyell fault zone, significant remobilised mineralisation does not occur in or near the fault zone. Lead and zinc appear to be the most mobile metals and occur in a very weakly mineralised zone in the fault above its intersection with the Prince Lyell orebody.

Minor copper - gold mineralisation was remobilised from haloes up to a few metres wide around late D_2 "flat faults". However, the faulting and associated veining were discontinuous and the degree of dissolution, irregular. As a result, only narrow zones of upgraded copper - gold mineralisation occur above some "flat faults".

REFERENCES

Alderton, 1980, Rare earth element mobility during granite alteration: evidence from southwest England. *Earth and Planetary Science Letters*, 49, 149 - 165.

Allen, R.L., 1988, False pyroclastic textures in altered silicic lavas, with implications for volcanic - associated mineralisation. *Economic Geology*, 83, 1424 - 1446.

Arnold, G.O., 1985, Mt. Lyell 1985: an exploration perspective. *Unpublished report, Gold Fields Exploration Pty Ltd*, Queenstown, Tasmania.

Arnold, G.O., 1989, Report to the Mt Lyell Mining and Railway Company Ltd in a system of geological mapping and logging for the Prince orebody. *Unpublished report, Mt Lyell Mining and Railway Co. Ltd*, Queenstown, Tasmania.

Arnold, G.O. and Carswell, J.T., 1990, The Mt Lyell deposits. *In:* Glasson, K.R. and Rattigan, J.H. (editors), Geological aspects of the discovery of some important mineral deposits in Australia. *Australasian Institute of Mining and Metallurgy Monograph*, 17, 135 - 140.

Arnold, G.O. and Fitzgerald, F.G., 1986, Mt Lyell: An exploration perspective. *In:* Large, R.R. (ed.), THE MT READ VOLCANICS AND ASSOCIATED ORE DEPOSITS. Geological Society of Australia, Tasmanian Division, Hobart, 21 - 23.

Banks, M.R. and Baillie, P.W., 1989, Late Cambrian to Devonian. *In:* Burrett, C.F. and Martin, E.L. (editors), Geology and mineral resources of Tasmania. *Geological Society of Australia Special Publication*, 15, 182 - 237.

Barrett, T.J. and MacLean, W.H., 1991, Chemical, mass, and oxygen isotope changes during extreme hydrothermal alteration of an Archaean rhyolite, Noranda, Quebec. *Economic Geology*, 86, 406 - 414.

Barrett, T.J., Cattalani, S. and MacLean, W.H., 1991a, Massive sulphide deposits of the Noranda area, Quebec. I. The Horne Mine. *Canadian Journal of Earth Sciences*, 28, 465 - 488.

Barrett, T.J., Cattalani, S., Chartrand, F. and Jones, P., 1991b, Massive sulphide deposits of the Noranda area, Quebec. II. The Aldermac Mine. *Canadian Journal of Earth Sciences*, 28, 1301 - 1327.

Barrett, T.J., MacLean, W.H., Cattalani, S., Hoy, L. and Riverin, G., 1991c, Massive sulphide deposits of the Noranda area, Quebec. III. The Ansil Mine. *Canadian Journal of Earth Sciences*, 28, 1699 - 1730.

Bartholmé, P., Koteska, F, and Ruiz, J.L., 1971, Cobalt zoning in microscopic pyrite from Kamoto, Republic of the Congo (Kinshasa). *Mineralium Deposita*, 6, 167 - 176.

Barton, P.B. jnr, 1970, Sulphide petrology. *Mineralogical Society of America Special Paper*, 3, 187 -198.

Barton, P.B. jnr and Bethke, P.M., 1987, Chalcopyrite disease in sphalerite : pathology and epidemiology. *American Mineralogist*, 72, 451 - 467.

Beane, R.E. and Titley, S.R., 1981, Porphyry copper deposits; Part II - Hydrothermal alteration and Mineralisation. *Economic Geology*, 75th Anniversary Volume, 235 - 269.

Beaty, D.W. and Taylor, H.P. jnr, 1982, Some petrological and oxygen isotope relationships in the Amulet mine, Noranda, Quebec, and their bearing on the origin of Archean massive sulphide deposits. *Economic Geology*, 77, 95 - 108.

Becker, R.H. and Clayton, R.N., 1976, Oxygen isotope study of a Precambrian banded iron formation, Hammersley Range, Western Australia. *Geochimica et Cosmochimica Acta*, 40, 1153 - 1166.

Berry, R.F., 1989, The history of movement on the Henty Fault Zone: an anlysis of fault striations. *Australian Journal of Earth Sciences*, 36, 189 - 206.

Berry, R.F., 1990a, Structure of the Rosebery deposit. In: Structure and Mineralisation of Western Tasmania. *Unpublished AMIRA project report*, P291, 17 - 26.

Berry, R.F., 1990b, Structure of the Queenstown area and its relation to mineralisation - interim report. In: Structure and Mineralisation of Western Tasmania. *Unpublished AMIRA project report*, P291, 27 - 68.

Bertenrath, R., Friedrichsen, H. and Hellner, E., 1973, Die Fraktionierung der Sauerstoffisotope $^{16}O/^{18}O$ im System Eisen - oxyd - Wasser (German with English abstract). *Fortschritte der Mineralogie*, 50, 32 - 33.

Bezmen, N.I., Yeremin, N.I., Narazauli, I.G., Pozdnyakova, N.V. and Sergeyeva, N.Y., 1978, Cobalt distribution and the pyrite - chalcopyrite geothermometer. *Geochemistry International*, 15 (2), 44 - 48.

Bird, M., 1982, An assessment of the economic geology of Mt Lyell. *Unpublished report, Mt Lyell Mining and Railway Co. Ltd*, Queenstown, Tasmania.

Bogush, I.A., 1983, Evaluation of productivity and mode of functioning of endogene sulphide-ore sources on the basis of growth zoning in pyrite. *Doklady, Academy of Sciences of USSR,* 258, 149 - 154.

Bowers, T.S., Jackson, K.J. and Helgeson, H.C., 1984, EQUILIBRIUM ACTIVITY DIAGRAMS FOR COEXISTING MINERALS AND SOLUTIONS AT PRESSURES AND TEMPERATURES TO 5 KB AND 600°C. Springer-Verlag, Berlin, 397p.

Boynton, W.V., 1984, Cosmochemistry of the rare earth elements: meteorite studies. *In:* Henderson, P. (editor), RARE EARTH ELEMENT GEOCHEMISTRY. Elsevier, Amsterdam, 63 - 114.

Bradinskaya, E.M., Kazachenko, Y.A. and Zavyalova, L.L., 1980, Heterogeneity of gold bearing pyrite composition (Russian with English abstract). *In:* Sidorenko, A.V. (editor), INHOMOGENEITY OF MINERALS AND CRYSTAL GROWTH. Academy of Sciences of USSR, 110 - 116.

Bradley, J., 1954, The geology of the West Coast Range of Tasmania, Part I - Stratigraphy and metasomatism. *Papers and Proceedings of the Royal Society of Tasmania,* 88, 193 - 243.

Bradley, J., 1956, The geology of the West Coast Range of Tasmania, Part II - Structure and ore deposits. *Papers and Proceedings of the Royal Society of Tasmania,* 90, 65 - 130.

Bradley, J., 1957, The geology of the West Coast Range of Tasmania, Part III - Porphyroid metasomatism. *Papers and Proceedings of the Royal Society of Tasmania,* 91, 163 - 190.

Braithwaite, C.J., 1985, Chlorite geochemistry and its relationship to aspects of lithology and mineralisation in the south-eastern margin of the Prince Lyell copper deposit, Tasmania. *Unpublished B.Sc (Hons.) thesis,* University of Sydney.

Bralia, A., Sabatini, G. and Troja, F., 1979, A revaluation of the Co/Ni ratio in pyrite as a geochemical tool in ore genesis problems. *Mineralium Deposita,* 14, 353 - 374.

Branov, E.N., Zasuskhin, G.N., Karpukhina, V.S., Loginova, L.A. and Bukharova, V.A., 1972, Occurrence of Cu, Zn and Pb and other elements in pyrite from aureoles of pyrite deposits. *Geochemistry International,* 9, 834 - 843.

Brett, R. and Kullerud, G., 1967, The Fe-Pb-S system. *Economic Geology,* 62, 354 - 369.

Brook, W.A., 1984, Mineralisation at Mt Lyell and exploration of the buffer zone, mine lease and E.L. 9/66. *Unpublished report, Gold Fields Exploration Pty Ltd,* Queenstown, Tasmania.

Brown, A.C. and Bartholmé, P., 1972, Inhomogeneities in cobaltiferous pyrite from the Chibuluma Cu-Co deposit, Zambia. *Mineralium Deposita*, 7, 100 -105.

Bryant, C.J., 1975, The geology and mineralisation of the corridor area, Mt Lyell, Tasmania. *Unpublished B. Sc. (Hons.) thesis*, University of Tasmanaia.

Cambel, B. and Jarkovsky, J., 1966, The possibility of utilising the nickel and cobalt in pyrites as indicators of ore genesis. *Geologicheskii Sbornik (Slov. Akad. Vied)*, 17, 17 - 34.

Carey, S.W., 1953, Geological structure of Tasmania in relation to mineralisation. *In:* Edwards, A.B. (ed.), Geology of Australian Ore Deposits, *5th Empire Mining and Metallurgical Congress Publication*, 1, 1108 - 1128.

Cas, R. A. F. and Wright, J. V., 1987, VOLCANIC SUCCESSIONS: MODERN AND ANCIENT. Allen and Unwin, London, 528 p.

Clark, A.M., 1984, Mineralogy of the rare earth elements. *In:* Henderson, P. (editor), RARE EARTH ELEMENT GEOCHEMISTRY. Elsevier, Amsterdam, 33 - 62.

Clark, L.A., 1960, The Fe-As-S system: Phase relations and applications. *Economic Geology*, 55, 1345 - 1381.

Connolly, H.J.C., 1947, Geology in exploration: Mount Lyell example. *Proceedings of the Australasian Institute of Mining and Metallurgy*, 147, 1 - 22.

Corbett, K.D., 1979, Stratigraphy, correlation and evolution of the Mt Read Volcanics in the Queenstown, Jukes - Darwin and Mt Sedgwick areas. *Geological Survey of Tasmania Bulletin*, 58.

Corbett, K.D., 1981, Stratigraphy and mineralisation in the Mt Read Volcanics, western Tasmania. *Economic Geology*, 76, 209 - 230.

Corbett, K.D., 1986, Geological setting of mineralisation in the Mt Read Volcanics. *In:* Large, R.R. (editor), THE MT READ VOLCANICS AND ASSOCIATED ORE DEPOSITS. Geological Society of Australia, Tasmanian Division, Hobart, 1 - 10.

Corbett, K.D. and Lees, T.C., 1987, Stratigraphic and structural relationships and evidence for Cambrian deformation at the western margin of the Mt Read Volcanics, Tasmania. *Australian Journal of Earth Sciences*, 34, 45 - 67.

Corbett, K.D., Reid, K.O., Corbett, E.B., Green, G.R., Wells, K. and Sheppard, N.W., 1974, The Mt Read Volcanics and Cambro-Ordovician relationships at Queenstown, Tasmania. *Journal of the Geological Society of Australia,* 21, 173 - 186.

Corbett, K.D. and Solomon, M., 1989, Cambrian Mt Read Volcanics and associated mineral deposits. *In:* Burrett, C.F. and Martin, E.L. (editors), Geology and mineral resources of Tasmania. *Geological Society of Australia Special Publication,* 15, 84 - 153.

Cox, S.F., 1981, The stratigraphy and structural setting of the Mt Lyell volcanic-hosted sulphide deposits. *Economic Geology,* 76, 231 - 245.

Crawford, A.J., 1987, Geochemistry of the Mt Read Volcanics: internal correlations and tectonic implications. In: Controls on gold and silver grades in volcanogenic sulphide deposits. *Unpublished AMIRA report,* 84/P210, 79 - 108.

Crawford, A.J. and Berry, R.F., 1992, Tectonic implications of Late Proterozoic - Early Palaeozoic igneous rock associations in western Tasmania, *Tectonophysics,* 214, 37 - 56.

Crawford, A.J., Corbett, K.D. and Everard, J.L., 1992, Geochemistry of the Cambrian volcanic - hosted massive sulphide - rich Mount Read Volcanics, Tasmania, and some tectonic implications. *Economic Geology,* 87, 597 - 619.

Crerar, D.A. and Barnes, H.L., 1976, Ore solution chemistry versus solubilities of chalcopyrite and chalcocite assemblages in hydrothermal solution at 200°C to 350°C. *Economic Geology,* 71, 772 - 794.

Date, J., Watanabe, Y. and Saeki, Y., 1983, Zonal alteration around the Fukazawa Kuroko deposits, Akita Prefecture, northern Japan. *Economic Geology Monograph,* 5, 365 - 386.

Duncan, A. R. and Taylor, S.R., 1968, Trace element analyses of magnetites from andesitic and dacitic lavas from Bay of Plenty, New Zealand. *Contributions to Mineralogy and Petrology,* 20, 30 - 33.

Edwards, A.B., 1939, Some observations on the mineral composition of the Mt Lyell copper ores, Tasmania, and the modes of occurrence. *Proceedings of the Australasian Institute of Mining and Metallurgy,* 114, 67 - 109.

Eldridge, C.S., Compston, W., Williams, I.S. and Walshe, J.L., 1989, Sulphur isotopic analysis on the SHRIMP Ion Microprobe. *In:* Shanks, W.C. and Criss, R.E. (editors), New frontiers in stable isotope research: Laser probes, ion probes, and small-sample analysis. *U.S. Geological Survey Bulletin,* 1890, 163 - 174.

Finlow-Bates, T. and Stumpfl, E.F., 1981, The behaviour of so-called immobile elements in hydrothermally altered rocks associated with volcanogenic submarine - exhalative ore deposits. *Mineralium Deposita,* 16, 319 - 328.

Fleet, M.E., MacLean, P.J. and Barbier, J., 1988, Oscillatory-zoned As-bearing pyrite from strata-bound and stratiform gold deposits: an indicator of ore fluid evolution. *Economic Geology Monograph,* 6, 356 - 362.

Fleischer, M., 1955, Minor elements in some sulphide minerals. *In:* Bateman, A.M. (ed.), ECONOMIC GEOLOGY FIFTIETH ANNIVERSARY VOLUME, Economic Geology Publishing Co., Urbana, 970 - 1024.

Fleischer, M., 1983, Distribution of lanthanides and yttrium in apatites from iron ores and its bearing on the genesis of ores of the Kiruna type. *Economic Geology,* 78, 1007 - 1010.

Floyd, P.A. and Winchester J.A., 1978, Identification and discrimination of altered metamorphosed volcanic rocks using immobile elements. *Chemical Geology,* 21, 291 - 306.

Frietsch, R., 1978, On the magmatic origin of iron ores of the Kiruna type. *Economic Geology,* 73, 478 - 485.

Frutos, J. and Oyarzún, J., 1975, Tectonic and geochemical evidence concerning the genesis of the El Laco magnetite lava flow deposits. *Economic Geology,* 70, 988 - 990.

Ghosh-Dastidar, P., Parjari, G.E. Jnr and Trembath, L.T., 1970, Factors affecting the trace element partition coefficients between co-existing sulphides. *Economic Geology,* 65, 815 - 837.

Gieré, R., 1986, Mobility of Ti, Zr and REE: mineralogical geochemical and isotope evidence from the Adamello contact aureole (Italy). *Chemical Geology,* 70, 161.

Gieré, R., 1990, Hydrothermal mobility of Ti, Zr and REE: examples from the Bergell and Adamello contact aureoles (Italy). *Terra Nova,* 2, 60 - 67.

Graf, J.L. jnr, 1977, Rare earth elements as hydrothermal tracers during the formation of massive sulphide deposits in volcanic rocks. *Economic Geology,* 72, 527 - 548.

Green, G.R., 1971, Geology and mineralisation of the Cape Horn - Lyell Comstock area, Mt Lyell. *Unpublished B.Sc (Hons.) thesis,* University of Tasmania.

Green, G.R., 1986, Stable isotope and alteration investigations of the Mt Read Volcanics: 1 - The Hercules and Boco areas. *In:* Large, R.R. (editor), THE MT READ VOLCANICS AND ASSOCIATED ORE DEPOSITS. Geological Society of Australia, Tasmanian Division, Hobart, 39 - 41.

Green, G.R., 1990, Rock alteration, mineral and isotope zonation in the Rosebery district, Tasmania. *10th Australian Geological Convention, Geological Society of Australia Abstracts,* 25, 15 - 16.

Green, G.R., Ohmoto, H., Date, J. and Takahashi, T., 1983, Whole rock oxygen isotope distribution in the Fukazawa-Kosaka area, Hokuroku district, Japan, and its potential application to mineral exploration. *Economic Geology Monograph,* 5, 395 - 411.

Green, G.R., Solomon, M. and Walshe, J.L., 1981, The formation of the volcanic-hosted massive sulphide ore deposit at Rosebery, Tasmania. *Economic Geology,* 76, 304 - 338.

Gregory, J.W., 1905, The Mt Lyell mining field, Tasmania. *Transactions of the Australasian Institute of Mining Engineers,* 10, 26 - 196.

Gulson, B.L. and Porritt, P.M., 1987, Base metal exploration of the Mt Read Volcanics, western Tasmania: Part II. Lead isotope signatures and genetic implications. *Economic Geology,* 82, 291 - 307.

Hall, G. and Solomon, M., 1962, Metallic mineral deposits. *Journal of the Geological Society of Australia,* 9, 285 - 309.

Hannington, M.D. and Scott, S.D., 1989, Sulfidation equilibria as guides to gold mineralisation in volcanogenic massive sulphides: evidence from sulphide mineralogy and the composition of sphalerite. *Economic Geology,* 84, 1978 - 1995.

Hawley, J.E. and Nichol, I., 1961, Trace elements in pyrite, pyrrhotite and chalcopyrite of different ores. *Economic Geology,* 56, 467 - 487.

Helvaci, C., 1984, Apatite-rich iron deposits of the Avnik (Bingol) region, southeastern Turkey. *Economic Geology,* 79, 354 - 371.

Henderson, P., 1984, General geochemical properties and abundances of the rare earth elements. *In:* Henderson, P. (editor), RARE EARTH ELEMENT GEOCHEMISTRY, Elsevier, Amsterdam, 1 - 32.

Hendry, D.A.F., 1972, The geochemistry of the Mt Lyell copper ores, Tasmania. *Unpublished Ph.D. thesis,* University of Cambridge.

Hendry, D.A.F., 1981, Chlorites, phengites and siderites from the Prince Lyell ore deposit, Tasmania, and the origin of the deposit. *Economic Geology,* 76, 285 - 303.

Hills, C.L., 1927, A synopsis of the geology of the Lyell district of Tasmania. *Proceedings of the Australasian Institute of Mining and Metallurgy,* 66, 129 - 148.

Hills, P.B., 1990, The Mount Lyell copper-gold-silver deposits. *In:* Hughes, F. (editor), Geology of the Mineral Deposits of Australia and Papua New Guinea. *Australasian Institute of Mining and Metallurgy Monograph,* 14, 1257 - 1266.

Huston, D.L., Bottrill, R.S., Creelman, R.A., Zaw, K., Ramsden, T.R., Rand, S., Gemmell, J.B., Jablonski, W., Sie, S.H. and Large, R.R., 1992, Geological and geochemical controls on the mineralogy and grain size of gold bearing phases, eastern Ausralian volcanic-hosted massive sulphide deposits. *Economic Geology,* 87, 542 - 563.

Huston, D.L. and Large, R.R., 1987, Genetic and exploration significance of the zinc ratio [100 Zn/(Zn + Pb)] in massive sulphide systems. *Economic Geology,* 82, 1521 - 1539.

Huston, D.L. and Large, R.R., 1989, A chemical model for the concentration of gold in massive sulphide deposits. *Ore Geology Reviews,* 4, 171 - 200.

Hynes, A., 1980, Carbonatization and mobility of Ti, Y, Zr in Ascot Formation metabasalts, S.E. Quebec. *Contributions to Mineralogy and Petrology,* 75, 79 - 87.

Ineson, P.R., 1989, INTRODUCTION TO PRACTICAL ORE MICROSCOPY. Longman, Earth Science Series, London, 181 p.

Ishikawa, Y., Sawaguchi, T., Iwaya, S. and Horiuchi, M., 1976, Delineation of prospecting targets for Kuroko deposits based on modes of volcanism of underlying dacite and alteration haloes (Japanese with English abstract). *Mining Geology,* 26, 105 - 117.

Itoh, S., 1973, Distribution of cobalt in pyrites from some cupiferous pyrite deposits, with special reference to its relationship to metamorphic grade. *Bulletin of the Geological Survey of Japan,* 24, 285 - 310.

Jago, J.B., Cooper, J.A. and Corbett, K.D., 1977, First evidence for Ordovician igneous activity in the Dial Range Trough, Tasmania. *Journal of the Geological Society of Australia,* 24, 81 - 86.

Jago, J.B., Reid, K.O., Quilty, P.G., Green, G.R. and Daly, B, 1972, Fossiliferous Cambrian limestone from within the Mt Read Volcanics, Mt Lyell mine area, Tasmania. *Journal of the Geological Society of Australia,* 19, 379 - 382.

Klemm, D.D., 1962, Untersushungen uber die Mischkristall bildung im Dreieck diagramm FeS2-CoS2-NiS2 und ihre Beziehungen zum Aufbau der naturlichen "Bravoite" (German with English abstract). *Neues Jahrbuch fur Mineralogie Monatshefte,* 76 - 91.

Large, R.R., Crawford, A.J. and Adrichem, S., 1986, Primary and alteration geochemistry of the Mt Read Volcanics. *In:* Controls on gold and silver grades in volcanogenic massive sulphide deposits. *Unpublished AMIRA progress report,* 38 - 45.

Large, R.R., Huston, D.L., McGoldrick, P.J. and Ruxton, P.A, 1988, Gold distribution and genesis in Australian volcanogenic massive sulphide deposits and their significance for gold transport models. *Economic Geology Monograph,* 6, 520 - 535.

Loftus-Hills, G., 1968, Cobalt, nickel and selenium in Tasmanian ore minerals. *Unpublished Ph.D. thesis,* University of Tasmania.

Loftus-Hills, G. and Solomon, M., 1967, Cobalt, nickel and selenium in sulphides as indicators of ore genesis. *Mineralium Deposita,* 2, 228 - 242.

Markham, N.L., 1968, Some genetic aspects of the Mt Lyell mineralisation. *Mineralium Deposita,* 3, 199 - 221.

McDonald, M.J., 1968, Progress report on the geology of the West Lyell orebodies at Mt Lyell, Tasmania. *Unpublished report, Mt Lyell Mining and Railway Co. Ltd,* Queenstown, Tasmania.

Morrison, M.A., 1978, The use of "immobile" elements to distinguish the paleotectonic affinities of metabasalts: applications to the Paleocene basalts of Mull and Skye, north-west Scotland. *Earth and Planetary Science Letters,* 39, 407 - 416.

Muehlenbachs, K., 1986, Alteration of the oceanic crust and the ^{18}O history of seawater. *In:* Valley, J.W., Taylor, H.P. jnr. and O'Neil, J.R. (editors), Stable isotopes in high temperature geological processes. *Mineralogical Society of America, Reviews in Mineralogy,* 16, 425 - 444.

Muller, L.D., 1977, Laboratory methods of mineral separation. *In:* Zussman, J. (ed.), PHYSICAL METHODS IN DETERMINATIVE MINERALOGY. 2nd edition, Academic Press, London, 1 - 34.

Nye, P.B., Blake, F. and Henderson, Q.J., 1934, Report on the geology of the Mt Lyell mining field. *Unpublished report, Tasmanian Department of Mines,* Hobart.

Nyström, J.O., 1985, Apatite iron ores of the Kiruna field, northern Sweden: magatic textures and carbonatitic affinity. *Geologiska Föreningens i Stokholm Förhandlingar,* 107, 133 - 141.

Ohmoto, H., 1986, Stable isotope geochemistry of ore deposits. *In:* Valley, J.W., Taylor, H.P. jnr. and O'Neil, J.R. (editors), Stable isotopes in high temperature geological processes. *Mineralogical Society of America, Reviews in Mineralogy,* 16, 491 - 559.

Ohmoto, H., Mizukami, M., Drummond, S.E., Eldridge, C.S., Pisutha-Arnond, V. and Lenaugh, T.C., 1983, Chemical processes of Kuroko formation. *In:* Ohmoto, H. and Skinner, B.J. (editors), The Kuroko and related volcanogenic massive sulphide deposits. *Economic Geology Monograph*, 5, 570 - 604.

Ohmoto, H. and Rye, R.O., 1979, Isotopes of sulphur and carbon. *In:* Barnes, H.L. (editor), GEOCHEMISTRY OF HYDROTHERMAL ORE DEPOSITS, 2nd edition, John Wiley & Sons, New York, 509 - 567.

Oyarzún, J. and Frutos, J., 1984, Tectonic and petrological frame of the Cretaceous iron deposits of northern Chile. *Mining Geology*, 34, 21 - 31.

Parak, T., 1973, Rare earths in the apatite iron ores of Lappland together with some data about the Sr, Th and U content of these ores. *Economic Geology*, 68, 210 - 221.

Parak, T., 1975, Phosphorus in different types of ore, sulphides in the iron deposits, and the type and origin of ores at Kiruna. *Economic Geology*, 80, 646 - 665.

Pearce, J.A. and Cann, J.R., 1973, Tectonic setting of basic volcanic rocks determined using trace element amalyses. *Earth and Planetary Science Letters*, 19, 290 - 300.

Peterson, M.D., 1983, The use of the 'immobile' elements Zr and Ti in lithogeochemical exploration for massive sulphide deposits in the Precambrian Pecos Greenstone belt of northern New Mexico. *Journal of Geochemical Exploration*, 19, 615 - 617.

Puchelt, H. and Emmermann, R., 1976, Bearing of rare earth patterns of apatites from igneous and metamorphic rocks. *Earth and Planetary Science Letters*, 31, 279 - 286.

Ramdohr, P., 1969, THE ORE MINERALS AND THEIR INTERGROWTHS. 3rd edition, Pergamon Press, Oxford, 1174p.

Reid, K.O., 1975, Mt Lyell copper deposits. *In:* Knight, C.L. (ed.), Economic geology of Australia and Papua New Guinea, 1. Metals, *Australasian Institute of Mining and Metallurgy Monograph*, 5, 604 - 619.

Reynolds, J.T., 1990, Workshop on application of fluid inclusions to mineral exploration. *Unpublished short course notes*, Fluid Inc., Denver.

Riley, J.F., 1968, The cobaltiferous pyrite series. *American Mineralogist*, 53, 293 - 295.

Robinson, B.W. and Kusakabe, M., 1975, Quantatative preparation of sulphur dioxide, for $^{34}S/^{32}S$ analyses from sulphides by combustion with cuprous oxide. *Analytical Chemistry*, 47, 1179 - 1181.

Roscoe, S.M., 1965, Geochemical and isotopic studies, Noranda and Matagami areas. *Canadian Mining and Metallurgical Bulletin*, 58, 965 - 971.

Rose, A.W., 1967, Trace elements in sulphide minerals from the Central district, New Mexico and the Bingham district, Utah. *Geochimica et Cosmochimica Acta*, 31, 547 - 585.

Rubin, J.N., Henry, C.D. and Price, J.G., 1989, Hydrothermal zircons and zircon overgrowths, Sierra Blanca Peaks, Texas. *American Mineralogist*, 74, 865 - 869.

Ryall, W.R., 1977, Anomalous trace elements in pyrite in the vicinity of mineralised zones at Woodlawn, N.S.W., Australia. *Journal of Geochemical Exploration*, 8, 73 - 83.

Shanks, W.C., Bischoff, J.L. and Rosenbauer, R.J., 1981, Seawater sulphate reduction and sulphur isotope fractionation in basaltic systems; interaction of seawater with fayalite and magnetite at 200 - 350°C. *Geochimica et Cosmochimica Acta*, 45, 1977 - 1995.

Shepherd, T.J., Rankin, A.H. and Alderton, D.H.M., 1985, A PRACTICAL GUIDE TO FLUID INCLUSION STUDIES. British Geological Survey, London, 239p.

Sheppard, N.W., 1987, Exploration rock geochemistry at Mt Lyell, Tasmania. *Unpublished Ph.D. thesis*, University of N.S.W.

Sillitoe, R.H., 1984, A reappraisal of the Mt Lyell copper deposits, Tasmania: Implications for exploration. *Unpublished report, Gold Fields Exploration Pty Ltd*, Queenstown, Tasmania.

Sillitoe, R.H., 1985, Further comments on geology and exploration at Mt Lyell, Tasmania. *Unpublished report, Gold Fields Exploration Pty Ltd*, Queenstown, Tasmania.

So, C. S., 1978, Geochemistry and origin of amphibolite and magnetite from the Yangyang iron deposit in the Gyeonggi metamorphic complex, Republic of Korea. *Mineralium Deposita*, 13, 105 - 117.

Solomon, M., 1964, The spillite-keratophyre association of west Tasmania and the ore deposits at Mt Lyell, Rosebery and Hercules. *Unpublished Ph.D. thesis*, University of Tasmania.

Solomon, M., 1967, Fossil gossans at Mount Lyell, Tasmania. *Economic Geology*, 62, 757 - 772.

Solomon, M., 1969, The copper - clay deposits at Mount Lyell, Tasmania. *Proceedings of the Australasian Institute of Mining and Metallurgy,* 230, 39 - 47.

Solomon, M., 1976, "Volcanic" massive sulphide deposits and their host rocks - a review and explanation. *In:* Wolf, K. (editor), HANDBOOK OF STRATABOUND AND STRATIFORM ORE DEPOSITS. Elsevier, Amsterdam, 21 - 54.

Solomon, M. and Carswell, J.T., 1989, Mt Lyell. *In:* Burrett, C.F. and Martin, E.L. (editors.), Geology and Mineral Resources of Tasmania, *Geological Society of Australia Special Publication,* 15, 125 - 132.

Solomon, M., Eastoe, C.J., Walshe, J.L. and Green, G.R., 1988, Mineral deposits and sulphur isotope abundances in the Mt Read Volcanics between Que River and Mt Darwin, Tasmania. *Economic Geology,* 83, 1307 - 1328.

Solomon, M. and Elms, R.G., 1965, Copper ore deposits of Mt. Lyell. *In:* McAndrew, J (editor), Geology of Australian ore deposits. *8th Commonwealth Mining and Metallurgical Congress Publication,* 1, 478 - 484.

Solomon, M., Rafter, T.A. and Jensen, M.L., 1969, Isotope studies on the Rosebery, Mt Farrel and Mt Lyell ores, Tasmania. *Mineralium Deposita,* 4, 172 - 199.

Solomon, M., Vokes, F.M. and Walshe, J.L., 1987, Chemical remobilisation of volcanic-hosted sulphide deposits at Rosebery and Mt Lyell, Tasmania. *Ore Geology Reviews,* 2, 173 - 190.

Springer, G., Schachner-Korn, D. and Long, J.V.P., 1964, Metastable solid solution reactions in the system FeS_2-CoS_2-NiS_2. *Economic Geology,* 59, 475 - 491.

Suzuoki, T., 1964, A geochemical study of selenium in volcanic exhalation and sulfur deposits. *Chemical Society of Japan,* 37, 1200 - 1206.

Sverjensky, D.A., Hemley, J.J. and D'Angelo, W.M., 1991, Thermodynamic assessment of hydrothermal alkali feldspar-mica-aluminosilicate equilibria. *Geochimica et Cosmochimica Acta,* 55, 989 - 1004.

Taylor, H.P. jnr, 1979, Oxygen and hydrogen isotope relationships in hydrothermal ore deposits. *In:* Barnes, H.L. (editor), GEOCHEMISTRY OF HYDROTHERMAL ORE DEPOSITS, 2nd edition, John Wiley & Sons, New York, 236 - 277.

Taylor, H.P. jnr and Sheppard, S.M.F., 1986, Igneous rocks: I. Processes of isotopic fractionation and isotope systematics. *In:* Valley, J.W., Taylor, H.P. jnr and O'Neil, J.R. (editors), Stable isotopes in high temperature geological processes. *Mineralogical Society of America, Reviews in Mineralogy,* 16, 227 - 271.

Urabe, T., Scott, S.D. and Hattori, K., 1983, A comparison of footwall-rock alteration and geothermal systems beneath some Japanese and Canadian volcanogenic massive sulphide deposits. *Economic Geology Monograph,* 5, 345 - 364.

Wade, M.L. and Solomon, M., 1958, Geology of the Mt Lyell mines, Tasmania. *Economic Geology,* 53, 367 - 416.

Walshe, J.L., 1971, Geology of the southern Mt Lyell field and trace element studies of the pyrite mineralisation. *Unpublished B.Sc (Hons.) thesis,* University of Tasmania.

Walshe, J.L., 1977, The geochemistry of the Mt Lyell copper deposits. *Unpublished Ph.D. thesis,* University of Tasmania.

Walshe, J.L. and Solomon, M., 1981, An investigation into the environment of formation of the volcanic - hosted Mt Lyell copper deposits using geology, mineralogy, stable isotopes and a six-component chlorite solid solution model. *Economic Geology,* 76, 246 - 284.

Ward, H.J., 1975, Barrambie iron-titanium-vanadium deposit. *In:* Knight, C.L. (editor), Economic geology of Australia and Papua New Guinea, 1. Metals., *Australasian Institute of Mining and Metallurgy Monograph,* 5, 207 - 211.

Wenner, D.B. and Taylor, H.P. jnr, 1971, Temperatures of serpentinisation of ultramafic rocks based on $^{18}O/^{16}O$ fractionation between coexisting serpentine and magnetite. *Contributions to Mineralogy and Petrology,* 32, 165 - 185.

White, N.C., 1975, Cambrian volcanism and mineralisation in south-west Tasmania. *Unpublished Ph.D. thesis,* University of Tasmania.

Williams, E., McClenaghan, M.P. and Collins, P.L.F., 1989, Mid-Paleozoic deformation, granitoids and ore deposits. *In:* Burrett, C.F. and Martin, E.L. (editors), Geology and mineral resources of Tasmania. *Geological Society of Australia Special Publication,* 15, 238 - 292.

Winchester,J.A. and Floyd P.A., 1977, Geochemical discrimination of different magma series and their differentiation products using immobile elements. *Chemical Geology,* 20, 325 - 343.

Young, E.J., Myers, A.T., Munson, E.L. and Conklin, N.M., 1969, Mineralogy and geochemistry of flourapatite from Cerro de Mercado, Durango, Mexico. *U.S. Geological Survey Professional Paper,* 650-D, D84 - 93.

Zaw, K, 1991, The effect of Devonian metamorphism and metasomatism on the mineralogy and geochemistry of the Cambrian VMS deposits in the Rosebery-Hercules district, western Tasmania. *Unpublished Ph.D. thesis,* University of Tasmania.

Zheng, Y-F, 1991, Calculation of oxygen isotope fractionation in metal oxides. *Geochimica et Cosmochimica Acta,* 55, 2299 - 2307.

APPENDIX 1.1

SAMPLE CATALOGUE

NOTES

* All seven digit field numbers refer to drill hole number and downhole depth.
  For example, 636135.5 refers to drill hole WL 636, 135.5 metres.

Abbreviations:
R - handspecimen
T - thin section
PT - polished thin section
PS - polished block
PD - powdered sample
PM - probe mount
F - fluid inclusion chips
GS - sulphides removed by gravity separation
XRF - whole rock XRF analysis
d34S - conventional sulphur isotope analysis
in situ d34S - SHRIMP sulphur isotope analysis
d18O - whole rock oxygen isotope analysis
REE - partial rare earth element analysis

CATALOGUE

University Catalogue No.	Field No.	Locality (* see note above)	Sample Description	Preparations	Chemical Analysis
109314	626047.0 (PL1)		pink sericitic altered felsic volcanic	R, PD	XRF
109315	626085.0 (PL2)		grey-orange sericitic altered felsic volcanic	R, PD	XRF
109316	633060.0 (PL3)		pinky grey, chlor flecked altered felsic volcanic	R, PD	XRF
109317	640127.0 (PL4)		grey-brown sericitic altered felsic volcanic	R, PD	XRF
109318	623065.0 (PL5)		dk grey, flecked altered dacite	R, PD	XRF
109319	623038.0 (PL6)		pink, sericitic altered felsic volcanic	R, PD	XRF
109320	623016.0 (PL7)		chloritic altered felsic volcanic	R, PD	XRF

University Catalogue No.	Field No.	Locality (* see note above)	Sample Description	Preparations	Chemical Analysis
109321	640063.0 (PL8)		massive pink sericitic altered felsic volcanic	R, PD	XRF
109322	633010.0 (PL9)		chloritic altered intermediate- mafic volcanic	R, PD	XRF
109323	624049.0 (PL10)		almost massive, pink sericitic altered felsic volcanic	R, PD	XRF
109324	627005.0 (PL11)		browny grey, sericitic and carbonate altered felsic volcanic	R, PD	XRF
109325	636060.0 (PL12)		chloritic altered intermediate- mafic volcanic, mnr mgt	R, PD	XRF
109326	637069.0 (PL13)		flecked, dk grey altered dacite	R, PD	XRF
109327	636017.0 (PL14)		chloritic altered intermediate- mafic volcanic	R, PD	XRF
109328	636116.5 (PL15)		grey sericitic altered felsic volcanic	R, PD	XRF
109329	636135.5 (PL16)		grey-pink, sericitic altered felsic volcanic	R, PD	XRF
109330	636091.5 (PL17)		dk grey, chloritic (+ ser?) altered felsic volcanic	R, PD	XRF
109331	636100.5 (PL18)		dk grey, partly rexst. altered dacite	R, PD	XRF
109332	637045.0 (PL19)		chloritic altered intermediate- mafic volcanic	R, PD	XRF
109333	637031.0 (PL21)		chloritic altered intermediate- mafic volcanic	R, PD	XRF
109334	637090.0 (PL22)		dk grey altered dacite with poorly aligned flecks	R, PD	XRF
109335	637075.0 (PL23)		v.siliceous, grey altered felsic volcanic	R, PD	XRF
109336	637135.5 (PL24)		carbonate altered pink sericitic felsic volcanic	R, PD	XRF
109337	637052.0 (PL27)		chloritic, grey, altered felsic volcanic	R, PD	XRF
109338	677078.5 (PL28)		mod flecked, dk grey altered dacite	R, PD	XRF
109339	637095.0 (PL29)		pink-grey, sericitic altered felsic volcanic	R, PD	XRF
109340	637056.0 (PL30)		dk grey, sericitic (+chlor ?) altered felsic volcanic	R, PD	XRF
109341	605085.0 (PL31)		chloritic grey altered felsic volcanic	R, PD	XRF
109342	637006.0 (PL32)		chloritic altered intermediate volcanic with dissem. mgt	R, PD	XRF
109343	636100.5 (PL25)		carbonate altered, ?lamprophyre with fine phenocrysts	R, PD	XRF
109344	115002	F/W drive - float, 115 Sublevel	volcanic breccia	R, PD, PT	d34S
109345	115012	55/56 pillar crosscut, 115 Sublevel	sphalerite-barite vein	R, PD, PT	d34S
109346	568A289.5		disseminated pyrite	PS, PD	d34S
109347	584330.5		pyrite vein	PS, PD	d34S
109348	584326 5		chalcopyrite in quartz-siderite vein	R, PD	d34S
109349	584389 0		pyrite vein	PS, PD	d34S
109350	586201.3		sphalerite vein	PS, PD	d34S
109351	596320.7		pyrite vein	PS, PD	d34S
109352	596343 9		pyrite vein	PS, PD	d34S
109353	596401 6		disseminated pyrite	R, PD	d34S
109354	596431.6		pyrite vein	PS, PD	d34S
109355	596454.8		pyrite vein	PS, PD	d34S

University Catalogue No.	Field No.	Locality (* see note above)	Sample Description	Preparations	Chemical Analysis
109356	605023.0		pyrite vein	PS, PD	d34S
109357	605050.2		pyrite vein	PS, PD	d34S
109358	605074.1		pyrite vein	PS, PD	d34S
109359	607068.8		pyrite vein	PS, PD	d34S
109360	619104.3		pyrite vein	PS, PD	d34S
109361	619017.3		pyrite vein	PS, PD	d34S
109362	619055.3		remobilised chalcopyrite	PS, PD	d34S
109363	619076.9		chalcopyrite in quartz-siderite vein	R, PD	d34S
109364	619086.8		pyrite vein	PS, PD	d34S
109365	619134.0		pyrite vein	R, PD	d34S
109366	622095.5		pyrite vein	PS, PD	d34S
109367	624050.4		pyrite vein	PS, PD	d34S
109368	634044.4		pyrite vein	PS, PD	d34S
109369	634085 6		pyrite vein	PS, PD	d34S
109370	634131.0		pyrite vein	PS, PD	d34S
109371	635010.0		pyrite vein	PS, PD	d34S
109372	635024.4		pyrite vein	PS, PD	d34S
109373	635069 9		pyrite vein and chalcopyrite	PS, PD	d34S
109374	635085.0		pyrite vein	PS, PD	d34S
109375	635119.6		chalcopyrite in quartz-siderite vein	R, PD	d34S
109376	635130.3		pyrite vein	PD	d34S
109377	636040.9		pyrite vein	PS, PD	d34S
109378	637029.6		pyrite vein	PS, PD	d34S
109379	698100.4		pyrite vein	PS, PD	d34S
109380	PX1	WL637, 0-10m	altered intermediate-mafic volcanic	PD	d18O
109381	PX2	WL637, 10-20m	altered intermediate-mafic volcanic	PD	d18O
109382	PX3	WL637, 20-30m	altered intermediate-mafic volcanic	PD	d18O
109383	PX4	WL637, 30-40m	altered intermediate-mafic volcanic	PD	d18O
109384	PX5	WL637, 40-50m	altered intermediate-mafic volcanic	PD	d18O
109385	PX6	WL637, 50-60m	altered intermediate and felsic volcanics	PD	d18O
109386	PX7	WL637, 60-70m	altered felsic and dacitic volcanics	PD	d18O
109387	PX8	WL637, 70-80m	altered felsic volcanics	PD	d18O
109388	PX9	WL637, 80-90m	altered felsic volcanics	PD	d18O
109389	PX10	WL637, 90-100m	altered felsic volcanics	PD	d18O
109390	PX11	WL637, 100-110m	altered felsic volcanics	PD	d18O

University Catalogue No.	Field No.	Locality (* see note above)	Sample Description	Preparations	Chemical Analysis
109391	PX12	WL637, 110-120m	altered felsic volcanics	PD	d18O
109392	PX13	WL637, 120-130m	altered felsic volcanics	PD	d18O
109393	PX14	WL637, 130-140m	altered felsic volcanics	PD	d18O
109394	PX15	WL637, 140-147m	altered felsic volcanics	PD	d18O
109395	PX16	WL637, 147-151m	Great Lyell fault zone	PD	d18O
109396	PX17	WL637, 151-153m	Owen Conglomerate	PD	d18O
109397	PX18	WL634, 0-13.4m	altered felsic volcanics	PD, GS	d18O
109398	PX19	WL634, 13.4-16.1m	altered felsic volcanics	PD, GS	d18O
109399	PX20	WL634, 16.1-34.0m	altered felsic volcanics	PD, GS	d18O
109400	PX21	WL634, 34.0-48.7m	altered felsic volcanics	PD, GS	d18O
109401	PX22	WL634, 48.7-50.5m	altered felsic volcanics	PD, GS	d18O
109402	PX23	WL634, 50.5-54.9m	altered intermediate-mafic volcanic	PD, GS	d18O
109403	PX24	WL634, 54.9-67.0m	altered felsic volcanics	PD, GS	d18O
109404	PX25	WL634, 67.0-80.0m	altered felsic volcanics	PD, GS	d18O
109405	PX26	WL634, 80.0-94.0m	altered felsic volcanics	PD, GS	d18O
109406	PX27	WL634, 94.0-106.1m	altered felsic volcanics	PD, GS	d18O
109407	PX28	WL634, 106.1-108.1m	altered felsic volcanics + mgt alteration	PD, GS	d18O
109408	PX29	WL634, 108.1-120.5m	altered felsic volcanics	PD, GS	d18O
109409	PX30	WL634, 120.5-126.2m	altered felsic volcanics + mgt alteration	PD, GS	d18O
109410	PX31	WL634, 126.2-139.7m	altered felsic volcanics	PD, GS	d18O
109411	PX32	WL634, 139.7-148.0m	altered felsic volcanics	PD, GS	d18O
109412	PX33	WL634, 148.0-156.5m	altered felsic volcanics	PD, GS	d18O
109413	115001	F/W drive - float, 115 Sublevel	flecked dacite with pyrite stringers	R, PT	
109414	115003	55 crosscut, 115 Sublevel	altered intermediate/mafic volcanic with pyrite stringers	R, PT, PM	in situ d34S
109415	115004	57 crosscut, 115 Sublevel	chloritic pink altered felsic volcanic	R	
109416	200003	No. 22 drawpoint, 200 Sublevel	mineralised pink altered felsic volcanic	R	
109417	525138.3		hematitic altered felsic volcanic	R	
109418	577124.6		flecked dacite	R, PT	
109419	580181.5		magnetite alteration	R	
109420	586201.3		sphalerite vein	R, PT	
109421	589065 7		volcanic breccia	R	
109422	589259 7		chloritic altered volcanic	R, PT, PM	in situ d34S
109423	598307.9		magnetite altered felsic volcanic	R, PT	
109424	599377.3		hematitic altered felsic volcanic	R, PT, PM	in situ d34S
109425	605100 5		sphalerite vein	R, PT	

University Catalogue No.	Field No.	Locality (* see note above)	Sample Description	Preparations	Chemical Analysis
109426	605104.3		volcanic breccia	R	
109427	605105.1		recrystallised volcanic breccia	R	
109428	605106.3		recrystallised volcanic breccia	R	
109429	607013.2		altered mafic dyke	R, T	
109430	607130.3		altered felsic volcanic	R, PT	
109431	618010.0		altered intermediate-mafic volcanic	R, PT	
109432	618051.8		altered felsic volcanic	R, PT	
109433	619098.6		silicified altered felsic volcanic	R, PT, PM	in situ d34S
109434	619079.1		altered felsic volcanic	R, PT, F	
109435	623076.6		magnetite alteration	R, PT	
109436	622171.5		altered felsic volcanic	R, T	
109437	623104.5		hematitic altered felsic volcanic	R	
109438	624096.9		Great Lyell fault zone	R, PT, PM	in situ d34S
109439	622095.5		flecked altered dacite	R, PT	
109440	626129.2		hematite altered dacite	R, PT	
109441	634017 8		mineralised altered felsic volcanic	R, PT	
109442	634066.1		mineralised altered felsic volcanic	R, PT	
109443	636019.9		altered intermediate-mafic volcanic	R	
109444	636126.8		magnetite alteration	R, PT	
109445	639116 4		mineralised altered felsic volcanic	R, PT	
109446	639121.3		Great Lyell fault zone	R, PT, PM	in situ d34S
109447	641040.1		magnetite alteration	R	
109448	641101.8		magnetite alteration	R, PT	
109449	580184.0		magnetite alteration	R, PD	d18O (mgt)
109450	582279.4		magnetite alteration	R, PD, PT	d18O (mgt)
109451	633068.9		magnetite alteration	R, PD	d18O (mgt)
109452	618112.8		magnetite alteration (apatite analyses)	R	REE (apatite)
109453	633050.8		magnetite alteration (apatite analyses) and qtz-sid vein	R, F	REE (apatite)
109454	633066.1		magnetite alteration (apatite analyses)	R	REE (apatite)
109455	629073.0		quartz-siderite vein	F	
	200001		magnetite alteration of felsic	PT	
	596459.1		magnetite alteration of felsic and shale	PT	

APPENDIX 2.1

DIAMOND DRILL HOLES LOGGED

D.D.H.	interval logged	Section	D.D.H.	interval logged	Section
WL 524	47.4 - 219.4 m	70	WL 622	0 - 176.5 m	70/71
WL 525	27.8 - 155.7 m	72	WL 623	0 - 119.0 m	74
WL 526	61.5 - 209.8 m*	71	WL 624	0 - 101.0 m	76
WL 528	0 - 104.3 m*	74	WL 626	0 - 134.3 m	74
WL 544	0 - 107.5 m	67	WL 627	0 - 140.0 m	76
WL 591	139.7 - 298.9 m	72	WL 629	0 - 154.5 m	73
WL 593	103.0 - 202.4 m	74	WL 633	0 - 116.0 m	67
WL 596	299.0 - 464.1 m	67/68	WL 634	0 - 156.5 m	68
WL 598	196.4 - 353.6 m	70	WL 635	0 - 140.0 m	68
WL 599	57.2 - 88.6 m	75	WL 636	0 - 138.7 m	71
	340.4 - 424.3 m	75			
WL 605	39.6 - 108.0 m	68	WL 637	0 - 153.2 m	71
WL 606	45.0 - 137.4 m	74	WL 638	0 - 131.0 m	73
WL 607	0 - 203.0 m	71	WL 639	0 - 121.6 m	74
WL 618	0 - 122.5 m	67	WL 640	0 - 139.5 m	74/75
WL 619	0 - 149.5 m	68	WL 641	0 - 131.7 m	73
WL 621	0 - 181.5 m	69	WL 679	0 - 179.0 m	73

Note: Downhole measurements are to the end of hole except where marked with *.

APPENDIX 3.1

LOW LEVEL (<1%) Na_2O DETERMINATIONS

LABORATORY PREPARATION

1. Due to the sensitivity of the AAS method, clean laboratory, glassware and polythene sample bottles thoroughly, with final rinse 3 - 4 times with distilled water.

PREPARATION OF RADIATION BUFFER SOLUTION

1. Dissolve 11.5 g $CaCl_2.2H_2O$ and 60.4 g $Sr(NO_3)_2$ in approximately 200 ml of distilled water.
2. Dissolve 3.125 g Fe filings and 6.25g Al powder in 50 ml concentrated hydrochloric acid. Heat slowly to complete dissolution, taking care it does not boil over, and cool.
3. Filter both solutions into a 500 ml volumetric flask and dilute to volume.

PREPARATION OF STANDARD SOLUTIONS

1. Make up 1000 ppm Na_2O stock solution by dissolving 0.9429 g dry NaCl in distilled water and dilute to 500 ml.
2. Dilute a 50 ml aliquot of stock solution to 500 ml to make a 100 ppm Na_2O solution. Repeat to produce a 10 ppm solution.
3. To each of five 100 ml volumetric flasks add 4 ml of radiation buffer solution and 0, 2.5, 5, 10, and 20 ml of the 10 ppm solution to make standards of 0, 0.25, 0.5, 1.0 and 2.0 ppm Na_2O.

PREPARATION OF SAMPLE SOLUTIONS

1. To a teflon crucible add 200 mg of powdered sample, 10 ml nitric acid and 5 ml hydrofluoric acid. Heat and decompose. Rinse walls with distilled water and evaporate dry.
2. Add 5 ml nitric acid, rinse walls and evaporate dry.
3. Add 2 ml perchloric acid, rinse walls, evaporate to white fumes, rinse walls and evaporate to no fumes.
4. Add 20 ml of 1% hydrochloric acid and heat. Dilute to volume with distilled water in a 200 ml volumetric flask. Shake and let settle.
5. To a 50 ml volumetric flask transfer 2 ml radiation buffer solution and 10 ml sample solution. Dilute to volume with distilled water (overall dilution now 5000x). Store in polythene bottles. Analyse as soon as possible.
6. Repeat steps 1 through 5 twice with no sample to give two reagent blanks, using the same batch of distilled water for the blanks as the samples.

Analysis and Data Reduction

1. Set atomic absorption spectrophotometer as follows: wavelength = 589.0 nm; slit = 0.33 nm; and slightly oxidized air/C_2H_2 flame.
2. Repeat standard solution analyses regularly to allow for machine drift during sample analysis.
3. The sample blanks must be averaged and subtracted from the samples to remove reagent contamination.
4. Sample Na_2O concentation in percent is equivalent to solution concentration in ppm.

APPENDIX 3.2

TRACE ELEMENT ANALYSES - WL 636

Depth (m)	ppm Ti	ppm Zr	ppm Nb	ppm Y	ppm Sc	ppm V	ppm Ga
0 - 2	3770	103	2	22	18	223	17
2 - 4	3690	119	8	24	12	207	13
4 - 6	3660	98	7	21	< 10	258	11
6 - 8	4000	105	5	23	13	305	16
8 -10	4090	104	8	24	26	286	16
10- 12	3830	101	4	25	21	275	14
12- 14	3710	93	7	23	13	287	18
14- 16	3540	93	7	20	19	314	17
16- 18	3450	98	5	19	< 10	236	13
18-20	3720	89	6	26	21	311	13
20-22	3110	69	7	14	11	320	18
22-24	3390	52	5	16	17	379	20
24-26	2890	44	9	19	35	342	15
26-28	3620	75	9	16	20	347	15
28-30	3000	72	9	16	10	257	16
30-32	3570	91	11	22	23	255	11
32-34	3460	82	10	18	12	245	17
34-36	3800	65	14	15	22	321	20
36-38	2150	35	11	8	13	179	11
38-40	2570	66	7	18	17	154	12
40-42	3600	96	16	19	31	311	14
42-44	2790	130	16	15	17	211	17
44-46	2940	111	15	20	23	237	15
46-48	2950	55	15	24	40	726	< 10
48-50	3960	68	13	15	26	357	17
50-52	3300	102	15	16	23	317	16
52-54	2630	61	13	14	23	291	14
54-56	3250	77	14	26	21	343	14
56-58	3550	45	18	27	26	447	16
58-60	3370	65	15	19	30	382	13
60-62	3730	69	16	20	17	325	11
62-64	4000	77	14	16	15	415	14
64-66	3630	90	19	40	22	466	18
66-68	3600	104	16	23	21	326	16
68-70	4090	91	18	20	40	402	15
70-72	4220	81	19	16	28	407	17
72-74	4010	88	22	21	27	486	15
74-76	1880	168	22	21	< 10	177	< 10
76-78	2070	182	21	28	23	151	10

Depth (m)	ppm Ti	ppm Zr	ppm Nb	ppm Y	ppm Sc	ppm V	ppm Ga
78-80	1770	182	22	29	< 10	166	< 10
80-82	1450	83	24	19	< 10	158	< 10
82-84	1850	206	27	23	10	142	< 10
84-86	1610	192	22	21	< 10	117	11
86-88	1750	200	14	22	16	137	10
88-90	1570	198	18	23	14	84	10
90-92	1770	162	18	28	16	173	12
92-94	2110	153	43	151	32	430	12
94-96	2020	238	29	38	12	109	13
96-98	1630	137	11	22	14	82	< 10
98-100	2230	148	8	34	15	136	14
100-102	2150	171	8	33	10	151	12
102-104	2080	177	10	36	19	131	14
104-106	1720	147	8	40	18	318	18
106-108	2120	126	8	31	14	318	15
108-110	2340	122	11	20	15	340	12
110-112	2400	132	8	26	17	273	15
112-114	1680	149	15	28	20	293	12
114-116	1500	185	17	41	< 10	267	17
116-118	1920	118	18	38	12	314	17
118-120	2580	154	15	27	14	221	12
120-122	2540	164	15	25	21	206	15
122-124	2310	139	12	35	18	280	16
124-126	1900	151	8	34	11	265	13
126-128	1780	126	9	86	14	344	13
128-130	2560	160	13	33	20	246	18
130-132	2090	162	15	28	18	208	17
132-134	2010	196	14	32	17	257	17
134-136	1960	184	16	31	21	165	12
136-138	2280	194	11	31	11	114	< 10

APPENDIX 3.3

TRACE ELEMENT ANALYSES - WL 637

Depth (m)	ppm Ti	ppm Zr	ppm Nb	ppm Y
0 - 2	4280	136	5	35
2 - 4	3910	134	9	31
4 - 6	4070	131	6	33
6 - 8	3950	119	6	31
8 -10	3990	111	6	31
10- 12	4130	106	11	32
12- 14	2190	64	5	25
14- 16	3840	99	8	26
16- 18	3270	74	6	36
18-20	3420	73	5	21
20-22	3120	121	11	27
22-24	3130	103	13	26
24-26	3520	93	13	27
26-28	2880	98	10	28
28-30	3220	100	11	23
30-32	3860	96	11	23
32-34	3760	91	14	25
34-36	3380	114	18	25
36-38	3500	85	15	25
38-40	3670	90	17	22
40-42	3300	103	14	26
42-44	3620	81	18	25
44-46	3720	92	16	23
46-48	4340	95	17	33
48-50	1420	168	13	24
50-52	1560	167	16	29
52-54	1460	160	14	41
54-56	1780	164	15	32
56-58	1800	187	14	25
58-60	1540	185	14	27
60-62	1770	176	13	37
62-64	1690	175	17	24
64-66	2160	173	19	31
66-68	2810	170	21	28
68-70	2760	167	31	34
70-72	1810	182	26	34
72-74	1610	193	22	30
74-76	1640	200	22	24
76-78	1670	208	23	31
78-80	1650	202	22	27
80-82	1590	199	19	27
82-84	1510	180	13	27
84-86	1400	174	14	40
86-88	1620	187	18	36
88-90	2160	184	16	47
90-92	2550	169	10	42
92-94	1590	168	10	35
94-96	1780	187	15	28
96-98	1670	186	10	24
98-100	1560	159	10	27
100-102	3810	46	23	35
102-104	2050	110	14	54
104-106	2010	84	9	31
106-108	2250	144	13	40
108-110	2510	148	15	36
110-112	1730	144	15	42
112-114	1210	167	14	36
114-116	1260	157	12	38
116-118	2170	169	21	46
118-120	2140	161	26	41
120-122	1490	156	20	42
122-124	1590	146	21	36
124-126	2610	166	14	28
126-128	1580	193	16	37
128-130	1830	161	14	49
130-132	1720	201	6	71
132-134	1530	206	8	74
134-136	1350	233	10	76
136-138	1390	228	9	66
138-140	1450	229	9	54
140-142	1410	216	8	57
142-144	1520	222	9	55
144-146	1430	227	8	45
146-148	1590	251	10	52
148-150	2010	207	9	35
150-152	1230	129	4	17
152-153	800	139	< 2	18

APPENDIX 3.4

RARE EARTH ELEMENT NEUTRON ACTIVATION ANALYSES
(all results in ppm)

Whole Rock Analyses

Sample No.	640063.0	637052.0
Element		
La	194.70	129.20
Ce	318.00	213.00
Nd	94.60	64.10
Sm	14.00	7.12
Eu	3.90	2.23
Tb	1.29	0.88
Ho	1.03	1.10
Yb	2.84	1.91
Lu	0.51	0.26

Apatite Analyses

Sample No.	618112.8	633066.1	699000.0*
Element			
La	4290.00	4950.00	3850.00
Ce	10100.00	11300.00	8400.00
Nd	3970.00	4310.00	3230.00
Sm	731.00	788.00	637.00
Eu	61.90	70.50	59.40
Tb	41.20	43.30	39.90
Ho	35.90	40.00	36.00
Yb	46.40	49.30	45.60
Lu	7.61	7.77	7.40

* Sample numbers normally refer to drill hole number and down hole distance. However, the exact location of this apatite is not known and a dummy sample number has been used.

APPENDIX 3.5

TRACE ELEMENT ANALYSES OF VOLCANICLASTIC BRECCIA CLASTS AND MATRIX

Sample No.	PL No.	ppm Ti	ppm Zr	ppm Nb	ppm Y	ppm Sc	ppm V	ppm Ga
115002	42	2405	130	1	21	13	192	13
115002	43	3385	140	2	15	14	165	14
586210.6	44	2920	61	13	25	16	319	11
586210.6	45	3010	79	7	25	27	328	14
586210.6	46	1980	44	3	38	25	381	9
586210.6	47	4455	11	6	19	36	483	20
586210.6	50	4585	67	10	24	33	533	17
589065.7	51	2465	140	<1	23	29	253	15
589065.7	52	2270	122	<1	22	22	236	14
589065.7	53	2620	134	1	23	22	215	16
589065.7	54	3600	177	<1	25	31	236	18
589065.7	55	3815	200	3	27	26	140	18
589065.7	58	1355	169	<1	49	20	57	11

Sample No.	PL No.	Ti/Zr	V/Sc	Ga/Sc	Description
115002	42	18.5	14.8	1.00	whole rock analysis
115002	43	24.2	11.8	1.00	altered dacite clast
586210.6	44	47.9	19.9	0.69	whole rock analysis
586210.6	45	38.1	12.1	0.52	altered dacite clast
586210.6	46	45.0	15.2	0.36	siliceous, pyritic matrix
586210.6	47	405.0	13.4	0.56	strongly altered clast
586210.6	50	68.4	16.2	0.52	altered dacite clast
589065.7	51	17.6	8.7	0.52	breccia matrix
589065.7	52	18.6	10.7	0.64	breccia matrix
589065.7	53	19.6	9.8	0.73	breccia matrix
589065.7	54	20.3	7.6	0.58	altered dacite clast
589065.7	55	19.1	5.4	0.69	altered dacite clast
589065.7	58	8.0	2.9	0.55	felsic volcanic clast

Note: Insufficient sample could be obtained for analysis of samples PL48, 49, 56 and 57.

APPENDIX 3.6

MAJOR AND TRACE ELEMENT ANALYSES
PRINCE LYELL ALTERED VOLCANICS

Sample No.	PL1	PL2	PL3	PL4	PL5	PL6	PL7	PL8	PL9	PL10
SiO2	68.49	56.13	52.27	59.87	56.13	66.83	56.77	69.18	45.62	65.55
TiO2	0.27	0.25	0.42	0.28	0.45	0.26	0.37	0.23	0.60	0.25
Al2O3	11.23	10.16	12.34	10.95	12.35	11.35	11.07	10.57	15.00	10.87
Fe2O3	7.98	15.97	18.39	10.97	15.16	7.90	19.35	7.42	20.41	11.94
MnO	0.07	0.37	0.06	0.24	0.12	0.11	0.42	0 07	0.30	0.08
MgO	1.18	1.97	2.13	1.83	2.20	1.56	3.08	1.39	3.76	0.83
CaO	0.38	0.83	0.56	1.72	0.91	0.80	0.15	0.74	1.34	0.05
Na2O	0.06	0.13	0.20	0.25	0.06	0.08	0.05	0.07	0.09	0.15
K2O	3.29	3.26	3.49	3.56	3.59	3.95	1.47	3.64	3.13	3.66
P2O5	0.15	0.49	0.34	0.34	0.65	0.21	0.17	0.16	0.46	0.08
Loss	4.04	8.38	7.72	7.10	5.64	4.93	6.16	4.77	8.33	6.16
CuO	2.12	1.75	2.25	2.38	2.50	2.25	1.00	1.50	1.88	0.75
Total	99.26	99.69	100.17	99.49	99.76	100.23	100.06	99.74	100.92	100.37
Sn	11	21	7	18	25	35	10	31	10	75
As	<10	<10	27	<10	<10	<10	11	<10	33	<10
Mo	39	21	150	336	6	27	21	33	19	23
Pb	13	33	30	12	19	12	16	8	1390	7
Zn	124	275	229	110	278	112	11	116	2110	39
Zr	182	161	172	194	157	190	171	140	95	195
Ti/Zr	8.9	9.3	14.6	8.7	17.2	8.2	13.0	9.8	37.9	7.7
Alteration Index	91.04	84.49	88.09	73.23	85.65	86.23	95.79	86.13	82.81	95.74

Sample No.	PL11	PL12	PL13	PL14	PL15	PL16	PL17	PL18	PL19	PL21
SiO2	62.13	38.94	45.33	45.45	53.53	57.83	56.32	56.53	45.44	45.24
TiO2	0.41	0.56	0.51	0.61	0.47	0.31	0.35	0.49	0.61	0.64
Al2O3	12.87	15.36	10.17	16.72	13.11	8.65	11.54	13.98	17.51	14.63
Fe2O3	12.85	27.52	24.27	23.34	16.69	16.64	16.07	13.53	19.97	24.07
MnO	0.21	0.36	0.19	0.28	0.17	0.21	0.05	0.20	0.14	0.24
MgO	1.32	4.48	2.25	4.03	2.37	1.51	2.02	2.63	3.11	4 22
CaO	0.15	0.55	0.98	0.19	0.81	0.54	0.26	1.50	0.65	0.80
Na2O	0.13	0.11	0.10	0.03	0.05	0.07	0.05	0.04	0.05	0.02
K2O	3.93	2.43	2.76	2.42	3.75	2.51	3.78	4.73	4.99	2.39
P2O5	0.09	0.40	0.79	0.18	0.45	0.32	0.29	0.21	0.22	0.32
Loss	6.18	8.41	8.52	6.11	5.96	7.96	5.81	5.49	6.88	6.93
CuO	0.13	0.88	4.26	0.40	2.13	2.88	3.13	0.63	0 75	0.50
Total	100.40	100.00	100.13	99.76	99.49	99.43	99.67	99.96	100.32	100.00
Sn	18	18	14	18	14	12	13	35	18	9
As	<10	113	66	14	<10	<10	27	<10	20	<10
Mo	7	19	89	9	29	41	282	18	9	7
Pb	<1	88	890	15	147	26	36	10	67	50
Zn	87	1535	1160	485	440	180	331	179	405	730
Zr	200	65	133	101	102	159	167	151	58	93
Ti/Zr	12.3	51.6	23.0	36.2	27.6	11.7	12.6	19.4	63.0	41.2
Alteration Index	94.94	91.28	82.27	96.70	87.68	86.83	94.93	82.70	92.05	88.96

Sample No.	PL22	PL23	PL24	PL25	PL27	PL28	PL29	PL30	PL31	PL32
SiO2	60.29	62.68	66.86	33.21	50.52	56.34	60.63	62.95	60.66	50.64
TiO2	0.46	0.28	0.25	0.70	0.31	0.55	0.23	0.23	0.21	0.70
Al2O3	14.11	11.89	10.92	16.68	10.81	13.46	10.32	10.54	9 62	17.14
Fe2O3	11.14	10.69	11.61	26.68	22.80	15.47	12.73	13.83	16.51	17.32
MnO	0.11	0.08	0.13	0.60	0.14	0.19	0.18	0.13	0.23	0.13
MgO	2.09	1 28	1.12	3.01	2.19	2.92	1.45	1.77	1.88	2.85
CaO	0.96	0.62	0.06	0.35	0.47	0.90	0.70	0.65	0.24	0.93
Na2O	0.32	0.92	0.11	0.29	0.02	0.10	0.07	0.02	0.04	0.60
K2O	4.83	5.21	3.64	4.10	2.02	2.94	3.40	2.87	1.67	4.90
P2O5	0 20	0.30	0.07	0.25	0.41	0.48	0.35	0.32	0.28	0.20
Loss	5.34	4.66	5.16	11.64	7.80	6.45	6.89	4.56	5.81	4.76
CuO	1.13	1.88	0.20	2.25	2.00	0.38	3.26	1.63	2.50	0.38
Total	100.98	100.49	100.13	99.76	99.49	100.18	100.21	99.50	99.65	100.55
Sn	41	9	40	10	17	16	13	13	5	10
As	<10	10	<10	<10	108	<10	<10	14	36	<10
Mo	21	66	23	17	44	18	34	90	237	5
Pb	7	23	20	31	134	17	18	83	179	11
Zn	118	177	96	397	2800	175	214	248	630	237
Zr	176	176	204	25	139	168	183	179	166	104
Ti/Zr	15.7	9.5	7.3	167.8	13.4	19.6	7.5	7.7	7.6	40.3
Alteration Index	84.39	80.82	96.55	91.74	89.57	85.42	86.30	87.38	92.69	83.51

Note: Samples PL20 and PL25 were analyses of University of Tasmania standards.

APPENDIX 3.7

LOCATION AND LITHOLOGICAL DESCRIPTIONS OF ALTERED VOLCANICS ANALYSED IN APPENDIX 3.6

PL No.	Location *	Description
1	626047.0	Pink sericitic felsic volcanic with coarse grained pseudofragmental texture
2	626085.0	Grey-orange, sericitic pseudofragmental felsic volcanic
3	633060.0	Massive, dark pinky-grey, chlorite flecked, felsic volcanic
4	640127.0	Grey-brown, sericitic, pseudofragmental felsic volcanic
5	623065.0	Dark grey, altered dacite with sericite flecks
6	623038.0	Pink, sericitic, coarsely pseudofragmental felsic volcanic
7	623016.0	Strongly chloritic, partly silicified volcaniclastic breccia
8	640063.0	Massive, pink, sericitic felsic volcanic with possible ghosts of feldspar phenocrysts
9	633010.0	Chloritic intermediate-mafic volcanic with pyrite bands
10	624049.0	Massive, pink, sericitic felsic volcanic
11	627005.0	Carbonate altered, brown-grey, sericitic, felsic volcanic
12	636060.0	Chloritic intermediate-mafic volcanic with minor pyrite-magnetite bands
13	637069.0	Weakly recrystallised, sericite flecked, dark grey dacite
14	636017.0	Chloritic intermediate-mafic volcanic with fine sericite flecks
15	636116.5	Grey, sericitic, pseudofragmental felsic volcanic
16	636135.5	Pale grey-pink, sericitic, pseudofragmental felsic volcanic
17	636091.5	Dark grey, chloritic, weakly pseudofragmental felsic volcanic
18	636100.5	Dark grey, partly silicified dacite with sericite flecks
19	637045.0	Chloritic intermediate-mafic volcanic with pyrite bands
21	637031.0	Chloritic intermediate-mafic volcanic with fine sericite flecks
22	637090.0	Dark grey, altered dacite with poorly aligned sericite flecks
23	637075.0	Very siliceous, grey, weakly pseudofragmental felsic volcanic
24	637135.5	Carbonate altered, pink, sericitic felsic volcanic
25	637101.5	Carbonate altered, fine grained ?lamprophyre with sericite flecks
27	637052.0	Chloritic, grey, felsic volcanic
28	677078.5	Fine grained, sericite flecked, dark grey altered dacite
29	637095.0	Pale pink-grey, sericitic, pseudofragmental felsic volcanic
30	637056.0	Dark grey, sericitic, weakly pseudofragmental felsic volcanic
31	605085.0	Chloritic, grey, felsic volcanic
32	637006.0	Chloritic intermediate-mafic volcanic with disseminated magnetite

* Note: Sample locations are denoted by seven digit numbers. The first three digits (eg: 637) refer to the diamond drill hole number in the WL series. The last four digits (eg: 095.0) refer to the downhole distance in metres.

APPENDIX 3.8

Error analysis - Whole rock geochemistry

Precision analysis - RGC Laboratories, Queenstown

	Detection limit	No. of check assays	Assay range	Average error	Median error
TiO2		8	0.28 - 0.93 wt%	3%	3%
Zr	5 ppm	8	<5 - 200 ppm	24%	21%
Pb	1 ppm	11	<1 - 24600 ppm	27%	27%
Zn		11	87 - 2170 ppm	9%	4%
Sn	5 ppm	5	< 5 - 19 ppm	44%	11%
As	10 ppm	5	< 10 - 116 ppm	10%	10%
Mo	5 ppm	5	< 5 - 280 ppm	4%	1%
Cu	1 ppm	3	<1 - 2680 ppm	35%	7%

Accuracy analysis - RGC laboratories assays of standard samples

	Detection limit	No. of check assays	Assay range	Average error	Median error
TiO2		5	0.29 - 2.31 wt%	5%	9%
Zr	5 ppm	4	44 - 260 ppm	11%	8%
Nb	2 ppm	3	1.4 - 60 ppm	10%	12%
Y		3	17 - 35 ppm	22%	23%
V	10 ppm	3	25 - 385 ppm	58%	80%
Sc	10 ppm	3	6 - 41 ppm	26%	35%
Pb	1 ppm	3	5 - 800 ppm	17%	11%
Zn		3	120 - 900 ppm	20%	18%

Single check analyses for Sn, As, Mo, Ag and Cu produced errors of 5 to 20%.

Relative precision between RGC and University of Tasmania laboratories

30 samples analysed for TiO2 at both laboratories produced an average 7% error between analyses with RGC analyses on average marginally lower.

APPENDIX 4.1

MAGNETIC SUSCEPTIBILITY CONVERSION

The measured magnetic susceptibility and magnetite content (measured by point counting) of five polished drill core samples are given below, along with the best fit line for the relationship between the two.

Magnetic susceptibility (c.g.s. x 10^3)	Magnetite content (volume %)
0.7	0.7
3.6	1.2
11	8.1
23	10.3
45	24.4

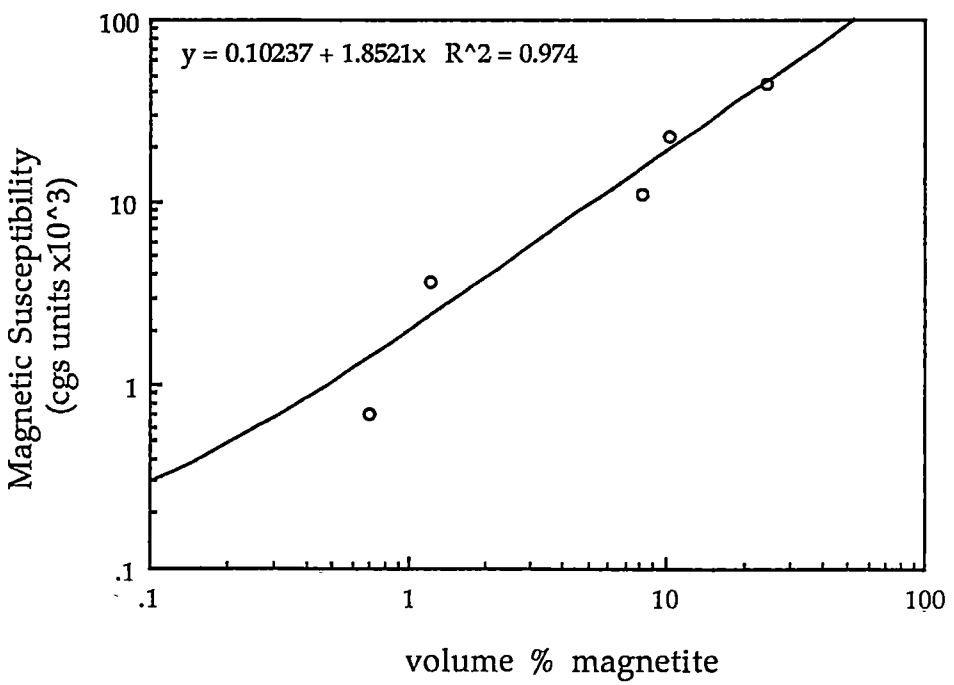

APPENDIX 5.1

SULPHIDE MINERAL ETCHING

PREPARATION OF ETCHING SOLUTION

1. Dissolve 1g $KMnO_4$ in 40 ml of distilled water.
2. Add 40 ml of 25% sulphuric acid.

SAMPLE ETCHING

1. Immerse and agitate a polished thin section in the etching solution for approximately 30 - 45 seconds for pyrite or 10 - 20 seconds for sphalerite.

Notes:

(i) The etching technique is destructive of chalcopyrite, imparting a heavy tarnish on the surface of chalcopyrite grains. The tarnish may be removed from chalcopyrite without removing pyrite etch marks by gentle polishing. Magnetite and hematite are unaffected by the etching solution.

(ii) Etching times may vary if a deeper etch is required or for large samples, such as polished slabs. After prolonged use of the solution, etching times may increase.

(iii) Keep the solution covered as vapours from it will corrode or rust some materials over time.

APPENDIX 5.2

DETECTION LIMITS OF MICROPROBE ANALYSES OF PRINCE LYELL SULPHIDES

Analyses of sulphide and oxide minerals were carried out using a Cameca SX-50 electron microprobe at the Central Science Laboratory, University of Tasmania. Operating conditions for sulphide analyses were progressively updated during the study until optimum detection limits for trace elements were reached. Arsenic could not be analysed in Label V due to equipment failure. Lead analyses are regarded as unreliable due to interference of lead and arsenic x-ray spectra. For the same reason, arsenic analyses may only be regarded as relative values.

Detection limits presented in the table below were calculated by the formula:

$$\text{Detection Limit (\%)} = \left[\frac{3 \times \sqrt{\frac{\text{Background counts/sec}}{\text{Background count time}}}}{\text{Standard counts /sec /nA /1\% pure standard}} \right]$$

Label #	nA	kV	Detection limit (ppm)							
			Co	Ni	Cu	Zn	As	Se	Ag	Pb
Ia	20	20	350	350	350	1450	200	-	-	-
I	50	20	200	200	250	450	150	850	250	-
II	50	20	200	200	250	450	150	450	250	-
III	100	20	100	100	100	350	50	350	150	-
IV	100	20	100	100	100	350	50	350	150	300
V	100	20	100	100	100	350	-	350	150	300

APPENDIX 5.3

ELECTRON MICROPROBE TRACE ELEMENT ANALYSES OF PYRITE

Thin Section	Label/Date	Py #	ppm Co	ppm Ni	ppm Cu	ppm Zn	ppm Ag	ppm Se	ppm As
115003	I	1	710	210	50	0	xxx	xxx	720
115003	I	2	90	10	210	0	xxx	xxx	430
115003	I	3	5300	80	310	0	xxx	xxx	740
115003	I	4	13470	0	0	0	xxx	xxx	720
115003	I	5	4920	1950	110	0	xxx	xxx	1080
115003	I	6	10	0	290	0	xxx	xxx	530
115003	I	7	950	320	190	0	xxx	xxx	710
115003	I	8	940	100	80	190	xxx	xxx	360
115003	I	9	320	170	210	360	xxx	xxx	760
115003	I	10	60	390	0	370	xxx	xxx	730
115003	I	11	1210	0	260	0	xxx	xxx	790
115003	I	12	1470	1580	0	0	xxx	xxx	870
115003	I	13	1410	850	970	330	xxx	xxx	1050
115003	I	14	2460	1250	150	400	xxx	xxx	610
115003	I	15	5870	850	0	0	xxx	xxx	540
115003	I	16	3860	1810	0	130	xxx	xxx	590
115003	I	17	4250	1910	200	0	xxx	xxx	780
115003	I	18	180	300	0	20	xxx	xxx	440
115003	I	19	0	0	30	0	xxx	xxx	750
115003	I	20	1580	1400	140	0	xxx	xxx	550
115003	Ia 1 3 90	21	4060	610	80	0	xxx	1070	440
115003	Ia 1 3 90	22	8350	10	120	0	xxx	0	1380
115003	Ia 1 3 90	23	0	150	6960	340	xxx	330	730
115003	Ia 1 3 90	24	12340	900	100	0	xxx	620	1430
115003	Ia 1 3 90	25	320	0	280	0	xxx	620	590
115003	Ia 1.3 90	26	11920	220	500	70	xxx	160	660
115003	Ia 1 3 90	27	1680	30	0	40	xxx	0	650
115003	Ia 1 3 90	28	210	60	0	140	xxx	590	680
115003	Ia 1 3 90	29	1270	460	0	90	xxx	140	720
115003	Ia 1 3 90	30	3650	260	0	210	xxx	500	540
115003	Ia 1 3 90	31	10	210	40	70	xxx	460	740
115003	Ia 1 3 90	32	2460	2400	80	0	xxx	430	770
115003	Ia 1 3 90	33	440	0	0	0	xxx	430	510
636126 8	II 27.3.90	34	750	1070	0	30	160	160	580
636126.8	II 27.3 90	35	4420	430	40	0	0	0	590
624096.9	Ia 1.3 90	36	150	0	0	0	xxx	510	900
624096.9	II 22.3 90	37	0	420	120	180	0	0	360
624096 9	II 22.3 90	38	0	30	0	0	260	0	400
624096.9	II 22.3 90	39	290	40	90	70	40	420	720
624096.9	II 22.3 90	40	1030	340	0	190	0	0	540
624096.9	II 22.3 90	41	60	160	0	0	0	40	460
624096 9	II 22.3.90	42	0	180	0	0	20	590	400
624096.9	II 22.3 90	43	0	130	0	150	0	0	540
624096.9	II 22.3 90	44	0	400	360	300	130	0	2550
624096.9	II 22.3 90	45	0	100	0	0	140	0	2780
624096.9	II 22.3 90	46	0	230	0	110	0	120	390
624096.9	II 22.3 90	47	160	20	120	0	0	900	590
624096.9	II 22.3 90	48	0	260	40	0	0	160	370
624096 9	II 22.3 90	49	0	0	150	190	60	0	560
624096 9	II 22.3 90	50	0	20	40	220	190	780	530
624096 9	II 22.3 90	51	0	140	150	0	170	30	590
624096.9	II 22.3 90	52	40	140	0	0	0	230	460
624096.9	II 22.3 90	53	0	170	90	0	0	220	450
599377 3	III 30.3 90	54	2750	10	10	10	0	0	490
599377.3	III 30.3 90	55	29880	120	100	0	0	260	510
599377 3	III 30.3.90	56	20950	0	170	30	0	0	480
599377 3	III 30.3 90	57	1600	80	120	110	0	0	950
599377 3	III 30.3 90	58	2270	3370	40	0	40	0	400
599377 3	III 30 3 90	59	70	0	120	30	10	0	580

Thin Section	Label/Date	Py #	ppm Co	ppm Ni	ppm Cu	ppm Zn	ppm Ag	ppm Se	ppm As
599377.3	III 30.3.90	60	900	50	10	30	0	300	450
599377.3	III 30.3 90	61	2260	110	0	80	0	40	400
599377.3	III 30.3.90	62	2690	140	0	120	110	20	530
599377.3	III 30.3 90	63	5680	0	150	0	210	0	480
599377.3	III 30.3.90	64	6020	300	70	0	20	330	420
599377.3	III 30.3.90	65	9240	310	60	50	30	150	510
599377.3	III 30.3.90	66	10320	330	80	70	30	0	590
599377 3	III 30.3.90	67	9810	100	0	60	0	0	460
599377 3	III 30.3.90	68	7800	0	10	60	0	0	560
599377.3	III 30.3 90	69	9350	240	0	0	0	0	450
599377.3	III 30.3.90	70	5580	60	20	30	60	560	470
599377.3	III 30.3 90	71	2260	100	0	0	0	120	370
599377.3	III 30.3.90	72	3250	160	10	10	30	0	470
599377.3	III 30.3.90	73	7510	170	0	0	50	100	820
599377.3	III 30.3.90	74	540	300	0	0	40	0	430
599377.3	III 30.3 90	75	50	40	0	0	0	340	510
599377.3	III 30.3 90	76	0	30	0	40	0	230	410
599377.3	III 30.3 90	77	0	40	40	0	90	0	430
599377 3	III 30.3.90	78	3550	60	0	100	0	140	480
599377.3	III 30.3.90	79	0	0	0	80	40	80	520
599377.3	III 30.3 90	80	0	70	0	0	0	220	500
599377.3	III 30.3.90	81	2230	80	0	0	0	0	450
599377.3	III 30.3.90	82	0	0	0	30	210	0	470
599377.3	III 30.3.90	83	6490	920	0	50	0	660	960
599377.3	III 30.3.90	84	6010	830	0	40	40	470	850
599377.3	III 30.3.90	85	4670	500	30	0	120	160	740
599377.3	III 30.3 90	86	8280	310	0	0	0	370	1180
599377 3	III 30.3.90	87	5910	290	70	0	0	130	1100
599377 3	III 30.3.90	88	7940	470	10	20	20	100	920
599377 3	III 30.3 90	89	7370	470	50	0	70	170	880
599377.3	III 30.3.90	90	4490	860	30	0	0	0	620
599377.3	III 30.3.90	91	5210	900	100	160	0	150	500
599377.3	III 30.3 90	92	7020	1040	0	10	0	0	370
599377 3	III 30.3.90	93	5250	1210	0	100	120	200	430
599377.3	III 30.3 90	94	2700	830	0	90	210	60	540
599377.3	III 30.3 90	95	2120	830	40	0	90	0	500
599377.3	III 30.3.90	96	1120	3920	140	70	0	0	480
599377 3	III 30.3.90	97	1580	50	0	60	0	180	320
599377.3	III 30.3.90	98	790	0	40	50	0	180	510
599377.3	III 30.3.90	99	1140	60	0	80	190	220	400
599377 3	III 30.3.90	100	0	60	10	30	30	0	300
599377.3	III 30.3.90	101	30	40	100	10	60	0	350
599377.3	III 30.3 90	102	0	10	10	0	0	260	550
599377.3	III 30.3 90	103	0	0	10	10	30	160	450
599377 3	III 30.3 90	104	0	40	40	40	280	90	520
599377 3	III 30.3 90	105	0	70	70	100	10	210	430
599377 3	III 30.3 90	106	130	40	40	0	60	140	440
599377 3	III 30.3.90	107	80	0	30	60	0	10	460
599377.3	III 30.3.90	108	40	20	10	0	50	180	520
599377 3	III 30.3 90	109	910	140	40	40	0	170	450
599377.3	III 30.3 90	110	530	110	0	0	240	40	450
599377.3	III 30.3.90	111	10	100	40	80	0	30	480
599377 3	III 30.3 90	112	1570	430	90	40	0	0	430
599377.3	III 30.3.90	113	3320	780	0	40	100	90	460
599377.3	III 30.3.90	114	6550	100	0	80	90	0	610
599377 3	III 30.3 90	115	7090	0	60	0	50	120	670
599377 3	III 30.3 90	116	2180	80	10	70	0	0	500
599377 3	III 30.3.90	117	280	0	0	50	150	0	420
599377 3	III 30.3 90	118	24070	10	0	0	0	290	530

Thin Section	Label/Date	Py #	ppm Co	ppm Ni	ppm Cu	ppm Zn	ppm Ag	ppm Se	ppm As
599377 3	III 30.3 90	119	17270	0	40	20	0	0	880
599377 3	III 30.3.90	120	24150	80	10	0	90	0	990
599377 3	III 30.3 90	121	0	0	0	140	220	90	420
599377.3	III 30.3 90	122	120	20	60	20	80	530	450
599377 3	III 30.3 90	123	20	0	0	0	0	0	470
599377 3	III 30.3 90	124	2770	170	60	50	0	0	350
599377.3	III 30.3 90	125	3400	70	0	120	0	0	1110
599377.3	III 30.3 90	126	4400	0	70	70	0	390	650
624096 9	III 30.3 90	127	0	0	0	80	0	340	450
624096 9	IV 2 4 90	128	0	10	0	90	0	0	540
624096 9	IV 2.4.90	129	0	70	10	120	0	0	540
624096 9	IV 2 4 90	130	80	50	70	410	0	300	3670
624096 9	IV 2 4 90	131	0	110	90	120	90	0	630
624096.9	IV 2 4 90	132	0	100	80	920	0	0	510
624096 9	IV 2 4.90	133	0	40	0	140	0	150	490
624096.9	IV 2 4 90	134	10	250	0	140	0	0	490
624096.9	IV 2 4.90	135	100	120	150	440	50	20	600
624096.9	IV 2 4.90	136	0	110	170	260	0	170	430
624096.9	IV 2.4.90	137	170	40	0	50	0	0	1450
624096.9	IV 2 4 90	138	0	110	80	60	0	280	3170
624096 9	IV 2.4 90	139	0	40	120	150	0	70	1370
624096.9	IV 2.4.90	141	0	110	0	60	100	0	500
624096.9	IV 2 4 90	142	260	130	140	100	150	270	2270
624096 9	IV 2 4 90	143	0	290	40	70	70	30	570
624096.9	IV 2 4 90	144	30	220	0	60	160	0	460
624096.9	IV 2 4.90	145	0	80	30	0	0	120	480
624096.9	IV 2 4 90	146	0	220	10	0	50	0	520
624096.9	IV 2.4 90	147	0	0	740	70	10	260	3960
624096 9	IV 2 4 90	148	20	80	130	0	160	0	2250
624096 9	IV 2.4.90	149	100	80	140	0	70	0	1760
624096 9	IV 2 4 90	150	0	140	50	30	80	0	460
624096 9	IV 2 4.90	151	0	160	90	100	20	0	860
624096 9	IV 2.4.90	152	0	20	770	360	0	10	480
115003	IV 1 4 90	153	1910	60	100	0	0	150	450
115003	IV 1.4.90	154	4430	320	100	50	0	10	550
115003	IV 1 4 90	155	310	10	130	0	0	390	510
115003	IV 1.4.90	156	460	20	0	0	0	210	530
115003	IV 1 4 90	157	0	0	50	80	230	510	600
115003	IV 1 4 90	158	4350	1200	120	0	40	500	530
115003	IV 1.4 90	159	3200	1610	80	90	80	30	520
115003	IV 1.4.90	160	550	80	0	0	180	0	480
115003	IV 1.4.90	161	600	760	0	0	0	0	590
115003	IV 1 4.90	162	1880	1520	160	0	120	250	610
115003	IV 1 4 90	163	5580	880	90	0	180	260	570
115003	IV 1 4 90	164	0	120	40	20	0	0	630
582255.6	IV 14.5.90	166	730	140	0	0	350	350	500
582255 6	IV 14.5 90	167	670	30	130	50	40	40	490
582255 6	IV 14 5 90	168	3980	20	30	50	0	0	910
599377.3	IV 17.5.90	170	9910	290	20	30	70	250	410
599377 3	IV 17 5 90	171	7810	980	50	60	0	0	540
599377 3	IV 17.5 90	172	4110	100	60	20	0	0	390
599377.3	IV 17 5 90	173	3550	130	70	110	120	140	430
599377.3	IV 17 5.90	174	29280	30	100	30	0	140	340
599377 3	IV 17.5 90	175	9180	0	120	30	50	80	440
599377.3	IV 17 5.90	176	80	70	140	0	50	190	460
599377 3	IV 17 5 90	177	160	30	310	0	0	0	490
599377.3	IV 17.5 90	178	8080	80	0	0	0	0	470
599377 3	IV 17 5 90	179	7130	110	50	0	30	0	570
599377 3	IV 17 5 90	180	0	50	80	0	0	210	520

Thin Section	Label/Date	Py #	ppm Co	ppm Ni	ppm Cu	ppm Zn	ppm Ag	ppm Se	ppm As
599377.3	IV 17 5 90	181	3710	40	0	0	0	40	420
599377 3	IV 17 5 90	182	0	10	60	20	0	40	530
599377.3	IV 17 5 90	183	0	0	190	0	10	0	440
599377 3	IV 17 5.90	184	4560	10	100	70	40	180	450
599377 3	IV 17.5.90	185	5250	80	110	0	70	60	460
599377 3	IV 17 5 90	186	620	0	0	0	0	130	560
599377.3	IV 17 5 90	187	0	90	10	0	0	0	410
599377.3	IV 17 5 90	188	1360	30	80	0	10	0	440
599377.3	IV 17 5 90	189	6760	80	170	70	270	140	690
599377.3	IV 17.5.90	190	0	10	150	0	210	0	390
599377.3	IV 17.5.90	191	0	60	80	0	0	120	420
599377 3	IV 17.5 90	192	4450	130	40	0	0	0	490
599377.3	IV 17.5 90	193	14610	180	140	80	0	120	440
599377.3	IV 17.5 90	194	5700	10	60	0	30	90	490
599377.3	IV 17.5.90	195	5870	0	20	0	20	0	510
599377.3	IV 17.5.90	196	2090	150	140	60	50	0	470
599377.3	IV 17 5.90	197	12620	100	80	20	70	170	480
599377.3	IV 17 5 90	198	340	130	40	0	0	0	390
599377.3	IV 17 5.90	199	2120	110	50	10	0	0	450
599377.3	IV 17 5 90	200	1960	100	0	0	70	30	410
599377.3	IV 17.5 90	201	550	40	90	0	40	230	500
599377.3	IV 17.5 90	202	160	60	30	100	20	0	420
599377.3	IV 17.5.90	203	27620	100	120	10	90	0	400
599377.3	IV 17 5.90	204	4720	30	70	80	0	0	730
599377.3	IV 17.5.90	205	6290	140	10	0	40	70	500
599377.3	IV 17 5.90	206	6690	80	60	40	0	220	740
599377.3	IV 17.5.90	207	7160	0	10	20	70	410	620
599377.3	IV 17.5 90	208	280	10	90	90	30	0	460
599377.3	IV 17.5 90	209	0	80	80	100	0	340	500
599377.3	IV 17 5.90	210	90	0	90	20	0	120	430
599377.3	IV 17 5 90	211	2630	10	10	70	0	0	470
599377.3	IV 17.5.90	212	190	0	70	60	120	30	490
599377 3	IV 17.5.90	213	2170	130	70	10	70	0	480
599377.3	IV 17.5 90	214	930	20	60	0	0	220	570
599377.3	IV 17 5 90	215	0	20	20	70	40	30	530
639121 3	IV 25.6 90	220	390	350	0	0	100	200	460
639121.3	IV 25 6 90	221	0	170	10	0	160	40	530
639121 3	IV 25 6 90	222	0	260	0	20	0	100	500
639121 3	IV 25.6 90	223	0	1510	0	40	40	600	440
639121.3	IV 25.6.90	224	0	1510	0	40	0	670	500
639121.3	IV 25 6 90	225	10	240	30	0	0	360	430
639121 3	IV 25.6 90	226	0	230	120	0	0	610	500
639121 3	IV 25.6 90	227	0	270	0	30	0	190	410
639121 3	IV 25.6 90	228	10	360	1160	0	70	250	450
639121 3	IV 25 6 90	229	30	60	60	120	150	70	980
639121.3	IV 25.6 90	230	0	20	20	40	210	0	480
639121 3	IV 25 6 90	231	0	0	30	0	0	300	470
639121.3	IV 25 6 90	232	0	160	50	40	0	190	600
639121 3	IV 25 6.90	233	420	270	30	90	0	0	540
639121 3	IV 25 6.90	234	190	280	0	30	40	20	420
639121 3	IV 25 6 90	235	360	1040	40	180	0	0	480
639121.3	IV 25 6.90	236	0	470	10	230	0	110	470
639121 3	IV 25 6 90	237	0	270	0	290	110	400	520
639121 3	IV 25 6 90	238	0	640	30	620	30	0	490
639121 3	IV 25 6 90	239	0	880	10	1280	120	40	570
639121 3	IV 25 6 90	240	60	770	40	260	0	0	400
639121 3	IV 25 6 90	241	0	640	0	100	0	0	530
639121 3	IV 25 6 90	242	0	630	0	750	70	0	500
639121.3	IV 25 6 90	243	0	590	30	0	20	0	440

Thin Section	Label/Date	Py #	ppm Co	ppm Ni	ppm Cu	ppm Zn	ppm Ag	ppm Se	ppm As
639121.3	IV 25 6 90	244	0	610	0	130	0	0	460
639121 3	IV 25 6 90	245	0	460	0	70	0	50	480
605100 6	IV 25 6 90	246	0	0	20	500	60	150	680
605100 6	IV 25 6 90	247	0	0	180	2840	10	190	390
605100.6	IV 25.6.90	248	70	10	1660	460	80	280	500
605100 6	IV 25.6 90	249	30	50	60	450	70	60	370
605100 6	IV 25.6 90	250	0	90	260	90	0	120	570
605100 6	IV 25.6 90	251	280	100	2830	1180	10	210	500
605100.6	IV 25.6 90	252	90	40	2520	330	90	0	570
605100 6	IV 25.6 90	255	0	30	10	430	0	0	440
605100 6	IV 25 6 90	256	0	130	0	260	30	0	490
605100 6	IV 25 6 90	257	2380	170	70	8050	180	0	720
605100 6	IV 25 6 90	258	3930	80	30	1880	60	0	570
605100 6	IV 25 6.90	259	0	0	0	2450	0	30	870
605100 6	IV 25 6 90	261	70	40	80	1290	0	340	9610
605100 6	IV 25.6.90	262	440	50	40	780	210	160	650
605100.6	IV 25 6 90	263	220	0	100	1040	170	160	6180
605100 6	IV 25 6 90	264	1410	40	10	4720	20	200	420
618051 8	IV 26 6.90	265	15210	20	120	60	10	160	540
618051.8	IV 26 6.90	266	170	10	2570	130	0	160	440
618051 8	IV 26.6 90	267	2970	290	190	40	0	140	1940
618051.8	IV 26.6 90	268	0	110	0	60	0	0	500
618051 8	IV 26 6 90	269	0	20	440	70	0	30	510
618051 8	IV 26 6 90	270	20	60	140	0	0	330	560
618051 8	IV 26.6 90	271	0	100	100	10	0	240	590
618051.8	IV 26 6 90	272	0	60	60	110	220	190	520
618051.8	IV 26 6 90	273	15160	80	10	50	0	0	670
618051 8	IV 26 6.90	274	14780	30	40	20	0	0	510
618051 8	IV 26 6 90	275	0	60	1810	0	250	260	460
619098 6	IV 28.6.90	276	80	60	80	10	0	20	2690
619098 6	IV 28 6 90	277	100	210	280	260	0	820	1900
619098 6	IV 28 6.90	278	620	40	160	60	110	0	10910
619098 6	IV 28 6 90	279	480	10	170	0	180	0	8770
619098 6	IV 28.6 90	280	0	70	100	0	190	350	480
618051.8	IV 28.6 90	281	2280	390	130	0	160	970	460
618051 8	IV 28 6 90	282	3650	220	0	90	0	790	600
618051.8	IV 28 6.90	283	40	100	370	50	0	450	790
618051 8	IV 28.6 90	284	0	0	0	90	90	0	590
598259.7	IV 28 6.90	286	3030	1160	230	100	0	640	460
598259 7	IV 28 6 90	287	6850	350	140	50	0	710	740
598259 7	IV 28 6 90	288	11150	60	690	0	0	50	1950
115003	IV 28 6 90	289	870	60	0	0	0	170	670
115003	IV 28 6 90	290	100	210	0	0	0	280	490
115003	IV 28 6 90	291	0	0	70	0	0	0	1840
115003	IV 28 6 90	292	120	70	2340	150	100	240	300
115003	IV 28 6 90	293	1080	350	1590	0	230	260	640
618051.8	IV 6 7.90	300	6060	400	0	0	0	0	
618051 8	IV 6 7 90	301	3960	510	30	100	70	0	450
618051 8	IV 6 7.90	302	680	60	130	50	0	0	570
618051.8	IV 6 7 90	303	350	60	80	20	120	0	510
618051 8	IV 6 7 90	304	130	110	10	50	0	150	490
618051 8	IV 6 7 90	305	290	0	30	0	0	420	540
618051 8	IV 6 7 90	306	870	40	40	0	50	10	490
		307	5390	490	90	0	60	390	480
618051 8	IV 6 7 90	308	3310	410	50	0	0	10	510
618051 8	IV 6 7 90	309	5780	190	0	0	40	40	660
618051 8	IV 6.7 90	310	7090	330	0	0	30	0	490
618051 8	IV 6 7 90	311	6190	300	0	90	10	100	510

Thin Section	Label/Date	Py #	ppm Co	ppm Ni	ppm Cu	ppm Zn	ppm Ag	ppm Se	ppm As
618051 8	IV 6 7.90	312	6500	420	0	0	30	0	500
618051 8	IV 6 7.90	314	830	320	90	0	140	170	530
618051 8	IV 6 7 90	315	1830	90	0	0	50	270	400
618051 8	IV 6.7.90	316	16200	30	0	60	0	80	430
618051.8	IV 6.7.90	317	240	60	20	160	0	20	660
618051 8	IV 6 7 90	318	2610	350	0	20	10	210	970
618051.8	IV 6 7 90	319	4140	100	30	80	0	90	640
618051.8	IV 6 7.90	320	2850	220	20	180	0	120	1080
618051.8	IV 6.7 90	321	15840	0	50	40	0	0	490
618051.8	IV 6 7 90	322	1090	220	180	30	0	400	540
618051.8	IV 6 7 90	323	9390	190	170	60	0	210	500
618051.8	IV 6.7.90	324	2000	250	900	50	210	0	500
618051 8	IV 6 7.90	325	2500	80	60	0	50	40	630
618051 8	IV 6.7.90	326	28040	40	260	0	50	190	540
618051.8	IV 6 7.90	327	10000	0	150	110	0	230	780
618051.8	IV 6.7.90	328	420	80	140	0	0	270	1190
618051 8	IV 6.7.90	329	440	0	160	40	180	0	770
618051 8	IV 6 7 90	330	6980	130	200	70	100	0	1270
640012.1	IV 10.7.90	332	0	80	3710	0	160	100	460
640012.1	IV 10.7.90	335	710	0	40	0	90	0	500
640012.1	IV 10 7 90	336	870	20	0	0	80	170	510
626037.0	IV 10.7 90	337	360	0	260	20	60	50	490
626037 0	IV 10.7.90	338	1300	0	70	40	80	40	540
626037 0	IV 10.7.90	339	870	730	2090	70	120	280	470
626037 0	IV 10.7 90	340	330	110	2910	0	0	300	600
626037.0	IV 10.7.90	341	1180	60	120	0	10	20	590
626037.0	IV 10 7 90	342	2960	150	160	20	0	390	500
626037 0	IV 10 7 90	343	300	100	1090	40	0	0	510
626037 0	IV 10 7 90	344	6940	470	10	30	180	0	2550
626037 0	IV 10 7.90	345	8310	430	0	20	0	80	2010
626037.0	IV 10 7.90	346	1630	450	0	40	20	170	970
626037.0	IV 10 7.90	347	4910	340	0	70	250	330	710
626037 0	IV 10 7.90	348	3350	800	0	0	110	30	770
626037.0	IV 10.7.90	349	7410	720	30	0	60	90	530
626037.0	IV 10.7.90	350	130	100	2320	0	70	0	500
626037.0	IV 10.7.90	351	1560	140	160	10	200	50	580
626037.0	IV 10 7.90	352	0	0	1180	20	170	0	450
626037.0	IV 10.7.90	353	120	20	150	30	0	0	500
626037 0	IV 10.7.90	354	1890	70	80	0	0	0	960
626037.0	IV 10.7.90	355	720	20	100	30	100	70	1060
626037.0	IV 10.7.90	356	1460	190	0	30	60	140	1840
626037.0	IV 10.7.90	357	3660	210	30	0	100	0	3610
626037.0	IV 10.7.90	358	3160	270	130	0	200	0	2530
626037 0	IV 10 7 90	359	2120	270	160	60	0	90	2870
626037.0	IV 10.7.90	360	3560	110	80	0	30	0	890
626037.0	IV 10.7.90	361	5360	10	70	0	0	0	560
626037 0	IV 10 7 90	362	5010	20	30	10	10	100	1240
626037 0	IV 10.7 90	363	1690	60	140	150	0	0	2480
626037 0	IV 10.7 90	364	1890	70	170	120	0	220	1920
626037 0	IV 10 7 90	365	1270	120	0	120	0	0	1660
626037 0	IV 10 7 90	366	1820	100	70	0	0	0	620
626037 0	IV 10.7 90	367	4980	0	120	80	110	340	470
626037 0	IV 10.7 90	368	3550	120	110	160	330	60	590
626037 0	IV 10.7.90	369	3990	120	0	60	0	70	1010
626037.0	IV 10 7.90	370	310	40	4860	20	190	0	650
618051.8	IV 1 8 90	400	170	120	0	10	0	0	580
618051 8	IV 1 8 90	401	480	170	10	50	50	0	790
618051.8	IV 1 8.90	402	760	90	80	90	0	200	790
618051 8	IV 1 8 90	403	1970	30	20	150	60	410	820

Thin Section	Label/Date	Py #	ppm Co	ppm Ni	ppm Cu	ppm Zn	ppm Ag	ppm Se	ppm As
618051 8	IV 1 8.90	404	16270	10	0	0	0	290	670
618051.8	IV 1.8.90	405	6330	450	40	30	0	380	1770
618051.8	IV 1 8 90	406	40	70	80	20	30	250	570
618051 8	IV 1 8.90	407	0	0	0	10	10	0	1740
618051 8	IV 1 8 90	408	13170	40	50	30	50	250	520
618051 8	IV 1 8.90	409	14860	540	40	0	10	540	500
618051 8	IV 1 8 90	410	0	100	10	0	110	0	1830
618051 8	IV 1 8 90	411	0	50	30	50	20	260	330
618051 8	IV 1 8.90	412	690	110	80	10	110	60	1070
618051.8	IV 1.8.90	413	2360	530	0	0	0	250	1200
618051 8	IV 1 8.90	414	10720	170	20	0	60	380	210
618051 8	IV 1 8 90	415	3590	170	20	80	50	370	550
618051 8	IV 1 8 90	416	3250	160	80	10	0	160	410
618051 8	IV 1 8.90	417	4060	190	50	40	100	570	610
618051.8	IV 1 8 90	418	5510	170	50	80	10	550	630
618051 8	IV 1 8 90	419	2320	260	10	6	50	140	570
618051 8	IV 1 8 90	420	1980	280	40	70	30	440	530
638086 9	IV 7 8 90	421	2360	330	800	80	50	0	800
638086 9	IV 7.8 90	422	1470	1660	490	30	140	90	730
638086 9	IV 7 8.90	423	7040	400	460	60	0	210	900
115002	IV 7.8.90	424	3230	390	90	0	0	0	470
115002	IV 7 8.90	425	0	10	40	50	90	90	610
115002	IV 7 8.90	426	70	130	50	0	0	0	510
115002	IV 7 8 90	427	900	130	80	40	70	20	490
115002	IV 7.8.90	428	410	40	50	0	0	140	660
115002	IV 7.8.90	429	4110	150	70	150	0	0	1430
115002	IV 7 8 90	430	610	0	1580	0	50	0	510
115002	IV 7.8.90	431	1080	130	200	30	0	40	850
115002	IV 7 8 90	432	2070	430	310	10	0	120	2700
115002	IV 7 8 90	433	1920	400	220	0	0	130	920
115002	IV 7 8.90	434	0	50	120	0	60	30	480
115002	IV 7 8.90	435	30	110	60	70	150	210	500
115002	IV 7.8 90	436	440	460	720	60	0	230	2240
115002	IV 7 8.90	437	4680	430	1210	80	0	10	760
115002	IV 7.8.90	438	2680	310	720	60	140	140	5110
115002	IV 7 8.90	439	7360	290	3290	50	0	400	3770
598307 9	V 21 8.90	440	1340	180	260	0	140	260	xxx
598307 9	V 21 8.90	441	7710	30	450	0	120	0	xxx
598307 9	V 21 8 90	442	1080	0	140	40	0	230	xxx
598307.9	V 21 8 90	443	13260	110	200	150	0	160	xxx
598307 9	V 21 8.90	444	14260	120	20	90	80	280	xxx
598307 9	V 21.8.90	445	13250	210	0	0	160	60	xxx
626067 1	V 21 8 90	446	780	360	230	80	0	0	xxx
582279 4	V 21.8 90	447	1500	850	180	0	0	560	xxx
582279 4	V 21 8.90	448	2170	4710	90	0	40	530	xxx
582279.4	V 21 8.90	449	4830	430	130	10	0	140	xxx
115002	V 21 8.90	450	2560	20	50	0	120	210	xxx
115002	V 21 8.90	451	70	100	20	10	150	300	xxx
115002	V 22 8 90	452	6020	150	30	0	10	270	xxx
115002	V 22 8.90	453	1080	50	80	0	20	100	xxx
115002	V 22 8 90	454	630	10	40	0	0	220	xxx
115002	V 22 8 90	455	740	90	40	10	140	80	xxx
115002	V 22 8.90	458	0	0	50	0	0	190	xxx
115002	V 22 8 90	459	290	540	20	40	10	0	xxx
115002	V 22 8 90	460	60	110	90	120	0	200	xxx
115002	V 22 8.90	461	0	120	0	70	0	250	xxx
115002	V 22 8 90	462	100	110	0	60	0	80	xxx
115002	V 22 8 90	463	0	90	30	0	0	100	xxx

Thin Section	Label/Date	Py #	ppm Co	ppm Ni	ppm Cu	ppm Zn	ppm Ag	ppm Se	ppm As
115002	V 22.8 90	465	40	50	30	0	0	0	xxx
115002	V 22.8 90	466	30	320	30	50	150	0	xxx
115002	V 22.8.90	467	920	10	260	0	10	330	xxx
115002	V 22.8.90	468	10910	180	190	50	160	160	xxx
115002	V 22.8 90	469	1160	230	250	60	0	200	xxx
115002	V 22 8 90	471	1300	50	40	60	110	80	xxx
115002	V 22.8 90	472	15420	90	50	140	0	290	xxx
115002	V 22.8 90	473	12610	190	0	30	50	0	xxx
115002	V 22.8.90	474	100	220	0	110	120	0	xxx
115002	V 22.8 90	475	570	670	150	0	0	150	xxx

APPENDIX 5.4

ELECTRON MICROPROBE ANALYSES OF TiO2 IN MAGNETITE

Thin Section	Date	TiO2 (wt%)	Remarks
636126.8	27.3.90	1.25	massive magnetite vein
636126.8	27.3.90	1.34	as above
636126.8	27.3.90	0.53	as above
636126.8	27.3.90	1.06	as above
636126.8	27.3.90	0.71	as above
638086.9	7.8.90	0.06	magnetite grain in groudmass
638086.9	7.8.90	0.11	as above
638086.9	7.8.90	0.16	as above
638086.9	7.8.90	0.36	massive magnetite vein
638086.9	7.8.90	0.42	as above
638086.9	7.8.90	0.12	magnetite grain in groudmass
638086.9	7.8.90	0.46	massive magnetite vein
638086.9	7.8.90	0.55	as above
638086.9	7.8.90	0.44	as above
638086.9	7.8.90	0.66	as above
638086.9	7.8.90	0.42	as above
638086.9	7.8.90	0.45	as above
638086.9	7.8.90	0.51	as above
618010.0	30.8.90	0.07	magnetite grain with ilmenite lamellae
618010.0	30.8.90	2.01	as above
618010.0	30.8.90	5.12	as above
618010.0	30.8.90	4.68	as above
618010.0	30.8.90	5.32	as above
618010.0	30.8.90	7.50	as above
598307.9	30.8.90	0.26	inclusion in pyrite
598307.9	30.8.90	0.03	as above
598307.9	30.8.90	0.02	as above
598307.9	30.8.90	0.04	as above
115002	30.8.90	0.00	magnetite grain in groudmass
115002	30.8.90	0.01	as above
115002	30.8.90	0.01	as above
115002	30.8.90	0.00	as above
115002	30.8.90	0.02	as above
115002	30.8.90	0.03	as above
115002	30.8.90	0.01	as above
115002	30.8.90	0.02	as above
582279.4	30.8.90	0.00	thin overgrowth in fractured magnetite vein
582279.4	30.8.90	1.17	as above
582279.4	30.8.90	1.74	massive magnetite vein
582279.4	30.8.90	1.59	thin overgrowth in fractured magnetite vein
582279.4	30.8.90	1.43	massive magnetite vein
582279.4	30.8.90	0.02	thin overgrowth in fractured magnetite vein
582279.4	30.8.90	1.32	massive magnetite vein
582279.4	30.8.90	0.00	thin overgrowth in fractured magnetite vein
582279.4	30.8.90	1.46	massive magnetite vein
582279.4	30.8.90	0.19	thin overgrowth in fractured magnetite vein

APPENDIX 5.5

THERMODYNAMIC DATA

Reaction	log K_{eq} 350°C	log K_{eq} 300°C	Ref.
$HSO_4^- = H^+ + SO_4^{2-}$	-6.90	-6.08	1
$H_2S = HS^- + H^+$	-8.98	-8.06	1
$HS^- + 2O_2 = SO_4^{2-} + H^+$	47.28	55.38	1
$H_2S + 2O_2 = SO_4^{2-} + 2H^+$	38.30	47.32	1
$H_2S + 2O_2 = HSO_4^- + H^+$	45.20	53.40	1
$3FeS_2 + 6H_2O = Fe_3O_4 + 6H_2S + O_2$	-44.48	-49.00	2
$3FeS_2 + 6H_2O = Fe_3O_4 + 6HS^- + 6H^+ + O_2$	-98.36	-97.36	2
$3FeS_2 + 6H_2O + 11O_2 = Fe_3O_4 + 6SO_4^{2-} + 12H^+$	185.32	234.92	2
$4FeS_2 + 8H_2O + 15O_2 = 2Fe_2O_3 + 8HSO_4^- + 8H^+$	311.44	372.21	2
$4FeS_2 + 8H_2O = 2Fe_2O_3 + 8H_2S + O_2$	-50.16	-54.99	2
$4FeS_2 + 8H_2O + 15O_2 = 2Fe_2O_3 + 8SO_4^{2-} + 16H^+$	256.24	323.57	2
$FeS_2 + H_2O = FeS + H_2S + {}^1/_2O_2$	-17.51	-19.57	2
$3FeS + 3H_2O + {}^1/_2O_2 = Fe_3O_4 + 3H_2S$	8.05	9.70	2
$3FeS + 3H_2O + {}^1/_2O_2 = Fe_3O_4 + 3HS^- + 3H^+$	-18.89	-14.49	2
$4Fe_3O_4 + O_2 = 6Fe_2O_3$	27.44	31.03	2
$Fe^{2+} + 2Cl^- = FeCl_2$	4.53	2.6	3
$2FeS_2 + 2H_2O + 4Cl^- + 4H^+ = 2FeCl_2 + 4H_2S + O_2$	-26.78	-31.88	4
$2FeS_2 + 2H_2O + 7O_2 + 4Cl^- = 2FeCl_2 + 4HSO_4^-$	154.02	181.73	4
$FeS + 2H^+ + 2Cl^- = FeCl_2 + H_2S$	4.12	3.63	4
$2Fe_3O_4 + 12H^+ + 12Cl^- = 6FeCl_2 + 6H_2O + O_2$	8.62	2.40	4
$2Fe_2O_3 + 8H^+ + 8Cl^- = 4FeCl_2 + 4H_2O + O_2$	-3.40	-8.76	4
$5CuFeS_2 + 2H_2O = Cu_5FeS_4 + 4FeS + 2H_2S + O_2$	-39.29	-43.93	2
$5CuFeS_2 + 2H_2S + O_2 = Cu_5FeS_4 + 4FeS_2 + 2H_2O$	30.75	34.33	2
$5CuFeS_2 + 2HSO_4^- + 2H^+ = Cu_5FeS_4 + 4FeS_2 + 2H_2O + 3O_2$	-59.65	-72.47	2

Reaction	log K_{eq} 350°C	log K_{eq} 300°C	Ref.
$15CuFeS_2 + 18H_2O =$ $3Cu_5FeS_4 + 4Fe_3O_4 + 18H_2S + O_2$	-85.67	-93.01	2
$15CuFeS_2 + 18H_2O =$ $3Cu_5FeS_4 + 4Fe_3O_4 + 18HS^- + 18H^+ + O_2$	-247.31	-238.09	2
$5CuFeS_2 + 6H_2O = Cu_5FeS_4 + 2Fe_2O_3 + 6H_2S$	-19.41	-20.66	2
$5CuFeS_2 + 6H_2O + 12O_2 =$ $Cu_5FeS_4 + 2Fe_2O_3 + 6HSO_4^- + 6H^+$	251.79	299.74	2
$5CuFeS_2 + 6H_2O + 12O_2 =$ $Cu_5FeS_4 + 2Fe_2O_3 + 6SO_4^{2-} + 12H^+$	210.39	263.26	2
$12Cu_5FeS_4 + 18H_2O =$ $30Cu_2S + 18HS^- + 18H^+ + O_2$	-262.14	-251.88	2
$4Cu_5FeS_4 + 2H_2O = 10Cu_2S + 4FeS + 2H_2S + O_2$	-44.24	-48.54	2
$2Cu_5FeS_4 + 3H_2O = 5Cu_2S + Fe_2O_3 + 3H_2S$	-12.18	-12.63	2
$2Cu_5FeS_4 + 3H_2O + 6O_2 =$ $5Cu_2S + Fe_2O_3 + 3HSO_4^- + 3H^+$	123.42	147.57	2
$Cu^+ + Cl^- = CuCl$	2.7	2.2	3
$4CuFeS_2 + 4Cl^- + O_2 + 4H^+ =$ $4FeS_2 + 2H_2O + 4CuCl$	20.68	20.57	4
$4CuFeS_2 + 4Cl^- + 4H^+ + 2H_2O =$ $4FeS + 4CuCl + O_2 + 4H_2S$	-49.36	-57.69	4
$12CuFeS_2 + 12Cl^- + 18H_2O + 12H^+ =$ $4Fe_3O_4 + 24H_2S + 12CuCl + O_2$	-115.88	-134.27	4
$2CuFeS_2 + 2Cl^- + 3H_2O + 2H^+ =$ $Fe_2O_3 + 2CuCl + 4H_2S$	-14.74	-17.21	4
$2CuFeS_2 + 2Cl^- + 3H_2O + 8O_2 =$ $Fe_2O_3 + 2CuCl + 4HSO_4^- + 2H^+$	166.06	196.39	4
$4Cu_5FeS_4 + 12H^+ + 20Cl^- + 17O_2 =$ $4FeS_2 + 20CuCl + 2H_2O + 8HSO_4^-$	342.00	392.72	4
$4Cu_5FeS_4 + 20H^+ + 20Cl^- + O_2 =$ $4FeS_2 + 20CuCl + 2H_2O + 8H_2S$	-19.60	-34.48	4
$4Cu_5FeS_4 + 20H^+ + 20Cl^- + 2H_2O =$ $4FeS + 20CuCl + O_2 + 12H_2S$	-89.64	-112.73	4
$6Cu_5FeS_4 + 5H_2O + 30H^+ + 30Cl^- =$ $2Fe_3O_4 + 30CuCl + 1/2\,O_2 + 24H_2S$	-118.36	-149.70	4
$2Cu_5FeS_4 + 3H_2O + 10Cl^- + 10H^+ =$ $10CuCl + Fe_2O_3 + 8H_2S$	-34.88	-44.73	4

Reaction	log K_{eq} 350°C	log K_{eq} 300°C	Ref.
$2Cu_5FeS_4 + 3H_2O + 16O_2 + 10Cl^- + 2H^+ = Fe_2O_3 + 10CuCl + 8HSO_4^-$	326.72	382.47	4
$Cu_2S + 2Cl^- + 2H^+ = 2CuCl + H_2S$	-4.54	-6.42	4
$Cu_2S + 2Cl^- + O_2 + H^+ = 2CuCl + HSO_4^-$	40.66	46.98	4
$KAl_2(AlSi_3O_{10})(OH)_2 + 6SiO_2 + 2K^+ = 3KAlSi_3O_8 + 2H^+$	-7.35	-6.92	5
$3Al_2Si_2O_5(OH)_4 + 2K^+ = 2KAl_2(AlSi_3O_{10})(OH)_2 + 2H^+ + 3H_2O$	-3.03	-3.60	1

References:

1. Huston and Large (1989)
2. calculated from Bowers *et al.* (1984)
3. Ohmoto *et al.* (1983)
4. calculated from 1, 2 and 3.
5. Sverjensky *et al.* (1991)

APPENDIX 6.1

TRACE ELEMENT ANALYSES - GREAT LYELL FAULT ZONE

(intersections of diamond drill holes with the Great Lyell fault, adjacent to the Prince Lyell South Lens)

Sample no.	WL Drill Hole No.	ppm Sn	ppm As	ppm Mo	ppm Ag	ppm Au	ppm Cu	ppm Pb	ppm Zn
LF 1	612	8	17	< 5	1	0.04	358	101	184
LF 2	611	< 5	22	< 5	4	0 04	358	3405	2150
LF 3	487	< 5	< 10	6	< 1	<.01	2590	16	125
LF 4	481	9	< 10	24	1	0.01	1940	30	108
LF 5	504A	23	11	18	< 1	0.03	2460	43	107
LF 6	544	< 5	< 10	< 5	1	<.01	940	43	188
LF 7	482	12	21	< 5	1	0.01	221	379	1100
LF 8	636	6	18	< 5	1	0.04	228	202	95
LF 9	639	9	< 10	< 5	2	0.02	274	2560	2680
LF 10	566	< 5	31	5	3	0.03	180	5800	281
LF 11	593	< 5	18	< 5	4	0.02	168	3630	2830
LF 12	562	10	15	8	2	0.03	393	167	338
LF 13	549	7	12	8	2	0.05	1120	504	209
LF 14	567	< 5	18	< 5	3	0.02	128	16400	112
LF 15	589	21	< 10	271	2	0.17	14200	29	92
LF 16	586	6	< 10	< 5	< 1	0.03	351	66	102
LF 17	595	5	< 10	< 5	2	0 06	223	351	246
LF 18	624	< 5	25	< 5	4	0.08	203	2410	3370
LF 20	637	8	< 10	< 5	3	0.05	30	2360	316
LF 21	629	9	< 10	9	2	0.03	2210	15	185
LF 22	603	< 5	< 10	< 5	1	0.02	358	41	1740
LF 23	640	24	< 10	119	3	0.22	11800	327	214
LF 24	594	8	< 10	7	1	0.04	500	162	202
LF 25	591	< 5	< 10	< 5	< 1	0.01	283	26	159

Note: Sample LF 19 was a University of Tasmania standard.

APPENDIX 6.2

ASSAY RESULTS OF DRILL CORE INTERVALS ACROSS ZONES OF "FLAT FAULTS" AND ASSOCIATED QUARTZ - SIDERITE VEINING

WL 591

depth (m)	Cu (%)	Au (ppm)	Ag (ppm)	Au/Cu
170 - 172	1.78			
172 - 174	2.31	0.6	3.1	0.25
174 - 176	2.90			
176 - 178	1.45			
178 - 180	1.71	0.4	1.7	0.21
180 - 182	2.49			
182 - 184	2.10			
184 - 186	2.05	0.4	1.6	0.21
186 - 188	1.57			
188 - 190	2.45			
190 - 192	2.27	0.6	2.5	0.27
192 - 194	1.82			
194 - 196	0.81			
196 - 198	0.94	0.2	1.1	0.19
198 - 200	1.45			
200 - 202	1.16			
202 - 204	1.08	0.2	1.5	0.18
204 - 206	1.15			
206 - 208	1.38			
208 - 210	1.94	0.4	1.1	0.26
210 - 212	1.37			
212 - 214	2.97			
214 - 216	2.20	0.6	2.3	0.22
216 - 218	2.90			
218 - 220	3.20			
220 - 222	1.20	0.5	1.9	0.26
222 - 224	1.32			
224 - 226	1.00			
226 - 228	1.72	0.1	0.8	0.06
228 - 230	2.71			
230 - 232	1.20			
232 - 234	1.00	0.1	1.0	0.10
234 - 236	0.88			
236 - 238	1.31			
238 - 240	1.70	0.3	2.2	0.18
240 - 242	2.03			

WL 599

depth (m)	Cu (%)	Au (ppm)	Ag (ppm)	Au/Cu
348 - 350	0.63	0.11	0.5	0.17
350 - 352	0.58	0.16	0.5	0.28
352 - 354	0.92	0.10	<0.5	0.11
354 - 356	0.80	0.39	1.0	0.49
356 - 358	0.82	0.18	0.5	0.22
358 - 360	1.03	0.23	1.0	0.21
360 - 362	0.48	0.10	<0.5	0.21

WL 607

depth (m)	Cu (%)	Au (ppm)	Ag (ppm)	Au/Cu
98 - 100	0.80			
100 - 102	0.88	0.2	2.8	0.14
102 - 104	2.52			
104 - 106	3.24			
106 - 108	2.22	0.7	3.3	0.29
108 - 110	1.76			
110 - 112	2.36			
112 - 114	2.18	0.4	3.2	0.17
114 - 116	2.32			
116 - 118	1.52			
118 - 120	0.64	0.3	2.0	0.21
120 - 122	2.10			
122 - 124	0.34			
124 - 126	1.72	3.0	2.6	1.24
126 - 128	5.16			
128 - 130	1.14			
130 - 132	0.90	0.2	0.8	0.17
132 - 134	1.40			
134 - 136	1.00			
136 - 138	1.86	0.2	0.5	0.16
138 - 140	0.90			
140 - 142	0.92			
142 - 144	1.14	0.2	0.8	0.19
144 - 146	1.12			
146 - 148	1.98			
148 - 150	1.58	0.4	1.5	0.22

WL 607 continued

depth (m)	Cu (%)	Au (ppm)	Ag (ppm)	Au/Cu
150 - 152	0.34			
152 - 154	0.22	<0.1	0.4	<0.25
154 - 156	0.40			
156 - 158	0.56			
158 - 160	0.70	0.1	0.9	0.13
160 - 162	1.08			

WL 621

depth (m)	Cu (%)	Au (ppm)	Ag (ppm)	Au/Cu
66 - 68	0.85	0.09	1.5	0.11
68 - 70	1.06	0.20	5.0	0.19
70 - 72	1.11	0.11	2.0	0.10
72 - 74	1.35	0.50	6.0	0.37
74 - 76	0.66	0.11	1.5	0.17
76 - 78	0.35	0.13	2.0	0.37
78 - 80	0.91	0.14	1.5	0.15
80 - 82	0.77	0.10	1.5	0.13
82 - 84	1.19			
84 - 86	1.86	0.4	5.3	0.26
86 - 88	1.58			
88 - 90	0.74	0.3	3.3	0.26
90 - 92	1.09			
92 - 94	1.24			
94 - 96	1.68	0.4	2.1	0.28
96 - 98	1.36			

WL 624

depth (m)	Cu (%)	Au (ppm)	Ag (ppm)	Au/Cu
4 - 6	0.42	0.08	0.5	0.19
6 - 8	0.43	0.15	1.0	0.35
8 - 10	0.30	0.07	<0.5	0.23
10 - 12	0.27	0.05	<0.5	0.19
12 - 14	0.18	0.10	1.0	0.56
14 - 16	0.24	0.05	<0.5	0.21
16 - 18	0.45	0.16	<0.5	0.36

WL 633

depth (m)	Cu (%)	Au (ppm)	Ag (ppm)	Au/Cu
54 - 56	2.35			
56 - 58	1.70	0.5	3.3	0.27
58 - 60	1.50			
60 - 62	2.14			
62 - 64	0.95	0.3	1.6	0.25
64 - 66	0.48			
66 - 68	0.57			
68 - 70	3.41	0.8	4.8	0.33
70 - 72	3.14			
72 - 74	0.48	0.26	<0.5	0.54
74 - 76	0.64	0.17	<0.5	0.27
76 - 78	1.12	0.33	0.5	0.29
78 - 80	0.89	0.21	1.0	0.24
80 - 82	0.90	0.28	0.5	0.31

WL 640

depth (m)	Cu (%)	Au (ppm)	Ag (ppm)	Au/Cu
14 - 16	0.35	0.10	<0.5	0.29
16 - 18	0.53	0.10	<0.5	0.19
18 - 20	0.37	0.36	<0.5	0.16
20 - 22	0.43	0.55	1.0	1.28
22 - 24	0.81	0.07	1.0	0.09
24 - 26	0.50	0.13	0.5	0.26
26 - 28	2.16	0.41	5.5	0.19
28 - 30	0.49	0.18	1.0	0.37

APPENDIX 6.3

FLUID INCLUSION DATA
FROM QUARTZ - SIDERITE ± FLOURITE VEINS

Sample #	Mineral	Th (°C)	Tf (°C)	Type
619079.1	quartz	161	-4.6	1
619079.1	quartz	141		1
619079.1	quartz	152		1
619079.1	quartz	141	-10.8	1
619079.1	quartz	154		1
619079.1	quartz	154		1
619079.1	quartz	199		1
619079.1	quartz	149		1
619079.1	quartz	157		1
619079.1	quartz	181		1
619079.1	quartz	150		1
619079.1	quartz	162		1
619079.1	quartz	155		1
619079.1	quartz	145		1
619079.1	quartz	204		1
619079.1	quartz	149		1
619079.1	quartz	151		1
619079.1	quartz	143		1
619079.1	quartz	154		1
619079.1	quartz	154		1
619079.1	quartz	152		1
619079.1	quartz	174		1
629073.0	flourite	112		2
629073.0	flourite	111		2
629073.0	flourite	110		2
629073.0	flourite	112		2
629073.0	flourite	117		2
629073.0	flourite	138	-5.2	1
629073.0	flourite	136	-4.9	1
629073.0	flourite	136	-2.7	1
629073.0	flourite	112		2
629073 0	flourite	118		2
629073.0	flourite	132		2
629073.0	flourite	123	-3.6	1
629073.0	flourite	125	-2 9	1

Sample #	Mineral	Th (°C)	Tf (°C)	Type
629073.0	flourite	125	-2.6	1
629073.0	flourite	127	-1.9	1
629073.0	flourite	128	-1.4	1
629073.0	flourite	117	-5.2	1
629073.0	flourite	121	-5.2	1
629073.0	flourite	121	-5.1	1
629073.0	flourite	123	-2.4	1
629073.0	flourite	120	-1.3	1
633050.8	quartz	151	-3.8	2
633050.8	quartz	158	-3.8	2
633050.8	quartz	141	-4.4	2
633050.8	quartz	150	-3.9	2
633050.8	quartz	154	-3.6	2
633050.8	quartz	156	-3.7	2
633050.8	quartz	157		2
633050.8	quartz	137	-5.0	2
633050.8	quartz	138	-4.0	2
633050.8	quartz	140	-3.6	2
633050.8	quartz	140	-3.6	2
633050.8	quartz	130		2
633050.8	quartz	132		2
633050.8	quartz	141		1
633050.8	quartz	143		1
633050.8	quartz	150		1
633050.8	quartz	151	-3.7	1
633050 8	quartz	145	-7.6	1
633050 8	quartz	140	-7.5	1
633050.8	quartz	151		1

APPENDIX 7.1

SULPHUR ISOTOPE DATA FOR SOUTHERN PRINCE LYELL SULPHIDES. (DATA FROM THIS AND PREVIOUS STUDIES)

Sample No.	$\delta^{34}S_{py}$	$\delta^{34}S_{cpy}$	$\Delta^{34}S_{py\text{-}cpy}$	$\delta^{34}S_{cpy}$ (D_2 veins)	$\delta^{34}S_{sph}$	Reference
115002A	5.9	(volcanic breccia clast)				1
115002B	8.8	(volcanic breccia matrix)				1
568A289.5	8.5					1
584326.5	7.3					1
584389.0	7.8					1
596320.7	7.4					1
596343.9	7.9					1
596401.6	9.0					1
596431.6	9.1					1
596454.8	9.8					1
605023.0	8.9					1
605050.2	7.3					1
605074.1	7.9					1
607068.8	11.1					1
607104.3	7.6					1
619017.3	8.1					1
619055.3	7.2	8.3	- 1.1			1
619086.8	6.8					1
619134.0	8.3					1
622095.5	7.4					1
624050.4	10.8					1
634044.4	7.9					1
634085.6	7.3					1
634131.0	7.0					1
635010.0	8.3	7.6	0.7			1
635024.4	6.3					1
635069.9	7.3	6.7	0.6			1
635085.0	10.8					1
635130.4	8.1					1
636040.9	8.5					1
637029.6	9.2					1
698100.4	7.6					1
104555A	5.6	5.2	0.4			2
104555B	7.0	6.6	0.4			2
104555C	5.9					2
104567	7.6	6.4	1.2			2
104606	8.1	7.5	0.6			2
104622A	6.7	5.9	0.8			2
104622B	7.5	6.4	1.1			2
104622C	6.5					2
104623	7.6	7.0	0.6			2
104639	7.9	7.3	0.6			2
104710	7.1	7.7	- 0.6			2

Sample No.	$\delta^{34}S_{py}$	$\delta^{34}S_{cpy}$	$\Delta^{34}S_{py\text{-}cpy}$	$\delta^{34}S_{cpy}$ (D_2 veins)	$\delta^{34}S_{sph}$	Reference
45749	7.3	7.5	- 0.2			2
Mt Lyell Co.	8.7					2
11227	6.3					3
11228	6.5					3
11229	8.7					3
11230	9.7					3
11231	10.0					3
31806A	7.7					3
31806B	6.5					3
31806C	8.6					3
10719		6.8				3
10733A		5.4				3
10733B		5.2				3
10736		5.8				3
10737		6.2				3
31200A		5.9				3
31200B		6.8				3
31200C		5.6				3
584330.5				8.2		1
619076.9				7.5		1
635119.6				8.5		1
115012					11.3	1
586201.3					10.3	1

1. Data from present study
2. Data from Walshe and Solomon (1981)
3. Data from Solomon *et al.* (1969)